

TEHNIČKI GLASNIK - TECHNICAL JOURNAL

Scientific-professional journal of University North

Volume 14
Varaždin, December 2020Number 4
Pages 403–545**Editorial Office:**

Sveučilište Sjever / University North – Tehnički glasnik / Technical journal
 Sveučilišni centar Varaždin / University Center Varaždin
 Jurja Križanića 31b, 42000 Varaždin, Croatia
 Tel. ++385 42 493 328, Fax. ++385 42 493 333
 E-mail: tehnickiglasnik@unin.hr
<https://tehnickiglasnik.unin.hr>
<https://www.unin.hr/djelatnost/izdavstvo/tehnicki-glasnik/>
<https://hrcak.srce.hr/tehnickiglasnik>

Founder and Publisher:

Sveučilište Sjever / University North

Council of Journal:

Marin MILKOVIĆ, Chairman; Anica HUNJET, Member; Goran KOZINA, Member; Mario TOMIŠA, Member;
 Vlado TROPŠA, Member; Damir VUSIĆ, Member; Milan KLJAJIN, Member; Anatolii KOVROV, Member

Editorial Board:

Chairman Damir VUSIĆ (1), Milan KLJAJIN (2)/(1), Marin MILKOVIĆ (1), Krešimir BUNTAK (1), Anica HUNJET (1), Živko KONDIĆ (1), Goran KOZINA (1), Ljudevit KRPAN (1), Krunoslav HAJDEK (1), Marko STOJIC (1), Božo SOLDO (1), Mario TOMIŠA (1), Vlado TROPŠA (1), Vinko VIŠNJIĆ (1), Duško PAVLETIĆ (5), Branimir PAVKOVIĆ (5), Mile MATIJEVIĆ (3), Damir MODRIĆ (3), Nikola MRVAC (3), Klaudio PAP (3), Ivana ŽILJAK STANIMIROVIĆ (3), Krešimir GRILEC (6), Biserka RUNJE (6), Predrag ČOŠIĆ (6), Sara HAVRLIŠAN (2), Dražan KOZAK (2), Roberto LUJIĆ (2), Leon MAGLIĆ (2), Ivan SAMARDŽIĆ (2), Antun STOIC (2), Katica ŠIMUNOVIĆ (2), Goran ŠIMUNOVIĆ (2), Ladislav LAZIĆ (7), Ante ČIKIĆ (1)/(2), Darko DUKIĆ (9), Gordana DUKIĆ (10), Srđan MEDIĆ (11), Sanja KALAMBURA (12), Marko DUNĐER (13), Zlata DOLACEK-ALDUK (4), Dina STÖBER (4)

International Editorial Council:

Boris TOVORNIK (14), Milan KUHTA (15), Nenad INJAC (16), Džafer KUDUMOVIC (17), Marin PETROVIĆ (18), Salim IBRAHIMEFENDIĆ (19), Zoran LOVREKOVIĆ (20), Igor BUDAK (21), Darko BAJIĆ (22), Tomáš HANÁK (23), Evgenij KLIMENKO (24), Oleg POPOV (24), Ivo ČOLAK (25), Katarina MONKOVA (26), Berenika HAUSNEROVA (8), Nenad GUBELJAK (27), Charlie FAIRFIELD (28), Stefanija KLARIC (28), Bertrand MARESCHAL (29), Sachin R. SAKHARE (30), Suresh LIMKAR (31), Mandeep KAUR (32), Aleksandar Sedmak (33)

Editor-in-Chief:

Milan KLJAJIN

Technical Editor:

Goran KOZINA

Graphics Editor:

Snježana IVANČIĆ VALENKO

Linguistic Advisers for English language:

Ivana GRABAR, Iva GRUBJEŠIĆ

IT support:

Tomislav HORVAT

Print:

Centar za digitalno nakladništvo, Sveučilište Sjever

All manuscripts published in journal have been reviewed.
Manuscripts are not returned.

The journal is free of charge and four issues per year are published
 (In March, June, September and December)

Circulation: 100 copies

Journal is indexed and abstracted in:

Web of Science Core Collection (Emerging Sources Citation Index - ESCI), EBSCOhost Academic Search Complete, EBSCOhost – One Belt, One Road Reference Source Product, ERIH PLUS, CITEFACTOR – Academic Scientific Journals, Hrcak - Portal znanstvenih časopisa RH

Registration of journal:The journal "Tehnički glasnik" is listed in the HGK Register on the issuance and distribution of printed editions on the 18th October 2007 under number 825.**Preparation ended:**

December 2020

Legend:

(1) University North, (2) Mechanical Engineering Faculty in Slavonski Brod, (3) Faculty of Graphic Arts Zagreb, (4) Faculty of Civil Engineering Osijek, (5) Faculty of Engineering Rijeka, (6) Faculty of Mechanical Engineering and Naval Architecture Zagreb, (7) Faculty of Metallurgy Sisak, (8) Tomas Bata University in Zlin, (9) Department of Physics of the University of Josip Juraj Strossmayer in Osijek, (10) Faculty of Humanities and Social Sciences Osijek, (11) Karlovac University of Applied Sciences, (12) University of Applied Sciences Velika Gorica, (13) Department of Polytechnics - Faculty of Humanities and Social Sciences Rijeka, (14) Faculty of Electrical Engineering and Computer Science - University of Maribor, (15) Faculty of Civil Engineering - University of Maribor, (16) University College of Teacher Education of Christian Churches Vienna/Krems, (17) Mechanical Engineering Faculty Tuzla, (18) Mechanical Engineering Faculty Sarajevo, (19) University of Travnik - Faculty of Technical Studies, (20) Higher Education Technical School of Professional Studies in Novi Sad, (21) University of Novi Sad - Faculty of Technical Sciences, (22) Faculty of Mechanical Engineering - University of Montenegro, (23) Brno University of Technology, (24) Odessa State Academy of Civil Engineering and Architecture, (25) Faculty of Civil Engineering - University of Mostar, (26) Faculty of Manufacturing Technologies with the seat in Prešov - Technical University in Košice, (27) Faculty of Mechanical Engineering - University of Maribor, (28) College of Engineering, IT & Environment - Charles Darwin University, (29) Université Libre de Bruxelles, (30) Vishwakarma Institute of Information Technology (Pune, India), (31) AISSMS Institute of Information Technology (Pune, India), (32) Permtech Research Solutions (India), (33) University of Belgrade

CONTENT	I
Reza Askarizad Evaluation of the Effective Factors on Social Interactions in the Design of Public Libraries	403
Emine Avşar Aydın*, Selin Yabaci Karaoğlu Reference Breast Phantoms for Low-Cost Microwave Imaging	411
Fereidoun Esmaeilzadeh, Kazem Askarifar*, Pegah Alamdari A Strategic Service Management Model in National Gas Distribution Projects	416
Emir Šarić*, Samir Butković, Muhamed Mehmedović The Effect of the Holding Pressure Profile on the Metal Injection Molded Component Dimensions after Sintering	423
Tomislav Hudika*, Igor Majnarić, Tomislav Cigula Influence of Varnishing the "Surface" Coverage on Optical Print Characteristics	428
Amalija Horvatić Novak*, Biserka Runje, Zdenka Keran, Marko Orošnjak Image Artefacts in Industrial Computed Tomography	434
Seyed Emad Hosseini, Amir Naser Akhavan*, Mohsen Bahrami Designing an Integrated Model of Oil and Gas Management with a SWOT Approach: The Case of NIOC	440
Margareta Premužić*, Almin Đapo, Željko Bačić, Boško Pribičević Accuracy Analysis of Point Velocities Determined by Different Software Packages and GNSS Measurement Processing Methods	446
Helena Ellingerová, Zora Petráková, Ingrida Skalíková* Statistical Methods in Building Industry to Determine Prices Indices	458
Zeljko Kos*, Yevhenii Klymenko, Kostiantyn Polianskyi, Andjelko Crnoja Research of the Residual Bearing Capacity and the Work of Damaged Reinforced Concrete Beams' Inclined Sections	466
Alena Tichá, Dana Linkeschová, Zdeněk Tichý, Zuzana Mrňová* Wages and Incentive Instruments for Enhancing the Performance of Construction Industry Employees	473
Vedran Mrzljak*, Sandi Baressi Šegota, Hrvoje Meštrić, Zlatan Car Comparison of Power Distribution, Losses and Efficiencies of a Steam Turbine with and without Extractions	480
Jovan Karamachoski*, Ninoslav Marina, Pavel Taskov Blockchain-Based Application for Certification Management	488
Hazim Bašić*, Ismet Demirdžić, Samir Muzaferija Calculation of the Plastic Metal Flow in the Cold Extrusion Technology by Finite Volume Method	493
Atanas Kochov*, Aleksandar Argilovski Case Study: Six Sigma Project for Reducing Manual Handling of Materials in Real Manufacturing Company	499
Carles Serrat*, Sebastian Banaszek, Anna Cellmer, Vicenç Gibert, Anna Banaszek UAV, Digital Processing and Vectorization Techniques Applied to Building Condition Assessment and Follow-up	507
Manoj Kumar Sahu*, Madhusmita Biswal, Jagan Mohana Rao Malla THD Analysis of a Seven, Nine, and Eleven Level Cascaded H-Bridge Multilevel Inverter for Different Loads	514
Fisnik Osmani, Atanas Kochov*, Betim Shabani, Mirjeta Ilazi The Importance of SD Goals Indicators 7, 8, 9 and 12 in the Industry Development by Using Multi Criteria and Decision Making Method	524
Predrag Čosić*, Zdenka Keran, Vedran Kokot Selection of an Optimal Supplier	531
Zvonimir Mihaljevic, Goran Dukic* The Simulation Model of a Student Restaurant	540
INSTRUCTIONS FOR AUTHORS	III



conferences.eg.org/eg2021

Evaluation of the Effective Factors on Social Interactions in the Design of Public Libraries

Reza Askarizad

Abstract: Nowadays, the interaction of people in the world is deemed a controversial topic and consequently, the creation of an appropriate context for interacting with individuals is one of the issues that is considered by architects in many designs. In this research, it has been endeavored to consider the factors affecting social interactions in the design of public libraries through the descriptive-inferential analysis. The results of this research reveal that in the architectural spaces that have been designed with open-configured plans, spatial integrity and sociability will increase. On the other hand, the factors such as depth and the level of privacy are also reduced. Therefore, in designing a public library with an approach toward social interaction, there should be a variety of open and closed-configured spaces in the plan that allow users to choose the space they optionally want and in which they would enjoy in their own presence by choosing their own activities.

Keywords: public library; Rasht National Library; social interactions; social sustainability; space syntax

1 INTRODUCTION

Human beings are social creatures in the sense that their survival condition depends on establishing communications and social interactions. Sociability is a procedure that prepares individuals for collective life [1]. Nowadays, the interaction of people in the world is a quite significant topic and consequently, the creation of an appropriate context for interacting with individuals is one of the issues that is considered by architects in many designs [2].

Studies have indicated that people are satisfied to be in the places which are the source of interactions [3]. The opportunity to see, hear and meet others can be the main attraction in urban spaces [4]. Being amongst others provides a rich sense of experience that brings a special quality to the environment. The attractiveness of the public environment is not only because of the buildings; rather, it depends on the presence of the people and the human events occurring there [5].

Meanwhile, a library is a kind of a public space; and a public space, according to its definition, should be a platform for the use and communication of citizens and can help users to increase the social interaction opportunities within it [6]. Based on its definition, a library is a building that preserves and stores books, papers and periodicals which may be read or lent out [7]. Nonetheless, public libraries have evolved in the present era and have changed from mere cultural institutions which preserve books, cultural heritage and in general, history and culture, into social, interactive and media environments where not only modern technologies take place in, but they can be considered as a manifestation of people's interactions, knowledge and public culture in its new form [8].

Despite the positive efforts made in the recent years, the active public libraries in Rasht still face challenges in attracting and retaining their users through the provision of au courant services to meet their scientific, cultural and recreational requirements. Most of the time, the existing libraries in Rasht are vacant, or the presence of users is just for studying their own educational books during the time of university or school examinations. Accordingly, the need to

create spaces with an approach toward audience attraction in public libraries seems to be necessary. In this way, it has been attempted to consider the factors affecting social interactions in the design of public libraries in order to maximize their level of attraction and the interaction of the audience, as much as possible, from the culture of reading books. In this regard, the following questions have been posed in order to obtain appropriate answers:

- 1) How can social interactions be considered in library designs?
- 2) What influences do social interactions have in the design of public libraries?

It seems that the spatial configuration of libraries can affect the level of the attraction and interaction of the audience as much as possible. Additionally, it is assumed that open-configured plans have a positive effect on interactional spaces and can improve the level of people's attraction toward public libraries.

2 THEORETICAL FRAMEWORK

2.1 Social Sustainability and Its Role on Sociability

Sustainable design is a sort of a scheme that aims to satisfy today's requirements without sacrificing the resources for future generations [9]. Social sustainability captures the human dimension of the sustainability discourse and accentuates the people and communities [10]. In other words, social sustainability is the ability of a society or an individual to cope with problems in a way that provides both their needs and the subsequent generations [11]. Therefore, social sustainability is a human and social discourse that investigates the human lifestyle and its effects on social interactions in the course of time. However, there is a consensus among the researchers that the social dimension of sustainable development has been severely neglected in its trinary facets [12].

Rapoport introduces urban space as an urban environment that includes a set of communications and interactions [13]. Sociability in a public space depends on promoting social interactions [14], attracting individuals and

groups [15], easy accessibility [16], social security [17], creating a mental image and legibility [18] and creating a lively & dynamic atmosphere [2]. Sociability in public spaces is based on the people's requirement to sense social belongings and interact with each other; and this will be possible in a supportive social space along with providing physiological comfort [19], claim of the realm, sense of ownership and social justice within the space [3].

If the social needs of people are balanced with the feeling of individual independence derived from privacy, then, social relations become easier. Physical privacy is the pre-requisite

for most social behaviors; in an environment in which physical secrecy exists, a wider range of personal choices is created [2]. That is precisely why people stay in a good place for a longer period than they really need - because they actually enjoy being there [4]. Therefore, in order to answer the questions and hypotheses of this research, and evaluate the effective factors on social interactions in the design of public libraries, various definitions of this variable have been considered from the viewpoint of the experts in this field (Tab. 1).

Table 1 Definition of Sociability from the Viewpoint of Experts

Theorist	Definition of Sociability	Keywords
Kevin Lynch	He considers legibility as one of the crucial factors affecting the sociability of an urban setting and defines it as recognizing the components of a city in an integrated framework in our minds [18].	Legibility, Mental Image
Bill Hillier	He identifies spatial configuration as the most important feature of sociability and declares that the intelligibility and permeability of a milieu have an indispensable role on attracting people [20].	Spatial Configuration, Intelligibility, Permeability
Jan Gehl	In defining urban sociability, he puts emphasis on the inviting sense of the space more than all its other features and considers it as an important factor in the overall attractiveness of the city [4].	An Inviting Space
Irwin Altman	He declares that the factors such as place attachment and sense of identity can be deemed as crucial factors on the creation of an unanimous community [21].	Place Attachment, Sense of Identity
Jon Lang	He describes social spaces as welcoming places and believes that such spaces are environments that can improve the human experience and that also have a human scale [19].	Welcoming Places, Human Scale
Robert Gifford	He remarks that the factors such as cognitive maps, territoriality, and sense of place are considered as effective factors on human behavior in public spaces [22].	Cognitive Maps, Territoriality, SOP
Lawrence Halprin	He considers spaces that allow citizens to choose freely with a great deal of diversity as societal spaces, and believes that these spaces give the city a special quality and personality [23].	A Great Deal of Diversity,
Paul Zucker	He names social spaces as elements that make the society in the true sense of community rather than the mere aggregation of individuals [24].	True Sense of Community

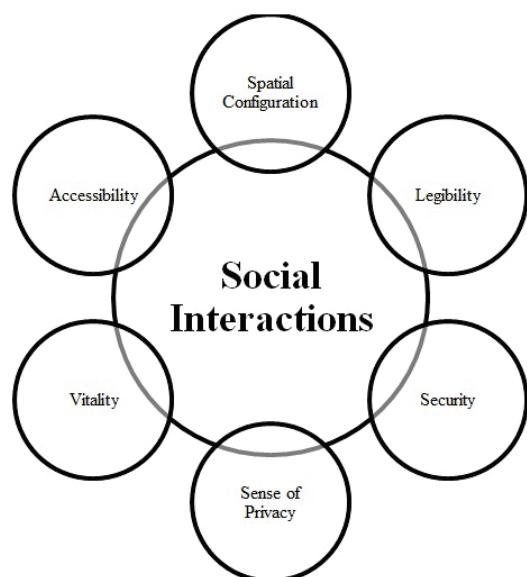


Figure 1 Factors Affecting Social Interactions in Public Spaces

2.2 Social Interactions

Social interaction means establishing a relationship between two or more people that leads to a reaction among them, and this kind of reaction is cognizant to both parties [25]. Therefore, meaningless relationships do not go under this definition [26]. According to Jan Gehl [4], three types of activities have been identified in public spaces and they are the following: necessary activities, optional activities, and social activities. Among them, social activities mainly refer

to the interaction that people engage in, such as playing with others, greeting others, and talking to others. Even passive contacts, such as eye contact, watching events, and listening to others, are considered to be social activities [27].

In his book, Humphrey Osmond uses the terms "Sociopetal" and "Sociofugal", which express the qualities of space that bring people together or separate them from one another [2]. In the poor quality areas of the city, it is only possible to find necessary activities; in other words, people only do the work that they are required to do. In high quality urban areas, not only are the essential activities done in proper conditions, but also, many recreational and societal activities are done in a good way [4]. According to the previous study literature on the assessment of the factors affecting socialization in public spaces and from the viewpoint of experts and theoreticians, six factors have been identified as influential items in order to promote social interactions in the design of public spaces (Fig. 1).

3 CASE STUDIES

Rasht is one of the major metropolises in Iran, the capital of the Gilan Province in northern Iran and it is recognized as the third most visited touristic city in Iran. The historical date of Rasht is likely to go back to the pre-Islamic period and at least the Sassanid era [28]. For many years, the Municipality Square has been the heart of Rasht and a place at which critical activities and traditional events take place. It is located in the central part of the city and near the main bazaar and the Green Square (another historical square in Rasht) and it houses many cultural and administrative buildings [25]. In

this research, the intention is to scrutinize two critical libraries in Rasht, named the **Rasht National Library** and the **Emam Hasan Mojtaba Library**.

The Rasht National Library is located in the central part of this city and it is adjacent to the Municipality Square. Based on the documents and evidence, its construction began in 1927 on a site granted by the former mayor of Rasht to the population community of the publishing house for the construction of a library. The construction of the building was carried out simultaneously with the construction of a series of administrative and public buildings in the north of Iran and in the First Pahlavi era, which is seen as a milestone for the formation of the city's historical texture (Fig. 2). The Rasht National Library is the first national library in Iran and one of the oldest public libraries independent from

governmental institutions. In this regard, due to the historical value of the building and its popularity among citizens, it has been chosen as a case study in this research. The library's total number of members is approximately 20,000 and on average, about 1,500 people use this library each day [29].

Another studied case is located in the Green Square of Rasht, which is 400 meters away from the National Library. The Emam Hasan Mojtaba Library was constructed in 1968, in the Second Pahlavi era, and is seen as another important public library in Rasht. The Green Square was designed based on the paradigms of the Persian Gardens and its library plays the role of a pavilion on it and its architecture is based on the vernacular architecture of Rasht (Fig. 3). Therefore, the intention was to assess these two case studies in order to generalize the subject matter.



Figure 2 Location of the National Library of Rasht, Iran

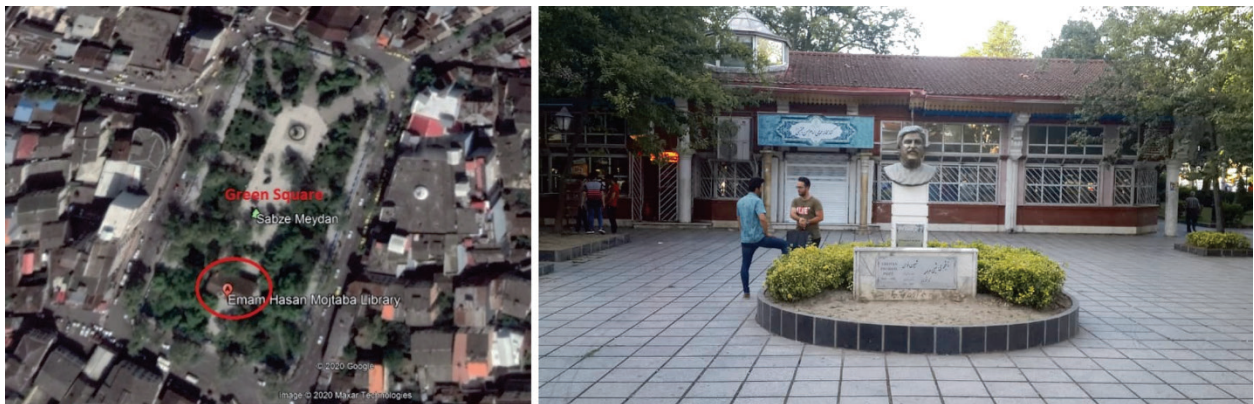


Figure 3 Location of the Emam Hasan Mojtaba Library of Rasht, Iran

4 RESEARCH METHODOLOGY

The research method has been applied quantitatively. In the first section, the library documents have been reviewed and through this, the theoretical principles of library design have been developed. In order to obtain the appropriate information from the existing conditions, field methods and taking notes have also been used in order to obtain the objectives of this research. Moreover, according to the questions elaborated in this research, by using the Space-Syntax methodology, the relationship between all spaces in the National Library of Rasht have been analyzed and the results have been presented as mathematical and graphical

parameters – with a descriptive-inferential analysis. The method for gathering data is using library resources (papers, books, journals and theses) and the research data have been evaluated by using scientific methods and simulations.

Furthermore, the **UCL Depthmap 10** software has been used to assess the social logic of the spatial configuration of the building in order to understand its legibility and syntactical logic. Therefore, after drawing the architectural floor plan of the case studies in the **AutoCAD** software, the file was imported to the **Depthmap** software. By using the variables and components affecting social interactions, the spaces within the Rasht National Library were then analyzed and the output was extracted in the form of graphs & digital

numbers. Accordingly, the principles derived from the research for designing a library with an approach toward social interaction were presented.

The Space-Syntax theory was introduced in 1976 by Professor Bill Hillier and his colleagues at the University College London. It is founded on the concept that the spatial configuration of the built environment determines how the space is experienced, explored and comprehended [20, 30]. By analyzing a series of spatial characteristics, Space-Syntax helps designers understand the role of spatial configurations in shaping the patterns of human behavior and it helps them estimate the social effects of their designs. This analysis model enables us to study the causal correspondence between the architectural forms and its impact on promulgating social interactions among people [31]. Numerous studies in the field of architecture have validated this method [8, 32, 33].

The variables used in this software in order to evaluate human behavioral patterns and their social impact estimation are Connectivity, Intelligibility, Mean Depth and Choice. In order to equate them with the components that affect social interactions, it can be argued that the functional concept of Connectivity is accessibility. Furthermore, the functional concept of Intelligibility is defined by the correlation between Integration and Connectivity, which can be considered tantamount to legibility. In order to equivalent the privacy component, the Mean Depth variable was used, and it is based on the separation of a particular space from the overall spatial configuration. Moreover, the Choice variable was used in order to measure the level of the security of the space.

5 RESULTS

5.1 Analysis of the Rasht National Library using Space Syntax

The results of the analysis for the interior space of the Rasht National Library using the Depthmap software in the test of the axial line indicate that the level of accessibility and integration on the second floor is more than the level of accessibility and integration on the first floor. According to the analysis carried out by the Space-Syntax methodology, the integration level of the first floor is 9.00, whereas the integration level of the second floor is 39.73. On the other hand, the level of connectivity on the first floor is 22, but on the second floor, the range of connectivity is 99 (Tab. 2).

Additionally, the results obtained from the analysis of the Emam Hasan Mojtaba Library reveal that the level of integration on the second floor is higher than on the first floor. Accordingly, the quantitative amount of integration on the first floor is 4.43. However, the level of integration on the second floor of this library is 8.87. Moreover, the quantitative range of connectivity on the first floor is 8, while the same range on the second floor is equivalent to 7. The data elucidate that despite better accessibility on the first floor, the sociability process on the second floor is much higher (Tab. 2). The analysis is visually denoted into a chromatic scale so that the integrated spaces are presented in red, while the segregated spaces are presented in blue.

Additionally, the results of the correlation test based on the correlation between integration and connectivity show that legibility on the first floor is higher than on the second floor. In other words, the first floor of the Rasht National Library has a higher degree of intelligibility compared to its second floor. Moreover, the value of R^2 for the first floor is 0.83 and 0.79 for the second floor.

Likewise, the findings obtained from the correlation between integration and connectivity illustrate that the intelligibility level on the first floor is higher than on the second floor. Quantitative data calculations indicate that the amount of R^2 for the first floor is 0.89, while the R^2 quantity for the second floor is 0.81. As a result, it can be interpreted that spaces which have an open-configured characteristic in their formation will present better integration but less legibility.

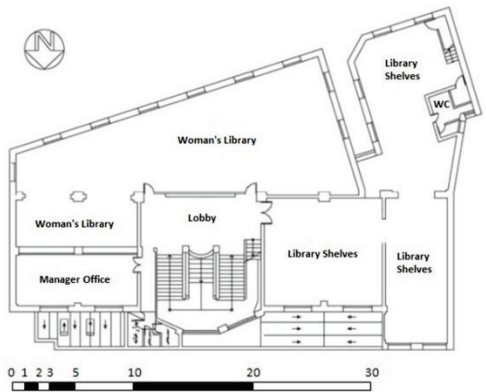
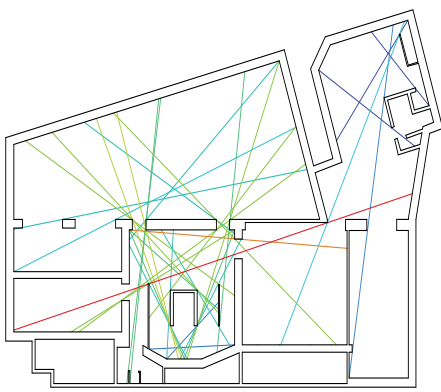
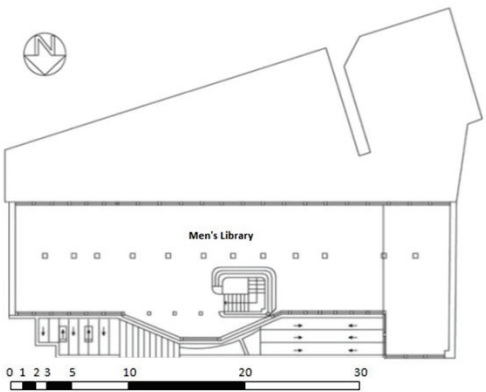
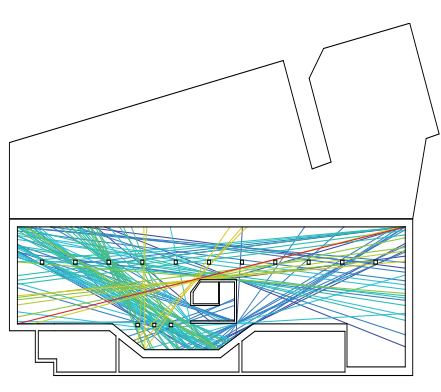
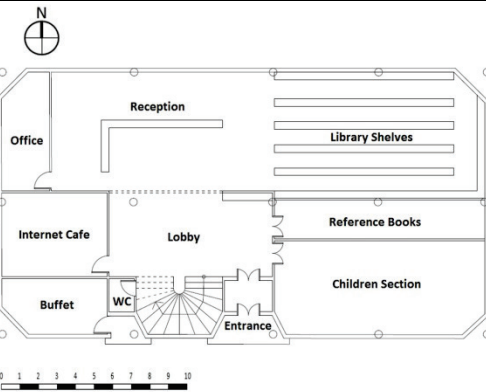
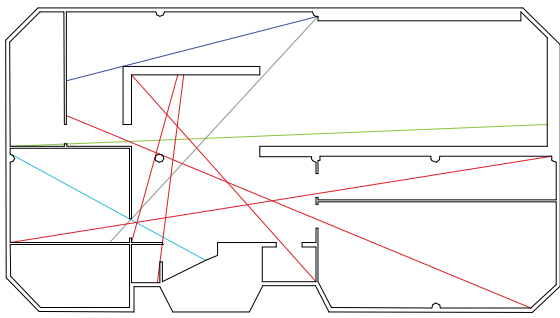
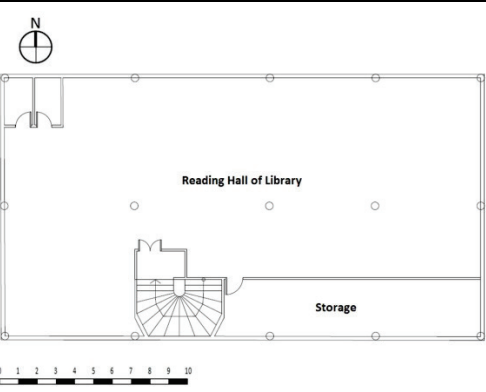
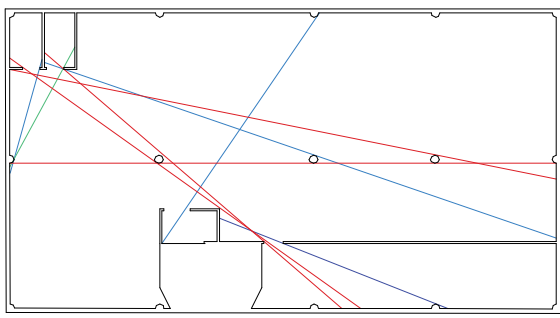
In terms of other variables affecting social interactions, the same can also be mentioned regarding components such as security, accessibility and privacy. Therefore, analyzing the variables affecting these components with the syntactical analysis in the Rasht National Library suggests that the spaces such as the Manager's Office and Library Shelves, with the choice value of 182, are more secure than other spaces. Furthermore, the assessment of the Accessibility variable indicates that the Manager's Office and Library Shelves adjacent to the staircase, with a connectivity rate of 22, have the best access on the first floor plan of the library. Moreover, in relation to the sense of privacy in the Rasht National Library, it should be noted that the Library Shelves and the toilet, located on the southwest side of the library and with the mean depth value of 2.74, have the highest spatial depth. This means that these spaces provide the highest sense of privacy and confidentiality in the Rasht National Library (Fig. 4).

The results obtained from the behavioral patterns of users in the spaces of the Rasht National Library by using the visibility graph analysis indicate that the Reading Hall of the library space, with an Isovist Area of 269.66, has the greatest effect on the behavioral pattern of users among the spaces of the Rasht National Library. After that, the Lobby space, with an Isovist Area of 172.94, has the greatest effect on the behavioral patterns of users. Accordingly, the space of the Main Reading Hall has more visibility and scope of view, which is visible from a particular point. Moreover, the analysis of the VGA test in the Emam Hasan Library has indicated that the Lobby space, with an Isovist range of 154.86, has the greatest effect on the behavioral patterns of the occupants (Tab. 4). As a result, simulation studies reveal that identifying spaces such as lobbies in the central organization of public places may have an indispensable role on interactional activities.

By analyzing the findings regarding the effective factors on social interactions in the studied libraries, it can be concluded that the rate of spatial integration will increase in the architectural spaces which have been designed with open plans. On the other hand, factors such as depth and the degree of privacy are also decremented. As it was mentioned in the analysis of the Space-Syntax methodology regarding the second floor plan of the library which resembles an open-

configured space, the library is equally well-versed in terms of spatial integrity, and reducing the rate of mean depth has made it livelier.

Table 2 Axial Line Test of the Studied Libraries

Plan	Axial Line	Floor
		1 st floor of the Rasht National Library
		2 nd floor of the Rasht National Library
		1 st floor of the Hasan Mojtaba Library of Rasht
		2 nd floor of the Emam Hasan Mojtaba Library of Rasht

There should also be specific propensity toward the creation of spaces with more depth in order to meet the requirements of the people's sense of privacy. In this way, security is also relative and influential on the factors such as vitality. According to the analysis, the range of integration in

high-depth spaces is lower than that of low-depth spaces. In other words, by increasing the degree of integration, the mean depth decreases, which is the conspicuous reciprocal synergy.

Table 3 Intelligibility Level of the Studied Libraries

First Floor	Second Floor	Plan
		National Library of Rasht
		Emam Hasan Mojtaba Library of Rasht

Table 4 Visibility Graph Analysis of the Studied Cases

First Floor	Second Floor	Plan
		Rasht National Library
		Emam Hasan Mojtaba Library

6 CONCLUSION

The objective of this study was to evaluate the factors affecting social interactions in the design of public libraries. Nowadays, the confinement of libraries in administrative buildings with a conventional and formal atmosphere and the

complete separation of such buildings from the daily life of people has prevented constructive interactions from happening between people, and in the libraries, which has greatly diminished the number of people visiting them in Iran. One of the reasons for the lack of interest in public libraries in Iran is the lack of attention of architects and

employers to the attractiveness of library spaces in their designs and planning phases. This makes it increasingly obvious that it is necessary to evaluate the factors affecting social interactions in the design of public libraries in order to expand the culture of reading within the society.

The results of the analysis regarding the interior space of the Rasht National Library by using Space-Syntax in the test of the axial line indicate that the level of spatial integration on the second floor is more than the integration level on the first floor. However, the results of the correlation test between integration and connectivity reveal that the first

floors of the studied cases have a higher level of intelligibility compared to the second floors. Moreover, the results from the Space-Syntax analysis in the Rasht National Library illustrate that the spaces such as the Manager's Office and Library Shelves are more secure than other spaces. Furthermore, spaces such as the Manager's Office and the Library Shelves, which are adjacent to the staircase, have the best accessibility on the first floor plan of the library. However, in the Emam Hasan Mojtaba Library, the Lobby space has the best sociability, accessibility and security potential among all other spaces.

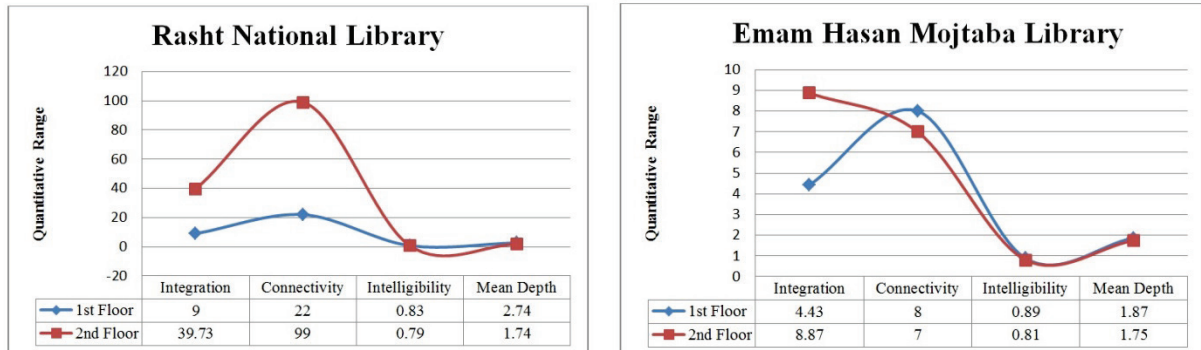


Figure 4 Quantitative Data Obtained from Syntactical Analysis of the Studied Cases

Based on the Space-Syntax analysis for the studied libraries, the following results can be considered for acquiring more sociable spaces in library designs:

- 1 – Plans that are compact and have less longitudinal and latitude stretches can be more legible.
- 2 – The location of the main entrance is better when it is near the central circulation space and in front of the visitor's point of vision.
- 3 – Paying attention to the private and public hierarchy that have been tailored to the function can lead to more legibility and can create a sense of privacy.
- 4 – The use of open-configured spaces that can provide convenient movement and visual communication can enhance the sociability and security of architectural spaces.
- 5 – The use of long or narrow corridors reduces the movement and visual accessibility and creates confusion among the users who are present within the space.
- 6 – Using furniture that leads to the creation of personal territory has a positive impact on the efficiency and sociability of libraries.

In general, it can be concluded that in the architectural spaces that have been designed with open-configured plans, the rate of spatial integrity and sociability will increase. On the other hand, the factors such as depth and the degree of privacy will also be diminished. There is also a particular need for the creation of spatial depth in order to meet people's privacy requirements. In this regard, security is also relative and influential on the factors such as vitality. Therefore, in designing a public library with an approach toward social interaction, there should be a variety of open and closed spaces available in the plan that would allow users to choose the space they optionally want and in which they would enjoy in their own presence by choosing their

own activities. Furthermore, according to the research findings, it can be concluded that the use of factors which are effective on social interactions in the design of public libraries can lead to the socialization of these spaces and their growing popularity among citizens regarding the culture of book reading. Finally, and in response to the hypothesis of this research, it can be declared that the spatial configuration of public spaces has an undeniable and indispensable role on interactional spaces. However, despite the positive effect of an open-configured plan on the social logic of spaces, it may also decrement the level of spatial legibility in these spaces in comparison to center-organized plans.

7 REFERENCES

- [1] Talen, E. (2007). Design for Diversity: Evaluating the Context of Socially Mixed Neighbourhoods. *Journal of Urban Design*, 11(1), 1-32. <https://doi.org/10.1080/13574800500490588>
- [2] Lang, J. (1987). *Creating architectural theory: The role of the behavioral sciences in environmental design*. New York: Van Nostrand Reinhold.
- [3] Alexander, C., Ishikawa, S., & Silverstein, M. (1977). *A Pattern Language: Towns, Buildings, Construction* (Center for Environmental Structure Series). Oxford, Oxford University Press.
- [4] Gehl, J. (1987). *Life between Buildings: Using Public Space*. New York: Island Press.
- [5] Bechtel, R. & Churchman, A. (2002). *Handbook of Environmental Psychology*. New York: John Wiley & Sons.
- [6] Thompson, J., History of Principles of Librarianship. 1977, London: Clive Bingley Press.
- [7] Moghadam, C. R. & Askarizad, R. (2019). *English for Architecture Students*. Rasht: Kadusan.

- [8] Askarizad, R. & Safari, H. (2020). Investigating the role of semi-open spaces on the sociability of public libraries using space syntax (Case Studies: Sunrise Mountain and Desert Broom Libraries, Arizona, USA). *Ain Shams Engineering Journal*, 11(1), 253-264.
<https://doi.org/10.1016/j.asej.2019.09.007>
- [9] Sassi, P. (2006). *Strategies for Sustainable Architecture*. London: Taylor & Francis.
<https://doi.org/10.4324/9780203480106>
- [10] Dempsey, N., et al. (2011). The social dimension of sustainable development: Defining urban social sustainability. *Sustainable Development*, 19(5), 289-300.
<https://doi.org/10.1002/sd.417>
- [11] Magis, K. (2010). Community Resilience: An Indicator of Social Sustainability. *Society & Natural Resources*, 23(5), 401-416. <https://doi.org/10.1080/08941920903305674>
- [12] Colantonio, A. (2007). *Social Sustainability, An Exploratory Analysis of its definition Assessment Methods, Metrics and Tools*. Oxford: The Oxford Institute for Sustainable Development.
- [13] Rapoport, A. (1984). *Culture & the Urban Order: The City in Cultural Context*. Boston: Allen and Unwin.
- [14] Sennette, R. (1974). *The Fall of Public Man*. New York: Reissue edition.
- [15] Whyte, W. (1980). *The Social Life of Small Urban Spaces*. Maryland: Tuxedo.
- [16] Carr, S., et al. (1992). *Public Space*. Massachusetts: Cambridge University Press.
- [17] Marcus, C. & Francis, C. (1998). *People Places: Design Guide Lines for Urban Open Spaces*. New York: Van Nostrand Reinhold.
- [18] Lynch, K. (1960). *The Image of the City*. Massachusetts: The M. I. T. press.
- [19] Lang, J. (1994). *Urban Design, American Experience*. New York: Van Nostrand Reinhold.
- [20] Hillier, B. & Hanson, J. (1984). *The Social Logic of Space*. Cambridge: Cambridge University Press.
<https://doi.org/10.1017/CBO9780511597237>
- [21] Altman, I. & Low, S. M. (2012). *Place Attachment (Human Behavior and Environment (12))*. New York: Springer.
- [22] Gifford, R. (1987). *Environmental Psychology: Principles and Practice*. Boston: Allyn and Bacon.
- [23] Halprin, L. (1972). *Cities*. Massachusetts: The MIT Press.
- [24] Zucker, P. (1970). *Town and Square, from the Agora to the Village Green*. Massachusetts: the MIT Press.
- [25] Askarizad, R. & Safari, H. (2020). The influence of social interactions on the behavioral patterns of the people in urban spaces (case study: The pedestrian zone of Rasht Municipality Square, Iran). *Cities*, 101, p. 102687.
<https://doi.org/10.1016/j.cities.2020.102687>
- [26] Argyle, M. (2009). *Social Interaction*. New Jersey: Aldine Transaction.
- [27] Huang, S. C. L. (2006). A Study of Outdoor Interactional Spaces in High-rise Housing. *Journal of Landscape and Urban Planning*, 78(3), 193-204.
<https://doi.org/10.1016/j.landurbplan.2005.07.008>
- [28] Askarizad, R., Safari, H., & Pourimanparast, M. (2017). The influence of organizing historical textures on citizenry satisfaction in the old texture neighbourhoods of Rasht. *Emerging Science Journal*, 1(3), 118-128.
<https://doi.org/10.28991/ijse-01114>
- [29] Guilan, C. H. O. O. (2010). *Rasht National Library*. Publishing of the Heritage and Tourism Industries Organization: Rasht.
- [30] Hillier, B., Leaman, A., & Stansall, P. (1976). Space Syntax. *Environment and Planning B: Urban Analytical and City Science*, 3(2), 147-185. <https://doi.org/10.1068/b030147>
- [31] Askarizad, R. (2017). Influence of Socio-Cultural Factors on the Formation of Architectural Spaces (Case Study: Historical Residential Houses in Iran). *Creative City Design*, 1(3), 44-54.
- [32] Asif, N., et al. (2018). Reflection of cultural practices on syntactical values: An introduction to the application of space syntax to vernacular Malay architecture. *Frontiers of Architectural Research*, 7(4), 521-529.
<https://doi.org/10.1016/j.foar.2018.08.005>
- [33] Jeong, S. K. & Ban, Y.U. (2011). Computational algorithms to evaluate design solutions using Space Syntax. *Computer-Aided Design*, 43(6), 664-676.
<https://doi.org/10.1016/j.cad.2011.02.011>

Author's contact:

Reza Askarizad
Department of Architecture,
Rasht Branch, ACECR, Rasht, Iran
reza.askarizad@gmail.com

Reference Breast Phantoms for Low-Cost Microwave Imaging

Emine Avşar Aydın*, Selin Yabaci Karaoğlu

Abstract: Microwave imaging provides an alternative method for breast cancer screening and the diagnosis of cerebrovascular accidents. Before a surgical operation, the performance of microwave imaging systems should be evaluated on anatomically detailed anthropomorphic phantoms. This paper puts forward the advances in the development of breast phantoms based on 3D printing structures filled with liquid solutions that mimic biological tissues in terms of complex permittivity in a wide microwave frequency band. In this paper, four different experimental scenarios were created, and measurements were performed, and although there are many vector network analyzers on the market, the miniVNA used in this study has been shown to have potential in many biomedical applications such as portable computer-based breast cancer detection studies. We especially investigated the reproducibility of a particular mixture and the ability of some mixes to mimic various breast tissues. Afterwards, the images similar to the experimentally created scenarios were obtained by implementing the inverse radon transform to the obtained data.

Keywords: cancer; conductivity; microwave imaging; permittivity; phantoms

1 INTRODUCTION

Breast cancer ranks second among female deaths all over the world. Breast cancer incidence is increasing in the United States and European Union countries [1].

Mammography facilitates the treatment of cancer by non-invasive techniques for the detection of small breast lesions [2, 3]. Recently, more new treatments as opposed to traditional surgery have been investigated to meet these demands. Microwave imaging technology for breast cancer detection has attracted much attention. The physical basis for the detection of breast cancer with microwave imaging is the difference between the dielectric properties of normal and malignant breast tissues. The significant difference between the dielectric properties of the normal and malignant breast tissue in microwave frequencies, the number of missed-detections and, false-positives are meagre, and this is considered to be the most important motivation for developing a microwave imaging technique for breast cancer detection. The contrast between the estimated malign-to-normal breast tissue is between 2:1 and 10:1, depending on the healthy tissue density. Another advantage of the microwave imaging technique is that the respective tissue properties are shown in a three-dimensional (3-D) volumetric map. Furthermore, microwave imaging is a non-invasive and even potentially a low-cost alternative to breast cancer imaging. For all the reasons mentioned above, microwave breast imaging has the potential to overcome some of the limitations of traditional breast cancer screening systems.

One of the most critical factors in the effective treatment of breast cancer is early diagnosis [4-6]. Early diagnosis is crucial both in increasing the success rate of treatment and decreasing the treatment costs. Hence, breast imaging is essential for early diagnosis and effective treatment.

There are many different techniques for breast imaging: mammography, ultrasound and magnetic resonance imaging [4-10]. The most common method used in breast imaging is mammography imaging, which provides a 2D image of the compressed breast. However, mammography may be inadequate in early and accurate diagnosis due to the

constraints caused by the overlapping of the displayed tissues.

Numerical breast microwave imaging is a new and increasingly widespread imaging technique that can display a high-resolution 3D imaging of the breast by using a limited number of 2D scans obtained with a limited scanning angle. This feature can be displayed in slices of the breast image obtained from 3D and it allows for a more detailed examination with in-depth information.

Numerical breast microwave imaging reduces the problems of traditional mammography imaging, such as the over-tightening of the breast during imaging and the overlapping of tissues, and the inability to overlook abnormal structures in the breast, whereas more dose problems arise [13].

The amount of the dose should be reduced so that it is an X-ray based imaging and that the X-ray can be used as a routine screening method due to the ionizing radiation effect. For this purpose, two-way studies have been carried out, including studies on hardware improvements and studies on image retraction techniques.

It is possible to obtain low dose images with developing a detector technology [1-15]. On the other hand, dose reduction is possible with compressed detection-based back-scattering techniques using a small number of projections. The use of the digital breast microwave imaging technique in breast imaging will increase in proportion to the decreasing dose amount.

Imaging techniques should have high sensitivity and sensitivity. However, the ease of use, low interference, high spatial resolution for sharp interpretation, low cost, etc. are sought after.

In recent years, an approach has been introduced that allows the imaging of the breast with a non-linear regression algorithm using a microwave-based imaging and electromagnetic radiation at a frequency of around 1 GHz [11-14].

Microwave applications [1-15] have been used to determine the dielectric properties of the living tissues such as fat, muscle, etc. These waves penetrating the human body

are scattered depending on the electrical properties of the displayed tissues. It is possible to map the electrical properties of the displayed tissues by processing the scattered waves by using a suitable model.

Electrical permittivity and conductivity are two critical parameters that determine the diffusion of microwaves in materials [15]. Different biological tissues in the microwave frequency range cause different spreading behavior. For example, fat and skin have low permittivity values, while blood and cancerous tissues have higher values. If the responses of the target tissues to the microwave signals are processed together in different angles, they allow the internal structure of the tissues to be visualized.

The back-scattering operation in Microwave Imaging is the process of solving the inverse problem by using the data collected by the antenna and scattered from the target. A cost function is defined to perform the back-scattering operation. The basic idea in the back-scattering algorithm is to update the displayed dielectric properties of the displayed target to minimize the difference of the calculated model.

Since microwave breast imaging is not an ionizing radiation hazard, there is a chance of being an efficient and reliable cancer detection method. In this study, four different experimental scenarios were created, and measurements were taken. Although there are many vector network analyzers on the market, miniVNA used in this study has been found to have a great potential in many biomedical applications, such as breast cancer detection studies, because of being more affordable, portable and computer-based.

However, many experimental systems and imaging algorithms have been studied, and promising results have already been obtained, using both radar-based and inverse scattering reconstruction algorithms. On the other hand, before inversion algorithms can be used in clinical studies, they need to be tested against the experimental data collected in controlled configurations on reference phantoms. Although the latter must be close to breast tissues in terms of dielectric properties, simple structures benefit instability over time and reproducibility over more complex structures.

2 HOMOGENOUS PHANTOMS PRODUCTION

To imitate a real human breast and tumor tissues, four different mixtures were produced in the form of "water-oil in gelatin" dispersions. Phantoms were built to simulate the real breast skin, fat, gland and tumor tissues in their dielectric properties. This method was chosen because of the simple style of the fabrication and the ease when obtaining the materials, stable mechanical properties and a long storage time [16, 17]. As for the chemicals, p-toluic acid, n-propanol and formaldehyde were purchased from Merck (Darmstadt, Germany). For deionized water, Elga Purelab Option-Q (UK) was used. 200 bloom gelatin (Tito, Turkey) and sunflower oil (Komili, Turkey) were purchased from the local market. Persil liquid detergent was used (Henkel, Germany) for the analysis. The specific amounts of the chemicals used in the phantom fabrication can be seen in Tab. 1. The method was adapted from Lazebnik, Madsen [18]. The production

method of the phantom is summarized as a flow diagram in Fig. 1.

Table 1 The specific amounts of the chemicals used in the phantom's fabrication

Material	Quantity			
	Fat	Gland	Skin	Tumor
p-toluic acid (g)	0.133	0.253	0.294	0.346
n-propanol (mL)	6.96	12.71	28.69	17
deionized water (mL)	132.7	241.9	279.5	328
200 Bloom gelatin (g)	24.32	43.27	50.02	58.67
Formaldehyde *(g)	1.53	2.74	3.33	3.72
oil (mL)	269.6	141.5	98.6	38.4
Detergent (mL)	12	6.79	5.86	2

*37% by weight

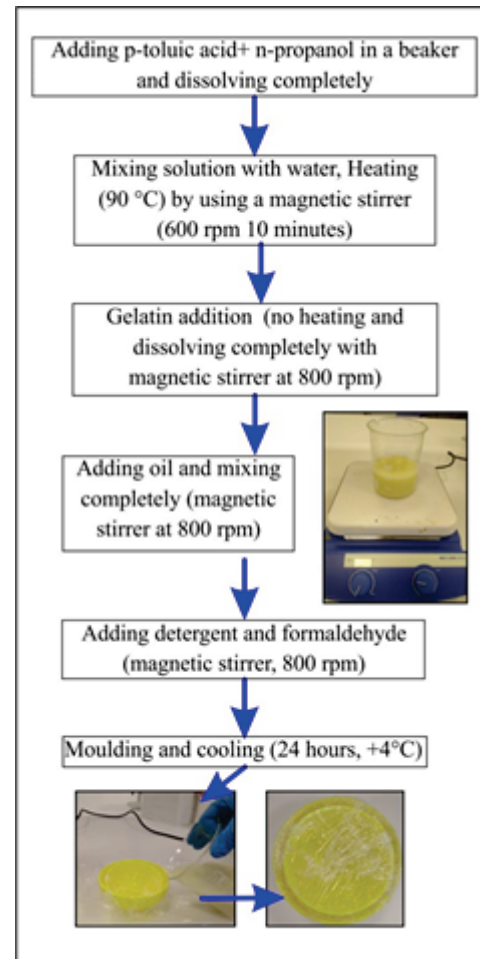


Figure 1 A summarizing flow diagram of the phantom fabrication

Firstly, p-toluic acid and n-propanol dissolved completely. The water part was then added with heating and stirring (by a magnetic stirrer- 90 °C, 600 rpm). After 10 minutes, the heating was stopped, and gelatin was added to the mixture to create a gel matrix with continuous stirring (800 rpm). After gelatin dissolved completely, the oil part was added into the matrix system, again with continuous stirring (800 rpm). At the end, detergent was added to emulsify the water and oil part and formaldehyde was added to preserve the system, homogenously. The mixture ("water-oil in gelatin" system) was molded and cooled in a refrigerator (+4 °C, 24 hours) to trap water and oil in the

gelatin matrix system and to solidify. Fig. 2 shows the last shape of the molded phantom. Tumor production was done in four different sizes such as 0.5, 1.0, 1.5 and 2 cm spherically, and it can be seen in Figure 3. For the analysis, these tumors were placed both in the center and sides of the breast phantom. Tissues should properly be stored without any air or moisture exposure. This situation can change the dielectric properties of the system. When they are closed hermetically by a plastic wrap or a container, the tissues will retain their structure for a longer time.

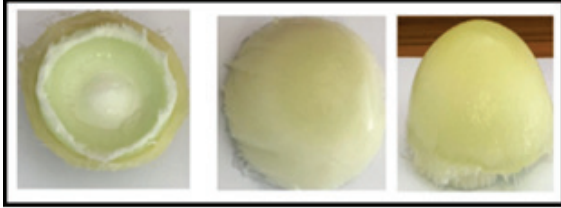


Figure 2 Breast phantom layers and the whole state

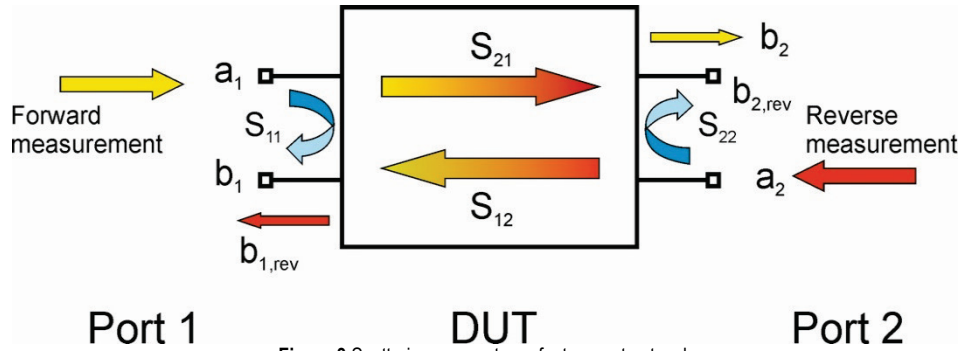


Figure 3 Scattering parameters of a two-port network

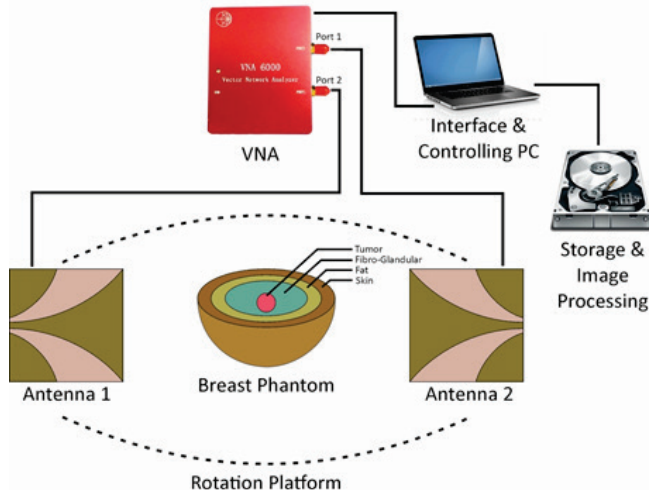


Figure 4 Microwave imaging system block schema

As shown in Fig. 5, a breast phantom of 12 cm in diameter was placed between two microstrip antennas, where one of them is a receiver, and the other is a transmitter. Tumors of different sizes were placed into the center, into the right of the center and into the left of the center of the fibro-

3 BREAST PHANTOMS' MEASUREMENT

The VNA contains two ports: one is used to send the signal, whereas the other receives the signal simultaneously. As shown in Fig. 3, two types of measurements are made by the VNA system: the forward and backward measurement [19].

In forward measurement, the signals are separated from port 1, and the signals are separated from port 2 in the inverse measurement [19]. If signals are emitted from a port and reflected back to the same port, this is called the reflection measurement. Otherwise, if the signal is output from a port and forwarded to the other port, it is considered as a transmission measurement.

S-parameters provide complete information about the linear behavior of RF and microwave components and are independent of the properties of the VNA [19]. By courtesy of VNA calibration, the device's defects are entirely removed from the measurement. Thereupon, the S-parameters are a highly delicate presentation of how the linear behavior of the tested component describes how it behaves and how it interacts with other devices when cascaded.

glandular layer of the breast phantom, respectively. Experiments were performed by turning off two antennas mutually. The microwave imaging system and experimental setup were given in Fig. 4 and Fig. 5.

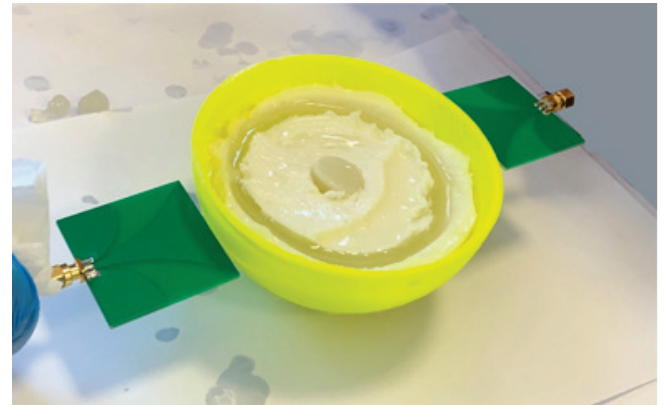


Figure 5 Experimental setup

The websites of major VNA producers such as Agilent and Rohde & Schwarz [20] show that a wide range of VNA equipment is available. For the most advanced users, VNAs

can provide high-precision signal measurements over a wide frequency range. This may confirm the use of GPRs and distinct areas, which often supply significant research results for a soil survey. The complexity of the equipment for more speculative research and field monitoring generally works at lower costs; some VNAs are now available as compact units suitable for field use.

Furthermore, many affordable portable PC-based VNAs are much cheaper on the market. The properties are given in Tab. 2. As a result, this device has the potential to be used in biomedical applications such as breast microwave imaging [20] and body bio-impedance measurement [21].

Table 2 The specifications of the miniVNA Tiny

Parameter	Value
Frequency range	1 MHz to 3 GHz
Ports	2 ports
Output power	-6 dBm at 500 MHz
Dynamic range	Up to 70 dB at 500 MHz
Connectors	2×SMA
Power consumption	370 mA at 5 V (USB)
Weight	70 g
Size	66×66×28 mm
Software	vna/J for Windows, Linux, and MacOS
Impedance range (Z)	1 to 1000 ohm

In the experimental setup, we tested the performance of the antenna and the miniVNA to detect tumor cells in the breast. The frequency range of the miniVNA is between 100 MHz and 3 GHz, and the number of points is 636. The miniVNA is connected to a PC via a USB port, and data are taken for further processing. The transmitted parameters bound up with the entire path between the two antennas

where the tumor has passed twice during the entire rotation. The reflected signals often represent shallow depths below the skin layer because the signals projected from the other side of the phantom must move twice through the phantom and are significantly weakened. The reflected signals generally introduce shallow depths below the skin layer since signals reflected on the other side of the breast phantom must move twice from the phantom and are significantly weakened. Therefore, antennas with an exceptionally low loss of original return are ideal for detecting weakly reflected signals. The collected images were then processed, and the inner breast images were reconstructed. In this study, firstly the skin, fat and fibro-glandular layers were formed from the outer to the inner side in the form of a hemisphere. Then, tumor phantoms were formed in four different diameters and placed in three different locations in the fibro-glandular layer and measurements were taken. Firstly, the smallest tumor was placed into the center of the breast, then it was placed 2 cm from the right and 2 cm from the left of the center of the breast, respectively and measurements were taken with the help of the miniVNA. Afterwards, this step was repeated for other tumors as well. Furthermore, after the image was obtained in an experimental study without a tumor in the tissue center, a second experiment was created for the tissue containing a tumor in the center in order to compare the performance, and the same procedure was repeated. Next, inverse radon transform [22] was used to display the data obtained, and the results were successful. In the following figure (Fig. 6), the images show when there is no tumor (a), when the tumor is in the center of the breast (b), and when the tumor is 2 cm away from the center of the breast.

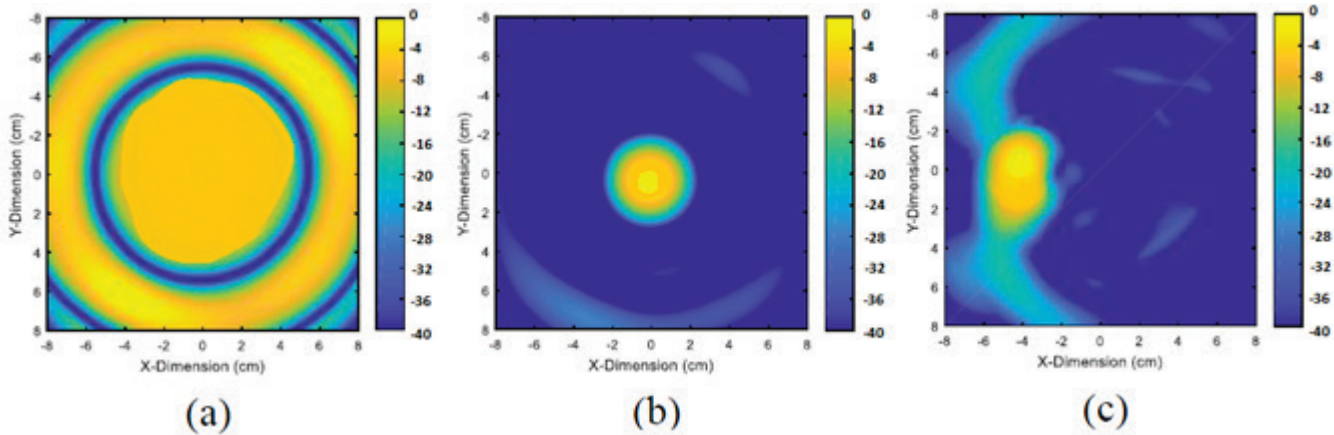


Figure 6 Images obtained by the inverse radon transform method (a) breast tissues without tumor, (b) when tumor is in the center of the breast (c) when tumor is 2 cm away from the center of the breast

4 CONCLUSION

In this study, the IRT (Inverse Radon Transform) method was used to reconstruct the appearance of a malignant tumor in the breast using the data obtained by experimental studies. Spherical tumors were obtained in four different diameters, and three different scenarios were established. The scenarios were as follows: measurements were taken by placing the first the smallest tumor at the center, then by placing it at a distance of 2 cm from the right of the center and then 2 cm

from the left of the center. The same steps were followed for all tumors. Throughout the experiment, the antennas were mutually rotated with specific steps. The experimental phantom was illuminated by using a miniVNA in the frequency domain. The resolution of the image was made higher by increasing the sample points. The images were successfully obtained, and the IRT algorithm performed well in detecting breast cancer with microwaves. Although there are many vector network analyzers on the market, the miniVNA used in this study, which is portable and computer-

based, has been shown to have potential in many biomedical applications such as breast cancer detection studies. Moreover, it can be seen that the IRT method is suitable for detecting breast cancer.

Acknowledgment

This research was partially supported by the Adana Alparslan Türkeş Science and Technology University Scientific Research Project Commission. Project Number: 18119003.

5 REFERENCES

- [1] Olivotto, I. A., Bancej, C., Goel, V., Snider, J., McAuley, R. G., Irvine, B., Kan, L., Mirsky, D., Sabine, M. J., & McGilly, R. (2001). Waiting times from abnormal breast screen to diagnosis in 7 Canadian provinces. *Canadian Medical Association or its licensors (CMAJ)*, 165(3), 277-283.
- [2] Fear, E. C., Li, X., Hagness, S. C., & Stuchly, M. A. (2002). Confocal microwave imaging for breast cancer detection: Localization of tumors in three dimensions. *IEEE Transactions on Biomedical Engineering*, 49(8), 812-822. <https://doi.org/10.1109/TBME.2002.800759>
- [3] Kurrant, D. J., Fear, E. C., & Westwick, D. T. (2008). Tumor response estimation in radar-based microwave breast cancer detection. *IEEE Transactions on Biomedical Engineering*, 55(12), 2801-2811. <https://doi.org/10.1109/TBME.2008.921164>
- [4] Servick, K. (2014). *Breast cancer: a world of differences*. American Association for the Advancement of Science. <https://doi.org/10.1126/science.343.6178.1452>
- [5] Kahar, M., Ray, A., Sarkar, D., & Sarkar, P. (2015). An UWB microstrip monopole antenna for breast tumor detection. *Microwave and Optical Technology Letters*, 57(1), 49-54. <https://doi.org/10.1002/mop.28773>
- [6] Siegel, R. L., Miller, K. D., & Jemal, A. (2019). Cancer statistics, 2019. *CA: A Cancer Journal for Clinicians*, 69(1), 7-34. <https://doi.org/10.3322/caac.21551>
- [7] Jacobsen, K. K., Abraham, L., Buist, D. S., Hubbard, R. A., O'Meara, E. S., Sprague, B. L., Kerlikowske, K., Vejborg, I., Von Euler-Chelpin, M., & Njor, S. H. (2015). Comparison of cumulative false-positive risk of screening mammography in the United States and Denmark. *Cancer Epidemiology*, 39(4), 656-663. <https://doi.org/10.1016/j.canep.2015.05.004>
- [8] Nikolova, N. K. (2011). Microwave imaging for breast cancer. *IEEE Microwave Magazine*, 12(7), 78-94. <https://doi.org/10.1109/MMM.2011.942702>
- [9] Irfan, N., Yagoub, M. C., & Hettak, K. (2012). Design of a microstrip-line-fed inset patch antenna for RFID Applications. *International Journal of Engineering and Technology*, 4(5), 558. <https://doi.org/10.7763/IJET.2012.V4.432>
- [10] Wang, L., Peng, H., & Ma, J. (2017). Microwave breast imaging techniques and measurement systems. *New Perspectives in Breast Imaging: IntechOpen*. Ed. A. Malik. <https://doi.org/10.5772/intechopen.69199>
- [11] Carr, K. L., Cevasco, P., Dunlea, P., & Shaeffer, J. (2000). Radiometric sensing: An adjuvant to mammography to determine breast biopsy. *IEEE MTT-S Int Microw Symp Dig*, 2(2), 929-932. <https://doi.org/10.1109/MWSYM.2000.863509>
- [12] Meaney, P. M., Fanning, M. W., Li, D., Poplack, S. P., & Paulsen, K. D. (2000). A clinical prototype for active microwave imaging of the breast. *IEEE Transactions on Microwave Theory and Techniques*, 48(11), 1841-1853. <https://doi.org/10.1109/22.883861>
- [13] Noghanian, S., Sabouni, A., & Pistorius, S. (2006). A numerical approach to microwave imaging based on genetic algorithm optimization. *Proc. SPIE 6177, Health Monitoring and Smart Nondestructive Evaluation of Structural and Biological Systems V*, 61771B (15 March 2006). <https://doi.org/10.1117/12.658572>
- [14] Fear, E. C., Meaney, P. M., & Stuchly, M. A. (2003). Microwaves for breast cancer detection? *IEEE Potentials*, 22(1), 12-18. <https://doi.org/10.1109/MP.2003.1180933>
- [15] Hancu, I., Roberts, J. C., Bulumulla, S., & Lee, S.-K. (2015). On conductivity, permittivity, apparent diffusion coefficient, and their usefulness as cancer markers at MRI frequencies. *Magnetic Resonance in Medicine*, 73(5), 2025-2029. <https://doi.org/10.1002/mrm.25309>
- [16] Porter, E., Fakhoury, J., Oprisor, R., Coates, M., & Popović, M. (2010). Improved tissue phantoms for experimental validation of microwave breast cancer detection. *Proceedings of the Fourth European Conference on Antennas and Propagation (EuCAP)*, 1-5.
- [17] Lan, S.-W., Weng, M.-H., Yang, R.-Y., Chang, S.-J., Chung, Y.-S., Yu, T.-C., & Wu, C.-S. (2016). Preparation of a carbon doped tissue-mimicking material with high dielectric properties for microwave imaging application. *Materials*, 9(7), 559. <https://doi.org/10.3390/ma9070559>
- [18] Lazebnik, M., Madsen, E. L., Frank, G. R., & Hagness, S. C. (2005). Tissue-mimicking phantom materials for narrowband and ultrawideband microwave applications. *Physics in Medicine & Biology*, 50(18), 4245. <https://doi.org/10.1088/0031-9155/50/18/001>
- [19] National Instruments. *Introduction to Network Analyzer Measurements - Fundamentals and Background*. http://download.ni.com/evaluation/rf/Introduction_to_Network_Analyzer_Measurements.pdf (Accessed: 30.04.2019)
- [20] Byrne, D., Sarafianou, M., & Craddock, I. J. (2017). Compound radar approach for breast imaging. *IEEE Transactions on Biomedical Engineering*, 64(1), 40-51. <https://doi.org/10.1109/TBME.2016.2536703>
- [21] Patil, A. S. & Ghongade, R. (2016). Design of bioimpedance spectrometer. *International Conference on Advances in Computing, Communications and Informatics (ICACCI)*, 2724-2728. <https://doi.org/10.1109/ICACCI.2016.7732473>
- [22] Boerner, W.-M., Ho, C.-M., & Foo, B.-Y. (1981). Use of Radon's projection theory in electromagnetic inverse scattering. *IEEE Transactions on Antennas and Propagation*, 29(2), 336-341. <https://doi.org/10.1109/TAP.1981.1142581>

Authors' contacts:

Emine Avşar Aydın, Assistant Professor
(Corresponding author)
Adana Alparslan Türkeş Science and Technology University,
Department of Aeronautics Engineering
Adana/TURKEY
+90-05318436781
eaydin@atu.edu.tr
rasvaenime@gmail.com

Selin Yabacı Karaoğlu, Assistant Professor
Adana Alparslan Türkeş Science and Technology University,
Department of Food Engineering
Adana/TURKEY
syabaci@atu.edu.tr

A Strategic Service Management Model in National Gas Distribution Projects

Fereidoun Esmaeilzadeh, Kazem Askarifar*, Pegah Alamdari

Abstract: The main purpose of this research was to develop a model regarding strategic service management in order to improve the performance of projects related to the oil and gas industry. To this end, this study was conducted in two steps. Firstly, the main practices of SSM were defined by a systematic review and completed by experts' interviews, and the data onto the expected and perceived about each practice were collected by using a questionnaire answered by the managers and direct experts of the Fars Gas Company, Iran, and its contractors in a five-year period. Finally, the SSM model was determined in a focus group. All participants were selected judgmentally and purposefully based on theoretical saturation. The findings show that the employer expects the contractor to improve the communication skills and the grooming and professional appearance of its staff and that they spend enough time processing the employer requests. As a result, the SSM model was developed based on four strategic cornerstones, including managerial attitude improvement, managing communications, improving business processes, and strengthening internal controls.

Keywords: construction projects; contractor; employer; gap analysis; public sector; Strategic Service Management (SSM)

1 INTRODUCTION

Construction projects generally play a vital role in developing the countries' infrastructure. Many organizations prefer to define their development tasks in the form of projects or to establish project-based institutions temporarily or even permanently [1]. The volume of construction projects in Iran, as a developing country, has allocated a significant part of financial, human and physical resources [2]. In this regard, the services of contracting companies have been developed as the axis of design services, engineering, implementation and supervision of these projects.

However, contracting companies need to perceive the higher levels of requirements in projects, in addition to the technical issues such as time and cost plans, in order to create value for the employer and to achieve the strategic goals of the business [3]. Despite the importance of projects in organizations, the research fulfilled in project management shows that contrary to the improvement of project management processes and systems, managers still face many challenges regarding the project success factors [4], and these challenges are evident for both the employer and the contractor.

To overcome this drawback, the employer must take into account all the necessary criteria in the process of contractor selection [5], and at the same time, the contractor must maximize the employer satisfaction at the various stages of project implementation by correct identification and management of the key success factors. Additionally, managers of contracting companies must be able to establish the closest relationship between their performance and their employer's expectations [6]. Therefore, they will be able to provide the most satisfaction to the employer with the proper management of key success factors in the sectors of design, consulting, implementation and supervision aspects of projects. One of the main steps of success factors, and as a result of strategic planning, is the gap analysis performing. In other words, by identifying the factors that have the greatest gaps in the perceptions and expectations of managers (contractors) and customers (employers), senior management can allocate limited organizational resources to strategic

priorities. Hence, the top managers of contracting companies could develop realistic and applicable strategic plans for project service management while defining the appropriate goals. This is especially important when the employer is in contact with several contractors and the criteria for evaluating the performance of a contractor is compared to its direct competitors.

Meanwhile, working for large governmental companies such as the Fars Province Gas Company, which has opened 128 projects in 2016 and started 85 projects [7], doubles the sensitivity of this issue. However, a lot of research in this area was focused on the issues such as contractor selection, and has paid less attention to the identification of the success factors of the service management of contracting companies. The contribution of this study can be considered from two perspectives. A look at the literature shows two major gaps in previous researches. The first gap is related to the general field of strategic service management (SSM), which, despite the development of its theoretical foundations, has been less explored in the applied studies. The second one related to the field of management of contracting companies so that despite the scope and importance of project activities and consequently the key factors of success in contracting companies, the concept of SSM in the contracting industry has not been developed as it should be. Accordingly, this study tries to provide an appropriate model for the nature of contracting activities by using all SSM levers with a strategic view on the issue of project management in contracting companies.

Therefore, the present study tried to present a model for improving the management of the activities of these companies with the aim of analysing the gaps in the SSM model in contracting companies. For this purpose, research has been performed in two main steps. In the first step, various practices that have to be carried out by a contracting company are extracted by reviewing studies and are completed and refined by interviewing experts. Then, by using the field data, the gap between the current and optimal status of these factors is determined. Finally, in the second stage, based on the existing gap and according to experts, a SSM model is presented.

2 RESEARCH BACKGROUND

Intensified competition has led many businesses to seek ways to differentiate themselves from their competitors. In this regard, one of the strategies that has been related to the success of these businesses is delivering qualified products and services as much or even beyond customer expectations [8]. With the growth of business models in manufacturing and services, the concern of managers and policy makers has become more dominant in terms of over-identifying priorities for improvement. Meanwhile, due to the challenge or opportunity of globalization on the one hand and the emergence of new concepts such as corporate social responsibilities (CSR) and international relations on the other hand has shifted the decision-making atmosphere to a new level [9].

One of the most important functions of an organization's management is service administration, which provides clarifying problems, optimized decision-making, and performing services based on the internal and external environment of the firms. Even though this area could be considered at the operational level, at the higher level, senior managers are always looking for identifying value-creating factors that can be explored and discussed in the context of strategic service management (SSM).

The (SSM) approach emerged in the 1990s as a branch of the strategic management of production [10], which was named as the missing link in the connection between organizational strategies [11]. In this new topic, management uses five levers: quality, reliability, service, delivery, and cost to overcome competitors while creating value for the customer in a turbulent market environment and intense market competition [12]. Therefore, production and service strategies brought up interrelated structural and infrastructural decisions and actions that empower the agency's production and service system. Eventually, the SSM provides a manner to achieve a set of organizational objectives consistent with the organization's goals, which is classified in the aforementioned five areas [13].

A look at the carried out research shows that each of the levers of SSM or a combination of several levers has been noticed by researchers in some way. Considering the cost and time [14], cost, quality, and time [15], or reliability and cost [16] in officious project management are some examples of these studies. However, apart from these five levers, there are other factors such as the risk addressed in the related studies [17], which originally somehow refers to the reliability of the main levers of SSM.

In their study, Yu and Liang [18] examined the role of corporate social responsibility in the strategic planning process. In this study, it was stated that in addition to reducing costs, integrating organizational resources and using the creativity and decision-making power of all employees at all levels, social responsibility was also perceived as strategic capability.

Another issue that can be seen as a research gap in this field is the lack of service providing strategies in contracting companies. In principle, there is a fundamental difference between the concept of strategic project management and classic project management in which the models require to help the project-oriented organizations to create competitive

advantages. In other words, in order to gain competitive advantages after which an organization's success will follow, managers must focus on the strategic aspects of projects and their processes in the organization [19].

As a summary of the background review, two major gaps can be seen in the previous research. The first gap is connected to the general field of strategic service management, which has been less exploited in applied studies. The second gap is illustrated in the field of the management of contracting companies due to the scarcity of the concept development of strategic service management. Accordingly, this study tried to provide an appropriate model based on the nature of contracting activities by using all the strategic management of service levers with a strategic view on the issue of project management in contracting companies.

3 RESEARCH METHOD

This research has an applied purpose; it is inferential in terms of nature and method, a mixed method from the variable aspect, and cross-sectional time, which has been implemented in contracting companies active in gas distribution infrastructures projects in the Fars province, Iran.

The subject context of this study is to use the model of strategic service management (SSM) and the gap analysis of strategic leverage in construction projects. The gathered data time zone is the period of March 2016 to September 2018. This research was carried out in two main steps. The first step included identifying the gap between the areas of SSM and the second one referred to the development of the SSM plan based on the outcomes of the gap analysis.

The statistical population of the first step of this research was all 47 managers and direct experts involved in the infrastructure projects of the Gas Company and in the contracting section, including 120 contractors in a recent five-year period (2012-2016). In the same way, the statistical population of the second step included the experts in service management, project management and strategic management. Due to the nature of the research, sample selection was done judgmentally and purposefully, in which the statistical sample of the gap analysis step included 21 employers and 34 contractors, and in the SSM model development step included 7 experts as shown in Tab. 1.

Table 1 Demographic Characteristics of Participants in the Research

Demographic characteristics	Levels	Participants as a statistical sample			
		1 st step			2 nd Step
		Contractor	Employer	Sum.	
	Total	34	21	55	7
Gender	Male	32	15	47	6
	Female	2	6	8	1
Education	With a diploma	6	4	10	-
	Technician	8	2	10	-
	Bachelor	18	10	28	-
	Masters and higher	2	5	7	7
Related work experience	<10	4	9	13	2
	10 < x < 20	19	5	24	3
	>20	11	7	18	2

Source: Created by the authors

In the first stage, service practices were extracted by using a systematic review of the studies as a conceptual model. These practices were then evaluated and refined by the experts' opinion considering the nature of the contracting entity in the case study. Meaning that these indicators were reviewed by seven experts before being surveyed in the form of a questionnaire, and based on their judgment, content validity ratio (CVR) was computed and the irrelevant indicators were removed. Therefore, in addition to determining valid indicators, the credibility of the conceptual model was also confirmed by the experts. On the other hand, the reliability of the questionnaire was confirmed by calculating the Cronbach's alpha coefficient ($\alpha = 0.73$).

A closed questionnaire was then designed based on the SERVQUAL approach that the expected importance of each practice was measured by an employer and contractor. Similarly, another questionnaire was designed to determine the gap of the current situation of each of the factors of the conceptual model from the point of view of the employer and the contractor as a perceptual gap. After the questionnaires were completed by the participants, by using inferential statistics, the significance of the gap in the importance of the factors of the conceptual model was examined, as well as the significance of the perceptual gap. At this step, the non-parametric Mann-Whitney and Wilcoxon tests were utilized in the SPSS 22 statistical software since the data were not normally distributed.

Finally, the SSM was designed and finalized based on the significant gaps determined by the panel of experts as a focus group.

4 FINDINGS

Based on the research method described in the previous section, 36 indicators were identified and then categorized by the researcher into four dimensions of the SSM, including quality, services, reliability, and delivery. It is noteworthy that according to the experts, the cost dimension was excluded from the conceptual model due to the inability to determine the appropriate indicators, as well as the restricted access to required data. In this case, the experts' reasoning was that in the public sector, cost estimation, budgeting, and the financial conditions of contracts such as payment terms, minus, or plus are subject to the upstream laws, and as a result, the cost factor is less flexible in management than the other dimensions of the model. Thus, its effects can be merged in other dimensions. Eventually, 27 indicators were finalized in four dimensions by the CVR calculation based on the seven experts' judgement as shown in Tab. 2.

In the following part, three main statistical hypotheses were expressed and tested to define the significant gap in the SSM leverages (dimensions) as well as the practices of each dimension:

Hypothesis 1 (H1): There is a significant difference between the employer's and contractor's expectations in the importance of each dimension (and practice) of SSM in construction projects.

Hypothesis 2 (H2): There is a significant difference between the perceptions and expectations of the employer in

the dimensions (and practices) of SSM in construction projects.

Hypothesis 3 (H3): There is a significant difference between the perceptions and expectations of the contractor in the dimensions (and practices) of SSM in construction projects.

Table 2 Dimensions and Indicators of the Strategic Management Model of Contracting Services*

Dimensions (Abbreviation)	Practices	Abbreviation
Delivery (DLV)	Completeness and clarity of information before project delivery	DLV-1
	On time project delivery	DLV-2
Service (SRV)	Spending enough time on the process as per the employer's requests	SRV-1
	Access to the contractor at the project site when needed	SRV-2
	Good will and polite behavior of the contractor staff	SRV-3
	Communication skills of the contractor staff	SRV-4
	Interest in responding to employer's requests	SRV-5
	Not wasting the employer's town	SRV-6
	Provide regular, timely and integrated reports	SRV-7
	Observation of moral rules and regulations	SRV-8
	Groomed and professional appearance of the staff	SRV-9
	Respect for the position of the employer	SRV-10
Reliability (REL)	Immediate action when a problem arises	REL-1
	Adequate technical knowledge of the contractor	REL-2
	Handling employer complaints	REL-3
	Provide sufficient information to the employer about the status of the project	REL-4
	A sense of responsibility and work conscience	REL-5
	Compensation for losses	REL-6
	Fulfillment of obligations (based on contract terms)	REL-7
	Observation of safety	REL-8
	Flexibility in specific conditions	REL-9
	Providing a suitable solution to solve problems	REL-10
Quality (QLT)	Flawless project delivery (FPD)	QLT-1
	Minimal deviation of the project from the pre-set expectations	QLT-2
	Having the necessary modern equipment	QLT-3
	Quality control of the material and consumables	QLT-4
	Workplace housekeeping	QLT-5

Source: Created by the authors

The conceptual model of research based on the defined hypotheses is shown in Fig. 1.

Afterwards, the importance and perception of each dimension and practices were defined based on the data collected through the questionnaires from the employer's and contractor's sample.

For testing the H1 hypothesis, the mean importance of the dimensions of the SSM model was calculated and the significance of the difference between the contractor and the employer were evaluated by the Mann-Whitney test. The results are shown in Tab. 3.

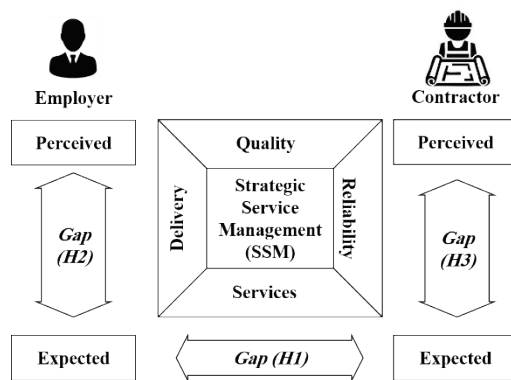


Figure 1 Conceptual model of the gap analysis
Source: Created by the authors

Table 3 The gap between the expectations of the employer and contractor in SSM Dimensions (Mann-Whitney test)

SSM dimensions	Mean of Expectations		Gap	p-value	Significance
	Contractor	Employer			
Quality	8.6	8.4	0.2	0.052	RE
Service	8.3	7.7	0.6	0.801	RE
Reliability	8.5	8.4	0.1	0.116	RE
Delivery	7.6	7.8	-0.2	0.022*	AC

* Significant at the 95% confidence level. AC: Accepted, RE: Rejected
Source: Created by the authors

The results of Tab. 3 show that the expectation of the employer and the contractor from the "delivery" dimension has a significant gap at the 95% confidence (p -value < 0.05), but in other cases, no significant gap is observed. In other words, what the employer expects in the importance of the delivery dimension is significantly more important than what the contractor is feeling in this dimension.

Table 4 The gap between the expectations of the employer and contractor in SSM indicators (Mann-Whitney test)

No.	Indicator	Mean of Expectations		Gap	p-value	Significance
		Contractor	Employer			
1	DLV-1	5.7	6.9	-1.2	0.01*	AC
2	DLV-2	8.5	8.6	-0.1	0.88	RE
3	SRV-1	6.0	7.5	1.5	0.01*	AC
4	SRV-2	7.4	8.8	1.4	0.01*	AC
5	SRV-3	6.9	7.0	-0.1	0.71	RE
6	SRV-4	8.0	6.1	1.9	0.00*	AC
7	SRV-5	7.7	7.0	0.7	0.08	RE
8	SRV-6	8.4	9.0	-0.6	0.08	RE
9	SRV-7	8.6	8.0	0.6	0.05	RE
10	SRV-8	7.7	8.0	-0.3	0.55	RE
11	SRV-9	8.3	6.6	1.7	0.01*	AC
12	SRV-10	8.1	8.9	-0.8	0.10	RE
13	REL-1	6.6	7.7	-1.1	0.04*	AC
14	REL-2	8.5	9.0	-0.5	0.20	RE
15	REL-3	8.4	8.2	0.2	0.58	RE
16	REL-4	9.3	8.8	0.5	0.14	RE
17	REL-5	8.5	9.1	-0.6	0.06	RE
18	REL-6	9.2	9.1	0.1	0.83	RE
19	REL-7	8.6	8.8	-0.2	0.62	RE
20	REL-8	7.2	8.2	-1.0	0.12	RE
21	REL-9	8.2	8.0	0.2	0.61	RE
22	REL-10	7.0	6.6	0.4	0.37	RE
23	QLT-1	9.1	7.8	1.3	0.00*	AC
24	QLT-2	7.9	8.7	-0.8	0.05	RE
25	QLT-3	9.2	9.0	0.2	0.41	RE
26	QLT-4	8.6	8.9	-0.3	0.67	RE
27	QLT-5	8.4	7.6	0.8	0.01*	AC

* Significant at the 95% confidence level. AC: Accepted, RE: Rejected
Source: Created by the authors

Similarly, to determine the significant gap in the practices' importance of the conceptual model, the Mann-Whitney test was performed at this level, and the results can be seen in Tab. 4. Based on these findings, the employer's and contractor's expectations have a significant gap in the DVL-1: completeness and clarity of information before project delivery, SRV-1: spending enough time to process the employer's requests, SRV-2: access to contractor at the project site, SRV-4: communication skills of the contractor staff, SRV-9: the groomed and professional appearance of the staff, REL-1: immediate action when a problem arises, QLT-1: flawless project delivery (FPD), and QLT-5: workplace housekeeping. Conversely, there is no gap in other practices, and the results are shown in Tab. 4.

Moreover, in the hypotheses 2 and 3 of the research, it was determined that the perceptions and expectations of the employer have a significant gap in all dimensions based on the data collected and the Wilcoxon test, (Tab. 5). In fact, contractors expect the level of performance to be present in all dimensions of SSM, which in practice is significantly lower, with the maximum and minimum gaps being "delivery" and "quality", respectively.

Table 5 The gap between the dimensions of SSM in the second hypothesis (Wilcoxon Test)

SSM Dimensions	Employer (mean)		Gap	p-value	Significance
	Expectation	Perceived			
Quality	7.7	5.0	2.70	0.001*	AC
Service	8.4	4.1	4.30	0.001*	AC
Reliability	7.8	5.0	2.80	0.001*	AC
delivery	7.7	4.1	3.61	0.001*	AC

* Significant at the 95% confidence level. AC: Accepted
Source: Created by the authors

Additionally, the employer has expectations from contractors in all dimensions of the SSM that significantly underestimate their actual performance, in which "delivery" and "service" show the highest and lowest gaps, respectively (Tab. 6).

Table 6 The gap between the dimensions of SSM in the third hypothesis (Wilcoxon Test)

SSM Dimensions	Contractor (mean)		Gap	p-value	Significance
	Expectation	Perceived			
Quality	8.7	6.9	1.8	0.001*	AC
Service	8.3	6.9	1.4	0.001*	AC
Reliability	8.5	7.0	0.5	0.001*	AC
delivery	7.6	5.9	1.7	0.001*	AC

* Significant at the 95% confidence level. AC: accepted
Source: Created by the authors

Similarly, in order to obtain the practices that have a significant difference in this hypothesis, the Wilcoxon test was performed at this level and the results are presented in Tabs. 7 and 8. Based on the findings of this stage, it was determined that the perceptions and expectations of the employer had a remarkable gap in all indicators except the SRV-3 and SRV-4; which means that the employer's perception of the contractor's performance in these indicators hides a significant difference from his/her expectations. Furthermore, this is more noticeable in the indicators of the DLV-2: On time project delivery, SERV-6: Not wasting the employer's time, and REL-4: Provide sufficient information

to the employer about the status of the projects shown in Tab. 7.

Table 7 The gap between the indicators of SSM in the second hypothesis (Wilcoxon Test)

Indicator	Employer (avg.)		Gap	p-value	Significance
	Expectation	Perceived			
1 DLV-1	6.9	5.4	1.5	0.04*	AC
2 DLV-2	8.7	2.8	5.9	0.01*	AC
3 SRV-1	7.5	3.8	3.7	0.01*	AC
4 SRV-2	8.8	5.9	2.9	0.01*	AC
5 SRV-3	7.0	5.7	1.2	0.05	RE
6 SRV-4	6.1	4.7	1.5	0.08	RE
7 SRV-5	6.9	4.2	2.7	0.01*	AC
8 SRV-6	8.9	3.5	5.4	0.01*	AC
9 SRV-7	8.0	4.9	3.1	0.01*	AC
10 SRV-8	8.0	5.7	2.3	0.01*	AC
11 SRV-9	6.6	3.5	3.1	0.01*	AC
12 SRV-10	8.9	6.8	2.1	0.01*	AC
13 REL-1	8.7	4.4	3.4	0.01*	AC
14 REL-2	8.9	5.0	3.9	0.01*	AC
15 REL-3	8.2	6.3	1.9	0.01*	AC
16 REL-4	8.8	3.5	5.3	0.01*	AC
17 REL-5	9.1	4.8	4.3	0.01*	AC
18 REL-6	9.1	5.1	4.0	0.01*	AC
19 REL-7	8.8	5.4	3.4	0.01*	AC
20 REL-8	8.2	5.7	2.5	0.01*	AC
21 REL-9	7.9	5.6	2.3	0.01*	AC
22 REL-10	6.6	4.1	2.5	0.01*	AC
23 QLT-1	7.8	5.7	2.1	0.01*	AC
24 QLT-2	8.7	6.1	2.6	0.01*	AC
25 QLT-3	9.0	5.2	3.8	0.01*	AC
26 QLT-4	8.9	6.9	2.0	0.01*	AC
27 QLT-5	7.6	5.1	2.5	0.01*	AC

* Significant at the 95% confidence level. AC: Accepted, RE: Rejected
Source: Created by the authors

Table 8 The gap between the indicators of SSM in the third hypotheses (Wilcoxon Test)

Indicator	Contractor		Gap	p-value	Significance
	Expectation	Perceived			
1 DLV-1	5.7	6.2	-0.5	0.26	RE
2 DLV-2	8.6	5.5	3.1	0.01*	AC
3 SRV-1	6.0	6.4	-0.4	0.36	RE
4 SRV-2	7.4	7.4	0.0	0.91	RE
5 SRV-3	6.9	6.6	0.3	0.85	RE
6 SRV-4	8.0	7.1	0.9	0.03*	AC
7 SRV-5	7.7	7.4	0.3	0.55	RE
8 SRV-6	8.4	6.4	2.0	0.01*	AC
9 SRV-7	8.6	5.3	3.3	0.01*	AC
10 SRV-8	7.7	7.9	0.1	0.75	RE
11 SRV-9	8.3	6.6	1.7	0.01*	AC
12 SRV-10	8.1	8.3	-0.2	0.69	RE
13 REL-1	7.6	6.0	1.6	0.01*	AC
14 REL-2	8.5	7.8	0.7	0.11	RE
15 REL-3	8.4	6.2	2.2	0.01*	AC
16 REL-4	9.3	6.6	2.7	0.01*	AC
17 REL-5	8.5	6.9	1.6	0.01*	AC
18 REL-6	9.2	6.7	2.5	0.01*	AC
19 REL-7	8.6	7.6	1.0	0.01*	AC
20 REL-8	7.2	7.4	-0.2	0.82	RE
21 REL-9	8.2	8.3	-0.1	0.51	RE
22 REL-10	7.0	6.6	0.4	0.49	RE
23 QLT-1	9.1	6.0	3.1	0.01*	AC
24 QLT-2	7.9	8.8	-0.9	0.01*	AC
25 QLT-3	9.2	5.7	3.5	0.01*	AC
26 QLT-4	8.6	7.3	1.3	0.01*	AC
27 QLT-5	8.4	6.9	1.5	0.01*	AC

* Significant at the 95% confidence level. AC: Accepted, RE: Rejected
Source: Created by the authors

It was also determined that contractor perceptions and expectations have a significant gap in the practices of DLV-2: On time project delivery, SRV-4: Communication skills of the contractor staff, SRV-6: Not wasting the employer's time, SRV-7: Provide regular, timely and integrated reports, SRV-9: The groomed and professional appearance of staff, REL-1: Immediate action when a problem arises, REL-3: Handling employer complaints, REL-4: Provide sufficient information to the employer about the status of the project, REL-5: A sense of responsibility and work conscience, REL-6: Compensation for losses, REL-7: Fulfillment of obligations (based on contract terms), QLT-1: Flawless project delivery (FPD), QLT-2: Minimal deviation of the project from the pre-set expectations, QLT-3: Having the necessary modern equipment, QLT-4: Quality control of the material and consumables, and QLT-5: Workplace housekeeping.

Finally, after the determination of the dimensions and indicators with a significant gap, the findings were presented in a focus group including seven experts, and the SSM model was finalized by reaching a collective agreement.

To do so, the results of the hypothesis tests were classified in four managerial fields as critical practices. Hence, in this classification, those practices that have a significant gap in the expectation and perception of the employer (H2) were defined as strategic communicative functions of the contractors.

Moreover, based on the findings of the hypothesis 1 testing, in order to bridge the gap between the contractor's expectations and the employer's expectations, as a critical goal, those practices that have a significant gap were placed in this strategic aspect. Furthermore, there are some practices that showed a significant gap in the expectation and perception of contractors (H3), while significantly affecting optimal service providing. These factors need to improve as internal factors, and they were therefore categorized into two groups as internal controls and business processes. A scheme of this classification is shown in Fig. 2.

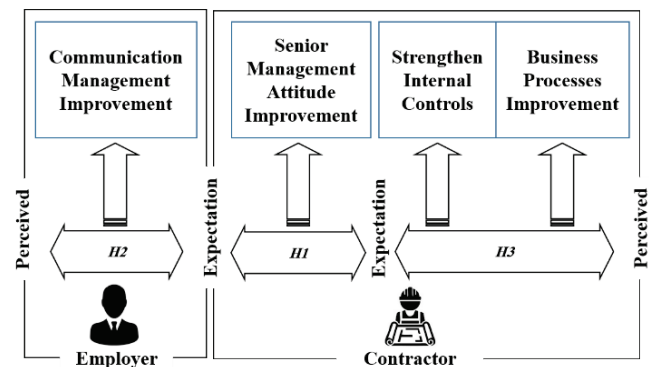


Figure 2 Strategic Management Model (SSM) extraction framework
Source: Created by the authors

Finally, based on the output of the focus group, critical practices were categorized as priorities for improvement in the management areas mentioned in Fig. 2, and they were sorted according to the observed gap ratings in the SSM model and presented as Fig. 3.

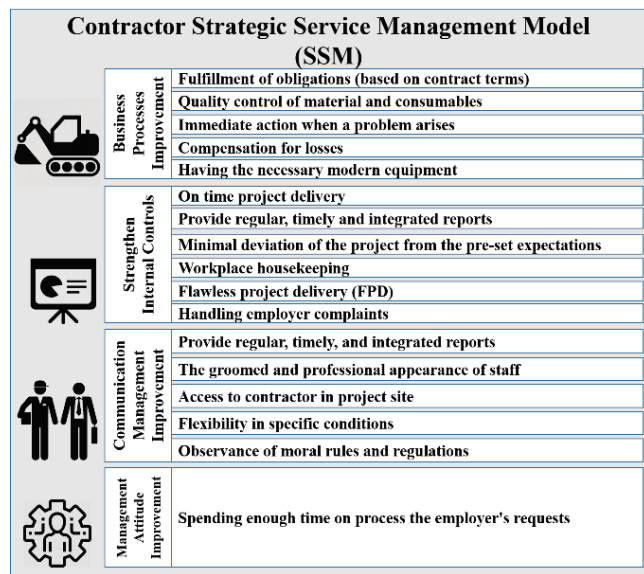


Figure 3 Contractor Strategic Service Management (SSM) Model in the public sector

Source: Created by the authors

5 DISCUSSION AND CONCLUSIONS

The purpose of this study was to present a service strategic management (SSM) model in contracting companies. Given that there has been limited research in the levers of SSM, the results of this study disclose that a notable gap between the employer's and contractor's expectations is related to the dimensions of the delivery of sufficient information about the project, as well as their completeness within a planned framework. The findings of the research are in line with what has been mentioned in other studies such as the one by Liu et al. [20], which puts emphasis on the effective relationship between contractor and employer.

Based on analysing the gap between the employer's perceptions and expectations, the biggest gap is related to the modernity of contractor equipment, which is related to the quality dimension of SSM. These factors should be important to contractors as key factors of success. In this regard, Alzahrani and Emsley [21] classified the key factors of success into nine groups: safety and quality, past performance, environment, technical and managerial aspects, resources, organization, experience, size of previous projects and financial capability, in which the indicators such as quality policies, workforce adequacy, and company image were shown to be the most important success factors for contracting companies. A closer look at research findings also shows that contractor accountability, on time project delivery, and having modern equipment play a considerable role in creating a good image in the construction project market which is why contractors must pay more attention to these practices.

Furthermore, based on research findings, in order to manage services strategically, it is suggested that contracting companies should focus on four areas of improving their managerial attitude, communication management, business processes, and internal controls.

More precisely, contractors must develop the mechanisms of communication management to ensure

providing sufficient information to the employer about the status of the project, the groomed and professional appearance of the staff, access to the contractor and its agents at the project site when needed, flexibility in specific conditions, and observance of moral rules and regulations.

Moreover, it is essential that managers strengthen internal control mechanisms, especially in the timely delivery of projects, regular and timely reporting, establishing actionable key performance indexes (KPI's) of project steps, workplace housekeeping, moving toward zero defect in a project at delivery, and handling employer compliances.

Another part of the SSM model is the business process management (BPM) in contracting companies.

Despite the importance of all business processes, according to the findings of this study, contractors should focus more specifically on the processes of modernization and even more on total preventive maintenance (TPM) of the equipment, compensation for losses, quality control of the material and consumables, and the fulfillment of obligations based on contract terms. However, all of the mentioned points can be achieved in the light of an oriented attitude of the senior management of the contracting companies to handle and take care of the employer's requests.

Comparing the findings of this study with other studies reported in the literature shows the concordance of these findings in this study. Hamaria et al. [22] considered service persistence as a different quality dimension of assurance, empathy, reliability, and accountability. Similarly, Lucianetti et al. [23] listed the competitive advantages of production as quality, cost, productivity, delivery, innovation, and reliability. Moreover, as it has been noted earlier, the managers of contracting companies must see employer requirements with half an eye in designing the work of an organization, as Mashwama et al. [24] emphasized in their study on contracting companies.

Although in this study the SSM model is presented based on service management levers, suggestions for the development and continuation of this research are mentioned, including the consideration of complementary factors such as cost, innovation [25], the risk management effect on the model [26], or the social responsibility of the contracting companies [27]. Finally, qualitative approaches such as phenomenology, grounded theory, or cognitive mapping could be used for determining the success factors and strategies, and therefore could also help develop the SSM model.

Acknowledgement

The authors are grateful to the Shiraz University for supporting this research.

6 REFERENCES

- [1] Fernandes, G., Ward, S., & Araújo, M. (2015). Improving and embedding project management practice in organisations - A qualitative study. *International Journal of Project Management*, 33(5), 1052-1067. <https://doi.org/10.1016/j.ijproman.2015.01.012>
- [2] Zanjirchi, S., Amani, M., & Azizi, F. (2016). Developing a model for prioritization automated car parking integration Taguchi design of experimental (DOE) and fuzzy

- AHP. *Geography and Environmental Planning*, 27(2), 131-146. <https://doi.org/10.1002/pm.j.20282>
- [3] Patanakul, P. & Shenhar, A. J. (2012). What project strategy really is: The fundamental building block in strategic project management? *Project Management Journal*, 43(1), 4-20.
- [4] Gupta, S. K., Gunasekaran, A., Antony, J., Gupta, S., Beg, S., & Rubaud, D. (2019). Systematic literature review of project failures: Current trends and scope for future research. *Computers & Industrial Engineering*, 127, 274-285. <https://doi.org/10.1016/j.cie.2018.12.002>
- [5] Cheaitou, A., Larbi, R., & Al Housani, B. (2018). Decision making framework for tender evaluation and contractor selection in public organizations with risk considerations. *Socio-Economic Planning Sciences*, In Press. <https://doi.org/10.1016/j.seps.2018.02.007>
- [6] Asgari, S., Awwad, R., Kandil, A., & Odeh, I. (2017). Impact of considering need for work and risk on performance of construction contractors: An agent-based approach. *Automation in Construction*, 65, 9-20. <https://doi.org/10.1016/j.autcon.2016.01.004>
- [7] Fars Province Gas Company website (2017). Actions to develop gas supply to Fars province cities, villages and industries in the government of tact and hope (Tadbir va Omid), retrieved from <http://nigc-fars.ir/Portal/File/ShowFile.aspx?ID=45c4e579-bc04-4a3b-9282-d26e5a949f1d> on 2017.
- [8] Jiang, J. J., Klein, G., Parolia, N., & Li, Y. (2012). An analysis of three SERVQUAL variations in measuring information system service quality. *Electronic Journal Information Systems Evaluation*, 5(2), 149-162.
- [9] Liao, P. C., Liao, J. Q., Wu, G., Wu, C. L., Xang, X. L., & Ma, M. C. (2018). Comparing international contractors' CSR communication patterns: A semantic analysis. *Journal of Cleaner Production*, 203, 353-366. <https://doi.org/10.1016/j.jclepro.2018.08.218>
- [10] Kellog, D. L. & Nie, W. (1995). A framework for strategic service management. *Journal of Operations Management*, 13(4), 323-337. [https://doi.org/10.1016/0272-6963\(95\)00036-4](https://doi.org/10.1016/0272-6963(95)00036-4)
- [11] Boyle, D. (2000). *Strategic Service Management beyond the Moment of Truth* (1st ed.). Vol. 7, Elsevier.
- [12] Lowson, R. H. (2002). *Strategic Operations Management*. London and New York: Routledge. <https://doi.org/10.4324/9780203361528>
- [13] Štefancová, V., Nedeliaková, E., & López-Escolano, C. (2017). Connection of dynamic quality modelling and total service management in railway transport operation. *Procedia Engineering*, 192, 834-839. <https://doi.org/10.1016/j.proeng.2017.06.144>
- [14] Alavipour, S. M. R. & Arditi D. (2019). Time-cost trade-off analysis with minimized project financing cost. *Automation in Construction*, 98, 110-121. <https://doi.org/10.1016/j.autcon.2018.09.009>
- [15] Mungle, S., Benyoucef, L., Son, Y. J., & Tiwari, M. K. (2013). A fuzzy clustering-based genetic algorithm approach for time-cost-quality trade-off problems: A case study of highway construction project. *Engineering Applications of Artificial Intelligence*, 26(8), 1953-1966. <https://doi.org/10.1016/j.engappai.2013.05.006>
- [16] Mehrafrooz, B., Edalat, P., & Dyanati, M. (2019). Cost consequence-based reliability analysis of bursting failure mode in subsea pipelines. *Journal of Marine Engineering*, 15 (29), 197-204. <https://doi.org/10.1016/j.joes.2019.01.001>
- [17] Mohammadipour, F. & Sajjadi, S. J. (2016). Project cost-quality-risk tradeoff analysis in a time-constrained problem. *Computers & Industrial Engineering*, 95, 111-121. <https://doi.org/10.1016/j.cie.2016.02.025>
- [18] Yu, S. H. & Liang, W. C. (2020). Exploring the determinants of strategic corporate social responsibility: An empirical examination. *Sustainability*, 12, 2368. <https://doi.org/10.3390/su12062368>
- [19] Soltani, A. & Marjani, T. (2015). Using strategic project management as a new approach to project management. *Technology Growth*, 12(45), 69-76.
- [20] Liu, R., Cui, L., Zeng, G., Wu, H., Wang, C., Yan, S., & Yan, B. (2015). Applying the fuzzy SERVQUAL method to measure the service quality in certification & inspection industry. *Applied Soft Computing*, 26, 508-512. <https://doi.org/10.1016/j.asoc.2014.10.014>
- [21] Alzahrani, J. I. & Emsley, M. W. (2013). The impact of contractors' attributes on construction project success: A post construction evaluation. *International Journal of Project Management*, 31(2), 313-322. <https://doi.org/10.1016/j.ijproman.2012.06.006>
- [22] Hamaria, J., Hannerb, H., & Koivisto, J. (2017). Service quality explains why people use freemium services but not if they go premium: An empirical study in free-to-play games. *Journal of Information Management*, 37, 1449-1459. <https://doi.org/10.1016/j.jinfomgt.2016.09.004>
- [23] Lucianetti, L., Jabbour, C. J. C., Gunasekaran, A., & Latan, H. (2018). Contingency factors and complementary effects of adopting advanced manufacturing tools and managerial practices: Effects on organizational measurement systems and firms' performance. *International Journal of Production Economics*, 200, 318-328. <https://doi.org/10.1016/j.ijpe.2018.04.005>
- [24] Mashwama, N., Aigbavboa, C., & Thwala, D. (2017). An assessment of the critical success factor for the reduction of cost of poor quality in construction projects in Swaziland. *Procedia Engineering*, 196, 447-453. <https://doi.org/10.1016/j.proeng.2017.07.223>
- [25] Setiawan, H., Erdogan, B., & Ogunlana, S.O. (2017). Innovativeness: A key factor to support contractors' business success. *Procedia Engineering*, 171, 379-386. <https://doi.org/10.1016/j.proeng.2017.01.347>
- [26] Mir, F. A. & Pinnington, A. H. (2014). Exploring the value of project management: Linking Project Management Performance and Project Success. *International Journal of Project Management*, 32(2), 202-217. <https://doi.org/10.1016/j.ijproman.2013.05.012>
- [27] Pal, R., Wang, P., & Liang, X. (2017). The critical factors in managing relationships in international engineering, procurement, and construction (IEPC) projects of Chinese organizations. *International Journal of Project Management*, 35(7), 1225-1237. <https://doi.org/10.1016/j.ijproman.2017.05.010>

Authors' contacts:

Fereidoun Esmaeilzadeh, PhD, Professor
Shiraz University,
School of Chemical, Petroleum, and Gas Engineering,
Mollasadra Street, Shiraz, Iran
Email: esmaeil@shirazu.ac.ir

Kazem Askarifar, PhD, Assistant Professor
(Corresponding author)
Shiraz University,
Department of Management, Eram sq., Shiraz, Iran
Tel: (+98) 7136134462 and 00989171114054,
Email: kaskarifar@shirazu.ac.ir

Pegah Alamdari, M.Sc. of Industrial Management
Zand Institute of Higher Education, Shiraz, Iran
Email: pegah_al89@yahoo.com

The Effect of the Holding Pressure Profile on the Metal Injection Molded Component Dimensions after Sintering

Emir Šarić*, Samir Butković, Muhamed Mehmedović

Abstract: The volumetric flow rate (injection velocity) and the holding pressure are metal injection molding (MIM) parameters that have a strong influence on the green parts density and density homogeneity, but their effect on sintered dimensions after sintering is still to a large extent unexplored. To reveal the relationship between the injection molding parameters and sintered dimensions, ring-shaped components were injection molded by using different values of injection velocities in combination with a rump-down and rump-up holding pressure profile. Afterwards, the green components were catalytically debound and sintered in the nitrogen (N_2) atmosphere. Finally, the component dimensions: the height, inner and outer diameter were measured by using a coordinate measuring machine. The ready-to-mold granules Catamold 310N made of heat resistant stainless steel X40CrNiSi 25-20 (according to the EN standard) powder and polyacetal based binder were used. The results showed that the interaction between the injection velocity and the holding pressure profile can be used to systematically adjust shrinkage after sintering. This approach is based on the dependence of the binder crystallization temperature on pressure, when the powder/binder proportion changes with the injection velocity.

Keywords: dimensional control; holding pressure profile; metal injection molding; shrinkage

1 INTRODUCTION

In recent times, MIM has been recognized as a technology for net shape production of small metallic components with complexity that can be achieved by injection molding techniques. The major technological phases of MIM, when producers rely on the commercial granulated mix of metallic powder and binder (feedstock) are:

- injection molding, where melted feedstock is transferred, pressurized and cooled in mold cavities forming the so-called green component,
- debinding, where most of the binder is removed from the green component to get a shaped porous and dominantly metallic part,
- and finally sintering, where the porosity and the part dimensions are significantly reduced at the sintering temperature to achieve metallic parts with a density of 96% or more.

Owing to the high solid loading (typical powder content 60% vol.), MIM feedstocks have the thermal conductivity and the viscosity one order higher, and the heat capacity about three times lower than plastic [1, 2]. Therefore, the injection molding of the MIM feedstock is more temperature sensitive and requires higher injection rates and pressures compared to plastic. Moreover, the MIM feedstock flowability is affected by the phenomena such as metal particle migration from a high to low shear rate region [3], powder agglomeration and powder-binder segregation in the runner and cavities. The density inhomogeneity induced in the injection molding phase cannot be rectified in subsequent processing steps. The industry standard for the dimensional precision in MIM is in the range from $\pm 0.3\%$ to 0.5% of the nominal dimensions [4]. The injection velocity and the holding pressure are the most important parameters of the injection molding phase for the dimensional precision of the final MIM components [5, 6].

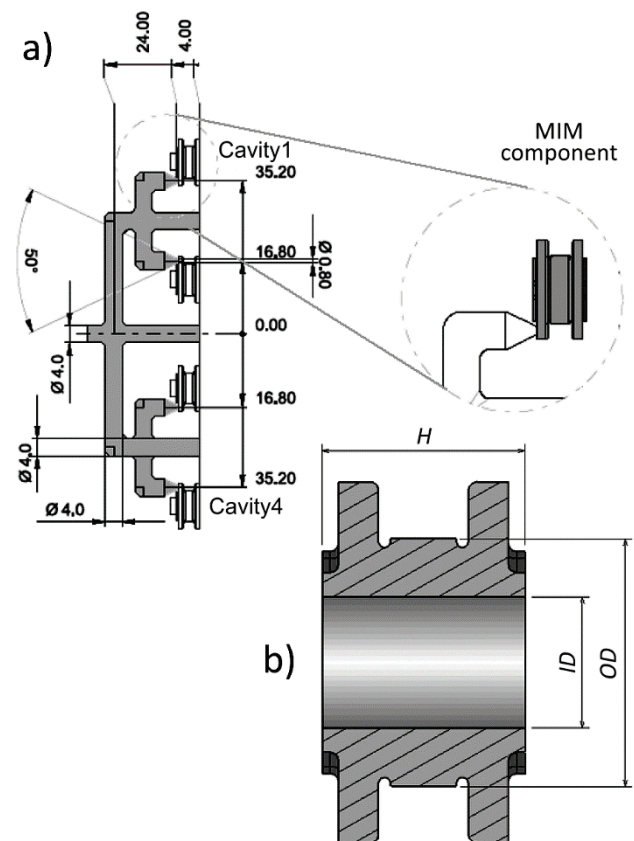


Figure 1 The runner system design and dimensions with the Pin-point gate location-detail and characteristic dimension: width (H), inner diameter (ID) and outer diameter (OD)

The amount of melted feedstock packed in a cavity depends on the packing intensity and packing time. Generally, the higher the cavity pressure-time integral is, the higher the packing intensity will be. The packing time lasts from the velocity/pressure (v/p) switchover point to the moment the gate is completely crystallized. The binder crystallization temperature is sensitive to the variation of

powder concentration, melt pressure and temperature. As a pure polymer, the MIM feedstock will crystallize at higher temperatures when pressure is applied, according to the pressure-volume-temperature (PVT) characteristic [7, 8]. However, increased metallic powder concentration (solid loading) in feedstocks diminishes the pressure sensitivity and shifts the feedstock crystallization point toward lower temperatures [8, 9].

Owing to the feedstock sensitivity to the injection, parameters' change and the complex interconnection between the technological phases, the influence of injection parameters in the final part quality in MIM remain to a large extent an unexplored territory. With this motivation in mind, the current paper researches the interactive effects of the holding pressure profile and the volumetric flow rate (injection velocity) on the final dimensions' change.

2 EXPERIMENTAL WORK

Green components were molded in a four-cavity split mold with a vertically positioned runner system by using pinpoint gates, Fig. 1a. The studied components were ring-shaped with an external groove in the middle, with the nominal mass after sintering of 1.27 g, Fig. 1b.

2.1 Material

The material used in this research was a highly viscous feedstock Catamold 310N, with high crystalline polyacetal based binder, produced by BASF, Fig. 2. The reported oversize factor (tool dimension/sintered dimension) has the nominal value of 1.1669 with a variation range of ± 0.004 based on a long term batch-to-batch variation.

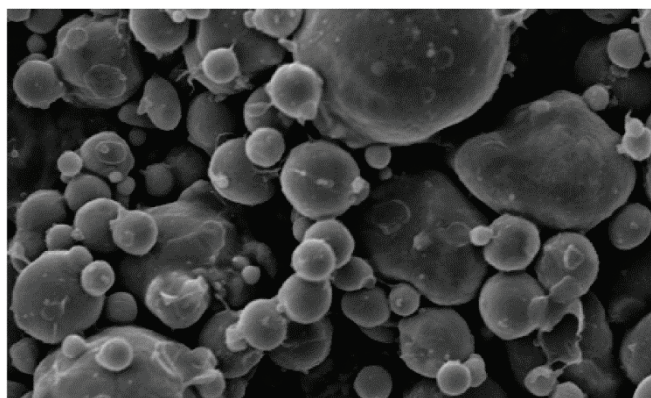


Figure 2 Etched surface of the green part (metal powder and residual binder), Catamold 310N, 1000×

2.2 Injection Molding

The Arburg 320C injection molding machine adopted for the MIM process with a low compression screw ($\varnothing 20$ mm) was used in injection experiments. The feedstock was plasticized by using the constant values of the screw speed of 30 rpm and the back pressure of 30 bar, while the barrel temperatures from the feeding zone to the nozzle were 160 °C, 170 °C, 180 °C and 190 °C. The cooling fluid

temperature of 115 °C was maintained by two "Regloplas" tempering units, where two insulating plates were placed at the tool/machine interface to improve temperature uniformity.

The injection velocity and the holding pressure profile are variables used in injection experiments. Both of them have the influence on the green part density [10-12] and consequently, on the dimensions after sintering [13]. The choice of parameters' variation ranges was based on the mold filling study, where the main criteria was to produce defect free green parts.

At first, the runner system was filled with 10 cm³/s, then velocity was reduced and varied in range from 5 to 7 cm³/s to avoid excessive shear heating in the gates area. The cavities were continued to be filled under reduced velocity until the switchover volume was reached. Then, the achieved injection pressure (with an average value of 1300 bar) was rapidly reduced to the packing phase of the initial pressure of 850 bar in 0,05 sec. Afterwards, the packing pressure was changed by using the rump-down (800 to 850 bar) and rump-up (850 bar to 900 bar) profiles, Fig. 3. It was found that the holding time of 2.1 sec was sufficient to assure gate crystallization (sealing) and prevent the back flow effect.

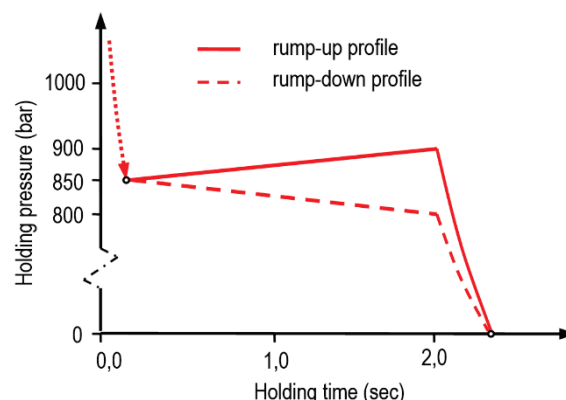


Figure 3 Holding pressure profiles used in injection experiments: "Rump-down" linear profile from 800 to 850 bar and "Rump-up" linear profile from 850 to 900 bar

Twenty injection cycles were performed between each parameter's change to assure that the parameters' change affected the process.

2.3 Debinding and Sintering

The green parts were placed on ceramic Al₂O₃ plates to prevent the diffusion between the samples and the supporting molybdenum shelves. Afterwards, the debinding process was performed in an Elnik 3002 CE oven at a temperature of 110 °C in a HNO₃ rich atmosphere (> 98%), according to the BASF process. The oven was supplied with 500 l/h pure nitrogen during the entire cycle. This catalytic debinding technique assured very fast binder degradation from the surface to the green parts' core. After debinding, the brown parts were replaced in an Elnik batch water cooled furnace MIM_3002, where one step thermal debinding and sintering took place. The density of the N₂ atmosphere lowered via the partial pressure of 400 mbar assuring the laminar flow over

the components' surface and temperature uniformity during the process. At first, the back-bone polymer (polyolephin) was completely burned in one hour at 600 °C, then sintering was performed in three hours at 1310 °C. The temperatures in six different furnace zones were kept in range from ± 3 to ± 7 °C during the sintering cycle.

2.4 Evaluation of the Sintered Parts

After sintering, the characteristic dimensions: the width (H), inner diameter (ID) and outer diameter (OD) were measured by a Coordinate Measuring Machine (CMM). For the purpose of the analysis, three sintered components per cavity (upper cavity 1 and lower cavity 4, Fig. 1a) were selected from the components' groups produced by using six different molding conditions. The average variation coefficients of sintered dimensions obtained with the same molding conditions were below 0.1%.

3 RESULTS AND DISCUSSION

To compare the results obtained by using different holding pressure profiles, the means with the \pm standard deviation (SD) for the part width, inner and outer diameter after sintering vs. the injection velocity were plotted on bar graphs.

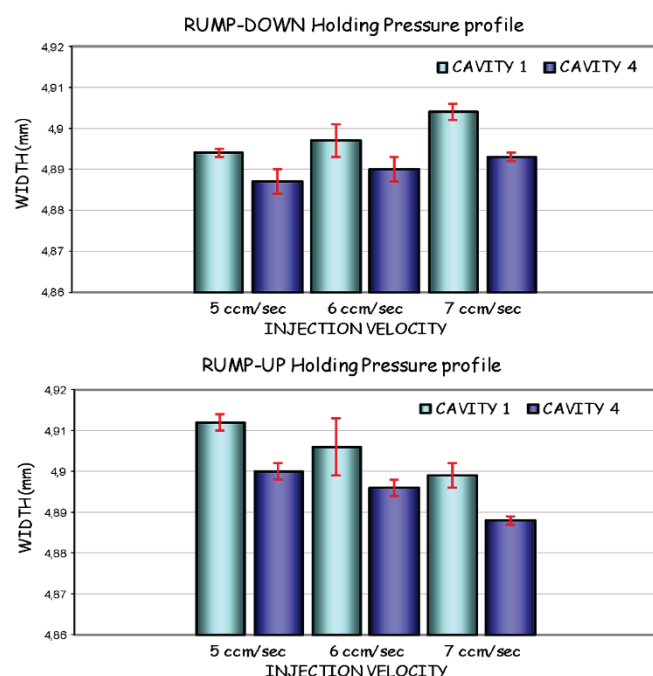


Figure 4 Sintered widths (mean \pm SD) obtained with a rump-down and rump-up holding pressure profile

The injection velocity and H correlation were a strong positive when the rump-down profile was used, with ($r = 0.887$; $p = 0.001$) for cavity 1 and ($r = 0.81$; $p = 0.008$) for cavity 4. However, with the rump-up profile, this correlation became a strong negative with ($r = -0.832$; $p = 0.005$) for cavity 1 and ($r = -0.959$; $p = 0.000$) for cavity 4, Fig. 4. Similar results were obtained for the correlation between the

injection velocity and OD after sintering. Namely, a very strong positive correlation for cavity 1 ($r = 0.825$; $p = 0.006$) and a strong positive for cavity 4 ($r = 0.696$; $p = 0.037$) were observed when the rump-down profile was used.

However, when the rump-up profile was used, this correlation was a moderate negative for cavity 1 ($r = -0.487$; $p = 0.183$) and a strong negative for cavity 4 ($r = -0.787$; $p = 0.012$), Fig. 5.

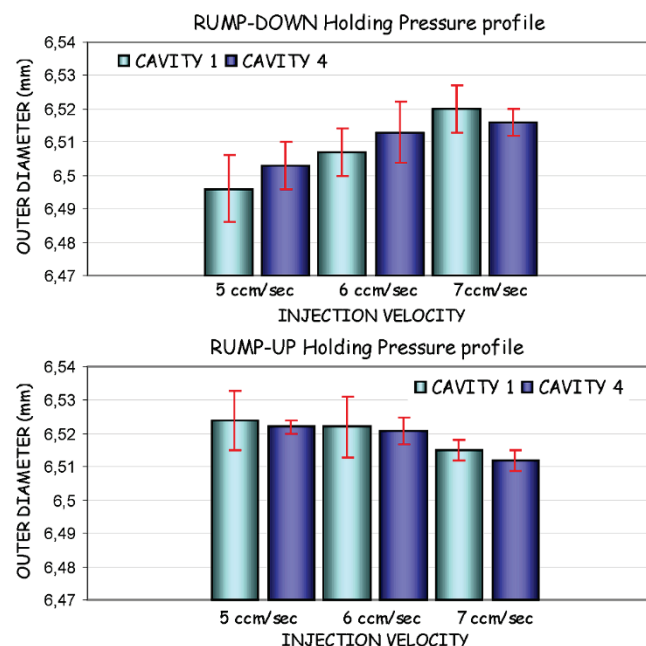


Figure 5 Sintered outer diameters (mean \pm SD) obtained with a rump-down and rump-up holding pressure profile

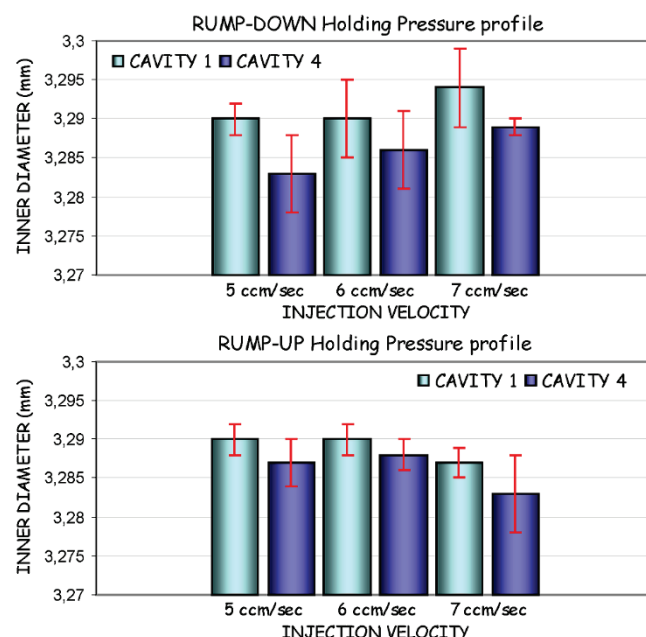


Figure 6 Sintered inner diameters (mean \pm SD) obtained with a rump-down and rump-up holding pressure profile

As for the inner diameter, the direction of obtained the relationship was the same, but with a moderate correlation for both cavities, Fig. 6.

The results showed that the average dimensions after sintering were positively correlated with the injection velocity when the rump-down holding pressure was used. As the injection velocity increases, the amount of shear heating, which is proportional to the square of the shear rate, also increases. Since the shear heat cannot be fully conducted away through the tool, the melt temperature rises. When the melt temperature is higher, the time until the gate has crystallized (effective packing time) is longer. Moreover, the higher the injection velocity is, the more intensive the packing will be. Subsequent packing pressure decreases from 850 bar to 800 bar, according to the MIM feedstock PVT characteristic, the binder crystallization temperature shifts toward lower values, causing additional prolongation of the effective packing time. The prolonged effective packing time due to the injection velocity increases and the holding pressure decrease is responsible for the obtained positive correlations.

However, in clear contrast with what we observed with the rump-down profile, the correlations became negative when the rump-up holding pressure profile was used. This can be explained by the pressure influence on binder crystallization. Namely, the holding pressure increases the shifts of the feedstock crystallization temperature toward higher values when the solid loading is sufficiently decreased [9]. Higher crystallization temperature causes earlier gates' sealing and consequently, the reduction of the effective packing time. Shear heating and powder segregation in the runner system with the velocity led to the lowering of the feedstock solid loading, which is the prerequisite for such feedstock behavior.

4 CONCLUSION(S)

The Catamold 310N feedstock batch-to-batch shrinkage factor variation range (± 0.004) produces the variation of the sintered part dimensions from the nominal of about $\pm 0.34\%$. This variation and inevitable machining error of the cavities consume almost the entire MIM tolerance budget without taking into account the variation induced in the processing steps. Producers relying on commercial feedstock do not have the ability to adjust the shrinkage factor by changing the feedstock formulation. Thus, to maintain the narrow part' tolerances, they often have to rework the mold cavities for new batches or they have to introduce post-sintering operations.

The results presented in this research prove that the input process variables – injection velocity and holding pressure – could be used to systematically control the shrinkage factor in MIM. Namely, the results showed the shrinkage factor decrease with the velocity for all dimensions with an average value of 0.002 mm/mm, after the application of the rump-down holding pressure profile from 800 to 850 bar. When the rump-up pressure profile from 850 bar to 900 bar was applied, the results showed an average shrinkage factor increase with the injection velocity of about 0.0017 mm/mm. The obtained shrinkage factor changes were evaluated as

significant since they cover about 50% of the reported batch-to-batch shrinkage range.

These findings reveal a new low cost approach to compensate for the batch-to-batch shrinkage factor variation and the variation due to the reuse of feedstock that could be valuable for MIM parts' producers who rely on commercial feedstocks.

5 REFERENCES

- [1] Martin, M. (1999). Powder Injection Moulding of Metals, Ceramics and Metal Matrix Composites. *Materials World*, 7(2), 71-75.
- [2] Bilovol, V. V. (2003). Mold filling simulation during powder injection moulding. *PhD Thesis*, Delft University of Technology, delft, Netherlands.
- [3] Kim, C. (2001). Migration in concentrated suspension of spherical particles dispersed in polymer solution. *Korea-Australia Rheology Journal*, 13(1), 19-27.
- [4] German, R. M. (2004). Green Body Homogeneity Effects on Sintered Tolerances. *Journal Powder Metallurgy*, 47(2), 157-160. <https://doi.org/10.1179/003258904225015563>
- [5] Luo, T. G., Qu, X. H., Qin, M. L., & Ouyang, M. L. (2009). Dimension precision of metal injection molded pre tungsten. *International Journal of Refractory Metals & Hard Materials*, 27(3), 615-620. <https://doi.org/10.1016/j.jrmhm.2008.10.003>
- [6] German, R. M. (1996). Statistical analysis of shrinkage variation for powder injection molding. *Journal of Material Processing Technology*, 59, 278-284. [https://doi.org/10.1016/0924-0136\(95\)02158-2](https://doi.org/10.1016/0924-0136(95)02158-2)
- [7] Cucarella, M. C. M. (1982). Effects of high pressure on polymer crystallization. *Latin American Journal of Metallurgy and Materials*, 2(1).
- [8] Hausnerova, B., Sedlacek, T., Slezak, R., & Saha, P. (2006). Pressure dependent viscosity of powder injection moulding compounds. *Rheol Acta*, 45, 290-296. <https://doi.org/10.1007/s00397-005-0036-4>
- [9] Chandra, A., Best, A., Meyer, W. H., & Wegner, G. (2009). P-V-T measurements on PMMA: PbTiO₃ polymer-ceramic composites with tunable thermal expansion. *Journal of Applied Polymer Science*, 115(5). <https://doi.org/10.1002/app.29819>
- [10] Petera, P. (2012). Holding pressure and its influence on quality in PIM technology. *Acta polytechnica*, 52(4). https://doi.org/10.17973/MMSJ.2012_07_201208
- [11] Islam, A., Hansen, H. N., & Rasmussen, T. T. (2013). Effects of holding pressure and process temperatures on the mechanical properties of molded metallic parts. *ANTECH 2013 Conference Proceedings*, Society of Plastic Engineers Incorporated.
- [12] Tseng, W. J. (1988). Statistical analysis of process parameters influencing dimensional control in ceramic injection molding. *Journal of Material Processing Technology*, 79(1-3), 242-250. [https://doi.org/10.1016/S0924-0136\(98\)00019-3](https://doi.org/10.1016/S0924-0136(98)00019-3)
- [13] Green, C. D. & Heaney, D. F. (2007). The PVT effect on final sintered dimensions of powder injection molded components. *Materials and Design*, 28, 95-100. <https://doi.org/10.1016/j.matdes.2005.05.023>

Authors' contacts:

Emir Šarić, PhD, Associate Professor
University of Tuzla,
Faculty of Mechanical Engineering,
Univerzitetska 4, 75000 Tuzla, Bosnia and Herzegovina
E-mail: emir.saric@untz.ba

Samir Butković, PhD, Associate Professor
University of Tuzla,
Faculty of Mechanical Engineering,
Univerzitetska 4, 75000 Tuzla, Bosnia and Herzegovina
E-mail: samir.butkovic@untz.ba

Muhamed Mehmedović, PhD, Associate Professor
University of Tuzla,
Faculty of Mechanical Engineering,
Univerzitetska 4, 75000 Tuzla, Bosnia and Herzegovina
E-mail: muhamed.mehmedovic@untz.ba

Influence of the Varnishing "Surface" Coverage on Optical Print Characteristics

Tomislav Hudika*, Igor Majnarić, Tomislav Cigula

Abstract: Varnishing is often used to protect or decorate the print, but it can also influence the print's colour appearance. Therefore, varnishing should enhance the print role, while colour change should be kept as low as possible. The aim of this paper is to evaluate inkjet UV LED varnishing by estimating optical print characteristics. Prepared offset prints were UV LED varnished in different surface coverage values (SCV) with a matte and gloss finish. The prints were evaluated by measuring gloss and colour coordinates. Secondly, varnishing was performed in a different SCV, which enabled assessing the optimal SCV, i.e. the most cost-efficient varnishing. The printing process was conducted in a standardized and controlled laboratory environment, regulated via the ISO 12647-2:2013 norm to ensure that the black colour was reproduced in the standard tolerance. The results showed that the colour difference is negligible (stays in the ISO tolerances), regardless of the varnishing SCV. On the other hand, the optimal printing gloss is at the SCV of 100%.

Keywords: colour difference (ΔE); inkjet; offset printing; print gloss; UV LED; varnishing

1 INTRODUCTION

The visual effect of segmental varnishing is becoming an increasingly desirable feature in the graphic industry. The initial usage of varnishing was to protect products. Today, almost every product, from commercial to personalized items, includes some type of varnishing. In terms of design, varnish is applied to the majority of products to increase their value by enhancing their visibility or to personalize the product for a customer. Varnishing could be, to some extent, conducted with most printing techniques, including screen printing, flexography, standard offset printing, drip-off offset systems and inkjet digital printing [1].

As the market leader in printing, offset printing is continuously developing so that it would remain at the top. The printing presses in offset printing have significantly improved their automatization, shortened the changeover time and various add-ons which enable customers to apply certain special effects, such as varnish, on the print in one go. On the other side, these highly productive printing presses include a higher price, workspace size and complexity, which is why other printing techniques are also developing.

One of the digital techniques which could be used for various applications is inkjet printing. Inkjet printing uses nozzles to spray ink in the form of a droplet which forms dots on the substrate's surface and therefore creates an image. Depending on the technological solution, it can print continuously or via "drop-on-demand", where it uses the UV curing technology (mercury vapor or LED).

Moreover, with inkjet, one can also print various varnish types, including the UV LED, in one or more layers, which gives the customer the possibility of relief on the print. When it comes to the market value, it is estimated that digital printing will grow from 21.35 Billion USD (2018) up to 33.49 Billion USD (2026). Hence, one must perceive it as a serious contender in the printing market [2, 3]. One of the reasons for this growth is a potential hybrid, where inkjet is used to print the added value (printed electronics, various coatings) over the standard offset-printed image. Some researchers have already made some research with the UV

LED overprinting varnishes (OPVs) by printing varnish in a pattern, which resulted in a conclusion that gloss may influence the print colour and that the substrate surface has a great impact on the varnish finish in terms of gloss [4, 5]. The purpose of this research is to determine the influence of the UV LED OPV on the offset prints that would be in accordance with the ISO 12647-2:2013 norm. Additionally, the research should give more insight on the relationship between the optical print characteristics and the varnishing tonal value.

1.1 UV LED Inkjet Varnishing Technology

Inkjet, as a printing technique, has the ability to print out layers by using only varnish. In the process of segmental UV LED varnishing by the means of inkjet printing machines, a thin transparent layer is formed on the surface of the desired substrate [6]. Varnishing could be done with a gloss and matt finish with the same varnish. The finishes are done by using a different light energy emission for curing. In the case of UV inks or varnishes, curing is performed by the photo-initiators' change under the UV light.

Varnish is composed of 10-20% acrylic amine synergist, 25-35% hexamethylene diacrylat hexane 1.6 diol diacrylate, 30-40% acrylic ester, 10-20% photosensitive monomers, 5-15% derivatives based on phosphine oxides [7]. The principle of inkjet printing is the same for colour printing and varnishing, i.e. the ink or varnish droplet forms a layer on the printing substrate. The formation of printing areas is performed by ripping the image via FM screening and transferring a binary image onto the substrate [8].

Overprint varnishes (OPVs) are coatings applied over the already printed substrate for the reasons of protection, decoration, gloss enhancement, stain resistance, security purposes, resistance to discoloration, etc. The UV LED varnish is basically a UV LED ink without the pigments that has the possibility to change its finish by applying different light energy for curing. One can also do textured OPVs with the use of different patterns and layer thickness. OPVs can be used with any printing technique and by means of all curing

types such as UV LED, oxypolymerization, air drying, IR curing etc. [9]. UV varnishes or inks do not evaporate or demand a high amount of solvents and due to these factors, they have great light, wear and temperature resistance to outer factors.

2 EXPERIMENTAL

The proposed research was conducted on samples prepared by combining two printing techniques, conventional offset printing with the printability tester and inkjet varnishing.

2.1 Materials

The printing substrate used in this research was the *WFC* gloss fine art paper 300 g/m², which is commonly used in commercial printing and packaging. Optical characterization of the substrate was first performed by measuring the gloss value and colorimetric coordinates.

The black ink (SUNCHEMICAL SUNLIT EXPRESS PROCESS BLACK) was printed on the substrate by the means of the PRÜFBAU multipurpose printability tester MZ II. The PRÜFBAU multipurpose printability tester MZ II is a laboratory printability tester which enables printing in defined conditions with low amounts of printing materials.

The printing conditions were the ink amount - 0.15 cm³, the printing speed - 1 m/s and the printing pressure - 150 N/cm². The prints were in accordance with the ISO 12647-2:2013 norm ($\Delta E_{ab} \leq 5$). Ink was applied with a micro pipette into the distribution system of the unit (the rubber-metal roller system with rotational and axial movement) with the spread of 30 seconds in order to get an even ink film which would be transferred to the printing roller. Printing was performed after the substrate was conditioned for 24 hours in a room with a temperature of 21 ± 1 °C and relative humidity of 50 ± 5 %, which is common in printing processes [8].



Figure 1 Digital printing form

The printed samples were then optically characterized by the measuring printing gloss and colorimetric coordinates. For the needs of the varnishing evaluation, the digitalized printing form is used, which includes a full tone patch and lines in positive and negative (Fig. 1). The digitalized printing form was before the varnishing process ripped in the

surface coverage of 60%, 70%, 80%, 90%, 100%. The 200% surface coverage was made as two overprints of the 100% printing form.

The digitalized printing forms (various surface coverage) were printed as an inkjet OPV by ROLAND VERSAUV LEC 300. The difference between the gloss and matte finish is in the UV drying technique, where to get the matte finish, UV drying receives a different energy than its gloss counterpart.

The matte finish requires two sets of UV LED lamps in which the first lamps cure the varnish, while the second lamps destroy the remaining cross-links in the polymer and create micro cracks in the surface. This is a common phenomenon in flexography plate making when the polymer is overexposed to the UV light. [4].

A total of 24 samples were prepared for this experiment. Samples were separated into four groups of six pieces denominated as WG (samples without black ink with a gloss finish), WM (samples without black ink with a matte finish), BG (samples with black ink and a gloss finish) and BM (samples with black ink and a matte finish). The samples in the group are denominated with the numbers 60 – 200 that come from the surface coverage of the ripped digital printing form.

3 MEASURING METHODS

The evaluation of samples was performed by using optical methods and by visual evaluation of microscopic images.

3.1 Optical Measurements of Paper, Prints and Varnished Samples

In order to assess the colorimetric characteristics of the prepared samples, the CIE $L^*a^*b^*$ values were measured by the reflective spectrophotometer X-rite eXact. The used spectrophotometer is compliant to the ISO 5-4:2009 norm. Measurement conditions were 0/45° geometry, 2° standard observer, D50 illuminant and M1 measuring filter.

The results of measurements were transferred to the computer and the colour difference was calculated according to the ΔE_{00} equation. Each sample was measured ten times. [10]

3.2 Print Gloss Method

The prepared samples, as well as the plain paper substrate (without varnishing or printed ink), were measured by using a glossmeter that measures the reflective glare in which light intensity is measured over a range of reflected angles. The intensity of the reflected light depends on the material and the angle used for illumination [11]. The remaining part of light that does not reflect is absorbed or diffuses per impact [12].

In this research, the Elcometer 407 glossmeter (measuring 60° geometry) was used for the measurements ('Statistical Glossmeter Operating Instructions', n.d.). Each

sample was measured ten times before UV varnishing and after it. Gloss was measured at the angle of 60°. [11, 13].

3.3 Microscopic Analysis of the Elements

A microscopic varnish element analysis was performed by means of the Leica DM 2500 microscope in order to assess the transfer of elements (positive and negative lines and text) that were printed in varnish with a gloss and matte finish. After taking the microscopic images at the enlargement of 25 \times , they were visually assessed.

4 RESULTS AND DISCUSSION

Every measuring method was performed ten times after which the average values and standard deviation were calculated.

4.1 CIE $L^*a^*b^*$ Coordinates and Colour Difference

In Figs. 2 – 4, one can see the colour coordinates of the evaluated samples. The dots in the diagrams are average values and the error bars represent the standard deviation of measurements.

One can observe that varnishing in both the gloss and matte finish acts as an overtop layer that makes the under image slightly darker (Fig. 2). With an increase in surface coverage, the values of the varnishing of the lightness do not substantially decrease.

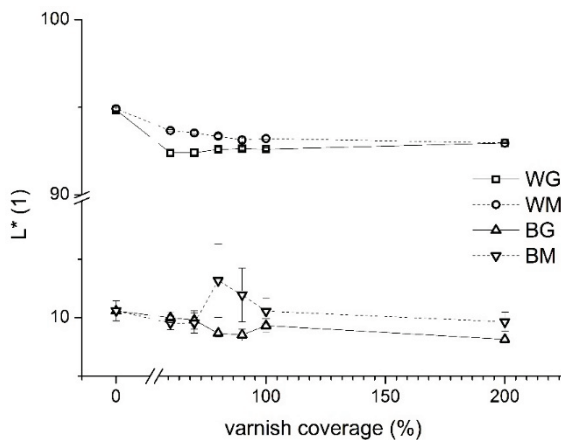


Figure 2 L^* coordinate of the evaluated samples

One can also see that the standard deviation of the printed samples (BM and BG) is higher than the one of the paper samples (WG and WM). This behaviour is probably due to the high lightness of paper samples. Additionally, the highest deviation of the results is on the printed samples with a matte varnish finish (BM). This effect can be a result of light refraction due the micro surface roughness of the matte finish (Fig. 3) with the usage of the FM screening technique that was used in inkjet varnishing within this case [14, 15].

Moreover, varnish is applied via inkjet in the form of a droplet which, especially in the case of TV/surface coverage lower than 100 %, is shaped as a dome on the surface. This could lead to distortion in the reflected light [16] and

therefore influence the measuring process, i.e. the measuring results.

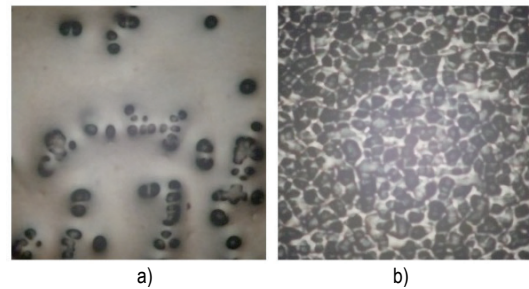


Figure 3 Varnished surfaces printed with a 100% surface coverage value on a black solid with a gloss (a) and matte (b) finish enlargement of 25 \times .

In the case of a^* and b^* coordinates (Figs. 4 and 5), one can see that on the researched samples, varnishing causes a very small colour shift. Apart from the BG (a printed sample with a gloss finish varnish), all samples show the same pattern – the b^* coordinate increases when applying varnish with a surface coverage value of 60 % and the values then drop.

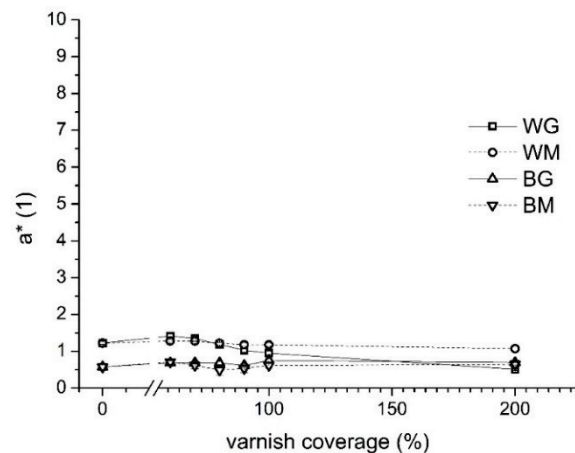


Figure 4 a^* coordinate of the evaluated samples

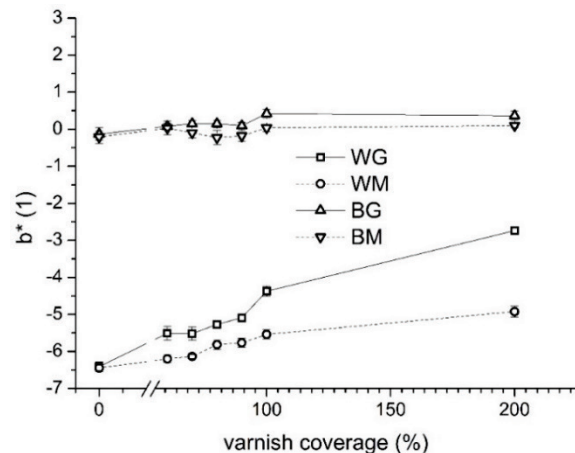


Figure 5 b^* coordinate of the evaluated samples

Although the paper and black print should be near the lightness axis (a^* and b^* near 0), it can be seen that there is a large difference between the paper and black print in the b^*

coordinate. Furthermore, opposite to the influence of the surface/tonal value of varnishing on the a^* coordinate, adding varnish on the surface causes an increase of the b^* coordinate on all researched samples (Figs. 4 and 5).

The varnish shifted the sample colour into the yellowish area, which is a common issue with all varnishing techniques. These results show that the usage of inkjet UV LED leads to the same issue and it cannot be avoided or decreased with lower surface coverage values.

Additionally, increasing the surface coverage of the varnish applied on the unprinted samples (WG and WM) causes a high increase of the b^* coordinate. This could be due to the fact that varnish layers the filters and blocks the operation of optical brighteners [17].

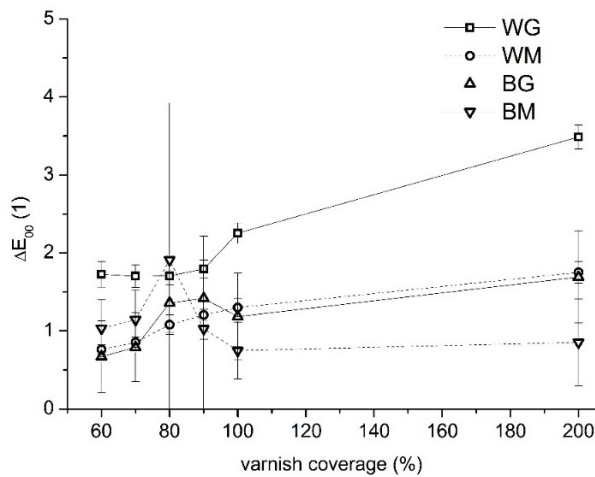


Figure 6 ΔE diagram

In the case of ΔE_{00} , both the gloss and matte finished samples show the same trend. Generally, the colour difference increases with the increase of the surface coverage of the applied varnish (Fig. 6). Nevertheless, the calculated colour difference is on all samples (except the WG-200) under three, which is almost not visible by the human eye [10].

4.2 Print Gloss

Gloss enhancement or the matt finish effect, as described in the text above, are the most important visual reasons why varnishing is being done onto printed samples. As expected, gloss finished samples have a gloss value peak when varnishing with a surface coverage of 200%. It can also be seen that on the black printed sample, the difference between varnishing with a surface coverage value of 100 or 200 % results with nearly the same gloss value, which is why double varnish consumption is not affordable. A high difference between gloss on the BG-90 and BG-100 can be linked to the fact that at 100% TVI, the surface is fully covered with varnish and therefore higher light reflection is caused [14].

On the other hand, the matte effect causes the gloss value to drop significantly on the black printed sample (BM), as the pattern of the matte finish, which is visible in Fig. 3b, has more cracks than the ink film itself.

As opposed to the ink film, the paper substrate has certain irregularities on the surface, which at higher surface coverage values of varnishing ((90 and 100 %) are mostly covered resulting with higher gloss value (Fig. 7). Doubling the varnish amount (varnishing with the tv/coverage of 200%) could be justified in the case of the paper substrate as the gloss value is lower than on the unvarnished sample (however, covering the surface would mean protecting the surface), but would not be affordable for the black printed sample.

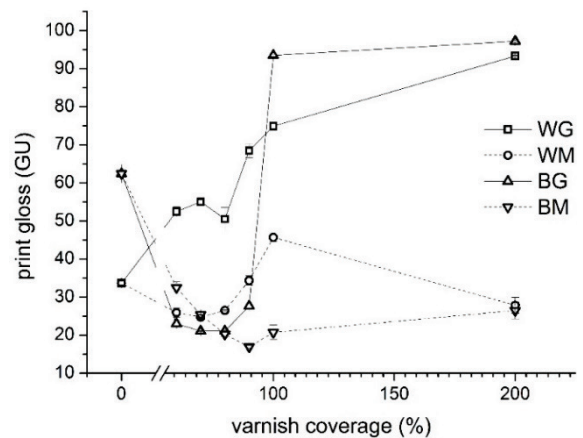


Figure 7 Gloss on the surface

4.3 Microscopic Varnish Elements' Analysis

The analysis of the elements printed with varnish was performed on the numbers 0 and 1 of the 6pt font size and a positive line with the width of 0,25 mm. These elements were chosen as they include elements with the areas in the direction of the printing head and other angles. The goal was to evaluate the surface appearance of the small elements and their applicability in the pattern varnishing with a smaller surface coverage and a surface finish (gloss or matte). The microscopic images are presented in Fig. 8, where numbers by rows denote the surface coverage value of varnishing, while the letters under columns denote a sample group.

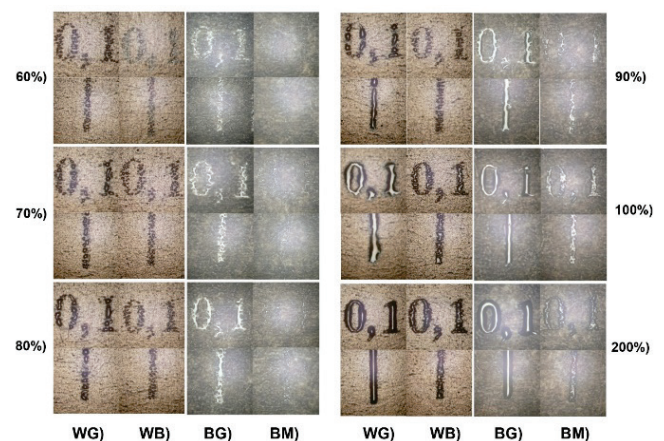


Figure 8 Microscopic images of the varnish printed elements (enlargement of 25x)

One can see that on the gloss finished samples, both on the paper substrate and black printed substrate, varnish printed elements are clearer to see than on the matte ones (Fig. 7). Moreover, it can be seen that on the black printed samples, varnish elements with a matte finish are not even visible if varnishing is conducted with a surface coverage under 90%. The gloss finish reflects the light in a way that creates a natural shadow which visually appears as an outline around the varnish printed element, creating a contrast which will differentiate the elements from the surface. In matte finish samples, the varnished area surface has a bigger amount of micro surface roughness that significantly distorts the light [4, 9, 14].

Assessing the printed pattern, one could clearly recognize the varnish printed elements on the printing substrate and the black printed sample when varnishing with a 60 % surface coverage, but the effect of the gloss is noticeable when varnishing with at least a 90% surface coverage.

On the other hand, the varnish printed elements with a matte finish are recognizable by 70% varnishing on paper and 100% varnishing on the black printed substrate. Varnishing with 200% decreases the glossy effect on the paper substrate, while it enables clearer varnish printed elements on the black printed substrate.

5 CONCLUSIONS

This research was conducted in order to research the usability of the UV LED inkjet varnishing in adding value to the prints produced in a conventional printing technique (offset). The prepared samples were optically characterized to see if there are any optical differences caused by the varnishing process. Furthermore, the evaluation of the different amounts of varnish and the application of pattern varnishing was also performed.

The results showed that the UV LED varnishing causes small colour differences which are in most cases not visible to the human eye. On the other hand, gloss measurements showed that varnishing with a gloss finish significantly increases gloss values on the substrate and the printed ink film.

Regarding pattern printing, it could be concluded that the use of lower amounts of varnish by applying varnish as a FM screen in coverage/tonal values lower than 100% will result with good results in the matte finish varnishing. On the other hand, if the print has to have a high gloss value due to the screening pattern, one must varnish in a 100% coverage value, but the double amount (a surface coverage of 200 %) is not affordable as it increases the print's gloss value by a few GU.

Additionally, it has been noticed that the handling of samples that were to be varnished caused some problems as any contamination of the surface, such as the ones from hand grease, creates patterns on the varnish film that are visible.

To conclude, varnishing with the UV LED technology would not be recommended as an offline process, but it could be useful as an inline hybrid technology as it offers more variations in varnishing processes (varnish amount, varnishing pattern) in comparison to conventional technologies.

6 REFERENCES

- [1] Kipphan, H. (2001). *Handbook of Print Media*. Berlin, Germany: Springer-Verlag Berlin, 45-60. <https://doi.org/10.1007/978-3-540-29900-4>
- [2] Smyth, S. & Smithers, P. (2017, April 13). Digital Printing to Continue to Take Market Share from Offset Presses. Retrived from https://www.inkworldmagazine.com/issues/2017-05-01/view_experts-opinion/digital-printing-to-continue-to-take-market-share-from-offset-presses/
- [3] Digital Printing Market Size, Share, Trends, Opportunities And Forecast. (2018, April) Retrived from <https://www.verifiedmarketresearch.com/product/digital-printing-market/>.
- [4] Majnaric, I., Bolanca Mirkovic, I., Birta, A., & Mustac, S. (2013). The Influence of the Extreme Thick Applied Layers of Varnish on Color Properties of LED UV curing inkjet prints. *AIC Color 2013*, 1269-1272.
- [5] Dolic, J., Pibernik, J., & Majnaric, J. (2014). Influence of UV Varnish pattern effect on Print Quality. *J. Imaging Tecnol.*, 58(6), 060501-060509. <https://doi.org/10.2352/J.ImagingSci.Technol.2014.58.6.060501>
- [6] Yang, L. (2003). Ink-Paper Interaction: A study in ink-jet color reproduction. *Dissertation*, Linkoping Studies in Science and Technology, no. 806, 21-28.
- [7] Magdassi, S. (2010). *The Chemistry of INK jet inks*. Singapore, World Scientific Publishing Co., 161-177.
- [8] Krizmanic, K., (2010). Kvalitativne Karakteristike digitalnog i konvencionalnog ofsetnog tiska. *Master thesis*, University of Zagreb, Faculty of Graphic Arts, 7-12. (in Croatian)
- [9] Majnaric, I., Golubovic, K., & Bolanca Mirkovic, I. (2012). New methods of varnishing and their influence on optical properties of cardboard packaging. *Matrib 2012 Book of abstracts*, Vela Luka, Croatia, 179-189.
- [10] Sharma, G., Wu, W., & Dalal, M. (2005). The CIEDE2000 color-difference formula: Implementation notes, supplementary test data, and mathematical observations. *Color Res. Appl.*, 30(1), 21-30. <https://doi.org/10.1002/col.20070>
- [11] Nadal, M. & Thompson, A., (2000). New Primary Standard for Specular Gloss Measurements. *Journal of Coatings Tecnology*, 72(991), 61-66. <https://doi.org/10.1007/BF02720526>
- [12] Hunter, R. S. (1934). Methods of determining gloss. *J. Res. Natl. Bur. Stand.*, 30(1), 28-29.
- [13] Elcometer Lim. (2009). *Statistical Glossmeter Operating Instructions*, instruction manual 406L.
- [14] Karlović, I. & Novaković, D. (2011). Effect of Different Coating Amounts on the Surface Roughness and Print Gloss of Screen Coated Offset Prints. *J. Imaging Sci. Technol.*, 55(2), p. 020501. <https://doi.org/10.2352/J.ImagingSci.Technol.2011.55.2.020501>
- [15] Car, I., Majnaric, I., & Lozo, B. (2018). Colorimetric Changes Caused by UV Varnishing. In *CIGT 2018*, 37-40.
- [16] Macinic, D. (2011). Utjecaj efekta lakiranja na optička svojstva otisaka. *Master thesis*, University of Zagreb, Faculty of Graphic Arts. (in Croatian)
- [17] Majnaric, I., Bolanca Mirkovic, I., & Golubovic, K. (2012). Influence of UV curing varnish coating on surface properties of paper. *Technical Gazette*, 19(1), 51-56.

Authors' contacts:

Tomislav Hudika, mag. ing., Research Assistant
(Corresponding author)
Department of Graphic Materials and Printing Forms,
Faculty of Graphic Arts, University of Zagreb,
Getaldićeva 2, 10000 Zagreb, Croatia
Tel: +385 (0)1 23 71 080
thudika@grf.hr

Igor Majnarić, PhD, Associate Professor
Department of Printing Processes,
Faculty of Graphic Arts,
University of Zagreb,
Getaldićeva 2, 10000 Zagreb, Croatia
Tel: +385 (0)1 23 71 080
imajnaric@grf.hr

Tomislav Cigula, PhD, Assistant Professor
Department of Graphic Materials and Printing Forms,
Faculty of Graphic Arts, University of Zagreb,
Getaldićeva 2, 10000 Zagreb, Croatia
Tel: +385 (0)1 23 71 080
tcigula@grf.hr

Image Artefacts in Industrial Computed Tomography

Amalija Horvatić Novak*, Biserka Runje, Zdenka Keran, Marko Orošnjak

Abstract: Computed tomography is a method that has been used for many years in medicine and material analysis, and recently it has also been introduced in dimensional measurements. The method has a lot of advantages compared to other 3D measurement methods, with the largest one being the possibility to perform a non-destructive measurement of an object's inner geometry. However, it is a complex method with a large number of parameters that influence measurement results. Some of these parameters are image artefacts that occur in the scanning and reconstruction process. An artefact is any artificial feature which appears on the CT image, but does not correspond to the physical feature of an object. In order to achieve metrological traceability, it is necessary to eliminate and minimize the influence of image artefacts on measurement results. This paper presents and explains image artefacts in industrial computed tomography as the consequences of different influence parameters in the CT system.

Keywords: computed tomography; dimensional measurements; image artefacts

1 INTRODUCTION

Computed tomography (CT) is one of the three-dimensional methods used in dimensional measurement. The method uses the nature of an X-ray to measure both the outer and inner objects' structures and geometries. The method was developed by Godfrey N. Hounsfield and Allan M. Cormack in the 1960s. The method was firstly used in medicine, where it still has great applicability and significance. Later on, the method was applied in material science, and in the last few decades, it has also found its application in dimensional metrology. Given the aforementioned, computed tomography can be divided into two groups – medical computed tomography and industrial computed tomography. Medical and industrial computed tomography differ in several components, such as radiation doses, the kinematic system, the method of scanning, and related to that, the performance of CT scanners. Fig. 1 shows a medical and industrial CT scanner.



Figure 1 CT scanner: a) medical CT scanner [1], b) industrial CT scanner

In industrial CT scanners, the object rotates during the scanning process, while the X-ray source and detector either move vertically (in line beam CT scanners) or do not move (in cone beam CT scanners). In medical CT scanners, patients are translated horizontally through the ring where the X-ray source and the detector are placed. In this paper, special emphasis is placed on industrial computed tomography.

Computed tomography is a method with a lot of advantages, for example:

- the possibility to measure and analyse inner objects' geometries in a non-destructive way
- the inspection of individual parts in assemblies
- the possibility of conducting many different analyses with one scan (e.g. the pore and inclusion analysis, analysis of polymer fibre orientation, dimensional measurements)
- suitable for deformable, reflective, transparent materials
- application in reversible engineering, etc.

However, it is a complex system where the process of dimensional measurement can be divided into three subprocesses: the subprocess of CT scanning, the model reconstruction subprocess and the subprocess of performing the analysis on the obtained 3D model, here the analysis of dimensional measurements (Fig. 2).

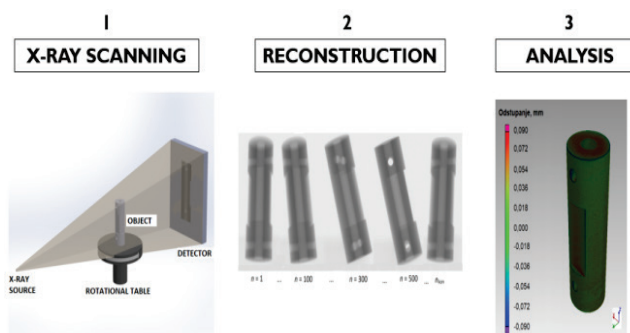


Figure 2 CT measurement process

The first subprocess, CT scanning, is conducted in CT scanners. CT scanning involves collecting the data generated by a passing X-ray through the object during its rotation on a rotational table for at least one cycle of rotation. In the process, the detector captures the remaining radiation which is attenuated while passing through the object and it records them in the form of a large number of 2D records.

Each 2D record corresponds to the image of the object taken from a specific angle. The next step includes the reconstruction of a 3D model from the captured 2D images. The reconstruction process is based on a filtered

backprojection. Since reconstruction includes processing a lot of information, a powerful computer configuration with adequate software support is required. The result of image reconstruction is a voxel model with different greyscale values. Voxel is a three-dimensional pixel. The final sub-process in the CT dimensional measurement involves the process of analysing and measuring features on the reconstructed 3D model.

Dimensional measurement with the use of computed tomography represents a complex system with a large number of influencing parameters. With the aim to achieve metrological traceability, all influencing parameters should

be identified and corrected. Until today, many different classifications of influencing parameters in CT dimensional measurements have been proposed. One of the classifications suggests the division of the influencing parameters according to the subprocess in which they occur [2]. Consequently, influencing parameters can be divided into: parameters influencing the scanning process, parameters influencing the reconstruction process and parameters influencing the measurement process. Fig. 3 shows the influencing parameters classified according to the subprocess in which they occur.

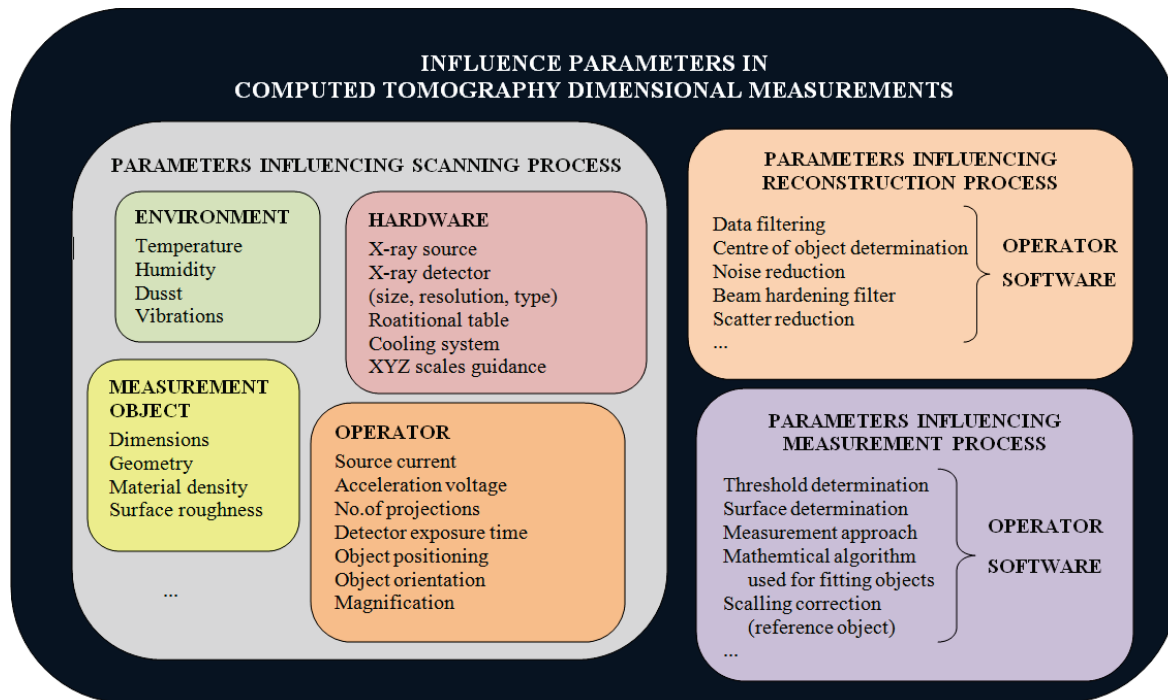


Figure 3 Classification of influencing parameters in computed tomography [2].

This paper present and explains image artefacts as the consequences of different influencing parameters in the CT system. According to the international standard ISO 15708-1, an artefact is any artificial feature which appears on the CT image, but does not correspond to the physical feature of an object [3]. Image artefacts mostly appear as apparent gradient changes inside homogeneous materials or as apparent darker or lighter lines between materials of different densities which do not exist in the object. These artefacts have a considerable influence on the greyscale profile and hinder the determination of an optimal greyscale threshold, which leads to significant deviations in measurement results [4].

2 IMAGE ARTEFACTS

During the CT scanning process, different phenomena occur as a result of: the physical nature of an X-ray, the interaction between the photons and measurement object, or imperfections of the CT scanner and its parts. These imperfections manifest as image artefacts. Given the cause of the occurrences, different authors classify artefacts in several

categories. Sun et al. [5] group artefacts in physics-based artefacts, scanner-based artefacts and computer-based artefacts. Amirkhanov et al. [6] classify artefacts in reconstruction and 3DXCT artefacts, while authors researching the use of the cone beam CT in medicine divide artefacts in physically-based artefacts, patient-based artefacts, scanner-based artefacts and motion artefacts [7, 8].

Artefacts caused by an imperfection of the CT measurement system are:

- beam hardening artefacts
- scattered radiation artefacts
- ring artefacts
- metal artefacts
- motion artefacts and
- partial volume artefacts.

The most common artefacts in cone beam CT scanning are beam hardening artefacts, scattered radiation artefacts and ring artefacts [9]. Below is an overview of the images that are generated in the process of scanning the object with the cone beam CT scanner.

2.1 Beam Hardening Artefact

Beam hardening artefacts are caused by the process of beam hardening. Beam hardening is a physical phenomenon resulting from the polychromatic nature of X-ray radiation. When X-ray beams pass through the object, photons which have less energy (softer beams) are more attenuated than those with higher energies (harder beams) [10].

During the absorption of polychromatic radiation, a nonlinear gradient of attenuation occurs during the propagation path of an X-ray through a material. However, most image processing algorithms assume a linear relationship between the propagated path and the number of photons attenuated, resulting 2D images show beam hardening artefacts, in the form of thin lines (streaks), brighter or darker edges compared to the based material also known as cupping and capping artefacts [4].

Fig. 4 shows the most significant errors of the 2D images resulting from beam hardening.

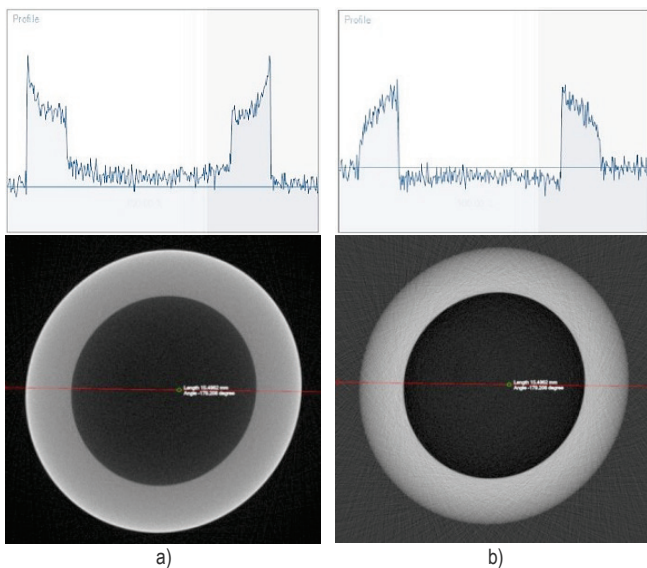


Figure 4 Beam hardening artefacts: a) cupping, b) capping.

Fig. 4a shows the error of the brighter object edges, the so-called cupping, while Fig. 4b shows the error of the darker object edges, the so-called capping. The grey value profiles shown in the figure, for the red-marked cross-sections, correspond to the cup shape in the left figure, i.e. the cup shape in the right figure.

Fig. 5 shows streak artefacts which occur in the reconstruction process of a cylinder.

The presence of beam hardening artefacts considerably affects the quality of 2D images and hinders proper determination of an object's edges. This directly affects the results of dimensional measurements [11]. Since beam hardening artefacts are considered to be one of the most significant influence parameters in CT measuring, their influence on the 2D image quality has to be eliminated or compensated. How the determination of a border between the material and background, or a border between two different

materials, influences the measurement uncertainty is explained in more detail by Lifton and Liu in [12].

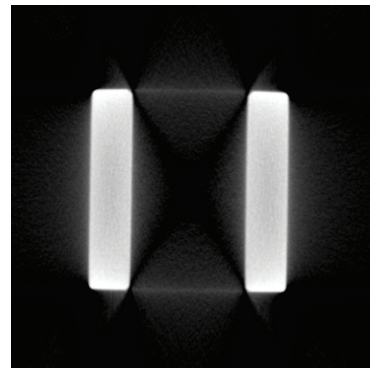


Figure 5 Streaking artefacts as a result of beam hardening

For beam hardening correction, several methods are suggested: scanning with a monochromatic X-ray, using different types of physical filters in order to limit the X-ray spectra, scanning with dual energy and using linearization methods based on polynomial curves. Moreover, authors in [13] use a polychromatic statistical image reconstruction for the reduction of beam hardening artefacts.

2.2 Scattered Radiation Artefacts

Scattered radiation artefacts are caused by scattered (secondary) radiation. One of the possible interactions between the incident photon and electrons in the scanned material is incoherent scattering, also known as Compton scattering. Scattering is defined as the redirection of radiation-beam photons caused by interactions with matter in their path [3]. During incoherent scattering, the incident photon uses a part of its energy to eject an electron from its host atom and a part of its energy is transferred to the ejected (recoiled) electron as its kinetic energy, while the rest of the energy is emitted as a new photon with less energy. The newly-emitted photons form secondary radiation [14]. This radiation is emitted at a specific angle, as a result of the law of the conservation of a momentum. Since photon energies observed here have much larger energies than the electron binding energy, the binding energy can be omitted so that the energy of the incident photon is given as (1):

$$E_i = E_e + E_f, \quad (1)$$

where: E_i - energy of the incident photon, E_e - kinetic energy of the recoil electron, E_f - energy of the scattered photon.

Fig. 6 illustrates the incoherent (Compton) scattering.

Because of incoherent scattering, some of the photons detected on the detector will be those of secondary radiation. Secondary photons cause deviations of the detected signal, compared to the wanted primary radiation signal, which results in shadows or lines on the reconstructed images [14]. Fig. 7 illustrates the impact of incoherent scattering on the detected signal. The scanned object in this case consists of a base material of lower density and a smaller object of higher density inside it, which absorbs and scatters more photons

than the base material, as seen in Fig. 7. Given that the path of scattered photons is arbitrary, the intensity distribution of secondary photons is seen as background noise with lower frequencies. The superposition of the primary and secondary signal results in a combined signal which lowers the image contrast and lowers the signal-to-noise ratio [14].

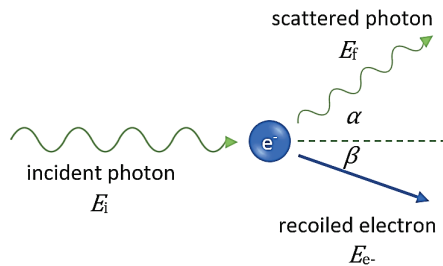


Figure 6 Incoherent scattering

The application of a simplified mathematical algorithm of a 3D model contributes to the formation of artefacts. In order to ease the reconstruction calculation, the detected signal is assumed to be equal with the linearly attenuated primary radiation [15].

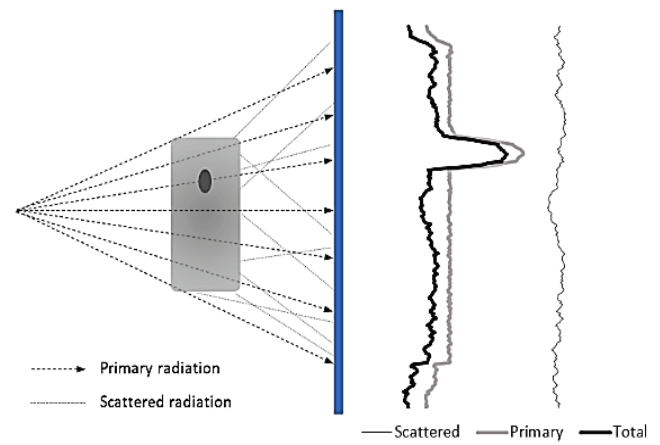


Figure 7 Impact of incoherent radiation

Fig. 8 shows artefacts caused by scattered radiation within the cross-sections of 3D models. The artefacts shown in Fig. 8 are observed as darker lines on the edges of the material and blurred borders on an object's surface.

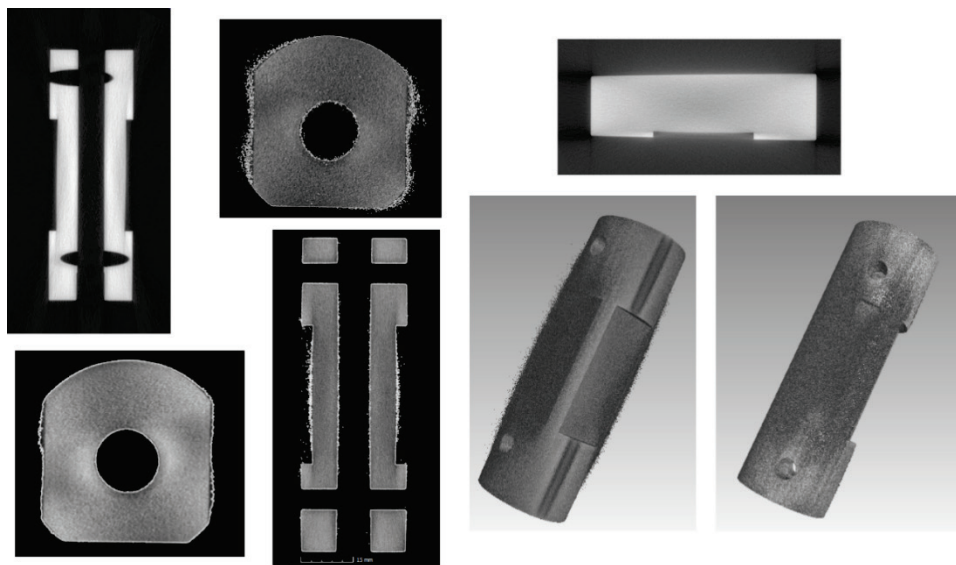


Figure 8 Reconstructed models with an observable impact of secondary radiation

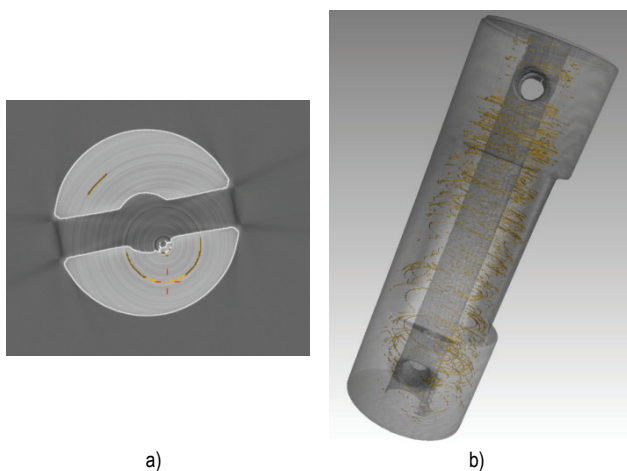


Figure 9 Ring artefact: a) in one slice, b) in a 3D model

2.3 Ring Artefact

Ring artefacts are systematic errors that occur due to a miscalibrated or defective X-ray detector [16]. Ring artefacts are manifested in the form of circles or circle arcs concentric to the rotational axis of the turning table. Artefacts are easily detectable and recognized due to its geometry and it is hard to misinterpret them as the object's geometry. However, the presence of ring artefacts can significantly disturb (impair) the performance of some analyses, e.g. the pore analysis where ring artefacts are wrongly recognized by the software analysis as pores in the material. The example of such a wrongly conducted analysis is shown in Fig. 9. The solution to the problems lies in detector calibration. With calibration, constant sensitivity along the entire detector can be achieved.

2.4 Metal Artefact

Metal artefacts result from the CT scanning of an object composed of or made of several materials with significantly different absorption coefficients, where at least one of the materials is metal. In the industrial application of computed tomography, metal artefacts usually occur when scanning polymer objects with inserted metal parts. Metal artefacts are more common in the medical use of CT if patients do not remove their metal jewellery before scanning, or in the case of implanted metal parts or dentures. The radiation absorbed in the metal parts of the objects is relatively high. As a result, the absorption detected just behind the metal parts is also artificially high [7]. This leads to misinterpretation of the attenuation coefficient in the material of lesser density while producing 2D images. The resulting metal artefacts appear in the form of brighter or darker lines on 2D images which lower the image quality [8]. Larger deviations in measurement results are expected when measuring parts with much higher absorption, e.g. metal parts, as well as when measuring those features that are closer to those (metal) components [17]. An example of metal artefacts in industrial computed tomography is given in [18], where metal artefacts manifested as brilliant stars that bound metal rods.

There are several different approaches in metal artefact corrections, but the most used ones are software correction methods, the so-called post-processing methods. A detailed overview of the available correction methods is given in [19, 20].

Some other image artefacts may occur as result of measurement system imperfections, such as motion artefacts and partial volume artefacts. However, the occurrence of these artefacts is more common in the medical application of computed tomography.

2.5 Motion Artefact

Motion artefacts, as their name says, are a result of motion during the CT scanning. Motion artefacts are more common in medicine computed tomography than in industrial computed tomography, where it is difficult to ensure complete absence of patient movement. Besides the controlled movements of a body part, motion artefacts are caused due to breathing or heartbeat. Unlike in medicine, in the industrial CT, motion artefacts are the result of poorly fixed objects during the scanning process, where the object may move relative to the rotational axis or table while rotating. The problem of object movement due to less stable fixation is described by the authors in [21].

2.6 Partial Volume Artefacts

Partial volume artefacts occur when the measurement object is not fully projected on the detector. The reasons for this can be incorrectly chosen geometrical magnification or scanning the object with a size that exceeds the detector size of the available CT scanner. Since reconstruction algorithms assume that the measurement object is fully visible on the detector at all viewing angles, should that not be the case, the

reconstructed images can contain truncated-view artefacts, i.e. partial volume artefacts [8]. In order to avoid partial volume artefacts, when placing the object on the table and adjusting the scanning parameters, the operator has to ensure that the whole object is visible on the detector in every rotation angle. The appearance of partial volume artefacts is not frequent in the use of industrial computed tomography [6]. Partial volume artefacts should not be confused with the region of interest (ROI) that results from the targeted scanning of a particular part of the object and/or the processing of that particular part of the object.

3 CONCLUSION

This paper presents image artefacts in industrial computed tomography. Image artefacts occur as result of measurement system imperfections and present errors that influence dimensional measurement results. In this paper, six different image artefacts are further explained: beam hardening artefacts, scatter artefacts, ring artefacts, metal artefacts, motion artefacts and partial volume artefacts. The artefacts cause the blurred edges of an object, hindering the proper determination of the borders between the object and background or the borders between different types of materials. Furthermore, image artefacts manifest as an appearance of noise in 2D images, which complicates the 3D reconstruction of a voxel model. Moreover, in the reconstruction process, the appearance of non-existing features in a model can occur. This is particularly the case with ring artefacts which can be wrongly detected as the parts of a scanned object, e.g. as inclusions. In order to minimize the influence of image artefacts on measurement results, extra care must be taken when adjusting the scanning and 3D reconstruction parameters. At the moment, the operator is the one that needs to recognize image artefacts and differentiate between the image artefacts that are a result of the measurement process or system shortcomings and the real state of the measured object. In order to minimize the influence of image artefacts, further research in this field is recommended. Research should focus on identifying and avoiding the presence of image artefacts. One of the possibilities which needs to be further investigated is the application of artificial intelligence in the measurement process, with the goal of recognizing all artificial features that appear on an image without corresponding to the physical feature of an object.

4 REFERENCES

- [1] https://img.medicalexpo.com/images_me/photo-mg/70354-13068301.jpg.
- [2] Horvatic Novak, A., Runje, B., & Stepanic, J. (2016). Capabilities of industrial computed tomography in the field of dimensional measurements. *Advances in Production Engineering & Management*, 12(3), 245-253. <https://doi.org/10.14743/apem2017.3.255>
- [3] ISO 15708-1:2002, Non-destructive testing – Radiation methods – Computed tomography – Part 1: Principles.
- [4] Lifton, J. J., Malcolm, A. A., & McBride, J. W. (2015). A simulation-based study on the influence of beam hardening in

- X-ray computed tomography for dimensional metrology. *Journal of X-Ray Science and Technology*, 23(1), 65-82. <https://doi.org/10.3233/XST-140471>
- [5] Sun, W., Brown, S. B., & Leach, R. K. (2012). *An overview of industrial X-ray computed tomography*. National Physical Laboratory, Teddington.
- [6] Amirkhanov, A., Heinzl, C., Kuhn, C., Kastner, J., & Gröller, M. E. (2013). Fuzzy CT Metrology: Dimensional Measurements on Uncertain Data. *29th Spring Conference on Computer Graphics*. Slovakia, Smolenice.
- [7] Lee, R. D. (2008). *Common Image Artifacts in Cone Beam CT*. Quarterly Publication of the American Association of Dental Maxillofacial Radiographic Technicians.
- [8] Jaju, P. P., Jain, M., Singh, A., & Gupta, A. (2013). Artefacts in cone beam CT. *Open Journal of Stomatology*, 3, 292-297. <https://doi.org/10.4236/ojst.2013.35049>
- [9] Müller, P., Hiller, J., Cantatore, A., & De Chiffre, L. (2012). A study on evaluation strategies in dimensional X-ray computed tomography by estimation of measurement uncertainties. *International Journal of Metrology and Quality Engineering*, 3(2), 107-115. <https://doi.org/10.1051/ijmqe/2012011>
- [10] Krumm, M., Kasperl, S., & Franz, M. (2008). Reducing non-linear artifacts of multi-material objects in industrial 3D computed tomography. *NDT&E International*, 41, 242-251. <https://doi.org/10.1016/j.ndteint.2007.12.001>
- [11] Hiller, J., Genta, G., Barbato, G., De Chiffre, L., & Levi, R. (2014). Measurement uncertainty evaluation in dimensional X-ray computed tomography using the bootstrap method. *International Journal of Precision Engineering and Manufacturing*, 15(4), 617-622. <https://doi.org/10.1007/s12541-014-0379-9>
- [12] Lifton, J. J. & Liu, T. (2020). Evaluation of the standard measurement uncertainty due to the ISO50 surface determination method for dimensional computed tomography. *Precision Engineering*, 61, 89-92. <https://doi.org/10.1016/j.precisioneng.2019.10.004>
- [13] Bismark, R.N.K. et al. (2019). Reduction of of beam hardening artifacts on real C-arm CT data using polychromatic statistical image reconstruction. *Zeitschrift für medizinische Physik*, 30(1), 40-50. <https://doi.org/10.1016/j.zemedi.2019.10.002>
- [14] Hsieh, J. (2009). *Computed tomography: Principles, Design, Artifacts and Recent Advances*. John Wiley & Sons Inc., New Jersey.
- [15] ISO 15708-2:2002, Non-destructive testing – Radiation methods – Computed tomography – Part 2: Examination practices.
- [16] Boas, F. E. & Fleischmann, D. (2012). CT artifacts: Causes and reduction techniques. *Imaging in Medicine*, 4(2), 229-240. <https://doi.org/10.2217/IIM.12.13>
- [17] Kruth, J.P., Bartscher, M., Carmignato, S., Schmitt, R., De Chiffre, L., & Weckenmann A. (2011). Computed tomography for dimensional metrology. *Cirp Annals-Manufacturing Technology*, 60(2), 821-842. <https://doi.org/10.1016/j.cirp.2011.05.006>
- [18] https://www.shimadzu.com/an/ndi/products/x_rylk/metal.html
- [19] Gjesteby, L., De man, B., Jin, Y., Paganetti, H., Verburg, J., Giantsoudi, D., & Wang, G. (2016). Metal Artifact Reduction in CT: Where Are We After Four Decades? *IEEE Access*, 4, 5826-5849. <https://doi.org/10.1109/ACCESS.2016.2608621>
- [20] Kesong Zhang, M. M. et al. (2020). Metal artifact reduction of orthopedics metal artifact reduction algorithm in total hip and knee arthroplasty. *Medicine*, 99(11). <https://doi.org/10.1097/MD.00000000000019268>
- [21] Kraemer, A. & Lanza, G. (2016). Assessment of the measurement procedure for dimensional metrology with X-ray computed tomography. *Procedia CIRP*, 43, 362-367. <https://doi.org/10.1016/j.procir.2016.02.018>

Authors' contacts:

Amalija Horvatić Novak, PhD
University of Zagreb,
Faculty of Mechanical Engineering and Naval Architecture,
Ivana Lucica 5, 10000 Zagreb, Croatia
amalija.horvatic@fsb.hr

Biserka Runje, PhD, Professor
University of Zagreb,
Faculty of Mechanical Engineering and Naval Architecture,
Ivana Lucica 5, 10000 Zagreb, Croatia
biserka.runje@fsb.hr

Zdenka Keran, PhD, Assistant Professor
University of Zagreb,
Faculty of Mechanical Engineering and Naval Architecture,
Ivana Lucica 5, 10000 Zagreb, Croatia
zdenka.keran@fsb.hr

Marko Orošnjak
University of Novi Sad,
Faculty of Technical Sciences,
Trg Dositeja Obradovica 6, 21000 Novi Sad, Serbia
orosnjak@uns.ac.rs

Designing an Integrated Model of Oil and Gas Management with a SWOT Approach: The Case of NIOC

Seyed Emad Hosseini, Amir Naser Akhavan*, Mohsen Bahrani

Abstract: In the recent years, the growing demand for energy on the one hand and the reduction of conventional hydrocarbon reserves on the other hand have made the proper extraction of oil and gas reserves, i.e. reservoir management issues, more important and hence proper management of these reserves is inevitable. Although renewable energies currently provide the bulk of the world's energy needs, hydrocarbon fuels remain the main source of energy until 2035. Despite the growing importance of the Integrated Reservoir Management Model (IRMI), as a rational solution to maximize economic production from oil and gas reservoirs, a comprehensive model that can cover all reservoir management modules has not yet been proposed. In this paper, by examining the current condition of reservoir management in one of the subsidiaries of the National Iranian Oil company and analyzing the obtained results, we offer some solutions to improve the condition and finally, we present a comprehensive model for reservoir management in this company.

Keywords: closed loop; control variable; data uncertainty; energy management; Integrated Reservoir Management Model (IRMI); SWOT

1 INTRODUCTION

New concepts and methods have been developed since the first definition of reservoir management presented by Thakur and Satter [1-3] that can be examined through modern approaches to reservoir management.

Since one of the most important factors in increasing the power of influence and bargaining in markets and

international organizations is the volume of strategic hydrocarbon reserves and the oil production capacity of countries, it seems that the realization of the goals of the resistance economy, especially the development of oil and gas production capacities, maximum efficient recovery, completion of the value chain and etc. will face fundamental challenges.

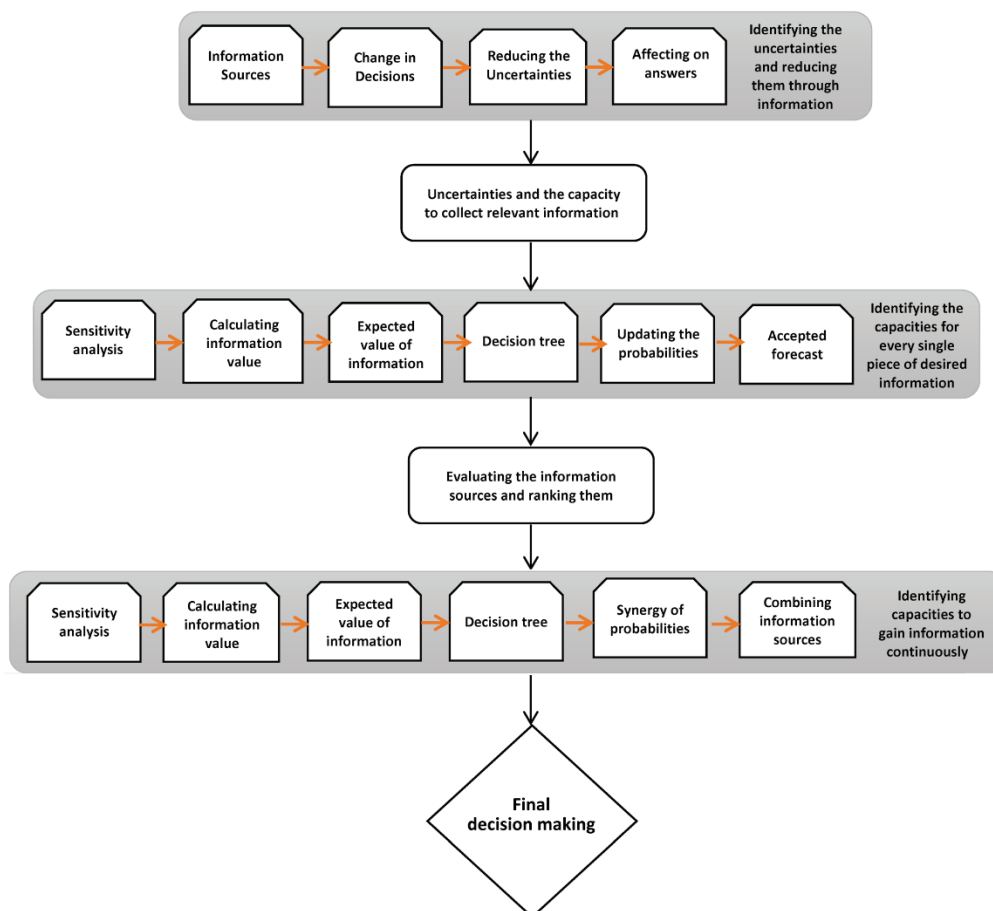


Figure 1 Data value analysis flowchart [4]

As a result, the need for a comprehensive model of integrated reservoir management which includes all effective criteria for a maximum efficient recovery and an increase in recycling oil and gas reservoirs is strongly felt. Familiarity with the reservoir and knowing the way of managing it and the elements affecting it are necessary for the effective utilization of hydrocarbon reservoirs.

Therefore, the aim of this paper is to present an integrated and dynamic model of oil and gas reservoir management as a tool to successfully implement the strategy of oil and gas field development, which at first considers the existing condition of reservoir management in the National Iranian Oil Co. and then identifies the requirements and challenges of oil and gas reservoir management and according to the upstream documents of the National Iranian Oil Co., presents a comprehensive model of reservoir management through the experts' opinions in one of the oil subsidiaries.

An example of the modern methods of reservoir management can be found in Schiozer's research. It is a comprehensive model for reservoir management (Fig. 1) which includes 12 steps that perform decision-making in the condition of data uncertainty with a lower risk. This method covers all stages of reservoir management including reservoir simulation, reservoir history matching and reservoir production and development strategy, and it helps reduce the risk over the life of the reservoir [4, 5].

The decision-making structure in reservoir management is multi-layered and hierarchical in the sense that it is separated by a scheduling structure. This structure in the reservoir management process can be explained as seen in Fig. 2 [6].

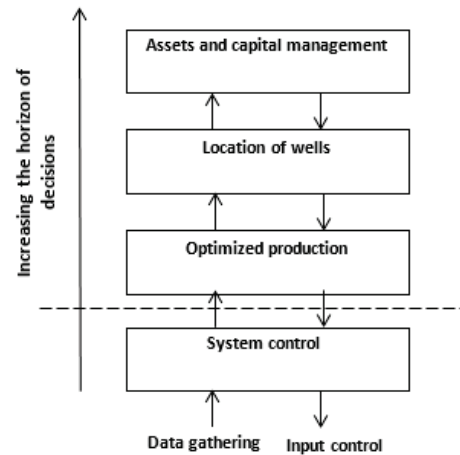


Figure 2 Hierarchy and control layers in reservoir management [6]

In this method, decision-making is divided into three periods of long-term, medium-term and short-term duration. The asset and capital management of a company in reservoir management is the one of long-term decisions that requires field development planning or production planning, which is usually the same as the life of depreciable assets.

Well placement optimization is a medium-term decision-making process aiming to provide a production strategy in each well and to optimize the location of wells and the production rate of each of them. Short-term planning considers the daily production of wells and solving the problems during exploitation operations. In this structure, control factors, which control technical issues, are also defined. The whole structure is defined in a closed process called the closed loop.

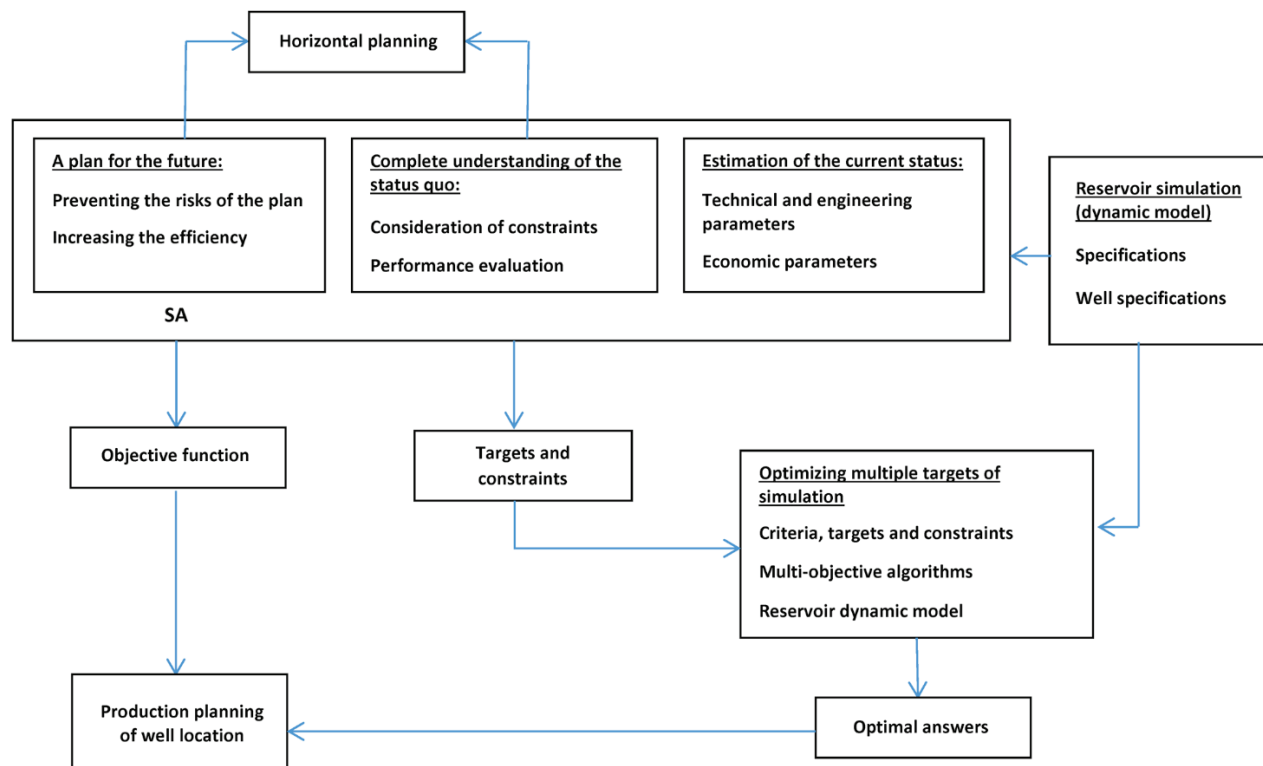


Figure 3 SA executive model for smart reservoir management using multi-criteria optimization models [7]

Smart reservoir management is also one of the novel methods being studied more and more every day. The model applied in one of these studies, presented by Moradi [7], is showed in Fig. 3. This method is called SA Simulation Awareness and it contains a cycle for planning all factors that influence reservoir management, i.e. factors such as capital planning, technical and operational management of the entire oil and gas reservoir system. In this model, the reservoir manager dynamically controls the reservoir conditions.

This kind of control includes the reservoir simulation model and the real data received from the exploitation operation which updates the executive model and improves the condition of reservoir management. The analysis of the obtained data and information and their evaluation for a better understanding of the efficiency of the implemented method and the extraction of the reservoir is the next step. Forecasting the future of the reservoir in order to achieve the highest and most optimal value and income from the reservoir is also the last step of decision-making.

One of the most important goals of reservoir management, which is studied in all research nowadays, is a correct, logical and responsible management of the existing resources, as well as obtaining the highest profit and, in fact, net value from oil and gas reserves. The first effective and useful step in managing the reservoir is to model and aggregate all influential variables in the reservoir for the best available model and to evaluate the model by examining the reservoir's past. However, despite examining the history of the reservoir, there is also a need for activating the algorithms that continuously control the optimal amount of production to determine the best net present value. Of course, it should be noted that the generalization of the model built for the whole field, due to the lack of sufficient information from the reservoir, creates problems. Therefore, certain algorithms have recently been defined to solve these uncertainties; algorithms such as Steepest Ascent (SA), Sequential Quadratic Programming (SQP), Variable Precision Rough Set (VPRS) and the Interior Point (IP) [8-10].

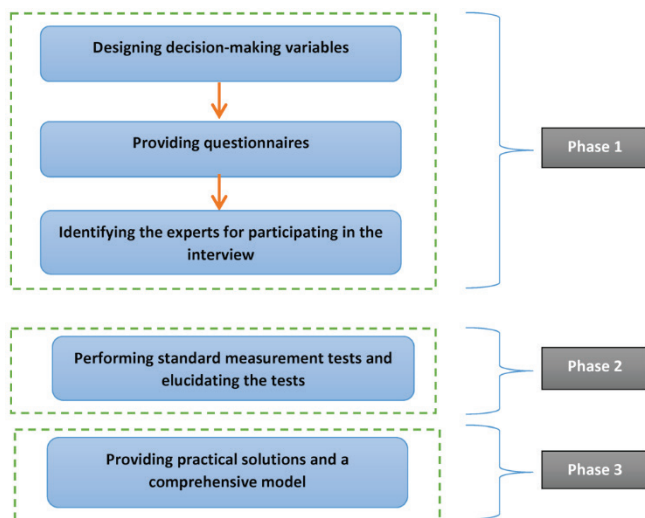


Figure 4 Theoretical research framework [author]

2 RESEARCH FRAMEWORK

This paper is divided into three phases (Fig. 4).

2.1 Designing Decision Variables in Reservoir Management

In this study, a group of industry experts and professors of the Amirkabir University of Technology and the Tehran University first gathered together, and a questionnaire in the field of reservoir management was designed according to the existing strengths, weaknesses, threats and opportunities of the oil industry. The questionnaire was distributed among 33 experts and managers of one of the subsidiaries of the National Iranian Oil Co., and the answers were evaluated based on certain indicators. Questions were about oil, gas and some other industries and were designed on the basis of the nature and technical and managerial structure of the research and its predetermined goals. The questionnaire was based on a Likert scale and in the five categories of 'I'm absolutely for it', 'I'm for it', 'I have no idea', 'I'm not for it' and 'I'm absolutely not for it'. Then, the numerical value of each category was determined, which seemed to be enough for the scores 1, 2, 3, 4 and 5.

Table 1 Influential variables in developing the reservoir management model of the National Iranian Oil Co.

1	The impact of technical knowledge and expert staff in the field of reservoir management in the National Iranian Oil Co.
2	The impact of the organizational structure in proportion to the implementation of reservoir management in the National Iranian Oil Co.
3	The impact of the political and economic conditions on the reservoir management model in the National Iranian Oil Co.
4	The impact of the international conditions on the reservoir management model in the National Iranian Oil Co.

The above-mentioned items led us to design a questionnaire to examine the condition in one of the subsidiaries of the National Iranian Oil Company.

2.2 How to Distribute the Research Variables Based on the Kolmogorov-Smirnov Test

This test is used to examine the claim made about the data distribution of a quantitative variable; e.g., is the distribution of the variable under the study Normal? Therefore, the normality claim of the distribution of all variables is examined through this study.

The statistical hypothesis of the study is as follows:

H0: Data follow the Normal distribution

H1: Data do not the Normal distribution

Based on the output of the SPSS software and the significance value, which is abbreviated to Sig, we examine the normality claim of the research variables. Sig is also known as the P-value. The lower the Sig value, the easier it is to reject the null hypothesis. Alpha (α) is the error level that the researcher considers (which is usually 5%). In general, we can say that:

IF Asymp. Sig. (2-tailed) < $\alpha = 0.05 \Rightarrow H0$: Reject

IF Asymp. Sig. (2-tailed) $\geq \alpha = 0.05 \Rightarrow H_1$: Not Reject

The results the of Kolmogorov-Smirnov Test for each of the research values are shown in Tabs. (2) and (3).

Table 2 Kolmogorov-Smirnov Test for the research variables

	Observing	Institutionalization	Familiarity of the macro level	Preparation of the company	Importance of implementing	Application of an integrated model	The role of the reservoir	Having an expert human resource
N	34	34	34	34	34	34	34	33
Nor	a	4.3	2.5	1.91	4.9	4.5	4.6	2.5
	d.	.81	1.0	1.7	1.19	.95	.58	1.3
Most e	A	.31	.24	.26	.337	.32	.383	.44
	P	.21	.24	.26	.337	.28	.29	.22
	e	-.37	-.14	-.24	-.222	-.32	-.44	-.14
Test Statistic	.31	.24	.26	.337	.32	.38	.44	.22
Asymp. Sig.	.06	.01	.03	.077	.10	.09	.07	.05

Table 3 Kolmogorov-Smirnov Test for the research variables

	Observing	Institutionalization	Familiarity of the macro level	Preparation of the company	Importance of implementing	Application of an integrated model	The role of the reservoir	Having an expert human resource
N	34	34	34	34	34	34	34	34
Nor	a	2.5	2.0	4.8	4.5	2.3	1.50	4.6
	d.	1.1	1.5	.45	.65	1.1	.99	.7
Most e	A	.32	.27	.53	.411	.33	.458	.31
	P	.32	.27	.30	.265	.33	.458	.27
	e	-.17	-.23	-.53	-.411	-.26	-.307	-.31
Test Statistic	.31	.32	.27	.503	.41	.353	.48	.31
Asymp. Sig.	.06	.08	.12	.221	.09	.325	.08	.17

If the value of the significance level is greater than the value of the error (alpha), we conclude the null hypothesis, and if the value of the significance level is smaller than the error, we conclude the research hypothesis. Since the value of the significance level of all research variables is greater than the error value of 0.05, we conclude that the distribution of all variables is Normal. Therefore, parametric tests (single-sample t-test) are used to test the research questions.

2.3 Examining the Existing Condition of Variables

A mean test of a statistical population is used to answer the research questions and to examine the condition of the variables (whether they are appropriate or inappropriate).

The statistical hypothesis of the test is presented as follows:

$H_0: \mu \leq 3$ (It Is Not in a Good Condition)

$H_1: \mu > 3$ (It Is in a Good Condition)

The result of the t-test consists of two outputs. The first output includes the descriptive statistics related to the hypothesis test, and the calculated numbers include the number of data, mean, standard deviation and mean standard error, respectively. The second output of the test includes the inferential statistics of the test which from left to right has the name of the variable in the first column, the statistic of t in the second column, the degree of freedom for each variable in the third column, the significance in the fourth column, the mean difference of each variable with three in the fifth column, and the last two columns for the upper and lower limits.

Table 4 Summary of the variables' situations in the company

Row	Variable title	Condition
1	Paying attention to the reservoir management	appropriate
2	Institutionalizing the knowledge of the reservoir management	inappropriate
3	Familiarity of the macro level managers with the basics of the reservoir management	inappropriate
4	Preparation of the company's organizational structure for implementing the integrated reservoir management system	inappropriate
5	The importance of implementing a comprehensive reservoir management system	appropriate
6	Applying a comprehensive reservoir management model	appropriate
7	The role of reservoir management in reducing different risks	appropriate
8	Possessing an expert human resource for implementing the comprehensive reservoir management model	inappropriate
9	Knowledge of engineers and technical experts of the operational headquarters	inappropriate
10	Coordination in team approaches	inappropriate
11	The role of reservoir management in maximizing profitability	appropriate
12	Improving and promoting the exploitation and recycling process through applying reservoir management knowledge	appropriate
13	Relevance of reservoir management knowledge for the use in oil and gas fields	inappropriate
14	Relevance of reservoir management knowledge for competing with foreign companies	inappropriate
15	Application of reservoir management knowledge in negotiating with foreign contractors	appropriate
16	Application of reservoir management knowledge in negotiating with the investors	appropriate

It should be noted that in examining the status of the components, an appropriate condition is a condition in which the mean score of the variable is greater than three, and on the contrary, an inappropriate condition is the one in which

the mean score of the variable is less than or equal to three. Given the mean values, the significance level (Sig) and the confidence interval obtained, we can summarize the status of variables in the company as described in Tab. 4.

According to the participants in the study, despite considering reservoir management in the macro strategies of the National Iranian Oil Co. and the application and importance of the integrated reservoir management model in the National Iranian Oil Company in reducing various

operational, economic and environmental risks and increasing the power of attracting foreign investors in developing oil fields, the reservoir management knowledge is at an inappropriate level and the level of the familiarity of the macro level managers of the National Iranian Oil Co. with the basics of reservoir management is low. Moreover, the current structure of the company is also not good enough for dynamic reservoir management.

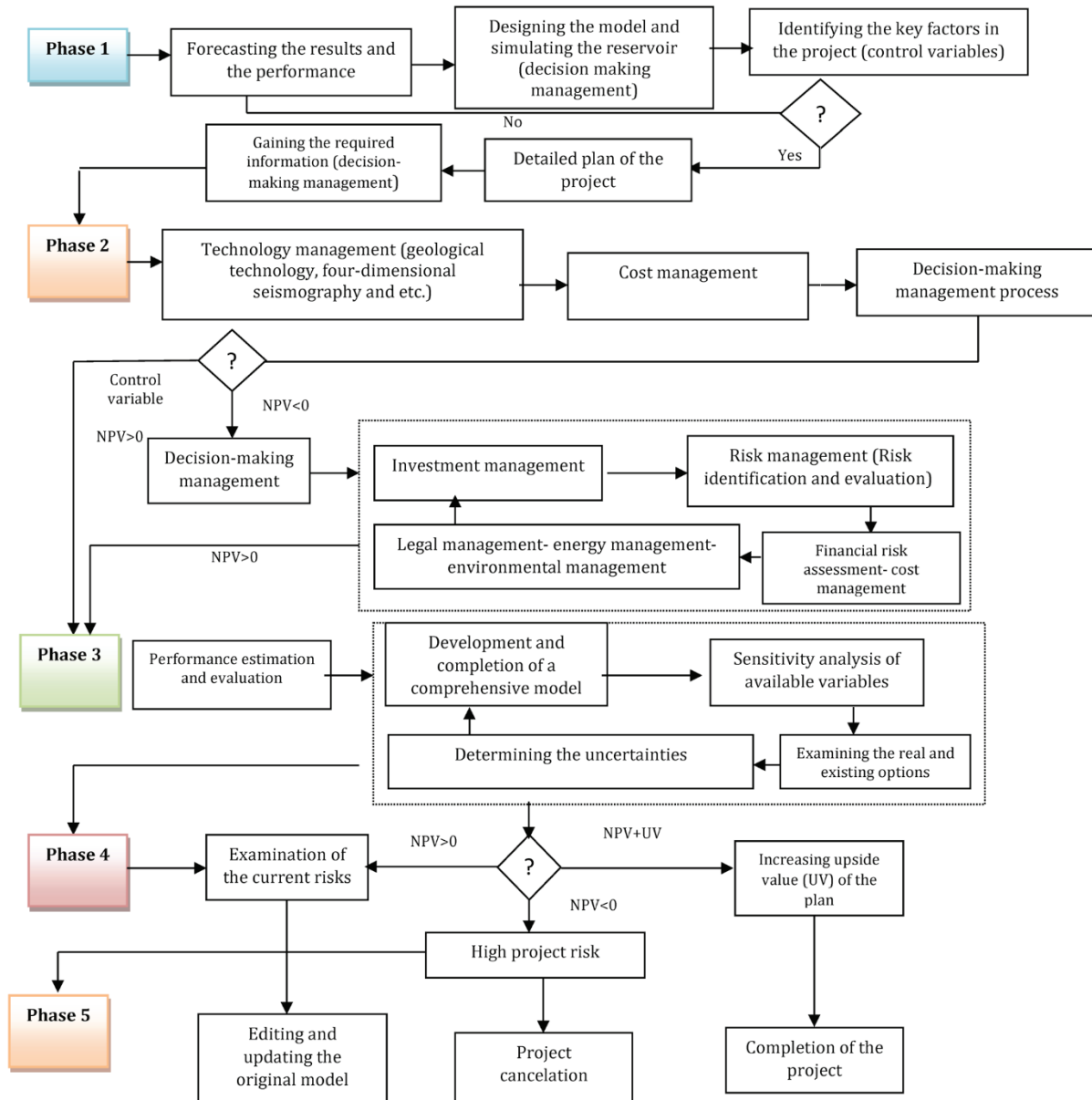


Figure 5 The process of developing a dynamic model in reservoir management (author)

3 DYNAMIC RESERVOIR MANAGEMENT MODEL

As it has previously been mentioned, the existing structure of the National Iranian Oil Co. and the static approach of reservoir management models are not effective in the today's complex and competitive environment, to which the reduction of conventional reserves has added

another challenge. Therefore, we propose a dynamic structure and framework for the stressful market of the oil industry.

The dynamic model of reservoir management must be innovative and forward-looking to seize opportunities and face challenges both inside and outside the country. Hence,

this model must have eight major modules in its dynamic structure.

Investment management: given that the oil industry in Iran needs investing in the development of current fields and exploring new fields (initial estimate of \$130 billion in the upstream sector), the dynamic model must be able to properly manage investments, especially foreign investments.

Decision-making management: due to the proliferation of simulation programs and mathematical decision-making models, decision-making in the upstream oil industry has moved away from its traditional way. Therefore, the dynamic model must be able to solve the situation real time by changing the situation and the variables affecting the decision. It also must be able to update its decisions by forming closed loops and receiving feedback.

Risk management is one of the riskiest industries for investment in the world. The uncertainty of the technical and economic data is a major challenge in this industry. Due to the dynamics of the project risks in the oil industry, eliminating or reducing these risks, i.e. risk management, with modern mathematical methods is one of the most important conditions for a dynamic model.

4 CONCLUSION

Due to certain problems in one of the subsidiaries of the National Iranian Oil Co. in the optimal and safe management of Iran's oil and gas reservoirs, and based on the decision variables, a questionnaire was designed with the help of experts. In order to study the current situation of deposit management in the company, efficient technology has been distributed. This was achieved with a skilled workforce and an appropriate organizational structure. The analysis of the results shows that there is no reservoir management with a new form that is dynamic and able to operate in the conditions of uncertainty in the oil industry and with a high level of risk. Therefore, in this paper, an appropriate model is designed.

As shown in Fig. 5, this model has five steps in which all reservoir management modules are involved in the decision-making process. Each step has a control variable which is responsible for matching the decisions made or the scenario selected with predefined goals. As a result, at each stage, when it is felt that the decision has moved away from the goals, the loop returns and the process is repeated with the new conditions, and the so-called real time optimization takes place.

5 REFERENCES

- [1] Wang, J.-J., Y.-Y., Jing, C.-F., Zhang, J.-H., Zhao, (2009). Review on multi-criteria decision analysis aid in sustainable energy decision-making. *Renewable and Sustainable Energy Reviews*, 13, 2263-2278. <https://doi.org/10.1016/j.rser.2009.06.021>
- [2] Thakur, G. C. (1990). Reservoir Management: A Synergistic Approach. Paper SEP 20138 presented at the *SPE Permian Basin Oil and Gas Recovery Conference*, Midland, Texas, March 8-9. <https://doi.org/10.2118/20138-MS>
- [3] Satter, A., et al. (1992). Reservoir Management Technical Perspective. SPE Paper 22350 presented at the *SPE International Meeting on Petroleum Engineering* held in Beijing, china, March 24-27. <https://doi.org/10.29118/IPA.2093.549.586>
- [4] Schiozer, D. J., Santos, A. A. S., & Drumond, P. S. (2015). Integrated Model Based Decision Analysis in Twelve Steps Applied to Petroleum Fields Development and Management. In: *SPE EUROPEC*, 1-4 June, Madrid, Spain. <https://doi.org/10.2118/174370-MS>
- [5] Arnold, D., Demyanov, V., Christie, M., Bakay, A., & Gopa, K. (2016). Optimisation of decision making under uncertainty throughout field lifetime: A fractured reservoir example. *Computers & Geosciences*, 95, 123-139. <https://doi.org/10.1016/j.cageo.2016.07.011>
- [6] Foss, B. A. & Jensen, J. P. (2011). Performance analysis for closed-loop reservoir management. *SPE J.*, 16(01), 183-190. <https://doi.org/10.2118/138891-PA>
- [7] Moradi, T. & Rasaei, M.-R. (2017). Automated reservoir management using multi-objective simulation optimization and SA model. *Journal of Petroleum Science and Engineering*, 150, 91-98. <https://doi.org/10.1016/j.petrol.2016.11.024>
- [8] Khosravi, M., Rostami, B., & Fatemi, S. (2012). Uncertainty Analysis of a Fractured Reservoir's Performance: A Case Study. *Oil & Gas Science and Technology – Rev. IFP Energies nouvelles*, 67(3), 423-433. <https://doi.org/10.2516/ogst/2011158>
- [9] Esmailzadeh, F. & Nourafkan, E. (2009). Calculation OOIP in oil reservoir by pressure matching method using genetic algorithm. *Journal of Petroleum Science and Engineering*, 64, 35-44. <https://doi.org/10.1016/j.petrol.2008.12.008>
- [10] Zabalza-Mezghani, I., Manceau, E., Feraille, M., & Jourdan, A. (2004). Uncertainty management: From geological scenarios to production scheme optimization. *J. Petrol. Sci. Eng.* 44(1-2), 11-25. <https://doi.org/10.1016/j.petrol.2004.02.002>

Authors' contacts:

Seyed Emad Hosseini, PhD Student
Future Study Engineering,
Amirkabir University of Technology,
No. 350, Hafez Ave, Valiasr Square, Tehran, Iran 1591634311
E-mail: seyedeemad@gmail.com

Dr. Amir Naser Akhavan, Professor
(Corresponding author)
Department of Mechanical Engineering,
Amirkabir University of Technology,
No. 350, Hafez Ave, Valiasr Square, Tehran, Iran 1591634311
E-mail: akhavan@aut.ac.ir

Dr. Mohsen Bahrami, Professor
Department of Mechanical Engineering,
Amirkabir University of Technology,
No. 350, Hafez Ave, Valiasr Square, Tehran, Iran 1591634311

Accuracy Analysis of Point Velocities Determined by Different Software Packages and GNSS Measurement Processing Methods

Margareta Premužić*, Almin Đapo, Željko Bačić, Boško Pribičević

Abstract: The paper analyzes the geodynamic network of the City of Zagreb for periodic campaigns carried out from 2006 to 2009 which were processed by different software packages. The first computations and processing results were obtained by using the scientific software Gamit/Globk and indicate the ongoing tectonic activity of the area. In this paper, all calculations were performed by using the scientific software Bernese. Processing strategies and applied error models in the Gamit and Bernese solution are analyzed. The results of the previous analyses show the need to perform GNSS measurements at intervals of up to one year, which is necessary for understanding the mechanism of the structural frame of the wider Zagreb area. The research and analysis performed in this paper indicate certain uncertainties in determining the velocities from periodic one-year GNSS measurements. When periodic GNSS observations are analyzed at time intervals shorter than 2.5 years, annual signals can cause significant errors in determining point velocities. The accuracy of determining velocities between annual time intervals depends on a number of factors: noise level in GNSS measurements, measurement sessions quantity and applied computation strategies. Previously, the time series analysis of observations was a key procedure in the context of geodynamic and geokinematic research and the FODITS algorithm was used for the analysis. A noise analysis on the daily time series of coordinates was performed for the purpose of understanding all influences on geodynamic points. Moreover, a correlation between the time series of observations was determined in order to estimate the final velocity uncertainty error. The purpose of this paper is to demonstrate the applicability of the methods and procedures used to determine the coordinates and velocities of points that can be reliably used for geodynamic and geokinematic analyses and consequently, timely responses to various geophysical phenomena due to earthquakes or other natural phenomena.

Keywords Bernese; CROPOS; FODITS; Gamit; Geodynamic Network of the City of Zagreb

1 INTRODUCTION

Previous calculations for establishing the reference frame and investigating geodynamics have made it possible to determine the character and parameters of the displacement of the Earth's crust in the territory of the Republic of Croatia [1-5]. However, measurement techniques such as the GNSS method are also a powerful tool for monitoring displacements and deformations in the local areas of interest, respectively for geodynamic and geokinematic analyses, and increasingly in the study of seismic activities. Because permanent stations are not densely distributed in the areas of interest, non-permanent, periodical observations on GNSS points are performed. An example of such a network that is analyzed in this paper is the geodynamic network of the City of Zagreb. The results of data processing indicate a constant presence of tectonic activity in the wider area of the City of Zagreb. The analysis of the processing results of the geodynamic network of the City of Zagreb [2] over a period of 20 years shows that, in the case of multi-year time intervals between GNSS campaigns, there is an averaging of the shifts or losses of certain information on the annual shifts, which are extremely valuable data needed for a reliable analysis. The results of previous analyses show the need to perform measurements at intervals of up to one year, which is necessary for analyzing the quality of the obtained results from the GNSS campaign and understanding the mechanism of the structural frame of the wider Zagreb area. The investigations carried out in this paper relate to examining the impact of the chosen error modeling method and the GNSS measurement processing strategy, while analyzing the time series of observations and the influence of time intervals between the observations on the accuracy and the precision of the points' coordinates and

velocities. The data processing of geodynamic campaigns is influenced by specific deviations due to the use of different processing parameters (antenna and receiver parameters, software changes), but also due to random errors (receiver noise and unmodified atmospheric effects). Coordinate and velocity variations may occur considering the network adjustment strategy used to detect local geodynamic impacts. Such solutions are ambiguous and dependent on the strategy employed [6]. Based on the collected observations of the Geodynamic Network of the City of Zagreb (GNCZ), the application of various error modeling methods and processing strategies for GNSS measurements has been analyzed, with the possibility of eliminating their systematic or random influences, which will ultimately enable their reliable use for geodynamic and geokinematic analyses.

The paper analyzes the time series of coordinates and velocities for discontinuities and jumps, which is today a key procedure for geodynamic and geokinematic analyses. A large number of discontinuities is caused by model updates (e.g. antenna calibration models) and changes in the GNSS data processing strategies or new ITRF implementations. Additionally, there are other sources that cause them, such as earthquakes that can cause discontinuities and velocity changes in the points near the epicenter. Discontinuities may also be present for some unknown reasons (construction of new objects around the antenna, dropping accumulated snow on the antenna, etc.), and they usually remain for longer periods (weeks) and, if identified, can be determined with accuracy below mm, and they can be applied to the time series of coordinates. The jumps are present in the time series of coordinates mainly due to systematic errors, e.g. due to bad atmospheric conditions (snow storms), anthropogenic influences, etc. Finding jumps depends on the assumptions determined by the statistical test and the level found to be

significant for the analysis of the datasets [7]. Jumps occur in a shorter period of time and the values are usually greater than those of discontinuities. By analyzing the daily solutions of the coordinates' time series, significant changes in the data in the predefined epochs are checked, i.e. discontinuities and jumps are determined. Multi-day coordinate solutions show fewer RMS values (*Root Mean Square*) than the daily ones, but they also use reduced data, hence it is important to use the daily solutions to determine discontinuities and jumps. A data analysis without averaging the time series of coordinates provides insight into the displacements and deformations of the location of interest, and the best insight can be obtained from continuous data analyses at permanent stations. The detection of geo-kinematic phenomena requires a data analysis of multiple daily GNSS solutions since determining displacement parameters requires a previous statistical analysis of the daily solutions that provide control for jumps. Daily solutions that have jumps, and remain in the processed dataset, can deform the established parameters, e.g. seismic deformations affect the time series of coordinates, accumulate over time and can significantly affect coordinates, not only from large earthquakes, but also from the accumulation of many small earthquakes. Seismic deformation modeling helps detect discontinuities in the time series of GNSS coordinates, which is one of the main sources of error in determining the ITRF frame today [8]. Numerous discontinuities induced by earthquakes are too small for visual detection due to seasonal variations and the GNSS noise that disable their identification. However, if not taken into account, they have a great influence on the determination of point velocities, considering the precision requirements for geodynamic and geokinematic analyses.

2 GNSS MEASUREMENT NOISE ANALYSIS

The noise analysis of GNSS measurements mainly assumes the presence of white noise in the time series of coordinates. Several previous studies [9] have shown that if correlated noise is neglected and if only the white noise model is used, then the uncertainty rate is significantly underestimated. Considering the combination of noise affecting GNSS measurements, it is difficult to accurately determine the source of the noise and, consequently, the reliability of the estimated time series of coordinates. Understanding noise content is very important in order to identify realistic uncertainties for the parameters to be determined. When applying the least squares adjustment, daily position errors are considered to be independent. However, using this method to calculate point velocities from time series coordinates gives some uncertainty. Studies have shown that the assumption that measurement errors are random and uncorrelated from an epoch-to-epoch (white noise) is unrealistic for GNSS measurements. Sources of time-correlated noise (colored noise) in the GNSS data include: orbits, atmospheric effects, stabilization shifts, etc. [10, 11]. For computing realistic errors, the approach of [11] is selected, who developed an empirical model to determine the GNSS error (σ_r) for individual velocity components (N , E , H) using the time series of coordinates with the presence

of white and colored noise. The final velocity uncertainty error is represented by the formula (1):

$$\sigma_r^2 \cong \frac{12\sigma_w^2}{gT^3} + \frac{a\sigma_f^2}{g^bT^2} + \frac{a\sigma_{rw}^2}{gT} \quad (1)$$

where: g is the number of measurements per year, T is the total time range of observations (T = period (in years)), and a and b are empirical constants: $a = 1.78$; $b = 0.22$.

White noise is a random noise (S_w "white"). There are two main types of colored noise: pink (S_f "flicker") inversely proportional to frequency and red (S_{rw} "random walk") inversely proportional to the square of frequency. In Fig. 1, the pink line represents the mean of white and pink noise, the blue dashed line is the maximum amplitude of white, pink and red noise [10], whereas the red dashed line is the minimum amplitude of the white and pink noise calculated from the time series of coordinates [12]. The magnitudes for white and pink noise are expressed in mm and for red noise in mm/yr.

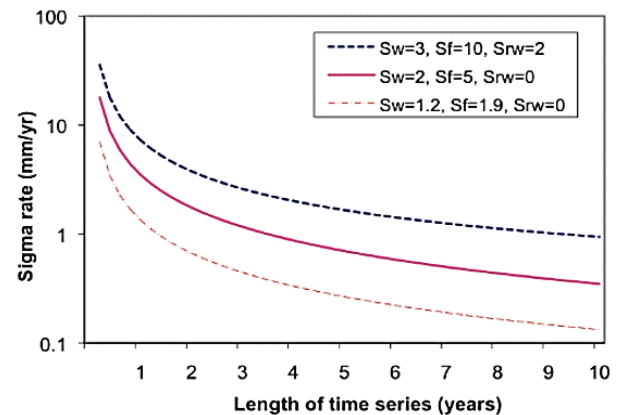


Figure 1 Analysis of measurement noise using the example of the GNSS network in the western Alps [12]

By investigating and analyzing the time series of coordinates according to [11], it was concluded that white and pink noise dominate the GNSS noise spectrum for the time series coordinates, while red noise is relatively small. Pink noise is spatially correlated and has a clear dependence on geodetic latitude. Although the pink noise amplitude decreases with time, it is still the most dominant. The vertical component is three times larger than the horizontal component. The red noise component is very difficult to detect since it requires a much longer time span of observations. Stabilization noise is characterized as red noise [10] and occurs with respect to the cycles of rain, freezing and atmospheric effects on rocks and soil. If the red noise is very small, the velocity error depends strongly on the time range of the observations (T) and less on the number of the observations (g). However, several studies have demonstrated the importance of red noise recognition in the GNSS data. According to [9] cumulative changes in the earth and atmosphere, stabilization shifts with respect to the deeper layers of the crust. The most common types of stabilization

in geodynamic networks are: metal pillars and deep concrete pillars. According to [10], there is no clear distinction between the deep concrete pillars and ordinary metal pillars related to the stabilization noise. Moreover, according to [10], larger noises do not occur from stabilization instability. Another study showed that deep concrete pillar stabilizations have a lower colored noise, but also slightly smaller velocity residuals [13] (Fig. 2).

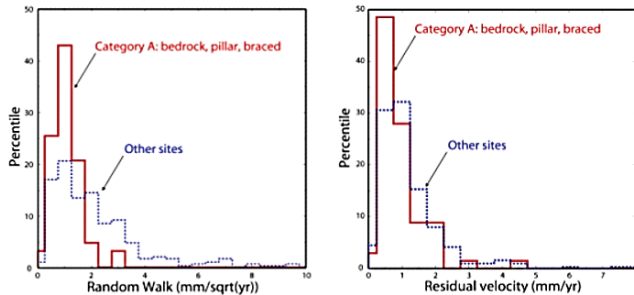


Figure 2 Analysis of the impact of red noise on velocity uncertainties with respect to the type of stabilization [13]

According to [11], a strong linear correlation between the weighted RMS values of the GNSS coordinate time series and the determined noise amplitudes for white and pink noise was observed with the linear equations shown in Tab. 1.

Table 1 The linear correlation of RMS and measurement noise [11]

Parameter	Formula
σ_w (N)	$0.613 \text{ wRMS (N)} + 0.259$
σ_w (E)	$0.767 \text{ wRMS (E)} - 0.183$
σ_w (H)	$0.843 \text{ wRMS (H)} - 1.772$
σ_f (N)	$1.139 \text{ wRMS (N)} + 0.117$
σ_f (E)	$1.041 \text{ wRMS (E)} - 0.342$
σ_f (H)	$0.668 \text{ wRMS (H)} + 5.394$

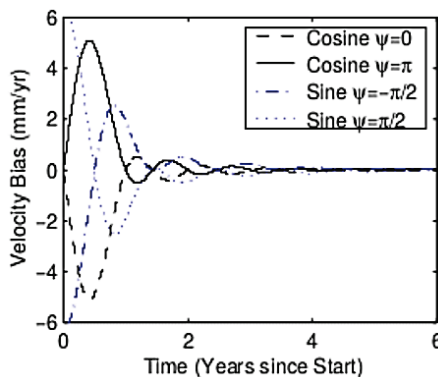


Figure 3 Theoretical velocity error from annual sinusoidal signals versus the time period [14]

Although previous analyses have shown that white and pink noise are dominant in the noise model for the coordinate time series, there are also various other sources of error, such as periodic (seasonal) signals that can be imposed as dominant, such as localized deformations with respect to changes in the groundwater (unknown colored noise). Therefore, the parameter of the annual and semi-annual sinusoidal signal must be introduced into the process of

determining point velocities, which must be determined simultaneously with velocities.

Using the least squares method, seasonal signals (annual and semi-annual) can be described by a simple formula (2):

$$x = A \cos(\omega t + \varphi) \quad (2)$$

where: A = amplitude, φ = phase, $\omega = 2\pi/T$ (T = period (in years)).

Seasonal signals contribute to the pole and ocean tide, which are usually corrected in GNSS processing by using the available models (the nutation model and sub-day pole model, ocean tide model and coefficients). Additionally, the earth's potential and solid earth tide are modeled. Errors caused by seasonal signals, which are not usually corrected in GNSS processing, and which must be taken into account are: atmospheric pressure, snow and soil moisture and the non-tidal ocean mass. It should also be emphasized that the accuracy and precision of coordinate and velocity determinations are also influenced by different computation or modeling strategies using different software packages for GNSS processing. Only with a complete understanding of the full spectrum of GNSS errors [15] (Tab. 2) could we obtain accurate and precise results that can be used in geodynamics and geokinematics.

Table 2 Contributions of Geophysical Sources and Model Errors to Annual Variations in the Site Position [15]

Sources of error	Range of effects
Pole tide	~ 4 mm
Atmospheric mass	~ 4 mm
Ocean tide	~ 0.1 mm
Non-tidal ocean mass	2-3 mm
Snow mass	3-5 mm
Soil moisture	2-7 mm
Bedrock thermal expansion	~ 0.5 mm
Error in network adjustment	~ 0.7 mm
Differences from the software	~ 2-3 mm, at some sites (5-7 mm)
Errors in the orbit, phase center, and troposphere models	No quantitative results from observations

The Western Alps are one of the most researched areas related to monitoring the mechanism of the structural frame and detailed geophysical surveys [12], [16]. The GPS ALPES group, made up of French, Swiss and Italian researchers, monitors the GPS network in the Western Alps. In the period from 1993 to 1998, more than 60 stations were observed with 3-day sessions at each station, and the data were processed by different software packages. The calculated solutions with the GAMIT/GLOBK software had a horizontal repeatability (N-E) of 4-7 mm in the year 1993 and 2-3 mm in the year 1998. A comparison of coordinates from the years 1993 and 1998 shows that the residual of GPS points velocities is less than 2 mm/year. Solutions were compared with the BERNESE software and the differences for the 1998 dataset are quite small, reaching an average of about 2 mm for the horizontal components and 5 to 10 mm for heights. The differences are slightly larger for the 1993 dataset with 4-7 mm for the horizontal components and 10-20 mm for heights. At several points observed in the year 1993, slightly higher values (greater than 10 mm) were obtained on the eastern

component and up to several tens of mm in height. This can be attributed to differences in the ambiguity resolution strategy of the two software solutions and it indicates the locations where shifts need to be carefully analyzed. However, for most sites, the differences generally remain within repeatability [16]. According to [17] GNSS, processing software packages play an important role in geodetic and geophysical studies. Error estimates or standard deviations do not have to be realistic values given their daily RMS repeatability. They present standard deviations as formal errors (FEs) and scale them according to RMS errors. The scale factor (SF) is defined as the ratio between the RMS error and the formal error.

3 PROCESSING AND ANALYSIS OF THE GEODYNAMIC NETWORK OF THE CITY OF ZAGREB

The aim of this study was to examine the application of appropriate error models and processing strategies for GNSS measurements by testing different software and processing methods that will allow reliably determined point coordinates and velocities to be used in geodynamic and geokinematic analyses. The impact of using a different reference frame in the adjustment (local vs. global network) was also examined. The GNSS measurements on the Geodynamic Network of the City of Zagreb (GNCZ) have been carried out for more than 20 years and they confirm the constant presence of tectonic activity in the area around Medvednica. The stabilization of geodynamic points was performed at most points in the form of deeply stabilized concrete pillars. All GNSS measurements campaigns of GNCZ [2] were processed in the same way using the scientific GNSS software GAMIT/GLOBK ver. 10.34 i 10.6 [19], which uses a Kalman filter to determine velocities from time-separated coordinates. When processing GNSS measurements of GNCZ by using the GAMIT / GLOBK software, all parameters were set for the local network, and the two most stable points in the study area were selected as the reference: the city's permanent CAOP (metal pillar on the building) GPS station and ZZP (metal pillar on the building) GPS station. The offsets of all other points in the network refer to the vector between the mentioned two points. The points of the baseline also had the possibility of a relative shift, but according to [18], they proved to be very stable. In this paper, the Bernese scientific software ver. 5.2 [20] was used for data processing and analysis of GNCZ for periodic campaigns from 2006 to 2009, using the least squares adjustment method. The results of the GNSS processing with the Bernese software were compared with the results of the processing obtained by the GAMIT / GLOBK software used in the realized campaigns. Using the prescribed standards for processing and analyzing GNSS data (IGS, EUREF), an investigation of the impact of various parameters on final processing results was performed. When processing and analyzing GNCZ with the Bernese software, IGS stations were selected as reference points: GRAZ (active since 1993), MATE (active since 1992) and MEDI (active since 1995). All three points are included in the IGS08 reference frame used in the adjustment. It was important to choose permanent

stations that have a continuum of observations given the long period of the observation of the GNCZ. These stations are close to the area of interest (Eurasian plate), but far enough from the regional / local structures and they are not located in tectonically very active areas (to reduce the possibility of reference points moving). Additionally, these stations are under the constant control of IGS (*International GNSS service*). Connecting to the ITRF frame can be done as a global or local/regional connection. The use of global IGS stations as a reference frame is considered to be the most accurate method, while the local/regional connection (e.g. with CROPOS stations) is achieved by an indirect connection with the ITRF frame. Each software package (Gamt and Bernese) was used with its recommended settings, i.e. with the implemented independent GNSS data processing strategies. At the same time, important processing parameters and common standard procedures prescribed by the IGS and EUREF were used, such as: applying the PPP (*Precision Point Positioning*) and DD (*Double Difference*) calculation methods, solving residuals with the outlier ejecting, using global tropospheric and ionospheric models, determination of weights in elevation-dependent observations, ocean correction model usage (FES2004), while the atmospheric correction model was not available. The IGS final orbits and corresponding Earth orientation parameters were used. Other parameters taken into account relate to the limitations and specificities of each software and the applied processing strategies (ambiguity solution method, adjustment method, application of different reference points), which can influence the final solution and must be taken into account (Tab. 3).

Table 3 The parameters of the Bernese and Gamit software solutions used in computing GNCZ campaigns 2006-2009

Parameter / SW	BERN52 (2006-2009)	GAMIT 10.34 (2006-2008) GAMIT 10.6 (2008-2009)
Reference frame	IGb08 1.1.2005.	Local
Fixed stations	GRAZ MATE MEDI	CAOP ZZFP
Processing method	1. step PPP (free) 2. step network solution (DD)	2 steps: free and network solution (DD)
Correlation strategy - baseline	L3	LC (L3-P3)
Residual resolution strategy	Normal, outlier ejected	Outlier ejected
Ambiguity resolution method	Quasi-Ionosphere- Free (L1&L2)	"Wide Lane" & "Narrow Lane"
Orbit, EOP and satellite clocks	from IGS (final)	from SOPAC, NGS (final)
Elevation mask	10°	10°
Interval	30 s / 15 s	30 s / 15 s
Ocean tide	FES2004	FES2004
Atmospheric tide	NONE	NONE
Tropospheric models	GMF(WET & DRY GMF)	GMF (WET & DRY GMF)
Ionospheric model	Global ionospheric	Global ionospheric
Adjustment method	The least squares	Kalman filter

One significant difference in the adjustment method is that the GLOBK uses a Kalman filter (equivalent to sequential least squares if there are no stochastic parameters) that calculates with covariance matrices rather than normal

equations (with which Bernese calculates), and it therefore requires an a priori limit for each estimated parameter. GAMIT produces a solution, which then uses GLOBK to calculate velocities with "weak" constraints on all parameters [19]. The Gamit solution aims to apply "weak" constraints to the entire reference frame: EOP (*Earth Orientation Parameters*), SV (*Space Vehicle*) and coordinate parameters, while the realization of the reference frame is implemented through seven Helmert transformation parameters. Bernese, on the other hand, uses the normal equations expanded with the point coordinate parameters. In the Bernese solution, the equation with minimum constraints is performed. The

parameters are fixed: EOP and SV to IGS standard products and apply "weak" constraints to coordinates only. The reference frame is implemented through four parameters of the Helmert transformation (without translation conditions). Periodic measurements at one-year time intervals for the year 2006, 2007, 2008 and 2009 were processed at the points observed in the GNCZ. By processing GNSS measurements via two software packages: GAMIT/GLOBK - G and Bernese - B, the velocities were calculated between one-year intervals: 2006-2007, 2007-2008, 2008-2009 and two year intervals 2006-2008.

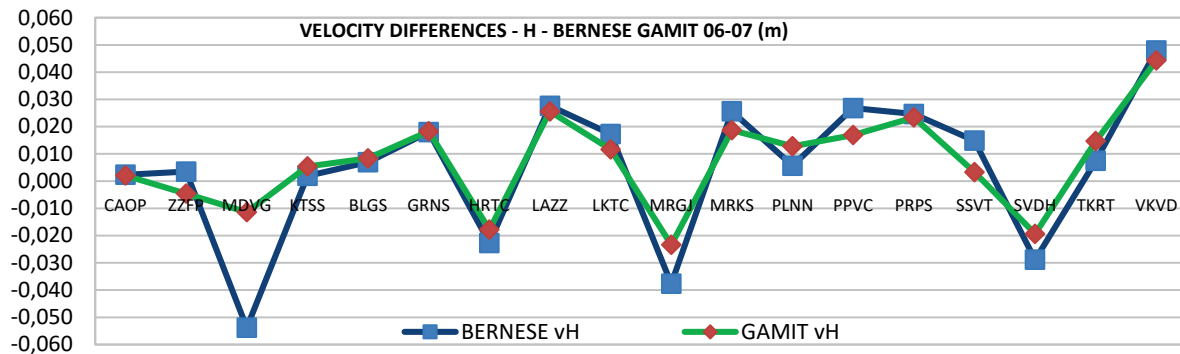


Figure 4 Velocity differences for the component H between the Bernese and Gamit solutions for 2006-2007

The results of the analyses show that in the period from 2006 to 2007, a relatively higher tectonic activity was present. It can be seen from the graph in Fig. 4 that the differences between the two solutions for the height component are at the mm level (mean $\Delta H = 2$ mm), but still, for some deviation points, the ΔH between the two solutions are at a cm level (example the MDVG point ~ 4 cm, MRGJ ~ 1.5 cm, SSVT and PPVC ~ 1 cm). For the horizontal components *E* and *N*, these differences are significantly smaller than for the height component; for all points they are at the mm level (mean $\Delta N = 2$ mm and $\Delta E = 1$ mm). The maximum height shift amplitudes in 2006-2007 were obtained simultaneously with both types of software and they are visible at the points: VKVD ~ 4 cm, LAZZ ~ 2.5 cm, PRPS ~ 2 cm, indicating the presence of the intensity of tectonic movements and a greater geodynamic activity in these areas. Moreover, at the points MDVG and MRGJ, there are higher values of displacement amplitudes (subsidence), however, deviations between the two solutions (Gamit and Bernese) are also visible, with max. values in Bernese solutions being MDVG ~ 5 cm and MRGJ ~ 3.5 cm; while for the Gamit solution, the values are significantly lesser – MDVG ~ 1 cm and MRGJ ~ 2 cm. The most important directions of the points horizontal shifts were towards the north and around the "Mountain" area towards the north-northwest, which is visible at the points: LKTC: north-northwest ~ 1 cm, PPVC: west ~ 1.5 cm, VKVD: west ~ 1 cm and MDVG: north ~ 1 cm. Towards the east, the points MRGJ and SVDH (~ 5 mm) move. Between the years 2007 and 2008, tectonic activities were reduced in comparison to the previous period, which was also reflected in the calculated solutions with both the Gamit and Bernese

software. The differences between the two solutions for the height component are at the mm level (mean $\Delta H = 3$ mm), with no significant deviations at individual points (the maximum value at HRTC, MRGJ and LAZZ is ~ 1 cm). For the horizontal components *E* and *N*, these differences are for all points at the mm level - mean $\Delta E = 2$ mm, while for the north component, a systematic deviation between two solutions $\Delta N \sim 5$ mm for all points is visible. However, relatively higher values of horizontal displacements of ~ 1 cm at the points: SSVT (southwest), PRPS (northeast) and VKVD (northeast) were obtained. Compared to previous displacements (2006-2007), a change in the direction of the displacement of those points is also visible. In the period from 2008 to 2009 the displacements at geodynamic points show a renewed increase in tectonic activity. The differences between the two software solutions for the height component are larger in this period at the cm level (mean $\Delta H \sim 1.5$ cm). Maximum differences between the two solutions were measured at PRPS ~ 4 cm and STPN ~ 2.5 cm, which also show different directions of the height deviation between the two software solutions. In this period, a slightly larger shift at the ZZFP point in the height direction (~ 3.5 cm for the Bernese solution) was observed, which was taken as a reference point in the GAMIT solution. The difference between the two solutions at the ZZFP point is $\Delta H = 2.5$ cm, which is very likely the reason for the systematic error at all points with a mean value of $\Delta H \sim 1.5$ cm. Furthermore, the maximum in the amplitude of displacement at the component H (subsidence) were recorded at the point MDVG in the Gamit solution, which is approximately 4 cm, while in the Bernese solution this maximum is 2 cm, then at points: BKVJ and ZLMG (~ 3.5 cm), which indicates the present intensity

of tectonic movements and a greater geodynamic activity in these areas. The highest rising, in addition to the ZZFP point, is also visible on the KPNC point (~ 3 cm). Here, due to the systematic shift of the entire network, it is considered that the cause of the difference between the two software solutions at all points is precisely the shift that comes from the ZZFP point, which is considered as a reference point in the Gamit solution. For position components E and N , these differences are significantly smaller, as they are for all points at the mm level (mean value $\Delta N = 1$ mm and $\Delta E = 3$ mm). Larger differences between software solutions at certain points in the horizontal components E and N are also visible here, where

differences in the direction are visible at the points: SSVT $\Delta N \sim 2$ cm, GRNC $\Delta E \sim 1.5$ cm and PRPS $\Delta E \sim 1$ cm. The maximum for the horizontal components for both solutions are $\sim 1 - 1.5$ cm, observed at the points: LAZZ, PLNN and PPVC (south), BLGS, SSVT, VKVD and ZLMG (east) and ZZFP in the southwest direction. Unlike previous campaigns, there was no trend of northward direction for all points. It should be emphasized here that the 2009 campaign was processed with the new version of GAMIT/GLOBK 10.6, while the previous campaigns of 2006, 2007 and 2008 were processed with the GAMIT/GLOBK solution 10.34.

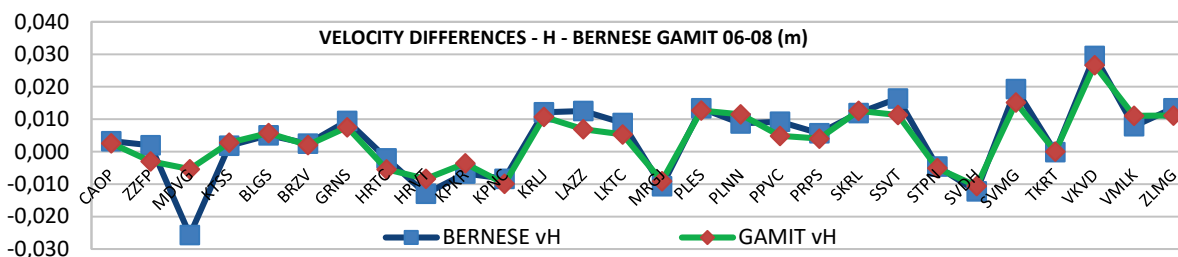


Figure 5 Velocity differences for the component H between the Bernese and Gamit solutions for 2006-2008.

The differences in the solutions obtained for the two-year period from 2006 to 2008 were also compared, and it can be seen that the differences between the solutions of the two software programs are significantly smaller, and an absolute decrease of the displacement amplitudes for both solutions can be observed (see Fig. 5).

It can be seen from the graph in Fig. 5 that the differences between the two solutions for the height component are below the mm level (mean $\Delta H = 0.2$ mm). With the exception of the MDVG point, where there is a discrepancy in the height between the two software programs (as was the case in the period from 2006 to 2007), it is noticeably smaller over a two-year period (~ 2 cm). The highest amplitudes of the displacement in height occur in both solutions at the point: VKVD (~ 3 cm) as in the period from 2006 to 2007, indicating greater geodynamic activities present at that point in 2006. The most important are the directions of points moving around the "Mountain" area towards the northwest and the elevation of these points, which can be interpreted as a sudden rise during 2006. For the horizontal components E and N , these differences are for all points at the mm level (mean $\Delta N = 4$ mm and $\Delta E = 2$ mm). The component N shows a small systematic shift between the two software solutions with a mean value of 4 mm, and it can be concluded that this shift came from the period from 2007 to 2008.

The processing results show that for each period, different values of displacement amplitudes were obtained at individual points, as well as different directions of displacement with two applied software solutions. This directly indicates the constant variability of the intensity of tectonic movements and the activity of the most important faults of the structural frame. The maximum differences that are obtained at individual points are 1 cm for the positional component and 1 - 2 cm for the height component for one-year intervals between periodic observations, and those

values are in accordance with the research results of [16]. The biggest difference between the two software solutions for the height component is visible on the MDVG point and the reason for that is the velocity resolution strategy. The Bernese solution uses normal equations extended with coordinate parameters, where the largest differences in the MDVG point of ~ 4 cm were obtained for the period from 2006 to 2007, while in the Gamit solution, velocity is calculated from covariance matrices with stronger parameter constraints (~ 1 cm). Larger discrepancies between the two software programs also appear in the period from 2008 to 2009 for the ZZFP reference point (velocity differences for the height component of ~ 2.5 cm), which also affects the calculated velocities for all points in the 2009 campaign, while the largest deviation for that period between the two software programs is visible on the PRPS point ~ 4 cm.

An additional analysis was performed by using a network of CROPOS stations (*CROatian POSitioning System*). As CROPOS stations were not available for the entire observation period of the periodic campaigns from 2006 to 2009, as the system started with the operation in December 2008, the use of the CROPOS reference points for comparisons and analyses was performed only for the year 2009. Although geophysical impacts are also present in global solutions and usually have more noise in observations than the local or regional network solutions [21], the regional and local impacts such as atmospheric or hydrological effects are usually not a priori modeled in global analyzes, but can be modeled for a regional or local station network if meteorological and hydrological data are available. Annual amplitudes of atmospheric influences can reach 4 mm for the radial component and are usually lesser than 0.5 mm for the horizontal component [15]. Global seasonal cycles in temperature and humidity depend on latitude, and the amplitudes of the north-south gradients are 40% larger than

the amplitudes of the east-west gradients. Longitude-dependent variations resulting from the local and regional effects show smaller mean amplitudes of east-west gradients compared to north-south gradients. According to [23], the amplitudes of annual and semi-annual signals in tropospheric gradients are generally smaller for the east-west component (mean absolute value of 0.17 mm) versus the north-south gradients (mean absolute value of 0.30 mm). However, the impact on heights is much greater than that on horizontal coordinates and the height is up to several tens of mm [23]. The analysis showed that the impact of the choice of reference stations (global/regional/local) on the calculated point coordinates was significant, mostly for the height component, where the differences of 2 cm were obtained between the global and local system (Fig. 6), while for the horizontal components (E and N), the differences were up to 1.5 cm. The differences between the IGS and CROPOS reference stations in the height component are about 5 mm. Therefore, it can be concluded that the selection of reference stations (global vs local) significantly affects the height component, while positionally, this influence is smaller.

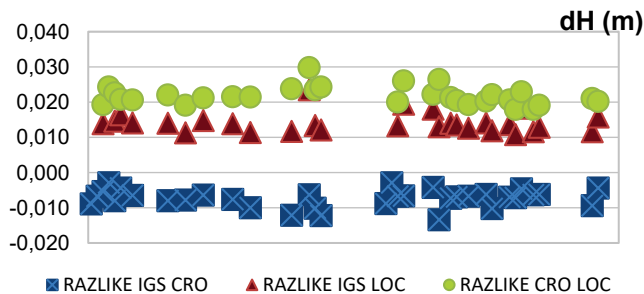


Figure 6 Global vs. regional vs. local reference stations' network differences

3.1 Noise Analysis of the Points of the Geodynamic Network of the City of Zagreb

A noise analysis was carried out for the campaigns from 2006 to 2009, and according to the formulas of [11] respectively, the values of σ_w and σ_f for all components were calculated according to the weighted RMS values for the calculated velocities. Generally, the RMS values are slightly higher for the northern component versus the eastern component, and most are for the height component. When it comes to small RMS values (mm level), which were mostly the case for all points in the campaigns processed and the noise level is of the same rank. The mean RMS values for the calculated velocities for the positional components (E and N) for all campaigns are ~ 0.6 mm, which means that the colored measurement noise is for $N \sim 0.8$ mm and for $E \sim 0.3$ mm. The mean RMS values for the calculated velocities for the height component (H) for all campaigns are ~ 2.2 mm, which means that the color measurement noise is ~ 6.9 mm for that component. The maximum observed RMS value is: 3.3 mm, which for the height component of colored noise is up to 7.6 mm. The final velocity uncertainty error σ_r for the maximum recorded noise values of periodic measurements at one-year intervals from the first session observations is ~ 1 cm. For the

purpose of the noise analysis at the points showing higher displacement amplitudes and greater differences between the two software programs, a kinematic analysis of daily sessions was additionally performed by using modules in the Bernese software in such a way that the coordinates were determined independently epoch by epoch. The detection and ejection of the outliers was also performed epoch by epoch in the iteration process. In this way, the analysis of noise in the daily solutions was performed. In the period from 2006 to 2007, the points that had the largest shift are MDVG and VKVD. For the VKVD point, a larger amplitude of displacement in both software solutions is clearly visible, and this point in the noise analysis also had the largest RMS error and therefore, the largest values of the colored noise and the final error of velocity uncertainty. The MDVG point shows the largest amplitudes of displacement in height in the period from 2006 to 2007, but also the biggest differences between the two software solutions.

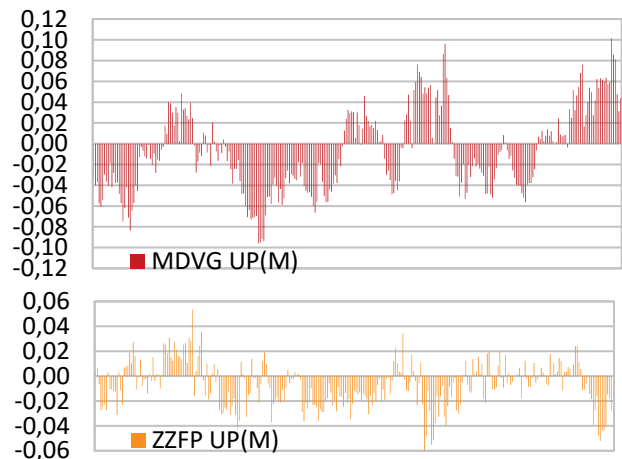


Figure 7 Kinematic analysis of the daily sessions at the MDVG and ZZFP stations for the 2006 campaign

Fig. 7 shows the kinematic analysis of the daily session for the 2006 campaign at the MDVG point - component H, compared to the ZZFP point for the same period (reference point). The graph in Figure 7 shows an increase in noise at the height component for MDVG versus the point ZZFP. At both reference points, CAOP and ZZFP, a lower presence of noise is visible, with jumps of up to $\max \pm 5$ cm, while points with larger displacement amplitudes VKVD and MDVG also have larger noises with jumps of up to ± 10 cm in the 2006 campaign. The reference point ZZFP in all campaigns has the noise level of ± 5 cm, and at the MDVG point, there is more noise in the 2006 campaign than in the 2007, 2008 and 2009 campaigns. Moreover, this point shows higher amplitudes of displacement in that period. Therefore, the amplitudes of displacements at the points for periodic campaigns should be interpreted with attention, because higher measurement noise also affects the higher final error of velocity uncertainty.

4 CROPOS STATION COORDINATE TIME SERIES ANALYSIS

The GNSS permanent station data have been widely used for positioning and navigation, as well as for studying geodynamics. In the last few years, the GNSS data have been used extensively for the exploration and analysis of geodynamic and geokinematic shifts. In determining the velocities of points from GNSS measurements, the existence of continuous and long-lasting GNSS observations is of great importance for quality analyses and the evaluation of the accuracy of calculated velocities. The analysis of the observations of these points enables, in addition to the detection of the shift trend, the detection of periodic phenomena as well as the phenomena that have nonlinear structures in the time series of coordinates. The analysis of changes in the coordinate time series is being increasingly used as an accurate and reliable source of information on local geodynamics. An example is the permanent IGS and EPN networks used for the global, regional and local geodynamics research. The GNSS networks of various institutions have been established for the research of local geodynamics from the analysis of the time series of coordinates: Geospatial Information Authority of Japan - GSI, Southern California Integrated GPS Network - SCIGN, Jet Propulsion Laboratory - JPL, Massachusetts Institute of Technology - MIT, Scripps Orbit and Permanent Array Center - SOPAC etc. [22]. With the establishment of the CROPOS station network at the end of 2008, the state network of the permanent stations of the Republic of Croatia was realized; while for the area of the City of Zagreb, such a network of permanent stations was not feasible for economic reasons. Therefore, periodic measurements (24 h observations with two to three sessions) on the points of the City of Zagreb network were used for geodynamic research. The closest permanent station in the surveyed wider area of the City of Zagreb was the CAOP station, which is no longer in operation as a permanent station, and since the establishment of CROPOS, the closest stations have been ZAGR at the Faculty of Geodesy and ZABO at the cadastral office building located on the north side of Medvednica. It should be said that the CROPOS stations are stabilized on the roofs of buildings on fixed metal pillars. For the ZAGR and ZABO stations, daily sessions were calculated on a monthly basis for 2018 and for a 10-year period (2009-2018), where an observation period was selected in the campaigns of the geodynamic network of the City of Zagreb (June-July) to eliminate the seasonal impact. The same strategy and reference network (IGS stations) were used for the processing and adjustment as for the processing of the Geodynamic Network of the City of Zagreb. The adjustment statistics for the CROPOS stations ZAGR and ZABO in the processing of annual sessions show that the RMS value is between 1.12 – 1.13 mm, while the "Chi-square" test for all years is between 1.39 - 1.79.

Previous research and analyses on the permanent GNSS stations that are established worldwide show annual variations with maximum amplitudes of ± 1 cm for the horizontal components and ± 2 cm for the vertical components [24]. The analyses performed in the daily

sessions over a 10-year period (2009-2018) show that the two CROPOS stations ZAGR and ZABO are very stable.

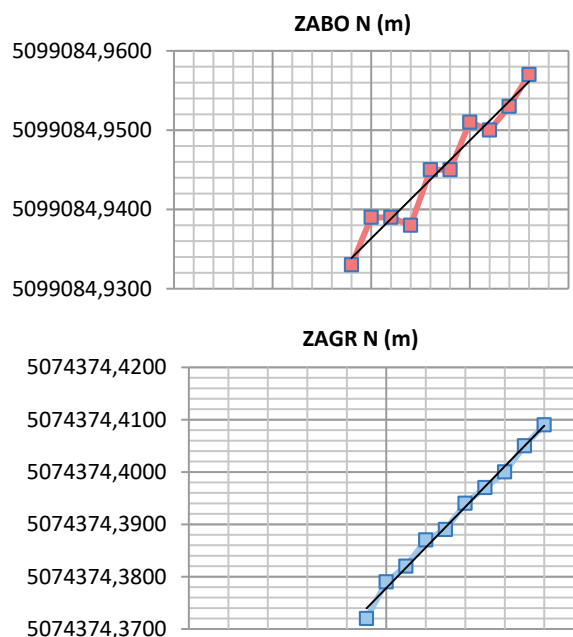


Figure 8 Time series analysis of coordinates for a 10-year period at the ZAGR and ZABO stations - component N

An analysis along the horizontal axis N shows a linear trend of increasing in the north direction by 2 cm for ZABO and 4 cm for ZAGR in a 10-year period, and there are no major jumps at points, hence we can conclude that the points are stable in terms of jumps and discontinuities (Fig. 8).

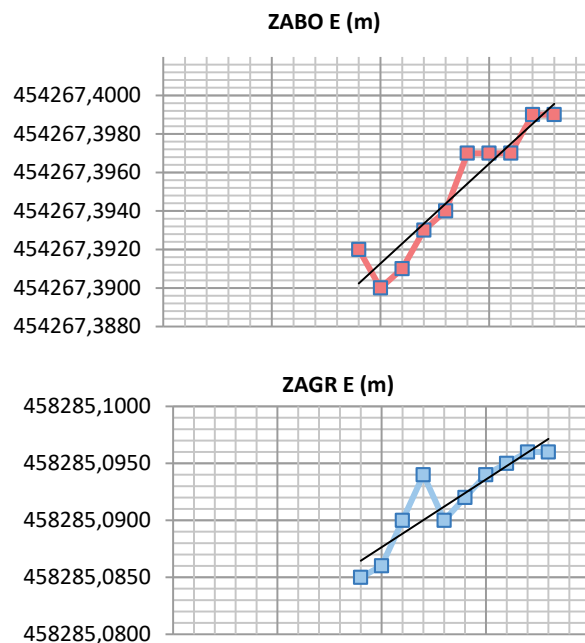


Figure 9 Time series analysis of coordinates for a 10-year period at the ZAGR and ZABO stations - component E

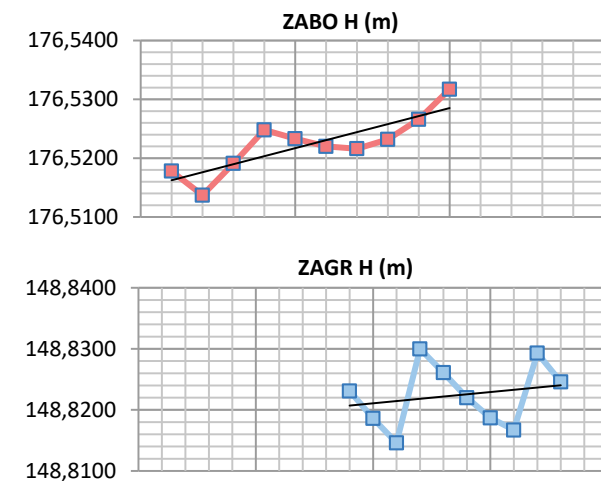


Figure 10 Time series analysis of coordinates for a 10-year period at the ZAGR and ZABO stations - component H

An analysis along the horizontal axis E shows a linear trend of increasing in the east direction by 1 cm, which means that the points move in the northeast direction without significant jumps and discontinuities at the ZAGR and ZABO locations in a 10-year period (Fig. 9). At ZAGR, a slight deviation was observed in 2012, which corresponds to the fact that in that year, September was chosen for observations, which is slightly later than for other sessions (atmospheric conditions are different), which were observed in June or July, which could be the reason for the differences of 4 mm.

The height axis - H shows displacements of up to 2 cm in the 10-year period, where the linear trend is a slight increase in height for the ZAGR and ZABO points (Fig. 10). For the ZAGR point, changes in the direction (jumps) were seen in the years 2011, 2012 and 2016, while variations for the ZABO point were less expressed in the same time period.

If we look at the one-year period in which the monthly data for the two stations ZAGR and ZABO for 2018 were processed, and which may contain seasonal variations during the year, we can see a slight increase along the N axis during one year and about 5 mm variations on both stations. A slight increase is also visible along the E axis with a variation of 7 mm and a jump (5 mm) in May with a similar trend on both stations. The H axis shows a linear trend of subsidence for both the ZAGR and ZABO stations by 1 cm, where a jump in April (7 mm) is visible for the ZAGR point, while monthly coordinate variations (changes of direction by 3 mm) are visible for the ZABO point. It should be emphasized here that the ZABO point is located on a high metal pillar which can cause these small variations, as well as seasonal conditions (atmosphere). The spatial distribution of the parameters of periodic signals and their correlation with changes in the atmospheric factors and other geophysical factors is necessary to consider the whole spectrum of errors. Atmospheric data were not determined at the ZAGR and ZABO stations, nor were any other geophysical influences recorded, however, the analysis of the time series of coordinates was performed, and the FODITS algorithm of the Bernese software was used for the analysis. The analysis of

time series of coordinates enables the detection of periodic signals (amplitude and phase of the signal), as well as other elements that can affect the coordinates of points. For the ZAGR and ZABO stations, the amplitude and phase of the periodic function were determined, as well as the basic components that were added to the functional model, and which correspond to the coordinates of the points and their linear velocities. Using the FODITS algorithm, new elements were determined in order to improve the functional model representing the time series of coordinates. For the ZAGR station, new elements of discontinuity were recorded for the observations in 2011, 2012, 2014 and 2016, which are visible primarily at the height component (Fig. 10). New elements of discontinuity for 2011, 2014 and 2016 have also been determined for the ZABO station, while for 2014, a new element for linear velocity was also determined. No significant deviations were recorded for any component, and no shifts were recorded due to earthquakes, equipment changes or other events. With the obtained new elements of the functional model, the coordinates and velocities in the adjustment process are recalculated. Periodic variations of the coordinates of up to 1 cm (in a 10-year period) were recorded for the height component, and according to [24], such variations are standard values for stable permanent networks in Europe. No correlation was noticed between the two stations ZAGR and ZABO in the time series of coordinates and related to the spatial component (distance of about 10 km), except for the already known fact that the points move in the northeast direction. In the height component, a descent was recorded for the two stations ZAGR and ZABO for the year 2018, however, for a ten-year period, a slight ascent was recorded for those two stations.

4.1 CROPOS Station Velocity Determination Analysis

An analysis of the displacements on the geodynamic network of the City of Zagreb from different epochs showed that it is necessary to carry out GNSS campaigns at the intervals of one year, since in the case of long-term intervals, an averaging of displacements occurs. However, the accuracy of determining the velocities from one-year periods depends on a number of factors: the intensity of the measurement noise, measurement sessions quantity and the applied computation strategies. Point velocities for periodic GNSS measurements correspond to the estimated linear rate of the daily solutions of two or more measurements. Because periodic measurements rely on two or more measurements with several days of data, periodic signals and jumps cannot be determined with certainty. These parameters represent the uncertainty of determining velocities from periodic measurements. Most campaigns are observed over the same time period to minimize the impact of the annual and semi-annual signals (seasonal impact), as it was the case with the City of Zagreb Geodynamic Network. However, according to [14], when processing GNSS observations over a period of less than 2.5 years, annual signals can cause significant errors in the determination of point velocities. When a period of more than 4.5 years between the observations is available, the velocity determination error drops significantly to negligible values [14]. Therefore, it is recommended that a minimum

period of 2.5 years be used as the standard for determining the velocity solution, so that the velocities of the points are reliably determined. Moreover, the velocity data for geophysical interpretations obtained in a shorter period of time should be taken with caution. According to [20], this recommendation was adopted for processing with the Bernese v5.2 GNSS software, and it is used in the FODITS module.

The uncertainty of velocities decreases with the expression: $1 / \sqrt{\text{the number of samples}}$, but is not a function of time (duration of measurement) that depends on the time span. The uncertainty of 1 mm / yr can be achieved at best in a one-year period, but also at worst in a 4.5-year period.

From one-year periods between observations, the velocities of point cannot be reliably determined on the basis of a linear velocity trend. By analyzing the calculated annual and multi-year velocities for the years from 2009 to 2018, results were obtained for the CROPOS stations ZAGR and

ZABO that correspond to previous studies [14]. On the example of the point ZAGR, determining the velocity in the height component for a one-year period versus multi-year solutions shows amplitudes of up to 1.4 cm (Fig. 11), while in the horizontal components (*E* and *N*), they are up to 7 mm. These differences can be attributed to periodic and stochastic influences on the determined velocity. For this purpose, it is necessary to determine the annual parameters of velocity corrections from the previous analysis of the time series of coordinates for annual periods. In this way, kinematic parameters containing periodic and stochastic influences can be determined, which enable the definition of real values of velocities for annual periods. According to [14], the errors in determining velocity considering the time component were compared (annual vs. 3.5-year), where the max. annual amplitudes of 0.3 - 4.4 mm in the horizontal direction and 1.1 - 10.9 mm in height were determined (Tab. 4).

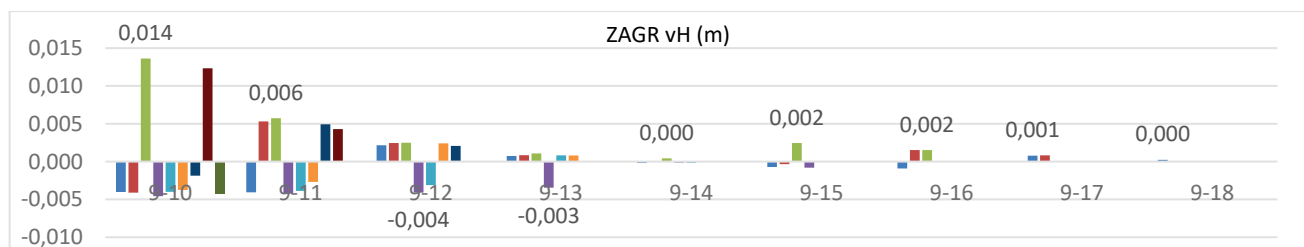


Figure 11 Differences in ΔH (m) for the CROPOS station ZAGR for one-year and multi-year solutions

Table 4 Range and RMS values for the annual and semi-annual amplitudes (Blewitt, G., Lavallee, D. 2002)

Velocity component	Annual signal RMS mm	Annual signal range mm	Semi-annual signal RMS mm	Semi-annual signal range mm
H	4.4	1.1 – 10.9	1.5	0.2 – 3.6
E	1.8	0.3 – 4.4	0.5	0.1 – 2.0
N	1.5	0.2 – 2.9	0.7	0.1 – 1.2

It can therefore be concluded that the research conducted in this paper shows similar results as in [14]. It can be seen from Fig. 11 that for periods longer than 2.5 years, the differences in velocities begin to equalize, while after 4.5 years, they are negligible. The variation of the annual component mainly comes from hydrological and atmospheric influences. Therefore, if annual signals are not taken into account, they can significantly reduce the accuracy of determining the point velocities used for highly accurate purposes such as plate tectonics or reference frames, and especially for geodynamic and geokinematic research.

5 CONCLUSION

Using the GNSS observation data from the geodynamic network of the City of Zagreb for the period from 2006 to 2009, different error models and GNSS measurement processing strategies were analyzed with the possibility of eliminating systematic and random influences. It all made it possible to determine the coordinate and velocity reliability and it showed the possibilities of using it for geodynamic and geokinematic analyses. This research has shown that when applying different parameters such as a local reference

solution versus a global one, the identity of the reference frame must be ensured, because otherwise, solutions can be interpreted ambiguously in a geodynamic analysis. Furthermore, certain differences in the coordinate and velocity solutions are visible when using two software programs (Bernese and GAMIT/GLOBK), which results from different adjustment and velocity calculation strategies. The research showed that when applying different software solutions for processing high-precision measurements that use different processing strategies, the differences in the velocity of up to 1 cm per the horizontal components *E* and *N* and of up to 2 cm per the height component are possible. However, the mean values are at the mm level. Uncertainties in determining velocities are visible in the annual periods since they contain a periodic and stochastic signal. It can be seen that for linear velocities in the 2.5 periods, these differences are below mm, which directly indicates the connection between a higher measurement noise and the processing strategies implemented in software solutions. Higher values were obtained at several points, and in the case of significant shifts, it is necessary to perform the analysis by using the time series analysis, because in this way, we obtain reliable mean values that are within repeatability. Therefore, in order to monitor the geodynamics of a particular area of interest, it is necessary to use a previously noise analysis on the daily time series of coordinates in the area of interest with the aim of determining the true character of the geodynamic change. The research and analyses performed in this paper indicate certain uncertainties in determining the velocities from periodic measurements. They are affected by periodic signals and can cause significant errors in determining point velocities. Therefore, several studies recommend a minimum

period of 2.5 years to be used as the standard for determining the velocity solution in order to reliably determine the velocities of geodynamic points. Velocities which are used as kinematic parameters for geophysical interpretations and that are obtained from the one-year period between the observations on geodynamic points must be interpreted with a detailed analysis. On the other hand, permanent GNSS stations brings a new quality to geodynamic research and the future of global and local geodynamic research is under constant monitoring. The analysis of changes in the time series of coordinates on permanent stations was also used in this paper as an accurate and reliable source of information on local geodynamics. At shorter time intervals (such as periodic observations on geodynamic networks), these values are influenced by the errors of different periodic and stochastic components. Moreover, one of the assumptions in the GNSS observation processing is that measurement errors are random and timeless (white noise), which leads to unrealistically estimated uncertainties in determining velocities, and affects the height component (~ 1 cm) the most. Previous research shows that white and pink noise dominate the GNSS noise spectrum for the time series of coordinates, hence it is necessary to calculate the true value of noise based on the analysis of the time series of the coordinates and the application of one of the models of the spectral analysis or empirical formulas. To determine the geokinematic parameters, the data of several daily GNSS solutions of the CROPOS stations were analyzed, since the determination of the displacement parameters requires a previous statistical analysis of the daily solutions, which provides control for the jumps and discontinuities. A permanent network of the CROPOS was available from 2009, therefore, the analysis of the time series of coordinates for the two stations ZAGR and ZABO was performed by using the FODITS algorithm and new elements of the functional model were determined. Such parameters can be used to determine the true character of the displacement/velocity of the geodynamic point (GMGZ) by using one of the methods of spatial interpolation. Further determination of parameters from the analysis of the time series of the CROPOS station coordinates will enable the use of the Geodynamic Network of the City of Zagreb for geodynamic and geokinematic purposes (the monitoring of the displacement parameters due to earthquakes or from other sources). The research conducted in this paper shows that in the geodynamic analyses for the interpretation of displacements, in addition to geological or seismological data, the influence of processing parameters for estimating reliability should be determined. The GNSS processing strategies analysis, as well as the determination of local geodynamic parameters from the analysis of the time series of coordinates, should be considered. The determination of the kinematic parameters at the points of the geodynamic network of the City of Zagreb will enable a further analysis of the observation epochs and determination of the kinematic model for the monitoring of the geodynamic and geokinematic phenomena. Additionally, an atmospheric impact analysis should be considered for an additional interpretation of the geodynamic and geokinematic parameters. Furthermore, for detailed analyses, it is necessary to establish denser permanent stations (~ 5 km or

more) in the area of interest (the City of Zagreb and Medvednica).

6 REFERENCES

- [1] Čolić, K., Bašić, T., Seeger, H., Gojčeta, B., Altiner, Y., Rašić, Lj., Medić, Z., Pribičević B., Medak, D., Marjanović, M., & Prelogović, E. (1996). Hrvatska u EUREF'94 i projekt CRODYN. *Geodetski list: glasilo Hrvatskoga geodetskog društva*, 50, 331-351. (in Croatian)
- [2] Đapo, A. (2009). Korelacija geodetskog i geološkog modela tektonskih pomaka na primjeru šireg područja Grada Zagreba, *doktorska disertacija*, Zagreb, Geodetski fakultet, 08.05.2009, iz: <https://www.bib.irb.hr/394400> (in Croatian)
- [3] Pribičević, B., Đapo, A., & Medak, D. (2011). Geodetsko-geološka istraživanja na širem zagrebačkom području oslonjena na Geodinamičku mrežu Grada Zagreba. *Geod. list* 1, 1-19, UDK 551.2/3:551.242.1:528.41(497.5):004.4 (in Croatian)
- [4] Marjanović, M., Bašić, T., & Bačić, Ž. (2012). Determination of Horizontal and Vertical Movements of the Adriatic Microplate on the Basis of GPS Measurements. *Conference: Geodesy for Planet Earth, Session 3: Geodesy and Geodynamics: Global and Regional Scales* At: Buenos Aires, Argentina, 31.08.-04.09.2009 Volume: International Association of Geodesy Symposia, Vol. 136, Kenyon, Steve; Pacion, Maria Christina; Marti Urs (eds), Springer Verlag, 683-688. https://doi.org/10.1007/978-3-642-20338-1_84
- [5] Pavasović, M., Marjanović, M., & Bašić, T. (2016). Latest study of Adriatic microplate over the territory of Republic of Croatia. *Conference: 18th General Assembly of WEGENER* At: São Miguel, Açores, Portugal Project: Geo+++ FO
- [6] Malkin, Z. M. & Voinov, A. V. (2000). Preliminary results of processing of EUREF observations using non-fiducial strategy. *IGS Network Workshop 2000*, Oslo, Norway, Jul 12-15.
- [7] Barnett, V. & Lewis, T. (1994). *Outliers in Statistical Data*. 3rd Edition, John Wiley & Sons, Kluwer Academic Publishers, Boston/Dordrecht/London.
- [8] Metivier, L., Collilieux, X., Lercier, D., Altamimi, Z., & Beauducel, F. (2014). Global coseismic deformations, GNSS time series analysis, and earthquake scaling laws. *Journal of geophysical Research Solid Earth*, 119. <https://doi.org/10.1002/2014JB011280>
- [9] Williams, S. D. P., Bock, Y., Fang, P., Jamason, P., Nikolaidis, R. M., Prawirodirdjo, L., Miller, M., & Johnson, D. J. (2004). Error analysis of continuous GPS position time series. *Journal of Geophysical Research*. <https://doi.org/10.1029/2003JB002741>
- [10] Langbein, J. & Johnson, H. (1997). Correlated errors in geodetic time series: Implications for time-dependent deformation. *Journal of Geophysical Research*, 102(B1), 591-603.
- [11] Mao, A., Harrison, C. G. A. & Dixon, T. H. (1999). Noise in GPS coordinate time series, *Journal of Geophysical Research*, 104(B2), 2797-2816. <https://doi.org/10.1029/1998JB900033>
- [12] Calais, E. et al. (2000). REGAL: a permanent GPS network in the Western Alps. Configuration and first results. *Comptes Rendus de l'Academie des Sciences, Series IIA Earth and Planetary Science*. 331. 435-442.
- [13] Calais, E., Han, J. Y., DeMets, C. & Nocquet J. M. (2006). Deformation of the North American plate interior from a decade of continuous GPS measurements, *Journal of Geophysical Research*, 111, B06402. <https://doi.org/10.1029/2005JB004253>
- [14] Blewitt, G. & Lavallee, D. (2002). Effect of Annual Signals on Geodetic Velocity. *Journal of Geophysical Research*, 107(B7). <https://doi.org/10.1029/2001JB000570>

- [15] Dong, D., Fang, P., Bock, Y., Cheng, M. K., & Miyazaki, S. (2002). Anatomy of apparent seasonal variations from GPS-derived site position time series, *Journal of Geophysical Research*, 107(B4), 2075. <https://doi.org/10.1029/2001JB000573>
- [16] Vigny, C. et al (2002). GPS network monitors the Western Alps deformation over a five-year period: 1993-1998. *Journal of Geodesy*, 76, 63-76. <https://doi.org/10.1007/s00190-001-0231-8>
- [17] Cetin, S., Aydin, C., & Dogan, U. (2019). Comparing GPS positioning errors derived from GAMIT/GLOBK and Bernese GNSS software packages: A case study in CORS-TR in Turkey. *Survey Review*, 51(369), 533-543. <https://doi.org/10.1080/00396265.2018.1505349>
- [18] Pribičević, B. & Đapo, A. (2016). Analiza pomaka na Geodinamičkoj mreži Grada Zagreba iz različitih vremenskih epoha. *Geodetski list*, 3, 207-230. <https://www.bib.irb.hr/846156> (in Croatian)
- [19] Herring, T. A., King, R. W., Floyd, M. A., & McClusky, S. C. (2018). *Introduction to GAMIT/GLOBK*. Department of Earth, Atmospheric, and Planetary Sciences Massachusetts Institute of Technology.
- [20] Dach, R., Lutz, S., Walser, P., & Fridez, P. (2015). Bernese GNSS Software Version 5.2 Astronomical Institute, University of Bern. <https://doi.org/10.7892/boris.72297>
- [21] Steigenberger, P., Rothacher, M., Dietrich, R., Fritsche, M., Rülke, A., & Vey, S. (2006). Reprocessing of a global GPS network. *Journal of Geophysical Research*, 111, B05402. <https://doi.org/10.1029/2005JB003747>
- [22] Herring, T. A., Melbourne, T. I., Murray, M. H., Floyd, M. A., Szeliaga, W. M., King, R. W., Phillips, D. A., Puskas, C. M., Santillan, M., & Wang, L. (2016). Plate Boundary Observatory and related networks: GPS data analysis methods and geodetic products. *Reviews of Geophysics*. <https://doi.org/10.1002/2016RG000529>
- [23] Meindl, M., Schaer, S., Hugentobler, U., & Beutler, G. (2004). Tropospheric Gradient Estimation at CODE: Results from Global Solutions. *Journal of the Meteorological Society of Japan*, 82, 331-338. <https://doi.org/10.2151/jmsj.2004.331>
- [24] Amiri-Simkooei, A. R., Tiberius, C. C. J. M., & Teunissen, P. J. G. (2007). Assessment of noise in GPS coordinate time series: Methodology and results. *Journal of Geophysical Research*, 112, B07413. <https://doi.org/10.1029/2006JB004913>

Authors' contacts:

Margareta Premužić, PhD
(Corresponding author)
State Geodetic Administration, Zagreb
Gruška 20, 10000 Zagreb, Croatia
margareta.premuzic@dgu.hr

Almin Đapo, Associate Professor, PhD
University of Zagreb, Faculty of Geodesy,
Kačićeva 26, 10000 Zagreb, Croatia
adapo@geof.hr

Željko Bačić, Full Professor, PhD
University of Zagreb, Faculty of Geodesy,
Kačićeva 26, 10000 Zagreb, Croatia
zbacic@geof.hr

Boško Pribičević, Full Professor, PhD
University of Zagreb, Faculty of Geodesy,
Kačićeva 26, 10000 Zagreb, Croatia
bpribic@geof.hr

Statistical Methods in Building Industry to Determine Prices Indices

Helena Ellingerová, Zora Petráková, Ingrida Skalíková*

Abstract. Tender price is often affected by the location of the construction, which is usually determined by the investor, and it has an impact on the traffic in the particular location. Individual time of supply and the method of realization play an important role as well. They both are determined by the investor along with the designer of the particular construction. Contractors often complain about the lack of time needed for the preparation of their tender prices. Therefore, it is necessary to look for the possibilities how to reliably speed up this process at the same time taking into account all of the specific features of a structure. This article deals with the application of two statistical methods. The Pareto analysis, which can be used during the design of the tender price, and the extrapolation method, which can be used for the estimation of the price development, based on the regression analysis of the time series. The results of the article particularly serve to contractors in the building industry to better prepare their price offers in tenders. The findings of this document may also be applicable in other countries which have a similar economic profile as Slovakia.

Keywords: building industry; Pareto analysis; prices indices; statistical methods

1 INTRODUCTION

Based on the needs of the construction practice, certain statistical methods are used more frequently. Their aim is to analyze several problems within the investment process during the preparation and the realization phase of the construction contract. For the contractor, the design of the tender price is one of the most difficult problems.

This price represents the price for which he is willing to perform the contract. The tender price must take into account all the specifics of the construction contract, which result from the individuality and the character of the particular construction, such as the layout, the design, the architectural solution, as well as the operational and ecological solutions of a structure [14].

The main role of a statistical method is typically to examine the mass phenomena and the variability of their expression. The essential element is the design of a database by collecting all the necessary information, define the set of statistical parameters, and finally to analyze all the examined phenomena. Methods of statistical analysis provide a particular set of techniques for quantification of the basic statistical set of regularities or the sample of files for the purpose of their use in the subsequent practical activities [4]. The issue of offers in the construction sector is the subject of interest of several scientific publications, not only in the Slovak Republic but also in other Central European countries such as Poland, Czech Republic and Hungary [13, 5].

Current trend in building industry is to reduce the workload in preparing the offering price of the commission. Traditional methods of determining the offering price using the detailed budget are being replaced by innovative approaches for evaluating the building flow already in the phase of construction preparation. One of these innovative approaches of determining the offering price is a form of parametric budgeting. This method using parametric estimate of expenses and other related mathematical statistical methods (regression function CER - Cost Estimating Relationships) is already showing results in Czech Republic [22].

Time factor is often being omitted in preparation of a bid, primarily for reasons of competitiveness, which is not always the correct procedure because some time always passes between the preparation of the bid and the final realization. The prices of building work and materials as well as other commodities change their value over time; therefore, it is sensible to account for this development, especially during times of greater value deviation, by adjusting the offering price by a reasonable amount. This article explores this problem and its solution using the second degree multinomial.

1.1 Literature Research

Ernest, Theophilus, Amoah & Emmanuel [6] conducted a quantitative survey in the form of a questionnaire containing 23 economic indicators. The results of the study point to the most important economic indicators to be taken into account in creating the offer in construction tenders. Those are as follows: the gross domestic product of the country (GDP), interest rates, exchange rate (exchange rate risk), and consumer price index.

Samani, Gregory, Leal, Mendes, & Correia [18] in their analysis point out, that LCCA (Life Cycle Cost Analysis) is a tool for assessing the costs associated with building life cycle phases in the building industry. The life-cycle phases of a building are the following: preparation, implementation, operation and change of the purpose of use, eventually liquidation.

The authors, in the conclusions of their study in American cities, believe that the location of the building with the impact of the rate of maintenance cost inflation (rising energy and safety costs) is also a factor that is not negligible in creating price offers in tenders. Amuda Yusuf & Mohamed [2] dealt with cost management and economy-effectiveness of the costs of the entire life cycle of the building. The authors came to the conclusion based on structured interviews and questionnaire surveys: adopting a pricing mechanism based on standards (of the most advanced countries in the world) could increase the quality of prediction of tender's price

offers in construction in all stages of the life cycle of a building. They also point to the use of mathematical-statistical methods in their creation.

The authors [17], point to the importance of statistical methods in pricing in tenders in the building sector, focusing in particular on the life cycle of the building. The authors point to the use of the Pareto optimum method and its boundary. The article highlights not only the benefits of using Pareto's optimum but also the shortcomings. In conclusion, the authors highlight the need for consultation and expert discussion using any statistical method used to predict an offer in the construction sector.

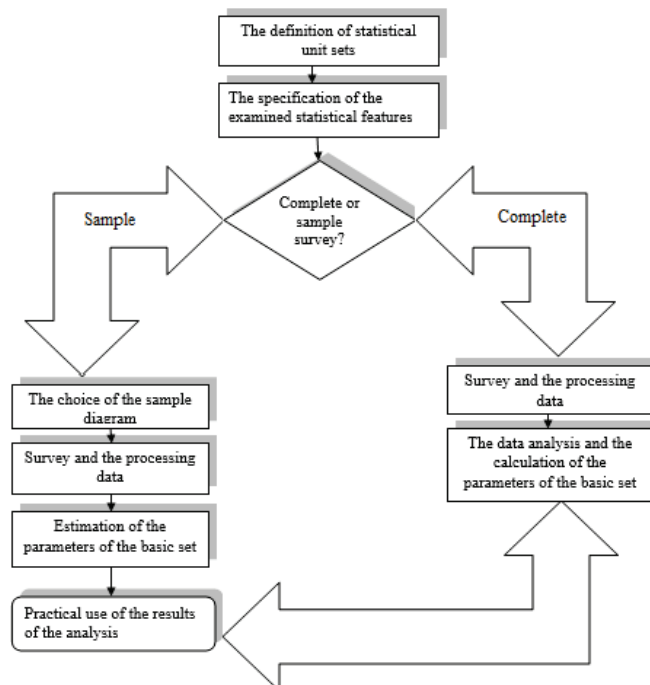


Figure 1 The general procedure for solving the statistical tasks.

In the construction practice, those statistical methods may also have a practical use, especially during the design of the tender price from the contractor's point of view, in his company's pricing policy [11].

1.2 The Specific of the Researched Phenomena within the Price Policy of the Contractor

The pricing policy is considered to be developed as the weakest, but it is also an applied tool for the marketing mix in the construction industry. Nevertheless, the price is an important factor of every construction company's success in the business [19].

Instead of the individual price policy, which responds to a specific part of a construction production, for the preparation of the construction contract Slovak construction companies still use the tender prices, which only indicate the approximate prices of all the construction works. These are annually published by several companies, which deal with the price settings within the construction industry. The explanation for this can be the fact that the Slovak market is

still not a well-functioning competitive market. At first it may seem that the construction companies which are fighting for contracts must be involved in a competitive battle, uncompromisingly forcing into the individual calculation of the tender price [16]. However, the commonly irresponsible approach of many public works authorities as well as many smaller developers to an agreement on the construction's price is negated by the amount of competition.

The construction production commitment to the location of a structure partially lowers down the competition pressure of the companies from farther locations. This is noticeable when they try to compete with the individual construction works. This kind of market does not motivate the construction companies to watch their own actual costs and neither to the creation of their own pricing database, which could take into account the specific needs of each and every construction company, and not only in the cost, but also in the profitable area.

This situation illustrates the common reaction of the construction companies to the question why they do not own their own pricing database. They claim that they do not need one, since those indicative approximate prices include sufficiently high percentage charges of the overheads and profits, which cover their cost, and they provide the necessary prosperity as well.

However, this situation changes due to the entry of foreign investors, as well as foreign construction companies. The foreign investors are used to the professionally performed offer control and to the supply activities of companies and their invoices. The foreign construction competition enters the distant markets only with their own management and technical capacity, hiring domestic subcontractors for the majority of the construction works whereupon they will have to comply with the conditions of the general contractors.

Therefore, the problematic dealing with the pricing policy of construction companies is extremely current. It requires the application of all available comprehensive approaches within the pricing itself, using all the existing mathematical-statistical methods in order to design the tender price which will be competitive for the contractor but also acceptable for the investor.

1.2.1 Pareto Analysis

During the design phase of the tender, every construction company should put into effect mainly their own, individually calculated prices. The individuality of the calculation does not mean that a fully new calculation of the price for every contract has to be made. However, this would definitely be the most precise way in terms of labor intensity, it would be unrealistic to manage this enormous number of items that would need to be calculated in certain time limit (of putting out the offer). Therefore, the company's own pricing database of construction works needs to be regularly updated. The other option would be to look for a way to speed up the designing process of the tender price by creating the tender budget. The Pareto analysis presents this kind of possibility [23].

The Pareto analysis is based upon the assumption that we own a database of statistical units which is divided in the ratio of 80/20, according to the particular criteria by the Pareto rule (upon the cost level, when dealing with the design of the tender price).

First, upon the specified report and assessment of the contracting authority, the contractor will design a cost budget using only approximate prices. As a next step, the final price of a structure will be adjusted from the approximate valuation, and it will be recalculated according to the individual conditions by adjusting part of the budget items into individual prices. For this purpose, the Pareto analysis will be applied. Items from the report and assessments, which represent 80% of the total price of a structure, will be taken out. According to the rule mentioned earlier, this should represent approximately 20% of all the items of the report and assessment. The remaining 80% of the total amount of items (with the share price of 20%) stays unchanged, without any changes of the unit price [21].

According to [24], the procedure steps of the Pareto analysis are the following: 1) The set of statistical units must be specified by the report and assessment items (it consists of numerous measurement units of works); 2) The amount of measurement units has to be priced by the approximate unit prices; 3) All the individual items according to the total price must be sorted in a descending order; 4) Corresponding cumulated sums of prices have to be calculated according to the order and the 80% border line of the total approximate price must be determined; 5) The limit of the amount of the items must be determined from the total amount of items which will be analyzed primarily (they will be individually calculated by company's rates); 6) Specific items and their unit prices have to be recalculated by the company's overhead and profit rates [3].

Thanks to this procedure, the numerical data dealing with the share of individual items on the total offer price will be available. Currently, there are several pricing programs in Slovakia, which allow the users to simulate the development of costs in the individual calculation within the price making process of a company.

For the contractor, the Pareto analysis output represents the information about the kinds of items and their serial numbers within the budget that can be considered bearing, and whose overall costs represent 80% of the total tender price of the contract. Another output of the Pareto analysis is the information about the percentage of the mentioned bearing items, which are present within the total amount of priced items in the budget.

However, the comprehensive comparison based on the analysis of total prices, profit, and individual cost items, which enter the price (such as material, salaries, machines, overheads, etc.), provides better information specified in the following levels:

- the calculation based on the indicative unit prices,
- the calculation based on the individually of calculated bearing items according to the company's overhead rates and the required profit of the contractor,
- the calculation based on the individually of calculated bearing items according to the company's overhead rates

and the required profit of the contractor including the possibility of discount on specific type of material.

The recalculation of bearing items by the company's overhead rates and profits will create a difference between the total price of the budget with the approximate prices and the individually calculated tender price of the contractor. This means that the contractor has applied the strategy of company's prices within the bearing items (individual calculation of unit prices according to the company's rates from the inner bookkeeping). This way, the contractor will be able to offer works along with the price taking into consideration the needs of the company; maybe even with lower prices than the presented offer, only based on the approximate prices, i.e., pricing the report and assessment by approximate unit prices of the existing database. Contractor's application of the Pareto analysis in practice, using the "bearing items" function of the existing pricing software, provides the creation of the tender price with less work involved. In case the company is provided with the well-prepared inner bookkeeping, the price offer should be even more accurate in regard to the planned economical effectiveness of the contract (ratability of costs, sales and profits).

1.3 The Method of the Price Development Forecast Based on the Analysis of the Time Series with the Seasonal Component

During the design of the tender price, due to the competitiveness, the time factor is often neglected. However, this is not the right approach, because there is always some time passed from the beginning of the design of the tender price until the end of the realization of a contract. The prices of construction work and materials, as well as other commodities, change their values in time. This trend is followed up by the Statistical Office of the Slovak Republic, which processes the index of development of prices. They are published monthly and quarterly on their website.

During the design of the tender, it is very smart to take into consideration the development of prices, especially during the price fluctuations. Therefore, this risk of price change shall be calculated into the offer price using a reasonably acceptable amount [8]; especially, if the developer constructor (investor) insists on the agreement on the tender price without any possibility of its adjustment (fixed price) [10].

The expected trend in the construction price development for the period of the next three years or for the estimated time of the construction can be created using individual features of MS Excel program. In our study mentioned below, with the time horizon since 2020, we have used this trend estimation, using the exact methods of prediction, such as the extrapolation method, which is based on the regression analysis of the time series with the seasonal component.

In the forecast of the development of prices, the price index of the construction works, materials and products used within the construction, will be representing the input data

during the time of the realization of a contract, and they will be quarterly published by the Statistical Office of the Slovak Republic. The overview of the past price development can be gained based on the mentioned statistical indices. They form the ultimate information for their next forecasts.

If no significant changes are anticipated within the price levels of the construction and mounting works, the appropriate method to use would be the method of extrapolation of trends. The purpose of this method is to analyze the time series of the examined statistical indices; to determine the trend line and to extend the trends into the future. By extending the trend, the estimated value of the index in the future quarters can be achieved.

The feature of the trend must be registered by a formalized relationship, i.e. by a particular mathematical formula, so that the calculation of predicted values is ensured [9]. In order to find a particular trend line, it is necessary to know their individual types and regression equations. The trend lines, which are used the most during the design of the extrapolation forecasts (prognosis), contain two or three parameters. Based on the significance of the estimation of the parameters of the trend line, a second-degree polynomial has been chosen [11].

1.4 Results

The time series of quarterly indices of prices in the construction industry since the first quarter of 2003 until the fourth quarter of 2019 for single-apartment buildings (family house type of buildings- according to ŠKS 1110 section of

JKSO 803 – residential buildings) will be analyzed and compared to the already known fact (first and fourth quarter of 2019), in the presented example (case study).

Table 1 The time series of the indices for buildings KS no. 111 (section no. 803 – Residential buildings).

	1	2	3	4	5	6
I	Year	QUARTER				Sum
		I.	II.	III.	IV.	
1	2003	1,013	1,010	1,013	1,009	4,04500
2	2004	1,025	1,019	1,021	1,009	4,07400
3	2005	1,013	1,008	1,009	1,008	4,03800
4	2006	1,013	1,010	1,009	1,009	4,04100
5	2007	1,017	1,009	1,011	1,011	4,04800
6	2008	1,021	1,018	1,013	1,007	4,05900
7	2009	1,008	1,009	0,995	1,000	4,01200
8	2010	1,000	0,997	1,002	1,001	4,00000
9	2011	1,003	1,001	1,003	1,000	4,00700
10	2012	0,998	1,003	1,002	0,998	4,00100
11	2013	0,999	1,001	1,005	1,005	4,01000
12	2014	1,002	1,003	1,003	1,001	4,00900
13	2015	1,006	1,004	1,006	1,003	4,01900
14	2016	1,001	1,004	1,004	0,999	4,00800
15	2017	1,014	1,016	1,004	1,003	4,03700
16	2018	1,013	1,008	1,008	1,007	4,03600
17	2019	1,017	1,007	1,009	1,004	4,03700
	Sum	17,163	17,127	17,117	17,074	68,481

*In Tab.1 the term $i = 1, 2, 3, \dots, 9$, where $i = 1$ corresponds to 2003.

Using the MS Excel program, it is possible to create the trend line and its formula (regression equation), which helps to determine the estimated development of index prices for the next period.

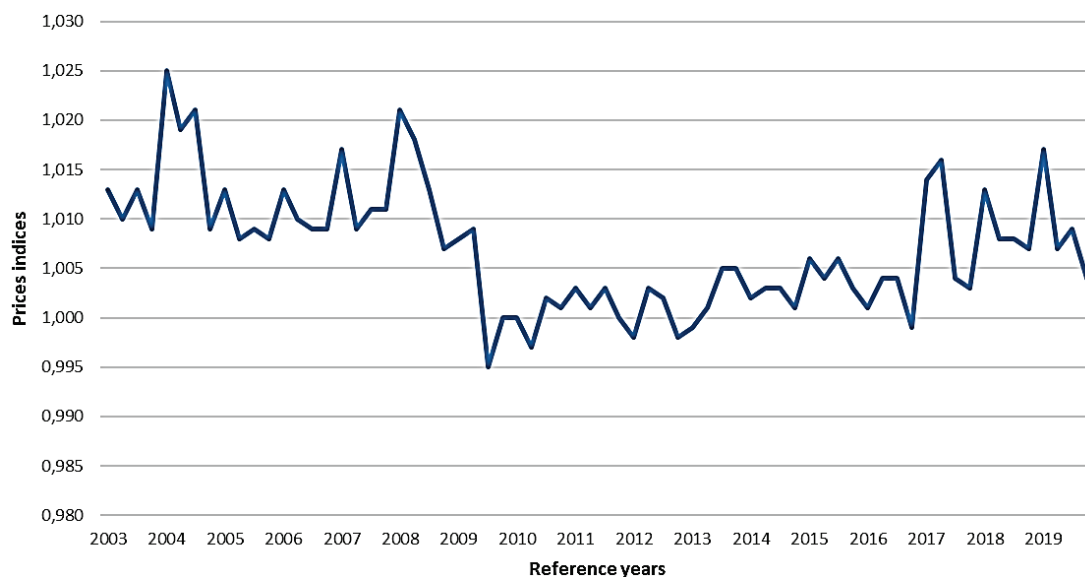


Figure 2 The quarterly index of the price development in the construction industry for the section no. 803 – Residential buildings (KS no. 111).

In the example mentioned above (Fig. 3), the trend line represents the second-degree polynomial. The formula of the trend line is following:

$$y(x) = 0.00001x^2 - 0.0008x + 1.019 \quad (1)$$

where x represents the particular time term to determine the value of the index $y(x)$.

The following Tab. 2 represents the forecast of the development of price indices for the next three years (the substitution of x in the equation of the trend line, for the value beginning with the value of 69, since the trend line, which is drawn according to the time series contains 68 input data).

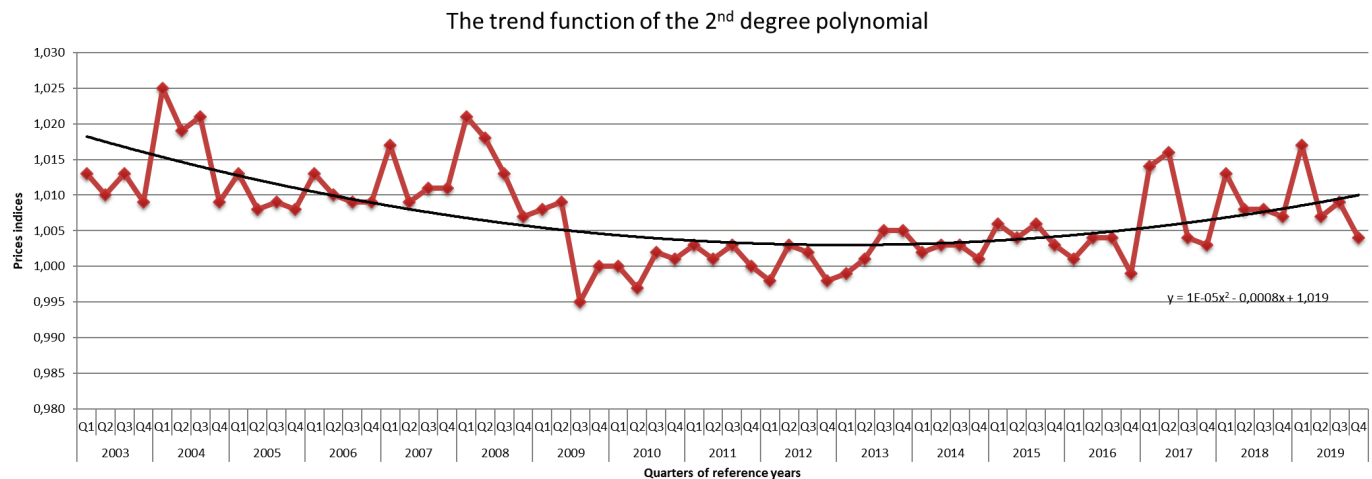


Figure 3 Quarterly index of the price development in the construction industry for the section no. 803 – Residential buildings (KS no. 111) with the trend function of the 2nd degree polynomial.

Table 2 The values of the quarterly indices for the section no. 803 – Residential buildings (KS no. 1110) for the next three years, using the trend without the seasonal component.

Quarter	Year		
	2020	2021	2022
1 st quarter	1,00962	1,00919	1,00878
2 nd quarter	1,00812	1,00769	1,00728
3 rd quarter	1,00798	1,00755	1,00714
4 th quarter	1,00976	1,00933	1,00892

This example only represents the general procedure of the trend setting. However, it is not recommended to use it in

this form. It is necessary to make an analysis of the seasonal component, because the trend does not say anything about the seasonality.

In case of time series with a seasonal component, it is necessary to individually analyze the trend section, as well as to individually analyze the seasonal section of time series. It has to be done, because in terms of the repeating seasonality the time series has a developing trend [12].

Table 3 Time series of price indices for residential buildings with the seasonal component.

1	i	Year	1	2	3	4	5	6	7	8
			QUARTER				Sum	y_i	$i \cdot y_i$	
			I.	II.	III.	IV.				
2	1	2003	1,013	1,010	1,013	1,009	4,04500	1,01125	1,01125	
3	2	2004	1,025	1,019	1,021	1,009	4,07400	1,01850	2,03700	
4	3	2005	1,013	1,008	1,009	1,008	4,03800	1,00950	3,02850	
5	4	2006	1,013	1,010	1,009	1,009	4,04100	1,01025	4,04100	
6	5	2007	1,017	1,009	1,011	1,011	4,04800	1,01200	5,06000	
7	6	2008	1,021	1,018	1,013	1,007	4,05900	1,01475	6,08850	
8	7	2009	1,008	1,009	0,995	1,000	4,01200	1,00300	7,02100	
9	8	2010	1,000	0,997	1,002	1,001	4,00000	1,00000	8,00000	
10	9	2011	1,003	1,001	1,003	1,000	4,00700	1,00175	9,01575	
11	10	2012	0,998	1,003	1,002	0,998	4,00100	1,00025	10,00250	
12	11	2013	0,999	1,001	1,005	1,005	4,01000	1,00250	11,02750	
13	12	2014	1,002	1,003	1,003	1,001	4,00900	1,00225	12,02700	
14	13	2015	1,006	1,004	1,006	1,003	4,01900	1,00475	13,06175	
15	14	2016	1,001	1,004	1,004	0,999	4,00800	1,00200	14,02800	
16	15	2017	1,014	1,016	1,004	1,003	4,03700	1,00925	15,13875	
17	16	2018	1,013	1,008	1,008	1,007	4,03600	1,00900	16,14400	
18	17	2019	1,017	1,007	1,009	1,004	4,03700	1,00925	17,15725	
19	Sum		17,163	17,127	17,117	17,074	68,481	17,120	153,8898	
20	y_i		1,010	1,007	1,007	1,004	4,028	1,007		
21	b_i		0,00178	0,00028	0,00014	0,00192				

Notes: $*y_i$, y_j - average values, b_j - deviation. The average values of the year indices for a particular year.

The average values of quarterly indices for each year are used for the description of the trend section. The average values of quarterly indices for each quarter are used for the description of seasonal section. Therefore, it is necessary to add data concerning average values to Tab. 1. These values are calculated in Tab. 3.

1.5 The Determination of the Seasonal Component within the Time Series

Fig. 4 represents the monitored indices of time series, which show unsystematic fluctuations within the particular year. This means, that in the first quarter the value of the

index is the highest. In the second and third quarter we can see a decline to approximately same values. Finally, the lowest value is in the fourth quarter. Therefore, the analyzed series can be considered as a time series with a seasonal component. The overall trend of time series is increasing.

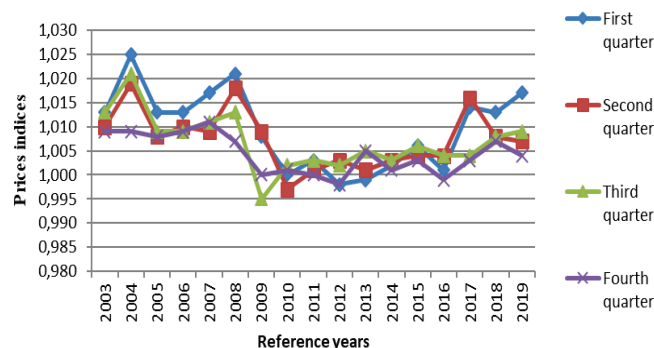


Figure 4 The average quarterly indices of prices for a particular year.

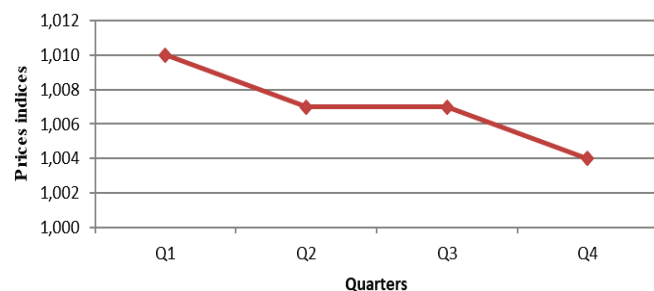


Figure 5 The average values of year indices of the development of prices within the construction industry for the section no. 803 – Residential buildings (KS no. 111).

Fig. 5 also shows the seasonality for the particular years. It is necessary to know the average values of quarterly indices in order to describe the seasonal component for particular years. They can be found in Tab. 3. The average value is determined out of these four values (line no. 20, column no.

7). The seasonal deviations of the averages for particular quarters also have to be determined and compared to the overall average.

1.6 The Determination of the Trend Component of the Time Series

Fig. 6 can be created based on the average values of quarterly indices for particular years. Based on the graph mentioned above, we can create the trend line along with a relevant trend equation using MS Excel program.

The created equation looks like this:

$$y(x) = 0.0002x^2 - 0.0033x + 1.0201 \quad (2)$$

In the next step, it is necessary to adjust the equation of the trend by using the deviations of particular quarters from Tab. 3 (line no. 21).

Following equations result from the mentioned sequence:

$$y(x) = 0.0002x^2 - 0.0033x + 1.0201 + 0.00178 \quad (3)$$

pre 1st quarter

$$y(x) = 0.0002x^2 - 0.0033x + 1.0201 + 0.00028 \quad (4)$$

pre 2nd quarter

$$y(x) = 0.0002x^2 - 0.0033x + 1.0201 + 0.00014 \quad (5)$$

pre 3rd quarter

$$y(x) = 0.0002x^2 - 0.0033x + 1.0201 + 0.00192 \quad (6)$$

pre 4th quarter

where x represents the year, $x = 1$ for the year 2003, $x = 2$ for the year 2004, $x = 3$ for the year 2005, etc.

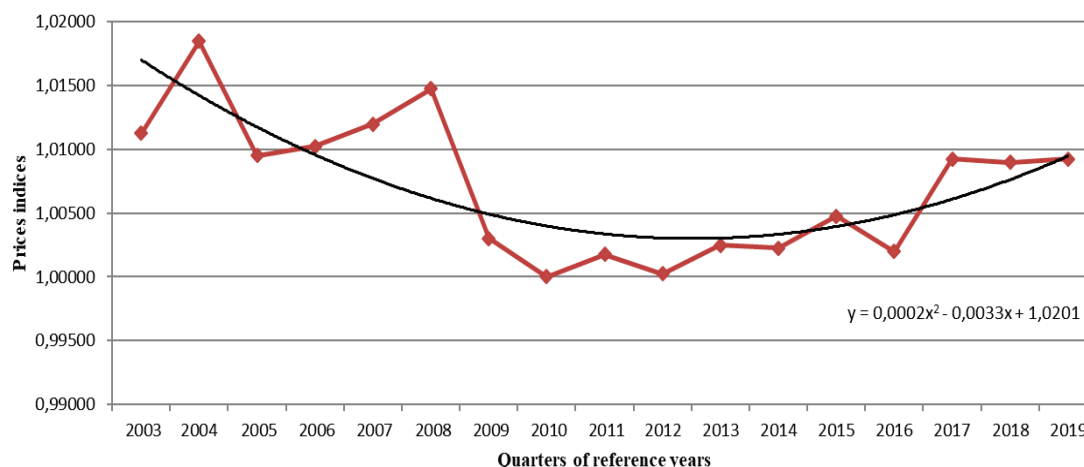


Figure 6 The average values of quarterly indices of price development within the construction industry for the section no.803 – Residential buildings (KS no. 111) during the monitored years.

Based on these relations, it is possible to determine the values of quarterly indices for the next period of quarters (Tab. 4).

If the realization of a construction is supposed to take for example from 2-3 years, it is recommended to do the forecast for this period. However, the accuracy of the calculation for

a longer period would be insufficient. The principle that should be applied when predicting for a period of a long time ahead is that there must be available minimum of three times more past information (data) than is the number of forecasted data [1].

Table 4 The values of quarterly indices for the section no. 803 – Residential buildings (KS no. 111) for the next three years.

QUARTER	Year		
	2020	2021	2022
1 st quarter	1,0273	1,0314	1,0359
2 nd quarter	1,0258	1,0299	1,0344
3 rd quarter	1,0256	1,0297	1,0342
4 th quarter	1,0274	1,0315	1,0360

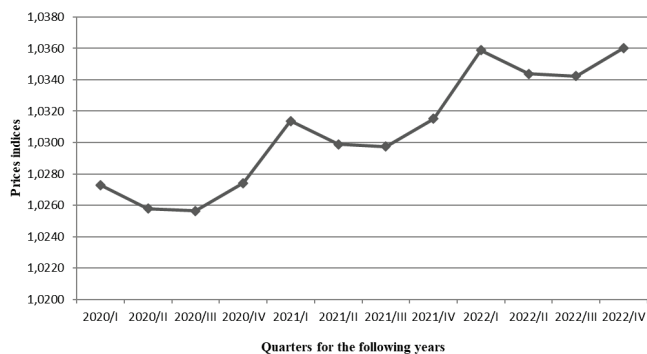


Figure 7 Graph of quarterly indices of price development in construction industry for the section no. 803 – Residential buildings (KS no. 111) for the next three years (year 2020, 2021, 2022).

The contractor can apply some of the other forecasting methods to determine the price development, as well as the increase of costs of the production. The contractor can also estimate this development for the required period (most often for the time of the realization of the construction) based on his experience and professional knowledge. Nevertheless, every contractor should definitely take into account the risk of the price development, especially in the times of price fluctuations, and include it in the tender price. Tab. 5 presents the comparison between the forecast and the reality, which is known so far for the year 2019. The following table shows the quarterly indices of the price development based on the Statistical Office of the Slovak Republic (www.statistic.sk) [20] for the section no. 803 and for the classification of structures no. 111.

Table 5 The values for quarterly indices for the section no. 803 – Residential buildings (KS no. 111) – the reality and predicted value.

Quarter	2019 – Section no. 803 Residential buildings (KS no. 111)	2019 – Trend without the seasonal component
1 st quarter	1,017	1,010
2 nd quarter	1,007	1,009
3 rd quarter	1,009	1,008
4 th quarter	1,004	1,010

2 DISCUSSION

The results of our study point to a growth in the construction price index. In 2005, Goh in his studies [7] pointed out to the need to apply sophisticated techniques

when determining prices in construction and housing policy tenders, among other in regard to the rising expansion of construction in the society. Authors in the reference [15] add that this is a very complicated process in which the lowest price may not automatically provide the tender to the contractor. No less important factors affecting the final costs are the following: the company's experience in similar tenders, the number of successful construction projects, and the number of projects that required an additional increase in funding.

The contractor can individually decide to implement the influence of time factor or not, based on the anticipated trend of price development for the construction and assembly work, the expected duration of construction and the fact that the offering price is subject to the time development of price. It is recommended to implement the time factor influence especially in cases when developer insists on the price without the possibility of changing it (Fixed price).

3 CONCLUSION

The findings of this paper may also be applicable in other Visegrad group countries (V4 - Hungary, Poland, Czech Republic, Slovak Republic), but also in countries with economic characteristics similar to the Slovak Republic. The authors are aware of the application of simpler statistical methods on the data sample of the Slovak Republic. However, they consider that their practical applicability is of importance in bidding since it takes into account the estimated contractual price developments in construction.

Acknowledgment

This paper is supported and funded from KEGA grant no. 019STU-4/2018, entitled "The process of integrating mentoring and coaching into teaching at technical universities".

Notice

The paper was presented at PBE2020 – International Scientific Conference "People, Buildings and Environment 2020". The 14th conference was held in the Rožnov pod Radhoštěm city, the Czech Republic, from 7 to 9 October 2020. The paper will not be published anywhere else.

4 REFERENCES

- [1] Abraham, B. & Ledolter, J. (1983). *Statistical Methods for Forecasting*. A John Wiley & Sons, Inc., New York. <https://doi.org/10.1002/9780470316610>
- [2] Amuda Yusuf, G. & Mohamed, S. F. (2014). Perceived benefits of adopting standard - based pricing mechanism for mechanical and electrical services installations. *Australasian Journal of Construction Economics and Building*, 14(2), 104-119. <https://doi.org/10.5130/AJCEB.v14i2.3864>
- [3] Bajaj, S., Garg, R., & Sethi, M. (2018). Total quantity management: a critical literature review using Pareto analysis. *International Journal of Productivity and Performance Management*, 67(1), 128-154.

- <https://doi.org/10.1108/IJPPM-07-2016-0146>
- [4] Boddy, R. & Smith, G. (2009). *Statistical Methods in Practice: for Scientists and Technologists*. John Wiley & Sons, Ltd. <https://doi.org/10.1002/9780470749296>
 - [5] Dziadosz, A., Tomczyk, A., & Kaplinski, O. (2015). Financial risk estimation in construction contracts. *Procedia Engineering*, 122, 120-128. <https://doi.org/10.1016/j.proeng.2015.10.015>
 - [6] Ernest, K., Theophilus, A., Amoah, P., & Emmanuel, B. B. (2019). Identifying key economic indicators influencing tender price index prediction in the building industry: A case study of Ghana. *International Journal of Construction Management*, 19(2), 106-112. <https://doi.org/10.1080/15623599.2017.1389641>
 - [7] Goh, B. H. (2005). The dynamic effects of the Asian financial crisis on construction demand and tender price levels in Singapore. *Building and Environment*, 40(2), 267-276. <https://doi.org/10.1016/j.buildenv.2004.07.012>
 - [8] Hyari, K. H., Tarawneh, Z. S., & Katkhuda, H. N. (2016). Detection Model for Unbalanced Pricing in Construction Projects: A Risk-Based Approach. *Journal of Construction Engineering and Management*, 142(12). [https://doi.org/10.1061/\(ASCE\)CO.1943-7862.0001203](https://doi.org/10.1061/(ASCE)CO.1943-7862.0001203)
 - [9] Chen, M. & Li, Q. M. (2009). Study on the Application of Price Adjustment Formulae in House Building. *International symposium on advancement of construction management and real estate*, Vol. 1-6, 2117-2121. ISBN: 978-962-367-675-5.
 - [10] Jarrett, J. (1987). *Business Forecasting Methods*, Basil Blackwell Publishers. Oxford and Cambridge. ISBN: 978-0631152897.
 - [11] Kissi, E., Adjei-Kumi, T., Badu, E., & Boateng, E. B. (2017). Factors affecting tender price in the Ghanaian construction industry. *Journal of Financial Management of Property and Construction*, 22(3), 252-268. <https://doi.org/10.1108/JFMPC-09-2016-0044>
 - [12] Kendall, M. G. & Hill, A. B. (1953). The Analysis of Economic Time-Series-Part I: Prices. *Journal of the Royal Statistical Society. Series A (General)*, 116(1), 11-34. <https://doi.org/10.2307/2980947>
 - [13] Kuda, F., Wernerova, E., & Endel, S. (2015). Selection of a Construction Contractor for Public Contracts in the Czech Republic according to Safe Tender Price. In: *Proceedings of the 2015 international conference on architectural, civil and hydraulics engineering. AER – Advances in Engineering Research*. Vol. 44, 65-68.
 - [14] Lacko, G. (2011). Modeling the residual market value of construction equipment under changed economic conditions. *Journal of Construction Engineering and Management*, 137(10), 806-816. [https://doi.org/10.1061/\(ASCE\)CO.1943-7862.0000279](https://doi.org/10.1061/(ASCE)CO.1943-7862.0000279)
 - [15] Lue, S. S., Son, P. V. H., & Nhung, P. T. H. (2015). Optimize negotiation price in construction procurement using Bayesian Fuzzy Game Model. *KSCE Journal of Civil Engineering*, 19(6), 1566-1572. <https://doi.org/10.1007/s12205-014-0522-2>
 - [16] Othman, A. A., Abd Rahman, S., Sundram, V. P. K., & Bhatti, M. A. (2015). Modelling marketing resources, procurement process coordination and firm performance in the Malaysian building construction industry. *Engineering Construction and Architectural Management*, 22(6), 644-668. <https://doi.org/10.1108/ECAM-02-2014-0030>
 - [17] Safaei, A., Freire, F., & Henggeler Antunes, C. (2015). A life cycle multi-objective economic and environmental assessment of distributed generation in buildings. *Energy Conversion and Management*, 97, 420-427. <https://doi.org/10.1016/j.enconman.2015.03.048>
 - [18] Samani, P., Gregory, J., Leal, V., Mendes, A., & Correia, N. (2018). Lifecycle cost analysis of prefabricated composite and masonry buildings: Comparative study. *Journal of Architectural Engineering*, 24(1). [https://doi.org/10.1061/\(ASCE\)AE.1943-5568.0000288](https://doi.org/10.1061/(ASCE)AE.1943-5568.0000288)
 - [19] Sinyaev, V. (2016). Analytical assessment of outsourcing services' marketing in construction industry. *Ekonomika. Biznes. Banki*. Vol. 8, 177-186. ISSN: 2304-9596. (in Russian)
 - [20] Statistical office of the Slovak republic. Available on: www.statistics.sk
 - [21] Surhone, L. M., Timpledon, M. T., & Marseken, S. F. (2010). Pareto Analysis. VDM Publishing, p. 76. ISBN: 978-613046141.
 - [22] Vrbka M. (2020). *Parametrické rozpočtování – inovace způsobu určování nabídkových cen ve stavebním podniku* (Parametric budget estimation – Innovation of the method of determining bid prices in a construction company). Dizertační práce, Ústav stavební ekonomiky a řízení, VUT Brno, 2020, p. 106. (in Czech)
 - [23] Wang, Z. Y. & Rangaiah, G. P. (2017). Application and Analysis of Methods for Selecting an Optimal Solution from the Pareto-Optimal Front obtained by Multiobjective Optimization. *Industrial & Engineering Chemistry Research*, 56(2), 560-574. <https://doi.org/10.1021/acs.iecr.6b03453>
 - [24] Chajdiak J. et al. (1997). *Štatistické metódy v praxi*, 2. vydanie, ISBN 8-85659-08-5 (in Czech)

Authors' contacts:

Ing. **Helena Ellingerová**, PhD, Assist. Prof.
Department of Building Technology,
Faculty of Civil Engineering,
Slovak University of Technology in Bratislava,
Radlinského 11, 813 68 Bratislava, Slovak Republic

Ing. **Zora Petráková**, PhD, Assist. Prof.
The Institute for Forensic Engineering,
Faculty of Civil Engineering,
Slovak University of Technology in Bratislava,
Radlinského 11, 813 68 Bratislava, Slovak Republic

Ing. **Ingrida Skalíková**, PhD
(Corresponding author)
The Institute for Forensic Engineering,
Faculty of Civil Engineering,
Slovak University of Technology in Bratislava,
Radlinského 11, 813 68 Bratislava, Slovak Republic
ingrida.skalikova@stuba.sk

Research of the Residual Bearing Capacity and the Work of Damaged Reinforced Concrete Beams' Inclined Sections

Zeljko Kos*, Yevhenii Klymenko, Kostiantyn Polianskyi, Andjelko Crnoja

Abstract: The article is devoted to studies about the stress-strain state and the residual bearing capacity of inclined sections of reinforced concrete beams with concrete damages in the compressed zone near support areas. The developed method of calculating the bearing capacity of the inclined sections of damaged beams is described. The numerical test of prototypes was performed in the LIRA-CAD 2017 software complex. A comparison of the results of laboratory tests, a numerical experiment and calculation results by the proposed method is shown. It is stressed that with an increase in the area of damage, the bearing capacity decreases. The nature of the change in the stress-strain state under the presence of damage is described. It is pointed out that in the damaged samples, there is an inclination of the neutral axis in the cross section of the element – it tilts, the neutral axis becomes, almost, parallel to the front of the damage.

Keywords: damaged RC beams; inclined section; method of calculation; residual bearing capacity; stress-strain state

1 INTRODUCTION

Reinforced concrete is a relatively durable material and may serve for a long time. Its active use began in the first half of the last century and continues to this day. The buildings and structures constructed at that time can be operated to this day. Over time, damages can appear and defects may be present. Damage can occur from various factors. Bonić Z. et al. [1] note the occurrence of damage from construction errors, the action of an aggressive atmosphere (which leads to the corrosion of concrete and reinforcement); Lu Z. et al. [2] note the occurrence of damage from exposure to elevated temperatures (in particular due to fires); Hayashi T, et al. [3, 4] note the occurrence of damage from accidental effects of freeze-thaw cycles; and etc.

Unfortunately, in the current codes [5, 6], there are no methods and guidelines for determining the residual bearing capacity of damaged elements. Due to the lack of guidance in the construction practice, when conducting a structural inspection, the decision to reinforce damaged elements is often applied intuitively, although the bearing capacity of such elements may still be provided.

A significant amount of work has been devoted to the study of reinforcing damaged elements. In particular, Kabir M. et al. [7] investigated the operation of reinforced beams by using CFRP; Burningham C. et al. [8] investigated the operation of reinforced beams by using the Steel Tendons Using Post-Tensioned Carbon Fiber-Reinforced Polymer Rods; Hou L. et al. [9] investigated the operation via reinforced beams repaired with ultra-high toughness cementitious composite.

There is a number of works on the probabilistic assessment of the reliability of damaged elements, among which Sakka, Z. et al. [10] can be noted, where the author proposed a technique using a probabilistic analysis of the statistics of random variables.

A number of studies were carried out by Klimenko E. et al. [11, 12] to determine the bearing capacity of damaged elements, as well as methods for calculating damaged

compressed concrete columns and bent beams from a normal section, it was also noted that changes occur due to a damage stress-strain state.

However, in all available literary sources, the determination of the residual bearing capacity by the inclined sections in the damaged beams was not found.

1.1 The Aim of the Work

The aim of the study is to obtain experimental data on the stress-strain state, the residual bearing capacity of the inclined sections of the damaged beams and the development of methods for revising calculations.

1.2 Materials and Characteristics of Experimental Samples

For the experiment, 15 samples were made. The materials for the samples were: concrete – grade of C25/30 working longitudinal reinforcement - grade of A500C $\varnothing 18$ mm, the vertical shear reinforcement in the form of closed clamps and structural reinforcement - grade of A240C $\varnothing 6$ mm. Reinforcement was designed so that the destruction occurred along an inclined section within the considered shear span. The cross-sectional size of the elements is 100×200 mm, length is 1200 mm, the working span of 1000 mm, the bearing is free.

The loading of the samples was in the form of a concentrated force F_u with uniformly increasing steps. The influence of three factors on the bearing capacity is studied – the shear span, the depth of damage and the angle of the inclination of the damage. Therefore, artificial damage to the compressed zone of the concrete of various depths h_1 (0, 50 and 100 mm) and the inclination angle β_1 (0° , 30° , 60°) were placed in the samples, and the load was applied at a relative shear span of a_v , $1d$, $2d$, and $3d$. The characteristics of samples are shown in Tab. 1 and in Fig. 1.

2 RESULTS OF LABORATORY TESTS

2.1 The Nature of the Destruction, Cracking and Deflection of Samples

During testing, all samples were destroyed by an inclined section because of the prevailing action of the transverse force, and as a rule, inclined cracks were significantly revealed in the samples and concrete was destroyed above the crack top. The angle of the tilt of the inclined crack was up to 22° at $a_v = 510$ mm, up to 30° at $a_v = 340$ mm, and up to 60° at $a_v = 170$ mm. The appearance of normal visible cracks fixed at 1-2 step loading is earlier than the inclined cracks. Visible inclined cracks along the undamaged face appeared 1-2 steps earlier than the damaged one, and they also had a greater length and width of the opening up to the penultimate or the last stage of loading, and they had a width of 0.4-0.5 mm.

The data of the ultimate deflections f_u showed that a reduction of the shear span, and an increase of the damaged area mainly leads to their reduction. The values of the obtained ultimate deflections in the experimental samples are shown in Tab. 2.

Table 1 Variable characteristics for samples

Call number	Depths of damage h_1 , mm	Angle of damage β_1 , °	Shear span a_v , mm
B1	0	0	3d
B2	50	30	3d
B3	50	60	3d
B4	100	30	3d
B5	100	60	3d
B6	0	0	2d
B7	50	30	2d
B8	50	60	2d
B9	100	30	2d
B10	100	60	2d
B11	0	0	1d
B12	50	30	1d
B13	50	60	1d
B14	100	30	1d
B15	100	60	1d

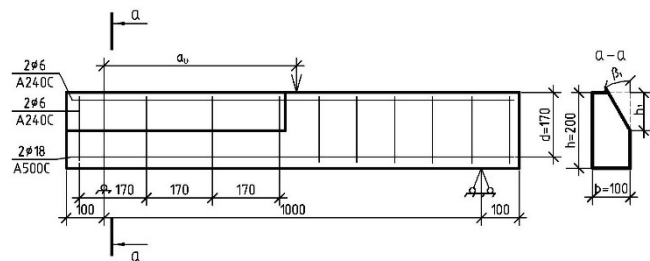


Figure 1 Characteristics of samples

2.2 Bearing Capacity of Samples

From the obtained laboratory data, it can be said that the bearing capacity decreases with an increase in the area of damage and the shear span. Within each shear span, specimens with a larger damage area are able to perceive less transverse force; specimens with a lower damage height and a greater angle of inclination are able to perceive a greater

load than the samples with a larger damage height and a smaller inclination angle.

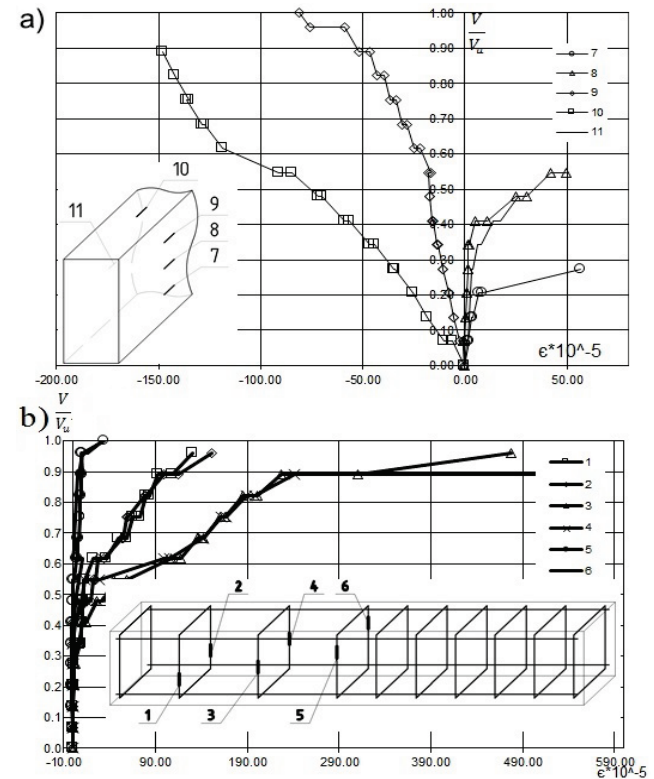


Figure 2 Nature of the strain state of the undamaged sample B1: (a) deformations of concrete and (b) deformations of transverse reinforcement

Table 2 Data of the ultimate deflections and ultimate deformations in experimental samples

Call number	Ultimate deflections f_u at $\approx 0.95 \cdot F_u$ mm	Ultimate concrete deformation $\epsilon_c^u \times 10^{-5}$	Ultimate shear reinforcement deformation $\epsilon_{sv}^u \times 10^{-5}$
B1	4.94	148	512
B2	4.03	283	323
B3	4.5	401	402
B4	4.68	377	287
B5	2.37	200	36
B6	3.92	163	712
B7	2.89	119	302
B8	2.88	177	285
B9	2.4	150	204
B10	2.59	152	24
B11	3.3	41	260
B12	2.04	49	184
B13	1.95	86	41
B14	2.45	45	64
B15	2.01	69	144

The bearing capacity at the shear span of $a_v = 510$ mm in the damaged samples of B2, B3, B4, B5 is 95.94%, 80.82%, 79.46%, 41.0% (respectively) of the bearing capacity of the sample B1; at the shear span of $a_v = 340$ mm in the damaged samples of B7, B8, B9, B10 is 74.98%, 69.99%, 54.99%, 42.5% of the bearing capacity of the sample B6; at the shear span of $a_v = 170$ mm in the damaged samples of B12, B13, B14, B15 is 94.74%, 88.42%, 78.95%, 67.31% of the bearing

capacity of the sample B11. The results of the bearing capacity are shown in Tab. 3.

Table 3 Data of the bearing capacity according to the results of laboratory tests, numerical experiment and calculation by the proposed method.

Call number	Bearing capacity of the laboratory tests V_{exp}^u , kN	Bearing capacity of the numerical tests V_{LIRA}^u , kN	Bearing capacity of the calculations $V_{calculated}^u$, kN
B1	59.54	54.51	54.16
B2	57.14	51.74	51.85
B3	48.16	44.51	47.23
B4	47.35	43.39	44.92
B5	24.49	22.64	31.38
B6	87.98	81.97	69.36
B7	65.97	80.13	66.4
B8	61.58	52.67	60.49
B9	48.38	51.48	57.53
B10	37.39	32.71	44.83
B11	131.36	113.3	133.4
B12	124.45	110.06	127.7
B13	116.15	103.58	116.3
B14	103.7	100.35	110.6
B15	88.5	72.09	77.29
ν , %		14.81	10.3

2.3 Nature of the Strain State of Samples

During laboratory tests, data were obtained on the ultimate deformations of the concrete ε_c^u and transverse reinforcement ε_{sw}^u . The data are presented in Tab. 2.

By analyzing the data, it can be concluded that the ultimate deformations of concrete decrease when the shear span decreases. An increase in the angle of damage leads to an increase in the ultimate deformation. The character of deformation indicates that the position of the neutral axis is tilted in damaged elements.

The final deformations of the transverse reinforcement and concrete are reduced with a decrease in the shear range. With an increase in the area of damage to the beams, the limiting deformations also reach lower values. It was noticed that at the initial stages of loading, the bars of transverse reinforcement are slightly compressed, but with an increase in load by several steps, they begin to experience tension. Another feature is that the bars located at the intact face had large deformations.

The character of the deformations of concrete and transverse reinforcement is shown in Figs. 2 and 3. Deformations were determined by using strain gauges; therefore, when the line breaks, it means that either the strain gauge is out of order, or that the strains reached values higher than the sensitivity of the measuring device.

3 RESULTS OF THE NUMERICAL EXPERIMENT

A simulation of the experimental samples was performed in the LIRA-CAD software complex based on the finite element method. An iterative calculation of nonlinear steps is performed. For the calculation, the actual stress-strain σ - ε diagrams were used. The criterion for the destruction of the samples was to one or several conditions: stresses in the compressed concrete have to reach ultimate values, stresses in the reinforcement have to reach ultimate values, there have

to be significant fast-growing movements (more than 10 mm) of the elements of the design scheme.

The obtained data on the residual bearing capacity are shown in Tab. 3.

In general, the bearing capacity data showed good convergence with the results of laboratory studies, as evidenced by the coefficient of variation $\nu = 14.81\%$.

Analyzing the character of destruction of the destruction of elements, it can be seen that it corresponds to the nature of the destruction during laboratory tests (destruction of concrete over the top of the inclined crack), but B1...B14 samples survived destruction due to the destruction of concrete on a support, which does not correspond to the tests.

The data of concrete deformation, as well as laboratory test data, show that the neutral axis tilts in the damaged samples – it becomes almost parallel to the damage front. A comparison of the position of the neutral axis of the cross section of the samples obtained in the simulation and in the laboratory test is shown in Fig. 4.

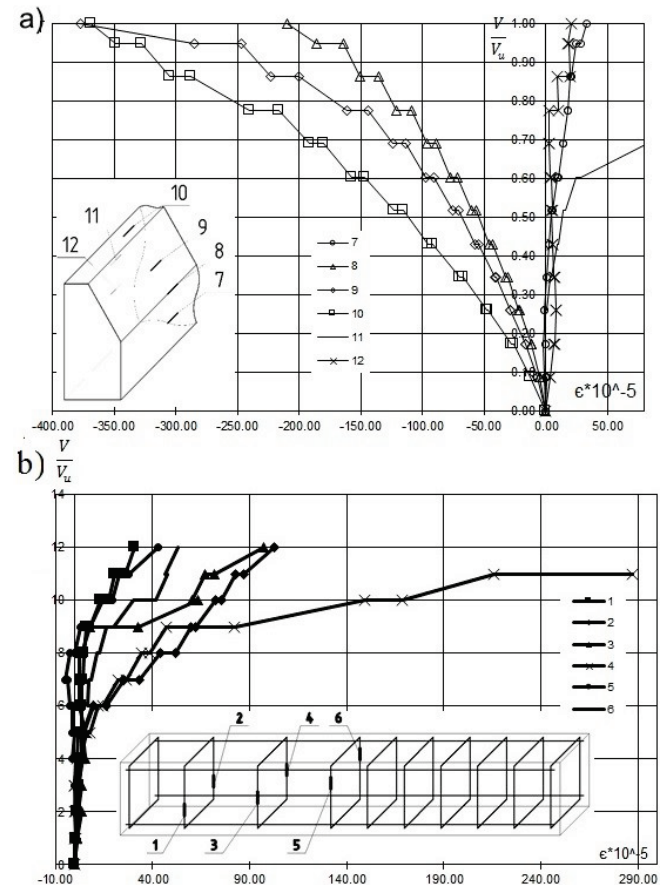


Figure 3 Nature of the strain state of the damaged sample B4: (a) deformations of concrete and (b) deformations of transverse reinforcement

The stress analysis in the bars of transverse reinforcement indicates that the nature of deformation generally corresponds to the test results; however, the yield strength was not achieved in any sample, although experiments showed that it was achieved in samples B1...B4, B6...B8, B11.

In general, conducting such calculations helps predict the nature of destruction and deformation of elements, however,

among the disadvantages of such a simulation, it should be noted that the whole process of constructing a calculation scheme to analyze the obtained values takes a substantial period of time, and the generally accepted criterion of failure in the software package is not developed and the user independently chooses what to take for the destruction of an element.

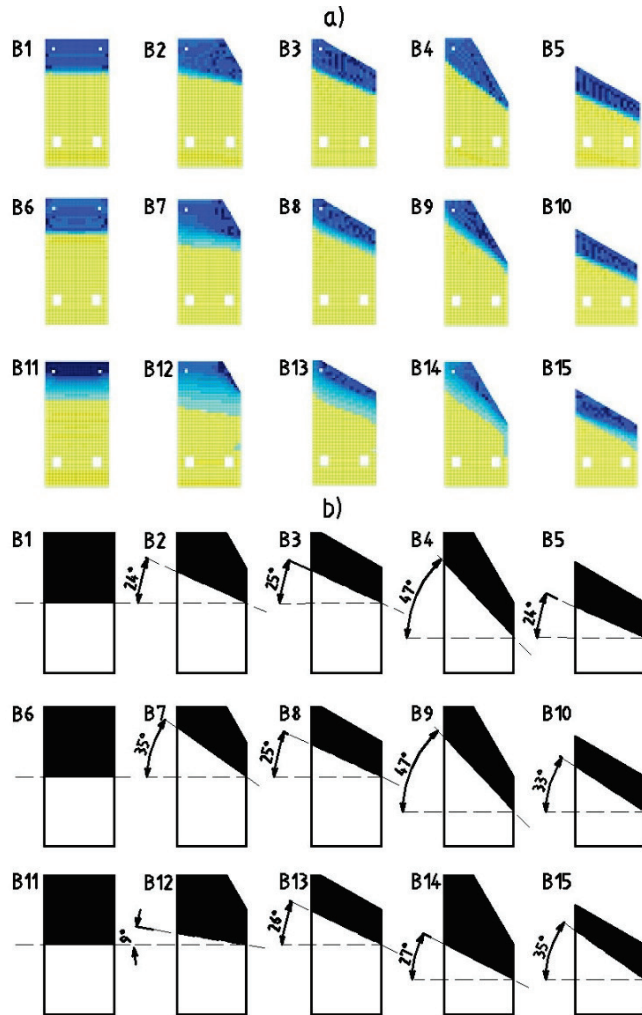


Figure 4 Position of the neutral axis of the cross section of the samples: (a) in the LIRA-CAD program complex and (b) in the laboratory test

The typical character of strain distribution and deflections in the damaged sample B4 is shown in Fig. 5.

4 PROPOSED METHOD OF THE CALCULATION OF THE INCLINED SECTIONS' DAMAGED BEAMS

The geometrical characteristics for the calculations for the proposed methodology are shown in Fig. 6. All non-indicated of the furthest methodical values recommended to be adopted by such values are recommended by the codes [5, 6].

In the current regulations [5, 6], to determine the bearing capacity of the inclined sections, the method of truss analogy is used. According to this method, the bearing capacity V_{Rd} is defined as:

$$V_{Rd} = V_{Rd,c} + V_{Rd,s} \quad (1)$$

where $V_{Rd,c}$ is defined as the maximum of the Eq. (2) and (3):

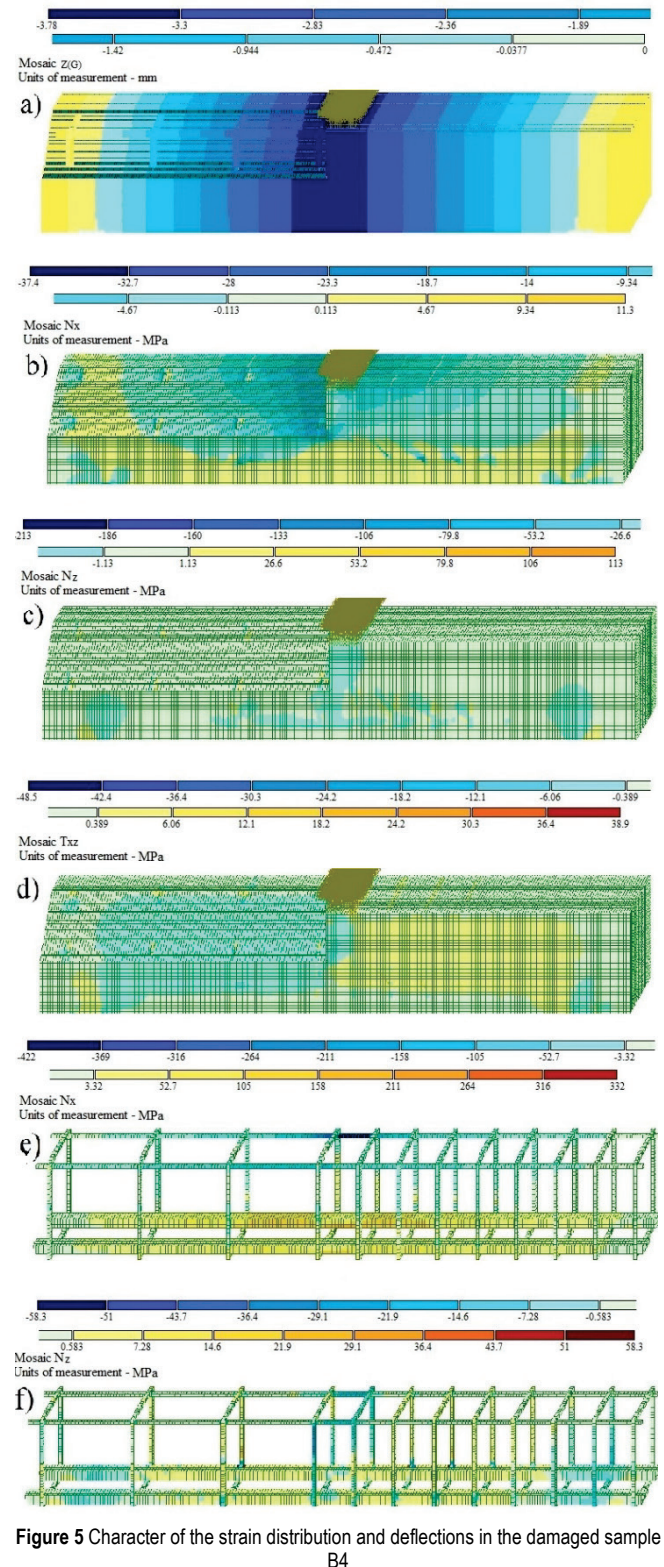


Figure 5 Character of the strain distribution and deflections in the damaged sample B4

$$V_{Rd,c} = \left(C_{Rd,c} \cdot k \cdot \sqrt[3]{100 \cdot \rho_1 \cdot f_{ck} - k_1 \cdot \sigma_{cp}} \right) \cdot b_w \cdot d \quad (2)$$

$$V_{Rd, c, \min} = \left(0.035 \cdot k^{\frac{3}{2}} \cdot f_{ck}^{\frac{1}{2}} + k_1 \cdot \sigma_{cp} \right) \cdot b_w \cdot d \quad (3)$$

and the value $V_{Rd, s}$ is defined as the minimum of the Eq. (4) and (5):

$$V_{Rd, s} = \frac{A_{sw}}{s} \cdot z \cdot f_{ywd} \cdot \cot \theta \quad (4)$$

$$V_{Rd, s} = \frac{\alpha_{cw} \cdot b_w \cdot z \cdot v_1 \cdot f_{cd}}{\cot \theta + \tan \theta} \quad (5)$$

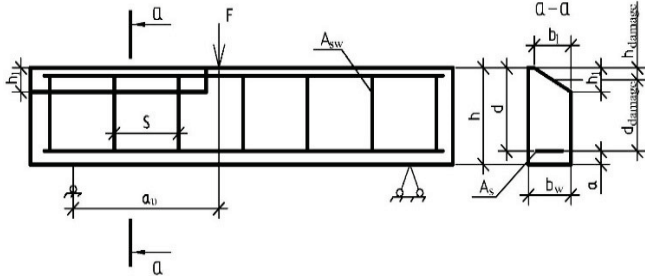


Figure 6 Characteristics used for calculations

By analyzing the data obtained during the research, it is found that a significant influence on the bearing capacity is exerted by the effect of the shear span – it can be noticed that with decreasing size of the shear, the bearing capacity of the experimental samples span increases by nonlinear dependence. But in the codes, the increasing of the bearing capacity is described by a linear expression:

$$\beta = \frac{a_v}{2d} \quad (6)$$

Due to the decrease of the acting shear force V_{Ed} by this value, at the shear span in the range of $0.5d \leq a_v \leq 2d$, whereas at the range of more than $2d$ it is not taken into account, the results of the experimental studies indicate that the shear span of $a_v = 3d$ affects the bearing capacity; in particular, the greatest impact was observed in the undamaged sample (B1) and the sample with the largest damage area (B5) experienced a decrease of up to 32-34% compared with a similar sample with $a_v = 2d$ (B6 and B10, respectively). At the shear span $1d$, an increase in the strength of the samples exceeds the stated in the Eq. (1).

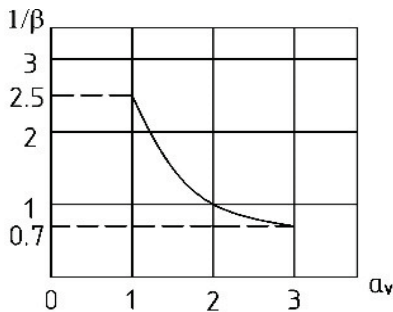


Figure 7 Dependence of $1/\beta$ of the shear span

When one takes into account the relative shear span (in the studied range of $1d \leq a_v \leq 3d$), it is recommended to determine the dependence of $1/\beta$ by using Fig. 7.

Based on the above, the Eq. (1) can be transformed into Eq. (7):

$$V_{Rd} = (V_{Rd, c} + V_{Rd, s}) \frac{1}{\beta} \quad (7)$$

As the results of experimental studies found that the area of damage affects the residual bearing capacity, in further calculations, it is necessary to introduce a number of changes. Due to the fact that the damaged elements have been calculated and it has been found that the shape of damage is not determinative, but its area is, then the value should be entered in the calculation as an equivalent height of the damage h_{damage} :

$$h_{damage} = \frac{A_{damage}}{b_w} \quad (8)$$

Instead of the working height element d , the equivalent working height with regard to the damage d_{damage} should be used:

$$d_{damage} = h - a - h_{damage} \quad (9)$$

The reinforcement ratio for the longitudinal reinforcement ρ_1 is then determined by the Eq. (10):

$$\rho_1 = \frac{A_s}{b_w \cdot d_{damage}} \leq 0.02 \quad (10)$$

The empirical coefficient k is determined by the Eq. (11) (d_{damage} use in mm):

$$k = 1 + \sqrt{\frac{200}{d_{damage}}} \leq 2.0 \quad (11)$$

In this case, in the Eq. (2) and (3), from the cross-sectional area of the element ($b_w \cdot d$) the area of the damage must be subtracted, which is denoted as A_{damage} . Considered to be action elements without the longitudinal force, the part $k_1 \cdot \sigma_{cp}$ must be ignored. The expressions then take the following form:

$$V_{Rd, c} = (C_{Rd, c} \cdot k \cdot \sqrt[3]{100 \cdot \rho_1 \cdot f_{ck}}) (b_w \cdot d - A_{damage}) \quad (12)$$

$$V_{Rd, c, \min} = \left(0.035 \cdot k^{\frac{3}{2}} \cdot f_{ck}^{\frac{1}{2}} \right) (b_w \cdot d - A_{damage}) \quad (13)$$

According to the results of the experimental studies, in the Eq. (4) and (5), the angle of the inclined cracks θ

respectively to the axe of the beam proposes to take the value of $\cot\theta$ based on the value of the shear span:

$$\cot\theta = \frac{a_v}{d} \quad (14)$$

The resulting value $\cot\theta$ should be limited to the range between $1 \leq \cot\theta \leq 2.5$.

The lever arm of the internal forces z should be adapted:

$$z = 0.9 \cdot d_{\text{damage}} \quad (15)$$

According to the proposals, a convenient calculation algorithm is created, which is shown in Fig. 8.

In the proposed method of calculation, test calculations were performed and the results are shown in Tab. 3. A comparison of the results of the calculation showed good convergence with the results of the experiment; the coefficient of variation is $v = 10,3\%$, which indicates the feasibility of using the developed methodology in the practice of design and construction.

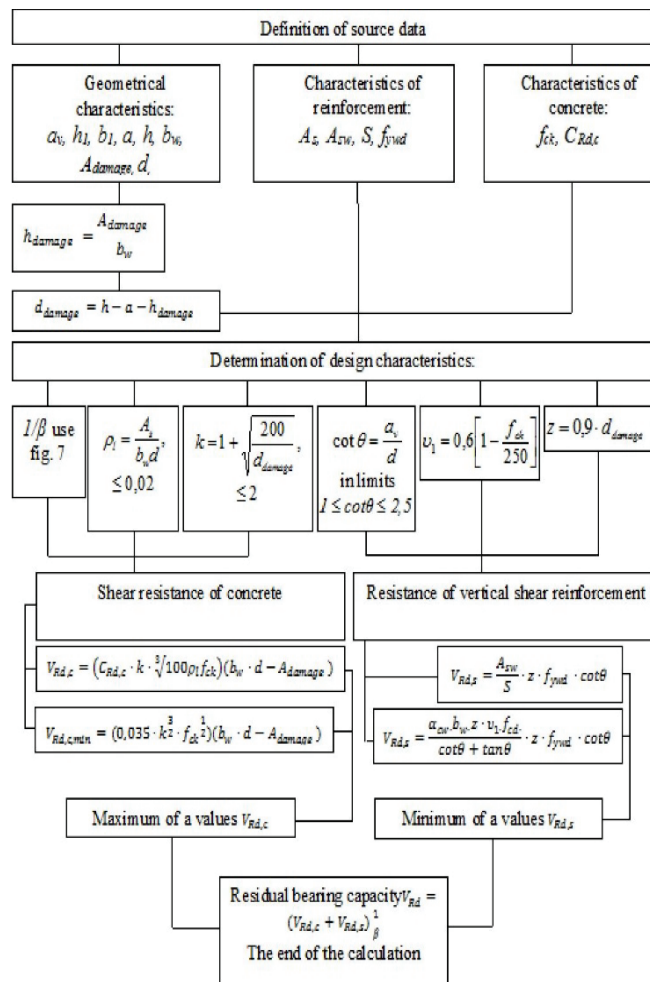


Figure 8 Proposed algorithm of the calculation of the residual bearing capacity of the damaged reinforced concrete beams' inclined sections

List of symbols in the calculation:

- A - cross-sectional area
- A_{damage} - total damage area
- A_s - cross-sectional area of longitudinal reinforcement
- A_{sw} - cross sectional area of shear reinforcement
- a - the axis distance of reinforcing steel from the nearest surface
- a_v - shear span
- b_l - width of the damage on the beam
- b_w - width of the web on the beam
- $C_{Rd,c}$ - value of the shear strength of concrete
- d - effective depth of a cross-section
- d_{damage} - equivalent damage depth of a cross-section
- F - action
- F_u - ultimate action
- f_u - ultimate deflection
- f_{ck} - characteristic value of the compressive strength of concrete
- f_{ywd} - characteristic yield of shear reinforcement
- h - overall depth of a cross-section
- h_l - damage depth of a cross-section
- h_{damage} - equivalent damage depth of a cross-section
- k - coefficient which depends on the effective depth of a cross-section d
- S - spacing between shear reinforcement
- V - shear force
- V_{Rd} - shear resistance
- $V_{Rd,c}$ - shear resistance of concrete
- $V_{Rd,c,min}$ - minimum of the shear resistance of concrete
- $V_{Rd,s}$ - resistance of vertical shear reinforcement
- V_u - ultimate shear force
- V_{exp}^u - ultimate shear force of laboratory tests
- V_{LIRA}^u - ultimate shear force of the numerical experiment
- z - lever arm of internal forces
- a_{cw} - coefficient of the state of stress in the compression chord
- $1/\beta$ - coefficient which depends on the shear span
- β_1 - angle of damage
- ε_c^u - ultimate deformations in the concrete
- ε_{sw}^u - ultimate deformations in shear reinforcement
- v - coefficient of variation
- ν_1 - strength reduction factor for the concrete cracked in shear
- ρ_1 - reinforcement ratio for longitudinal reinforcement
- θ - angle of the inclined crack

5 CONCLUSION

Experimental studies were conducted, and their results determined the residual bearing capacity of the inclined sections and the stress-strain state of the damaged reinforced concrete beams.

It was determined that with a decrease in the shear span, the elements perceive a larger transverse force. The presence of damage leads to a decrease in the bearing capacity, and during destruction, smaller ultimate deflections are reached (because the dangerous crack needs to cross a lower height of the cross-section to destroy the element). The presence of damage also leads to changes in parameters of the stress-

strain state – a decreasing of the ultimate deformations of the concrete (because of the same reason), an inclination of the neutral axis in the cross section of the element.

Modeling in LIRA-CAD software complex allows to predict the work elements and determine the bearing capacity, but in comparison with the real data, there are still some differences and the process takes considerable time.

The developed method for determining the residual bearing capacity is quite simple to apply, it allows quick calculation and shows good convergence with the experimental data, as indicated by the coefficient of variation $v = 10.3\%$.

6 REFERENCES

- [1] Bonić, Z., Topličić Ćurčić, G., Davidović, N., & Savić, J. (2015). Damage of concrete and reinforcement of reinforced-concrete. *Procedia Engineering*, 117, 411-418. <https://doi.org/10.1016/j.proeng.2015.08.187>
- [2] Lu, Z., Chai, J., & Yu, J. (2015). A numerical approach for calculating the mechanical performance of the fire-damaged reinforced concrete continuous beams. *Tongji Daxue Xuebao / Journal of Tongji University*, 43(1), 16-26. <https://doi.org/10.11908/j.issn.0253-374x.2015.01.003>
- [3] Hayashi, T., Yamauchi, T., Kudoh, H. (1984). Repair Works of the Earthquake Damaged Building by the Nihonkai-Chubu Earthquake, 1983. *Concrete Journal*, 22, 32-40. https://doi.org/10.3151/coj1975.22.9_32
- [4] Ou, Z.-M. & Sun, L. (2017). Flexural fatigue-life reliability of frost-damaged concrete. *Zhejiang Daxue Xuebao (Gongxue Ban) / Journal of Zhejiang University (Engineering Science)*, 51, 1074-1081 and 1103. <https://doi.org/10.3785/j.issn.1008-973X.2017.06.003>
- [5] BS EN 1992-1-1:2004. Design of concrete structures. General rules and rules for buildings, The European Union Per Regulation 305/2011, Directive 98/34/EC, Directive 2004/18/EC
- [6] DBN B.2.6.-98:2009. Concrete and reinforced concrete structures. General rules. Kyiv, 2009, 101 p.
- [7] Kabir, M., Subhani, M., Shrestha, R., & Samali, B. (2018). Experimental and theoretical analysis of severely damaged concrete beams strengthened with CFRP. *Construction and Building Materials*, 178, 161-174. <https://doi.org/10.1016/j.conbuildmat.2018.05.038>
- [8] Burningham, C., Pantelides, C., Reaveley, L. (2014). Repair of Prestressed Concrete Beams with Damaged Steel Tendons Using Post-Tensioned Carbon Fiber-Reinforced Polymer Rods. *ACI Structural Journal*, 111, 387-3954. <https://doi.org/10.14359/51686529>
- [9] Hou, L., Wang, J., Huang, T., Shen, C., Aslani, F., Chen, D. (2019). Flexural behaviour of corroded reinforced concrete beams repaired with ultra-high toughness cementitious composite. *Construction and Building Materials*, 211, 1127-1137. <https://doi.org/10.1016/j.conbuildmat.2019.03.214>
- [10] Sakka, Z., Assakkaf, I., & Qazweeni, J. (2018). Reliability-based assessment of damaged concrete buildings. *Structural Engineering and Mechanics*, 65, 751-760.
- [11] Orešković, M., Klymenko, I., Aniskin, A., & Kozina, G. (2018). Analysis of Damaged Concrete Columns of Circular Cross-Section. *Tehnički vjesnik* 25(2), 337-343. <https://doi.org/10.17559/TV-20160621085905>
- [12] Klimenko, Y., Chtrnieva, O., & Ismael, A. (2013). Tests results of the damaged T-section beams. *Tehnički glasnik*, 7(4), 344-346. <https://hrcak.srce.hr/112055>

Authors' contacts:

Zeljko Kos, PhD, Assistant Professor
(Corresponding author)
University North, Department of Civil Engineering
Jurja Krizanica 31B, 42000 Varazdin, Croatia
+38598757989, zkos@unin.hr

Yevhenii Klymenko, PhD in Engineering Science, Professor
Odessa State Academy of Civil Engineering and Architecture,
4 Didrihsona st., 65029 Odessa, Ukraine
klimenkoew57@gmail.com

Kostiantyn Polianskyi, post-graduate student
Odessa State Academy of Civil Engineering and Architecture,
4 Didrihsona st., 65029 Odessa, Ukraine
kostyapolyanski@gmail.com

Andjelko Crnoja, post-graduate student
Odessa State Academy of Civil Engineering and Architecture,
4 Didrihsona st., 65029 Odessa, Ukraine
+385992755466, acnoja@hotmail.com

Wages and Incentive Instruments for Enhancing the Performance of Construction Industry Employees

Alena Tichá, Dana Linkeschová, Zdeněk Tichý, Zuzana Mrňová*

Abstract: The aim of the article is to present quantitative development of wages and incentive instruments in the Czech Republic during the recent period and at the same time to provide an insight into the emerging changes in the labor market brought by the industry and the construction industry digitization. Strong demand for increased corporate social responsibility of the companies in the technical, economic and environmental protection and care sectors, and in particular in mutual communication between market partners, has had and will have an impact on wage policy and creation of employer wage systems. This article briefly gives the insight into what visions and strategies this situation brings into the construction industry field.

Keywords: development of wages; incentive instruments; wage policy; wages

1 INTRODUCTION

Construction industry is a beautiful profession. It allows you to see and show the results of the work of individuals and entire teams even after decades, which is not common in every industry. And it is precisely this view of this complex work that enables to motivate employees in various ways to achieve business plans. Incentive instruments have been developing in the same way as the technical and technological developments in the construction industry have. In particular, however, they adapt and modify according to the changes that are brought by the shift in people's behavior and attitudes to construction work. The post-war BB generation called "baby boomers" (born 1945–1964) gradually entered the labor market, followed by X generation (born 1965–1979) and later the Y generation, more commonly referred to as "millennials" (born 1980–1994).

People born between 1995 and 2010 are included in the Z generation, sometimes referred to as "centenarians". First representatives of this generation entered the work process around 2015, and now the first university educated graduates of Z generation follow. According to the research, the very Z generation will be the hatchery of digital talents for the upcoming digital age. In the work environment, however, the centenarians behave in a different way than any previous generation, including the millennials. They represent a fully technological generation with tremendous confidence, but at the same time with an autonomous willingness to work hard and in more assertive and much more demanding way than the millennials. Completely different and new incentive instruments are connected with this situation.

Nevertheless, it is clear that the classical wage incentive instrument will also appeal to this generation. Providing wages to employees is a daily part of the employer's work. This process is complicated by different and often contradictory expectations of the employer and their employees. On the one hand, wages are a means to meet the needs of employees and their families, but on the other hand, they are a significant cost item for the employer. At the same

time, they are an instrument of material stimulation of employees to achieve the employer's business plans. Moreover, the impact of the remuneration process significantly affects both the business and economic situation of the company and the social situation of the employee. Furthermore, the conditions for the provision of wages are quite significantly regulated by legislation.

The aim of the article is to present quantitative development of wages and incentive tools in the Czech Republic during the recent period and at the same time to provide an insight into the emerging changes in the labor market brought by the industry and the construction industry digitization. Strong demand for increased corporate social responsibility of the companies in the technical, economic and environmental protection and care sectors, and in particular in mutual communication between market partners, has had and will have an impact on wage policy and creation of employer wage systems.

2 REMUNERATION FOR WORK, WAGES AND THE DEVELOPMENT OF MINIMUM AND GUARANTEED WAGES

The legal regulation of wages in the Czech Republic results from the Constitution, namely from Article 28 of the Charter of Fundamental Rights and Basic Freedoms. Details are regulated by Act No. 262/2006 Coll., Labor Code, as amended. In addition to this constitutional principle, the principles arising from international conventions and European Union directives must apply in the area of wages. Wage rights and their protection are an organic part of labor relations. The fundamental principles of labor relations in the field of wages are given by the constitutional right to equitable remuneration [1].

The Labor Code distinguishes between remuneration for work in the business sector (it is called a wage) and in the sphere of public services and administration (it is called a salary). The employee is entitled to wage, salary or remuneration from the agreements on work performed (Tab. 1).

Table 1 The system of remuneration in employment relations [1]

Remuneration under the Labor Code	Remuneration for work WORK	Remuneration in an employment relationship EMPLOYMENT	Remuneration for work in the business sector WAGE
		Remuneration for work outside employment relationship REMUNERATION FROM THE AGREEMENT	Remuneration for work in public services and administration SALARY
			Agreement on work activities AWA
	Remuneration for work readiness		Work performance agreement WAP

Table 2 Guaranteed minimal wage in 2019 and in 2020 [2]

Work category	Hourly guaranteed wage in 2019 (CZK)	Hourly guaranteed wage in 2020 (CZK)	Monthly guaranteed wage in 2019 (CZK)	Monthly guaranteed wage in 2020 (CZK)
1	79.80	87.30	13,350.00	14,600.00
2	88.10	96.30	14,740.00	16,100.00
3	97.50	106.40	16,280.00	17,800.00
4	107.40	117.40	17,970.00	19,600.00
5	118.60	129.70	19,850.00	21,700.00
6	130.90	143.20	21,900.00	24,000.00
7	144.50	158.10	24,180.00	26,500.00
8	159.60	174.60	26,700.00	29,200.00

The minimum wage is a protection against the provision of unduly low wages. It is the lowest allowable amount of remuneration for work in an employment relationship, i.e. the lowest allowable amount of wage, salary or remuneration from the agreement. In the Czech Republic it is determined by the Government Regulation. The minimum wage category is a very sensitive variable perceived quite contradictory by individual partners in the labor market. Nevertheless, at optimal levels, the minimum wage has a protective function for both employees (protection against poverty) and employers (a uniform level of lowest earnings introduces equal conditions of competition). Similarly, the minimum wage is conceived in most EU countries. In some EU countries (Denmark, Finland, Austria, Sweden, Cyprus), the minimum wage is ensured by collective supranational agreements covering most employees. Employees whose wages are not negotiated by a collective agreement are protected against the provision of unduly low wages by a "guaranteed minimum wage". The work carried out is graded according to its complexity, responsibility and effort into eight individual categories, for each of which there is the lowest level of guaranteed minimum wage (Tab. 2). Thus, not only the minimum wage is binding for the employer, but it must be remunerated at least at the level of the respective groups of guaranteed minimum wages. It grows with every minimum wage increase.

Indicative examples of work falling within individual categories:

1st category: kitchen assistant, seamstress, cleaning woman, delivery man, porter
 2nd category: digger, scaffolder, medical orderly, chambermaid, tobacconist, plumber
 3rd category: bricklayer, plumber, tinsmith, heating engineer, waiter, bartender, barber, hairdresser
 4th category: general nurse, midwife, cook, tailor
 5th category: bus driver, foreman, dispatcher, paramedic, salary accountant, kindergarten teacher
 6th category: business clerk, IT system creator, independent designer of complex buildings
 7th category: financial expert, doctor, dentist, pharmacist, marketing expert or programmer
 8th category: expert on financial and business strategy, top scientist.

For the sake of interest and comparison, the following table (Tab. 3) shows the income scales or claim or guaranteed component of the income of academic, scientific and research workers at a selected technical university in the Czech Republic, which were in force on 1st January 2020.

Table 3 Income tariffs – academic, scientific and research workers in 2019

Job title	Professor	Assistant professor	Senior lecturer with PhD title	Senior lecturer without PhD title	Lecturer (Ing.)	Reader
Salary tariff (CZK)	33,600	28,400	24,500	22,600	19,400	19,400
Salary tariff (EUR)	1,344	1,136	980	904	776	776

Table 4 Development of the minimum wage in the Czech Republic since its introduction in 1991

Year	Minimal wage amount			
	CZK/month	CZK/hour	EUR/month	EUR/hour
1991	2,000	10.80	80.00	0.43
1992	2,200	12.00	88.00	0.48
1996	2,500	13.60	100.00	0.54
1998	2,650	14.80	106.00	0.59
1999	3,600	20.00	144.00	0.80
2000	4,500	25.00	180.00	1.00
2001	5,000	30.00	200.00	1.20
2002	5,700	33.90	228.00	1.36
2003	6,200	36.90	248.00	1.48
2004	6,700	39.60	268.00	1.58
2005	7,185	42.50	287.40	1.70
2006	7,955	48.10	318.20	1.92
2007	8,000	48.10	320.00	1.92
2013	8,500	50.60	340.00	2.02
2015	9,200	55.00	368.00	2.20
2016	9,900	58.70	396.00	2.35
2017	11,000	66.00	440.00	2.64
2018	12,200	73.20	488.00	2.93
2019	13,350	79.80	534.00	3.19
2020	14,600	87.30	584.00	3.49

The current development of the minimum wage in the Czech Republic is shown in the following overview (Tab. 4). To estimate the conversion between the currency in Euro and Czech crowns it is stated on average that 1 EUR corresponds

to approximately 25 CZK. For comparison, Tab. 5 also lists the minimum wages in selected countries in Europe.

The evolution of the minimum wage in the time series from January 2009 to January 2019 is shown in the following chart (Fig. 1) for countries in which a minimum wage is introduced in the European Union as well as a comparison with non-EU countries.

Evidently the highest minimum income is in Luxembourg, where it exceeds 2,000 EUR/month. It is therefore 3.42 times higher minimum income than in the Czech Republic. The lowest minimum income is in Bulgaria.

The development of the minimum wage is related to the income growth. The following chart (Fig. 2) shows the growth of the average income in the Czech Republic in CZK.

The minimum and average income ratio is shown in Table 6 in the time series. As can be seen, between 2009 and

2012 the minimum income stagnated and its ratio to the average income was decreasing. Gradually, the whole system found itself in a situation where it was not worth to work for a minimum wage and it was better to live on social benefits. There has been a tendency to reverse this trend in recent years.

Table 5 Minimum wage in selected countries in 2019 [3]

Country	Bulgaria	Czech Republic	Greece	Spain
EUR/month	286	519	684	1050
Country	Latvia	Hungary	Poland	Portugal
EUR/month	430	464	523	700
Country	Romania	Slovenia	Slovakia	UK
EUR/month	446	887	520	1453
Country	Netherlands	Ireland	Belgium	Germany
EUR/month	1616	1656	1594	1557

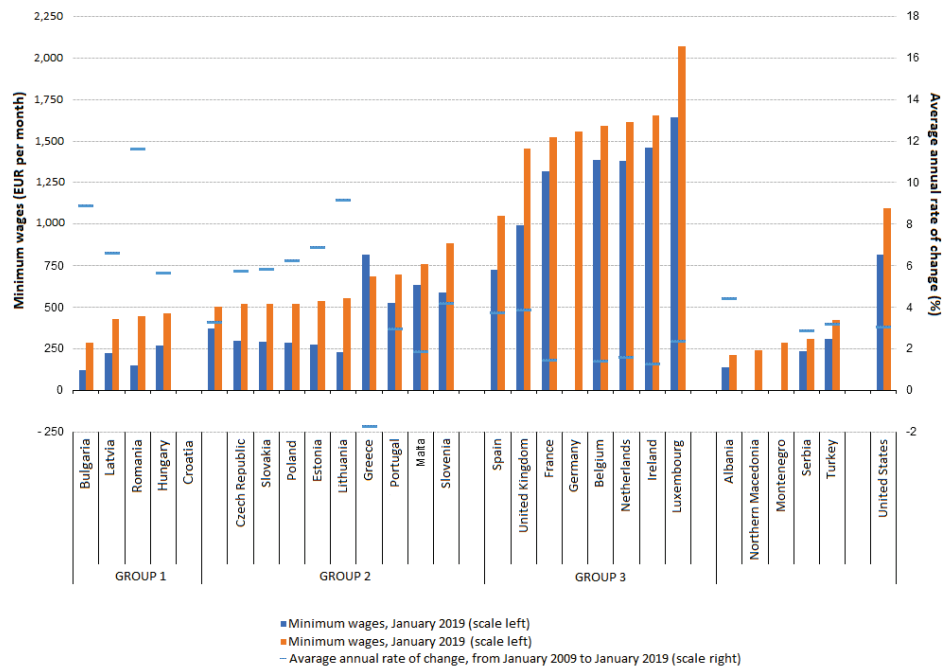


Figure 1 Minimum wages in selected EU countries in 2009 and 2019 [3]



Figure 2 Development of the average wage in CZK in the Czech Republic between 2005 and 2019

For the further development of the labor market, it is certainly necessary to consider not only the income as an incentive instrument, but also the benefits provided by

employers to employees. In connection to the industry, construction and services digitalization onset, there will be changes in the perspective on remuneration. The importance

of corporate social responsibility towards the ecological, economic and social sustainability of the world significantly strengthens. All of these have and will increasingly have an impact on workers' performance.

Table 6 Ratio of minimum income to average income in the Czech Republic in time series

Year	Average income	Minimum income	Ratio of minimum and average income (%)
2005	18,270	7,185	39
2006	21,269	7,955	37
2007	22,641	8,000	35
2008	24,309	8,000	33
2009	25,418	8,000	31
2010	25,591	8,000	31
2011	26,211	8,000	31
2012	27,055	8,000	30
2013	26,525	8,500	32
2014	27,261	8,500	31
2015	28,258	9,200	33
2016	29,491	9,900	34
2017	31,802	11,000	35
2018	33,871	12,200	36
2019	33,697	13,350	40
2020	35,000	14,600	42

3 WORK COMPETENCES, JOB POSITIONS AND INCENTIVE INSTRUMENTS (BENEFITS)

Working in the digitized industry and construction industry requires new **competences**. Individuals are expected to be **flexible, independent** and capable of addressing **project-oriented** work tasks more and more frequently. In addition to professional competences, these are basic "skills for the 21st century", such as the ability to (virtually) **cooperate in teams** made up of different experts with different responsibilities. Today's workers need to be able to **acquire knowledge independently** according to their current needs – often directly in the workplace. This requires knowledge of **new media technologies** and devices (web 2.0, mobile media) and knowledge of the risks and dangers associated with the **data use** and virtual systems (data security and protection). However, all this will not work without continuing education (**lifelong learning**).

In the broader meaning of **Industry 4.0**, there is one key element – **interconnection**. The **automation and process optimization** in the field of production, logistics and services goes hand in hand with it. While the first three stages of industrial production were characterized by innovations in the fields of mechanics (industry 1.0), electronics (industry 2.0) and information technology (industry 3.0), it is typical for industry 4.0 that classic, industrial processes are increasingly interconnected with communication and data technique to create so-called **cyber-physical production systems**, thus enabling the realization of the vision of **self-managed production**.

Z generation employees prefer their own work environment – they **do not like sharing space** with others. Their intimate relationship with devices makes them **less sociable** than the millennials. From the beginning they are interested in how they will contribute to the running of the company. They long for doing beneficial things and **leaving**

a trace. In the construction industry, the introduction of **digital building information modelling/management (BIM)** represents such an initial trace of the digital revolution. The centennials greatly **value their time** and want to know in detail the **model** by which they will be **remunerated**. They expect **regular promotion** or at least salary increase in exchange for the **loyalty to the employer**. They are pragmatic and interested in **non-monetary compensation** such as above-standard health care, retirement benefits and long-term benefits – in which they are closer to generations X and BB than to millennials of Y generation. [4]

Along with the changing behavior of the forthcoming generation and the progress in digitization and work automation, there are many vulnerable professions. Some professions can be expected to disappear completely (Tab. 7); however, new professions can be expected to emerge that cannot be imagined now. At the same time, the current predictions expect that the number of newly created positions will be lower than those that have disappeared. [6]

Table 7 Twenty professions with the highest digitization vulnerability index [6]

ISCO-3 Code	Job title	Digitization vulnerability index
431	Numerical data processing clerks	0.98
411	General administrative staff	0.98
832	Motorcycle and car drivers (except lorry drivers)	0.98
523	Cashiers and ticket vendors	0.97
621	Skilled workers in forestry and related areas	0.97
722	Blacksmiths, toolmakers and related workers	0.97
441	Other clerks	0.96
412	Secretaries (in general)	0.96
834	Operation of mobile equipment staff	0.96
612	Animal breeders for the market	0.95
921	Agricultural, forestry and fishery assistants	0.95
811	Operation of equipment for mining and processing of raw materials	0.94
814	Operation of machines for production and processing of rubber, plastic and paper products	0.94
432	Clerks in logistics	0.94
821	Assembly workers for products and equipment	0.93
816	Operation of machinery for food and related products	0.93
961	Waste workers	0.93
421	Treasurers in financial institutions, bookmakers, money lenders, receivables collectors and related workers	0.93
831	Engine drivers and staff providing assembly and train operation	0.92
818	Other operators of stationary machinery and equipment	0.92

Digitization era is becoming part of everyday life, and in many aspects, we may not have noticed it. In 2015, digital economy accounted for 4.2% of global GDP and provided work for 17 million people worldwide, with additional 15 million jobs indirectly supported. The period of the Fourth Industrial Revolution will change the view of work and employment as perceived today, education will not be adapted to one profession as it has been until now, but will

emphasize interdisciplinarity, complexity, creativity and flexibility.

Table 8 Necessary and the least vulnerable professions in the period of work digitization and automation. Twenty professions with the lowest digitization vulnerability index [6]

ISCO-3 Code	Job title	Digitization vulnerability index
142	Retail and wholesale managers	0.000
221	Doctors (except dentists)	0.001
222	General nurses and midwives with specialization	0.002
134	Managers in education, health, social and other areas	0.002
122	Managers in business, marketing, research, development, advertising and public relations	0.005
231	Lecturers at universities and colleges	0.008
133	Managers in the field of information and communication technologies	0.008
141	Managers in accommodation and catering services	0.010
131	Managers in agriculture, forestry, fisheries and related fields	0.011
226	Other health care specialists	0.011
215	Specialists in the field of electrical engineering, electronics and electronic communications	0.015
252	Specialists in databases and computer networks	0.021
143	Other managers	0.021
312	Foremen and related workers in mining, manufacturing and construction industry	0.022
214	Specialists in production, construction industry and related fields	0.044
111	Legislators and top officials of public administration, political and interest organizations	0.048
213	Specialists in biological and related fields	0.050
263	Specialists in social, church and related fields	0.054
132	Managers in manufacturing, mining, construction, transport and related industries	0.054
242	Specialists in strategy and personnel management	0.056
264	Writers, journalists and linguists	0.058

4 CORPORATE SOCIAL RESPONSIBILITY AND INDUSTRY 4.0

Corporate Social Responsibility (CSR) means sustaining economic success and gaining a competitive advantage by building a company good reputation and **gaining the trust of people working for it** or living in the community within its business field. It represents an important aspect of strategic corporate behavior and is recognized as such at European Union level. Within this concept, the company behaves responsibly not only in the area of business decisions and strategy, but also in the area of the environment and social impact of the company functioning.

Customers expect not only high-quality products and services from the company, but also to be a reputable and respected supplier on the market. The company suppliers want to sell to customers who return to their products or services and pay for the products within the deadlines. The people and community in which the company operates want to know that the company behaves responsibly to the society and the surrounding environment. **Employees** like to work

for a company they are proud of and which values their work.

The role of companies in the society has currently been changing. The public assesses and evaluates them not only according to the quality of their services and products, but also according to the degree of responsibility of their activities in the society. Responsible behavior brings not only **greater loyalty of its employees** but also strengthening of the brand value and good reputation, good relations within the region, and last but not least, significant potential for solving possible crisis situations. Corporate social responsibility behavior is a long-term investment in its overall development.

A company that chooses this strategy should ask the following questions right from the very beginning: which area it will support, in which regions, what it wants to achieve, and what resources it will use to do so. It appears that the interconnection of the commercial sector with the public benefit area is also important in the exchange of know-how by involving employees in the provision of professional services. [7]

The trend will result in the growth of services, as the customer demands not only quality products, but also related services that increase their comfort. Such a market brings a **new view of the skills of work teams**: "In our view, the **key skills for the 21st century** are the following **abilities**: to orientate oneself, to adapt, to convince, to cooperate, to lead, and to express empathy."

5 INFLUENCE OF WAGE AND BENEFITS ON WORKERS' BELONGING TO THE COMPANY

The impacts of Industry 4.0 on the labor market are really complex, but also contradictory. Due attention has not been paid to their investigation in the Czech Republic yet. One of the exceptions is the study called **Impacts of digitization on the labour market in the Czech Republic and the EU** [6] from the Department of EU Strategy and Trends of the Office of the Government of the Czech Republic. The text deals only with the effects of narrowly conceived digitization and attempts to estimate the risk of employment in occupational groups on the basis of coefficients that are taken from the study dealing with the US labor market. The calculations made so far on the cessation and creation of jobs differ in relation to the methodology used. Specifically for the Czech Republic, it is estimated that 10% of jobs will be strongly threatened by automation over the next 20 years and that 35% of jobs will experience significant changes in activities carried out. If this estimate published in the OECD study (Employment Outlook 2016) is related to the number of employees in 2015, about 408,000 jobs will be highly threatened and 1.4 million jobs will undergo substantial changes.

In 2017, at the conference Towards Work 4.0, Prime Minister Advisory Director Vladimír Špidla said that **the digitization and robotization of industry will cause a radical change in the organization of work and many jobs will disappear**. It is estimated that there will be as many as

53% of them in the Czech Republic. It follows from the above that **the industrial revolution will have a negative impact on unemployment**. However, it will be a longer time horizon and if the education system is reformed, the labor market will be prepared for these changes. The Czech Republic has one of the lowest unemployment rates in the EU as a whole and **currently companies have difficulty finding skilled workforce**.

The second aspect is **average wages**, which are among **the lowest in the EU**. This prevents the rapid accession of modern technologies. This access of modern technologies and the massive purchase of technologies will be influenced primarily by the business cycle, when economists are already discussing a "overheated economy" (e.g. Governor of the Czech National Bank Jiří Rusnok, 2018) and political determination to bring wages in the Czech Republic closer to the European Union average. As the Czech Republic is a small open economy, the influx of foreign investment will have a major impact on the rapid access of Industry 4.0.

When comparing the share of unemployed persons and the general unemployment rate for individual regions and the Czech Republic as a whole, significant differences can be seen. Given the fact that the authors of scientific articles state that the redundancies will mainly affect low-skilled workers, further deepening of regional disparities can be expected. According to the analysis carried out, the importance of the manufacturing industry for the Czech Republic results to be clear. **Industry 4.0 is expected to shift employment from industry to the knowledge-intensive services sector**. The implementation of Industry 4.0 principles into industry is of limited significance, as long as the surroundings of the factories, including towns, will operate in "old-fashioned" way without applying Industry 4.0 principles. These apply mainly at fundamental conceptual changes in energy, transport, Smart Cities sectors, etc. [9]

6 CONCLUSION

Czech companies regularly update their remuneration systems; however, half of the managers do not use them correctly. **More than 70% of Czech companies have updated their remuneration system in the last two years. This points to the fact that companies are aware of the importance of setting remuneration and wage systems in line with labor market trends and developments on the labor market. However, the question is: Do companies use their remuneration systems correctly?**

Czech companies update payroll systems not only to attract new employees, but also to stabilize existing ones and not let them run away to the competition. **This year, the wage system has been updated by 27% of Czech companies; last year it was 33% of companies; and two years ago 10% of companies started updating their wage system.** This results from a survey [10] among Czech companies on the topic of setting up payroll systems.

However, the results of the survey also showed that **in half of Czech companies, the wage system is not perceived as an instrument for managing people and influencing labor productivity**. In one third of the companies surveyed,

managers do not feel the need to have an instrument to influence employee work productivity, and in a quarter of companies, managers with this approach are a minority. Czech companies thus face a challenge for greater involvement of managers in people management.

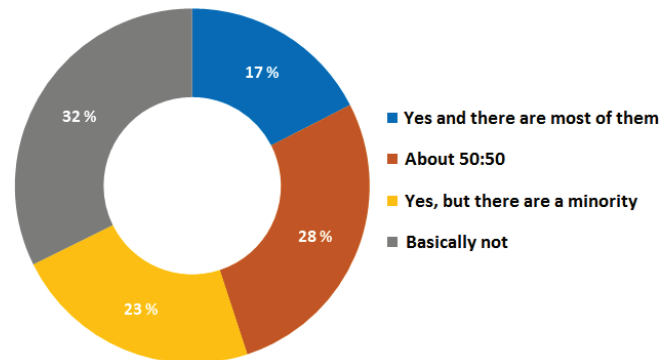


Figure 3 Managers' pressure on changes in remuneration systems [10]

Wages and incentive systems are essential for the functioning of Czech companies. Companies regularly try to improve their quality. A quality and well-set payroll system should fulfil **four basic attributes** in order to complete its main role, namely to motivate employees to perform well:

1. **Transparency** – all employees and of course managers and team leaders should know how remuneration is set up in the company, what their wages consist of, and for what and how they are valued.
2. **Clarity** – the system may be transparent, but at the same time unclear for most of the employees. Everything should be set so that each employee can understand it.
3. **Motivation** – the benefit system should motivate all employees in all categories, not only certain groups, and in others raise the impression that they are neglected and their work is less important and less valued.
4. **Fairness** – payroll system setting should be fair, not disadvantageous, and fairly rewarding all employees according to their job title and competences. [11]

Across the world, a successful solution is one that benefits both people and the environment that is actually our natural home. Similarly to nature, it applies to the teams at workplaces, that if the individual members or elements of the system do not "win" each on its own, then the team as a whole will not "win" as well. [12], [13]

Notice

The paper was presented at PBE2020 – International Scientific Conference "People, Buildings and Environment 2020". The 14th conference was held in the Rožnov pod Radhoštěm city, the Czech Republic, from 7 to 9 October 2020. The paper will not be published anywhere else.

7 REFERENCES

- [1] Tomší, I. (2008). *Mzdy a mzdové systémy*. Praha: ASPI Wolters Kluwer, ISBN 978-80-7357-340-9.

- [2] Zaručená mzda 2020. *Kurzy.cz* [online]. [cit. 2020-02-03]. Available at: <https://www.kurzy.cz/mzda/zarucena-mzda/>
- [3] Statistika minimálních mezd. *Ec.europa.eu* [online]. [cit. 2020-02-03]. Available at: https://ec.europa.eu/eurostat/statistics-explained/index.php?title=Minimum_wage_statistics/cs
- [4] Čičváková, M. (2017). *Část 1: Průmysl 4.0 a jeho vliv na svět práce* [online]. [cit. 2020-02-03]. Dostupné z: <http://www.nuv.cz/vystupy/cast-1-prumysl-4-0-a-jeho-vliv-na-svet-prace>
- [5] Kuhnová, E. (2017). *Digitalizace změny trh práce* [online]. 29.12.2017 [cit. 2020-02-03]. Available at: www.bozpinfo.cz/josra/digitalizace-zmeni-trh-prace
- [6] Chmelař, A. et al. (2015). *Dopady digitalizace na trh práce v ČR a EU* [online]. Oddělení strategie a trendů Evropské unie (OSTEU), [cit. 2017-09-18]. Available at: <https://www.vlada.cz/assets/evropske-zalezitosti/analyzy-EU/Dopady-digitalizace-na-trh-prace-CR-a-EU.pdf>
- [7] *Co je společenská odpovědnost firem* [online]. [cit. 2020-02-03]. Available at: <http://www.businessprospolecnost.cz/lbg/spolecenska-odpovednost-firem.html>
- [8] Revoluce práce je tu In: Komora, měsíčník hospodářské komory České republiky, ročník 20, prosinec 2019-leden 2020, p. 80
- [9] Hedvičáková, M. (2018). Dopady iniciativy Průmyslu 4.0 na nezaměstnanost a vývoj mezd. *XXI. mezinárodní kolokvium o regionálních vědách*, Kurdějov, 13. - 15. června 2018 [online]. Brno: Masarykova univerzita, 201-207 [cit. 2020-02-03]. <https://doi.org/10.5817/CZ.MUNI.P210-8970-2018-26>
- [10] České firmy pravidelně aktualizují své odměňovací systémy, polovina manažerů je však nepoužívá správně. *Trexima.cz* [online]. [cit. 2020-02-03]. Available at: <https://www.trexima.cz/aktualita/ceske-firmy-pravidelne-aktualizuji-sve-odmenovaci-systemy-polovina-manazeru-je-vsak-nepouziva-spravne>
- [11] 13. vlna HR Monitoru. *Trexima.cz* [online]. [cit. 2020-02-03]. Available at: <https://www.trexima.cz/13-vlna-hr-monitoru>
- [12] In: Třetí alternativa Stephen R.Covey: Praha Management Press 2013 (ISBN 978 – 80 – 7261 – 256 – 7) p. 366

Authors' contacts:

Assoc. Prof. **Alena Tichá**, M.Sc., Ph.D.
Brno University of Technology, Faculty of Civil Engineering,
Institute of Structural Economics and Management,
Veveří 331/95, Brno, 602 00, Czech Republic
E-mail: ticha.a@fce.vutbr.cz

M.A. **Dana Linkeschová**, Ph.D.
Brno University of Technology, Faculty of Civil Engineering,
Institute of Structural Economics and Management,
Veveří 331/95, Brno, 602 00, Czech Republic
E-mail: linkeschova.d@fce.vutbr.cz

Zdeněk Tichý, M.Sc.
Brno University of Technology, Faculty of Civil Engineering,
Institute of Structural Economics and Management,
Veveří 331/95, Brno, 602 00, Czech Republic
E-mail: tichy.z@fce.vutbr.cz

Zuzana Mrňová, M.Sc.
(Corresponding author)
Brno University of Technology, Faculty of Civil Engineering,
Institute of Structural Economics and Management,
Veveří 331/95, Brno, 602 00, Czech Republic
E-mail: 157909@vutbr.cz

Comparison of Power Distribution, Losses and Efficiencies of a Steam Turbine with and without Extractions

Vedran Mrzljak*, Sandi Baressi Šegota, Hrvoje Meštrić, Zlatan Car

Abstract: The paper presents an analysis of two steam turbine operation regimes - regime with all steam extractions opened (base process) and regime with all steam extractions closed. Closing of all steam extractions significantly increases turbine real developed power for 5215.88 kW and increases turbine energy and exergy losses with simultaneous decrease of turbine energy and exergy efficiencies for more than 2%. First extracted steam mass flow rate has a dominant influence on turbine power losses (in comparison to turbine maximum power when all of steam extractions are closed). Cumulative power losses caused by steam mass flow rate extractions are the highest in the fourth turbine segment and equal to 1687.82 kW.

Keywords: efficiencies; losses; power distribution; steam extractions; steam turbine

1 INTRODUCTION

Steam turbines are integral components of steam power plants of any kind (land based [1-3] or marine steam power plants [4, 5]). In the most of the cases its main function is electricity production (or ship propulsion in marine steam power plants) [6, 7].

In marine propulsion, new complex propulsion systems are completely or at least partially based on steam turbine processes [8]. Steam turbine processes are also inevitable components of combined [9-11], cogeneration [12, 13] or multi-generation power systems [14, 15].

In various power systems, low power steam turbines are also used for several auxiliary purposes (for pumps drive [16, 17], for the drive of additional (or main) electrical generators [18], etc.). It should be noted that such auxiliary steam turbines usually did not possess any steam extractions [19].

Along with the production of electricity (or ship propulsion) the purpose of the main steam turbine in any system is to provide a sufficient steam mass flow rate for condensate/feed water heating (at condensate/feed water return line from the steam condenser to steam generator) [20, 21].

In this paper, the analysis of steam turbine with nominal power of 66 MW is presented. Two possible steam turbine operation regimes were investigated: operation regime with all steam extractions opened (base process) and operation regime when the all steam extractions are closed. Obtained results suggest that closing of steam extractions significantly increases turbine developed power, but simultaneously it increases turbine energy and exergy losses and decreases turbine energy and exergy efficiencies. Cumulative turbine power losses and turbine power losses in each turbine segment caused by steam extractions are calculated and discussed.

2 CHARACTERISTICS AND OPERATING PROCESS OF THE ANALYZED STEAM TURBINE

The analyzed steam turbine has a nominal power of 66 MW and operates in Al-Hussein power plant in Jordan [22]. For proper turbine analysis, it is important to know the steam mass flow rate as well as steam pressure and temperature at the turbine inlet, outlet and at each turbine extraction [23]. Steam turbine scheme and necessary operating points required for the performed analysis are presented in Fig. 1.

Superheated steam at the turbine inlet is delivered to the analyzed turbine direct from the steam generator [24-26], Fig. 1. At each steam turbine extraction, a certain steam mass flow rate was lead to regenerative condensate/feed water heating system (in this power plant regenerative condensate/feed water heating system consists of two low-pressure condensate heaters [27, 28], deaerator [29] and two high-pressure feed water heaters [30, 31]). After expansion in the analyzed turbine, remaining steam mass flow rate is delivered to steam condenser [32, 33].

Unlike most other conventional steam power plants, where the steam condenser is cooled with water [34, 35], in this power plant condenser is cooled with air. Steam condenser air cooling enables that steam, after expansion in the analyzed steam turbine – operating point 7, Fig. 1 and Fig. 2, is still superheated (not saturated as usual) [36, 37]. Air cooling performs additional cooling of superheated steam and enable its condensation.

Numerical analyses (energy and exergy analyses) performed in this paper do not require knowledge of the steam turbine or any other steam system component's internal structure [38-40]. Those methods are widely used in the analyses of various steam turbines [41, 42], gas turbines [43] and the entire power plants [44, 45] (black box methods).

It should be noted that in Fig. 1 the numeration of condensate/feed water heaters (water heaters) is arranged from steam condenser to steam generator (water heater mounted closer to steam condenser has lower number).

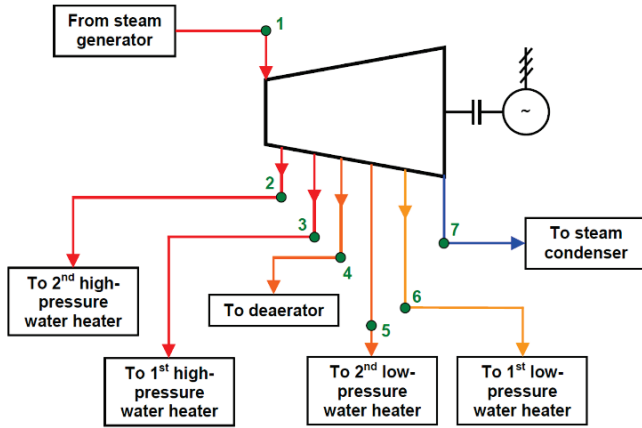


Figure 1 Scheme of the analyzed steam turbine with steam extractions along with marked operating points required for the analysis

Steam expansion processes inside the analyzed turbine in h - s (specific enthalpy-specific entropy) diagram are shown in Fig. 2. Real (polytropic) steam expansion process is presented with operating points from 1 to 7 - dark red curve (according to Fig. 1). Ideal (isentropic) steam expansion process is presented with operating points from 1 to 7 - blue line. Ideal (isentropic) steam expansion process assumes that steam specific entropy during the whole expansion process remains the same as at the beginning of the expansion (as in operating point 1) [46]. Steam mass flow rates extracted from the analyzed turbine are marked with red arrows.

Proper energy analysis of any steam turbine, as well as of turbine analyzed in this paper, requires comparison of real (polytropic) and ideal (isentropic) steam expansion processes [47], while the exergy analysis of any steam turbine requires only the real (polytropic) steam expansion process [48, 49].

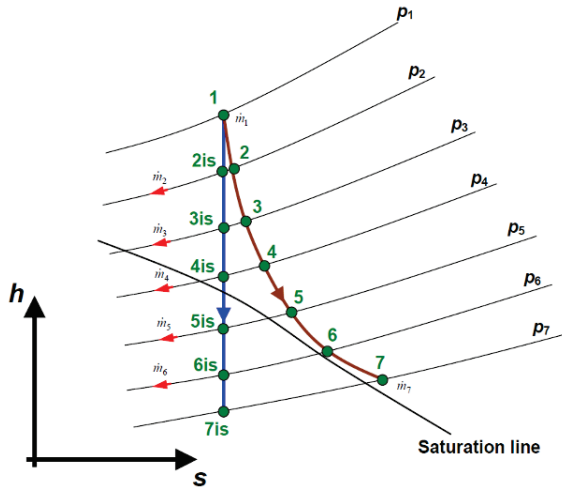


Figure 2 Ideal (isentropic) and real (polytropic) steam expansion processes inside the analyzed turbine in h - s diagram

3 EQUATIONS REQUIRED FOR THE COMPARISON OF STEAM TURBINE PROCESSES WITH AND WITHOUT EXTRACTIONS

All the equations for the steam turbine analysis in this paper are presented according to operating points from Fig. 1

and according to turbine expansion processes (ideal and real) from Fig. 2.

Real (polytropic) power of the analyzed steam turbine for the process with steam extractions is:

$$P_{RE,WSE} = \dot{m}_1 \cdot (h_1 - h_2) + (\dot{m}_1 - \dot{m}_2) \cdot (h_2 - h_3) + (\dot{m}_1 - \dot{m}_2 - \dot{m}_3) \cdot (h_3 - h_4) + (\dot{m}_1 - \dot{m}_2 - \dot{m}_3 - \dot{m}_4) \cdot (h_4 - h_5) + (\dot{m}_1 - \dot{m}_2 - \dot{m}_3 - \dot{m}_4 - \dot{m}_5) \cdot (h_5 - h_6) + (\dot{m}_1 - \dot{m}_2 - \dot{m}_3 - \dot{m}_4 - \dot{m}_5 - \dot{m}_6) \cdot (h_6 - h_7), \quad (1)$$

while for the turbine process without steam extractions (entire steam mass flow rate at the turbine inlet expanded through the turbine), real (polytropic) power is:

$$P_{RE,WOSE} = \dot{m}_1 \cdot (h_1 - h_7). \quad (2)$$

Ideal (isentropic) power of the analyzed steam turbine for the process with steam extractions is:

$$P_{ID,WSE} = \dot{m}_1 \cdot (h_1 - h_{2is}) + (\dot{m}_1 - \dot{m}_2) \cdot (h_{2is} - h_{3is}) + (\dot{m}_1 - \dot{m}_2 - \dot{m}_3) \cdot (h_{3is} - h_{4is}) + (\dot{m}_1 - \dot{m}_2 - \dot{m}_3 - \dot{m}_4) \cdot (h_{4is} - h_{5is}) + (\dot{m}_1 - \dot{m}_2 - \dot{m}_3 - \dot{m}_4 - \dot{m}_5) \cdot (h_{5is} - h_{6is}) + (\dot{m}_1 - \dot{m}_2 - \dot{m}_3 - \dot{m}_4 - \dot{m}_5 - \dot{m}_6) \cdot (h_{6is} - h_{7is}), \quad (3)$$

while for the turbine process without steam extractions, ideal (isentropic) power is:

$$P_{ID,WOSE} = \dot{m}_1 \cdot (h_1 - h_{7is}). \quad (4)$$

Energy losses of the analyzed steam turbine for the process with steam extractions are:

$$\dot{E}_{en,LOSS,WSE} = P_{ID,WSE} - P_{RE,WSE}, \quad (5)$$

while for the turbine process without steam extractions, energy losses are:

$$\dot{E}_{en,LOSS,WOSE} = P_{ID,WOSE} - P_{RE,WOSE}. \quad (6)$$

The exergy power of any fluid flow (i = index of each operating point from Fig. 1 or Fig. 2) is calculated according to [50, 51] as:

$$\dot{E}x_i = \dot{m}_i \cdot ex_i. \quad (7)$$

In the Eq. (7) ex_i is fluid flow specific exergy (for each operating point from Fig. 1 or Fig. 2). Fluid flow specific exergy is calculated according to [52, 53] as:

$$ex_i = (h_i - h_0) - T_0 \cdot (s_i - s_0). \quad (8)$$

Conditions of the ambient for the calculation of fluid flow specific exergy in each operating point (0 is the index of the ambient conditions) are ambient temperature of 298.15 K and ambient pressure of 0.1013 MPa, as proposed in the literature [22, 54].

Exergy losses of the analyzed steam turbine for the process with steam extractions are:

$$\dot{E}_{\text{ex,LOSS,WSE}} = \dot{E}x_1 - \dot{E}x_2 - \dot{E}x_3 - \dot{E}x_4 - \dot{E}x_5 - \dot{E}x_6 - \dot{E}x_7 - P_{\text{RE,WSE}}, \quad (9)$$

while for the turbine process without steam extractions, exergy losses are:

$$\dot{E}_{\text{ex,LOSS,WOSE}} = \dot{E}x_1 - \dot{m}_1 \cdot ex_7 - P_{\text{RE,WOSE}}. \quad (10)$$

The energy efficiency of the analyzed steam turbine for the process with steam extractions is:

$$\eta_{\text{en,WSE}} = \frac{P_{\text{RE,WSE}}}{P_{\text{ID,WSE}}}, \quad (11)$$

while for the turbine process without steam extractions, energy efficiency is:

$$\eta_{\text{en,WOSE}} = \frac{P_{\text{RE,WOSE}}}{P_{\text{ID,WOSE}}}. \quad (12)$$

The exergy efficiency of the analyzed steam turbine for the process with steam extractions, according to [55] is:

$$\eta_{\text{ex,WSE}} = \frac{P_{\text{RE,WSE}}}{\dot{E}x_1 - \dot{E}x_2 - \dot{E}x_3 - \dot{E}x_4 - \dot{E}x_5 - \dot{E}x_6 - \dot{E}x_7}, \quad (13)$$

while for the turbine process without steam extractions, exergy efficiency is:

$$\eta_{\text{ex,WOSE}} = \frac{P_{\text{RE,WOSE}}}{\dot{E}x_1 - \dot{m}_1 \cdot ex_7}. \quad (14)$$

Each steam mass flow rate extracted from the turbine does not expand throughout the whole turbine. When compared with the same turbine without steam extractions, each extracted steam mass flow rate causes turbine power losses and reduces turbine maximum power. For each extracted steam mass flow rate turbine power losses (cumulative power losses and power losses for each turbine segment) can be calculated with regard to turbine maximum power. Analyzed turbine is divided into six segments (one turbine segment is defined between each two consecutive operating points from Fig. 1 and Fig. 2).

Cumulative turbine power losses for each extracted steam mass flow rate and for the real (polytropic) steam expansion are calculated, according to Fig. 1 and Fig. 2, as:

-Turbine cumulative power losses for the first extracted steam mass flow rate (\dot{m}_2):

$$P_{\text{LOSS,RE,m2}} = \dot{m}_2 \cdot (h_2 - h_3) + \dot{m}_2 \cdot (h_3 - h_4) + \dot{m}_2 \cdot (h_4 - h_5) + \dot{m}_2 \cdot (h_5 - h_6) + \dot{m}_2 \cdot (h_6 - h_7). \quad (15)$$

-Turbine cumulative power losses for the second extracted steam mass flow rate (\dot{m}_3):

$$P_{\text{LOSS,RE,m3}} = \dot{m}_3 \cdot (h_3 - h_4) + \dot{m}_3 \cdot (h_4 - h_5) + \dot{m}_3 \cdot (h_5 - h_6) + \dot{m}_3 \cdot (h_6 - h_7). \quad (16)$$

-Turbine cumulative power losses for the third extracted steam mass flow rate (\dot{m}_4):

$$P_{\text{LOSS,RE,m4}} = \dot{m}_4 \cdot (h_4 - h_5) + \dot{m}_4 \cdot (h_5 - h_6) + \dot{m}_4 \cdot (h_6 - h_7). \quad (17)$$

-Turbine cumulative power losses for the fourth extracted steam mass flow rate (\dot{m}_5):

$$P_{\text{LOSS,RE,m5}} = \dot{m}_5 \cdot (h_5 - h_6) + \dot{m}_5 \cdot (h_6 - h_7). \quad (18)$$

-Turbine cumulative power losses for the fifth extracted steam mass flow rate (\dot{m}_6):

$$P_{\text{LOSS,RE,m6}} = \dot{m}_6 \cdot (h_6 - h_7). \quad (19)$$

Cumulative turbine power losses for each extracted steam mass flow rate and for the ideal (isentropic) steam expansion are calculated by using the same equations from Eq. (15) to Eq. (19) with a note that steam specific enthalpies must be taken for the same operating points but for ideal (isentropic) expansion process, Fig. 2. Steam mass flow rates extracted in each turbine extraction remain the same for real and ideal steam expansion processes.

4 DATA FOR THE OBSERVED STEAM TURBINE ANALYSIS

Analysis of the observed steam turbine requires knowing the steam temperature, pressure and mass flow rate in each turbine operating point from Fig. 1 and Fig. 2. Such steam operating data were found in [22] and presented in Tab. 1. Mentioned data were obtained by measurements during turbine exploitation, therefore, they represent operating parameters of real (polytropic) steam expansion process. For each turbine operating point steam specific enthalpy, specific entropy and specific exergy were calculated by using NIST REFPROP 9.0 software [56], which are also presented in Tab. 1.

Table 1 Data for each steam turbine operating point (base process) [22]

O.P.*	Temperature (K)	Pressure (MPa)	Steam mass flow rate (kg/s)	Steam specific enthalpy (kJ/kg)	Steam specific entropy (kJ/kg·K)	Steam specific exergy (kJ/kg)
1	793.15	9.1233	76.389	3436.3	6.7168	1438.25
2	618.55	2.4231	4.944	3118.1	6.8419	1082.75
3	547.85	1.3244	4.144	2986.9	6.8835	939.15
4	463.65	0.5690	4.556	2831.4	6.9511	763.49
5	394.35	0.2060	3.878	2707.7	7.1173	590.24
6	360.45	0.0628	1.775	2655.2	7.5169	418.60
7	343.15	0.0272	57.092	2626.9	7.8193	300.14

* O.P. = Operating Point (according to Fig. 1 and Fig. 2)

For the ideal (isentropic) steam expansion process, all the required operating parameters were calculated by knowing the steam pressure in each operating point from Fig. 1 and Fig. 2 (Tab. 1) as well as by knowing always the same steam specific entropy during ideal expansion through the turbine.

5 THE RESULTS OF THE STEAM TURBINE ANALYSIS AND COMPARISON OF ITS PROCESSES

Steam turbine real (polytropic) and ideal (isentropic) power with and without steam extractions are presented in Fig. 3. Steam extractions closing significantly increases real turbine power (for 5215.88 kW) and simultaneously increases ideal (isentropic) turbine power for 10117.61 kW.

Along with the turbine power increase, closing of all steam extractions simultaneously increases analyzed turbine energy and exergy losses - energy losses increase for 4901.73 kW while exergy losses increase for 4748.09 kW, Fig. 3. Therefore, closing of all steam turbine extractions has a higher influence on turbine energy losses, which increase is higher in comparison to exergy losses.

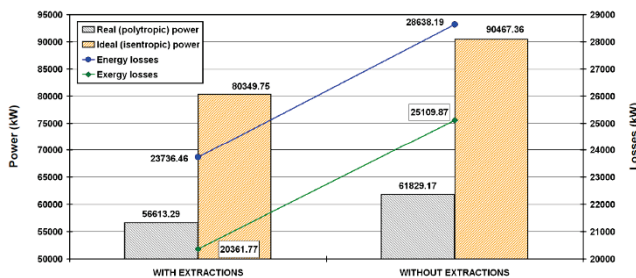


Figure 3 Change in developed power and losses of the analyzed turbine with and without steam extractions

Base turbine operation (when all steam extractions are open) results with turbine energy efficiency of 70.46 % and turbine exergy efficiency of 73.55 %, Fig. 4. Closing of all steam extractions resulted in a decrease in both efficiencies - turbine energy efficiency decreases for 2.11 %, while turbine exergy efficiency decreases for 2.43 %. From the obtained results it can also be concluded that closing of all steam extractions has a higher influence on the turbine exergy efficiency decrease (in comparison to turbine energy efficiency decrease).

Finally, regarding the analyzed turbine it can be concluded that closing of all steam extractions significantly increases turbine power (ideal or real power, Fig. 3), but simultaneously increases turbine energy and exergy losses and decreases turbine energy and exergy efficiencies, Fig. 4.

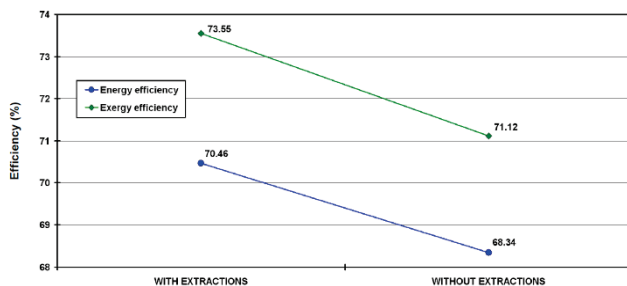


Figure 4 Change in energy and exergy efficiency of the analyzed turbine with and without steam extractions

Each steam mass flow rate extraction from the analyzed turbine (base process) participates in the reduction of maximum real or ideal turbine power. Maximum real or ideal

power, which can be developed with the same steam operating parameters at the turbine inlet and outlet (operating points 1 and 7, Tab. 1) without any steam mass flow rate extraction, is presented in Fig. 3 and equal to 61829.17 kW for real (polytropic) steam expansion and 90467.36 kW for ideal (isentropic) steam expansion.

Each steam mass flow rate extracted from the analyzed turbine will expand throughout the whole turbine (to the pressure at the turbine outlet) if steam extractions were closed. Therefore, each extracted steam mass flow rate causes turbine power losses which are calculated by using equations from Eq. (15) to Eq. (19) and which are presented in Fig. 5. Power losses are the highest for the first extracted steam mass flow rate from the turbine (\dot{m}_2), regardless of the fact whether the steam expansion is ideal or real - Fig. 2, because of the highest pressure differences between which that steam mass flow rate can expand. Following the above, power losses (again, both real and ideal) are the lowest for the last extracted steam mass flow rate (\dot{m}_6), Fig. 5.

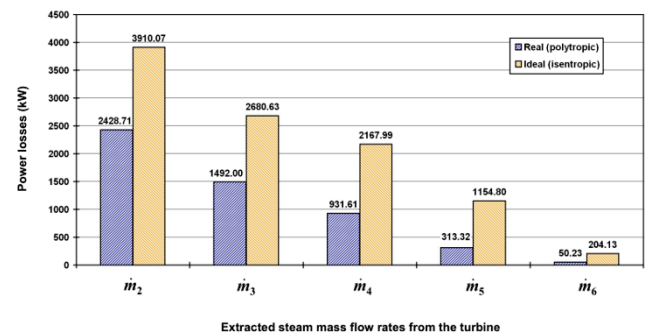


Figure 5 Real (polytropic) and ideal (isentropic) power losses due to steam mass flow rate extractions from the analyzed turbine

Analyzed turbine is divided into the segments and each turbine segment is defined between turbine operating points presented in Fig. 1 and Fig. 2. Therefore, analyzed turbine has six segments. In each turbine segment developed turbine power is calculated with and without steam extractions as well as cumulative power losses from all extracted steam mass flow rates, Fig. 6.

As can be seen from Fig. 6, in the first turbine segment developed turbine power with and without steam extractions is the same (because in the first turbine segment the entire steam mass flow rate which enter in the turbine expands). In all the other analyzed turbine segments developed turbine power without extractions is higher than power with steam extractions. In any case, the first turbine segment develops the highest, while the last turbine segment develops the lowest power.

The difference between turbine power with and without steam extractions in each turbine segment represents cumulative power losses caused by steam extractions. It can be seen from Fig. 6 that cumulative power losses caused by steam extractions are the highest in the fourth turbine segment and equal to 1687.82 kW.

Cumulative power losses caused by steam extractions in each turbine segment are the sum of power losses from each extracted steam mass flow rate. Distribution of power losses

on each extracted steam mass flow rate in any turbine segment is presented in Fig. 7. Power losses in the first turbine segment are not shown in Fig. 7, because the first turbine segment does not contain any steam extraction, so power losses on the first turbine segment are equal to zero, Fig. 6.

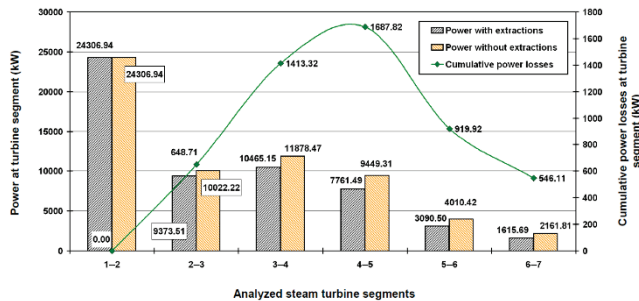


Figure 6 Developed power and cumulative power losses at each segment of the analyzed steam turbine

An extracted steam mass flow rate, which has a dominant influence on power losses in each turbine segment is the first extracted steam mass flow rate (\dot{m}_2). In the second turbine segment (2--3), the first extracted steam mass flow rate (\dot{m}_2) is the only component which defines cumulative power losses, Fig. 7, while in the other turbine segments sum of at least two extracted steam mass flow rates defines cumulative power losses. In the last turbine segment, all of the extracted steam mass flow rates define cumulative power losses.

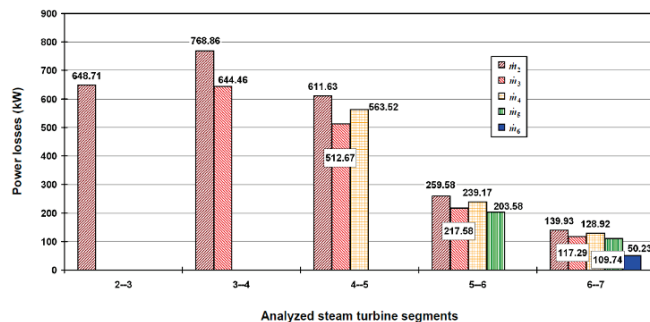


Figure 7 Distribution of power losses at each analyzed turbine segment due to steam mass flow rate extractions

Further research, reduction of power losses and possible optimization of the steam turbine analyzed in this paper will be performed by using various artificial intelligence methods [57-61].

6 CONCLUSIONS

This paper presents an investigation of two possible steam turbine operation regimes – a regime with all steam extractions opened (base process) and a regime with all steam extractions closed. Major conclusions obtained from this analysis are as follows:

- Closing of all steam extractions significantly increases turbine real developed power in comparison to the

regime when all steam extractions are opened (from 56613.29 kW to 61829.17 kW).

- All steam turbine extractions closing, in comparison to the regime when all steam extractions are opened, significantly increases turbine energy and exergy losses (from 23736.46 kW to 28638.19 kW for energy losses and from 20361.77 kW to 25109.87 kW for exergy losses).
- Closing of all steam turbine extractions decreases turbine energy and exergy efficiencies when compared to the base process when all steam extractions are opened (from 70.46 % to 68.34 % for energy efficiency and from 73.55 % to 71.12 % for exergy efficiency).
- First extracted steam mass flow rate has a dominant influence on turbine power losses (in comparison to maximum turbine power without steam extractions).
- Analyzed turbine develops the highest power (24306.94 kW) in its first segment.
- Cumulative power losses caused by steam mass flow rate extractions are the highest in the fourth turbine segment and equal to 1687.82 kW (in comparison to the turbine regime when all of the extractions are closed).

Acknowledgments

This research has been supported by the Croatian Science Foundation under the project IP-2018-01-3739, CEEPUS network CIII-HR-0108, European Regional Development Fund under the grant KK.01.1.1.01.0009 (DATACROSS), project CEKOM under the grant KK.01.2.2.03.0004, CEI project "COVIDAi" (305.6019-20), University of Rijeka scientific grant uniri-tehnic-18-275-1447 and University of Rijeka scientific grant uniri-tehnic-18-18-1146.

NOMENCLATURE

Latin symbols:

ex	specific exergy, kJ/kg
\dot{E}	fluid flow power, kW
h	specific enthalpy, kJ/kg
\dot{m}	mass flow rate, kg/s
p	pressure, MPa
P	power, kW
s	specific entropy, kJ/kg·K
T	temperature, K

Greek symbols:

η	efficiency, %
--------	---------------

Subscripts:

0	ambient state
en	energy
ex	exergy
i	operating point index
ID	IDEal (isentropic)
RE	REAL (polytropic)
WOSE	WithOut Steam Extractions
WSE	With Steam Extractions

7 REFERENCES

- [1] Ahmadi, G. R. & Toghraie, D. (2016). Energy and exergy analysis of Montazeri steam power plant in Iran. *Renewable and Sustainable Energy Reviews*, 56, 454-463. <https://doi.org/10.1016/j.rser.2015.11.074>
- [2] Kumar, V., Pandya, B., & Matawala, V. (2019). Thermodynamic studies and parametric effects on exergetic performance of a steam power plant. *International Journal of Ambient Energy*, 40 (1), 1-11. <https://doi.org/10.1080/01430750.2017.1354326>
- [3] Babaelahi, M., Mofidipour, E., & Rafat, E. (2020). Combined Energy-Exergy-Control (CEEC) analysis and multi-objective optimization of parabolic trough solar collector powered steam power plant. *Energy*, 201, 117641. <https://doi.org/10.1016/j.energy.2020.117641>
- [4] Koroglu, T. & Sogut, O. S. (2018). Conventional and advanced exergy analyses of a marine steam power plant. *Energy*, 163, 392-403. <https://doi.org/10.1016/j.energy.2018.08.119>
- [5] Mrzljak, V., Poljak, I., & Prpić-Oršić, J. (2019). Exergy analysis of the main propulsion steam turbine from marine propulsion plant. *Brodogradnja: Teorija i praksa brodogradnje i pomorske tehnike*, 70(1), 59-77. <https://doi.org/10.21278/brod70105>
- [6] Kostyuk, A. & Frolov, V. (1988). *Steam and gas turbines*. Mir Publishers, Moscow.
- [7] Taylor, D. A. (1998). *Introduction to marine engineering*. Elsevier Butterworth-Heinemann.
- [8] Fernández, I. A., Gómez, M. R., Gómez, J. R., & Insua, Á. B. (2017). Review of propulsion systems on LNG carriers. *Renewable and Sustainable Energy Reviews*, 67, 1395-1411. <https://doi.org/10.1016/j.rser.2016.09.095>
- [9] Lorencin, I., Andelić, N., Mrzljak, V., & Car, Z. (2019). Genetic Algorithm Approach to Design of Multi-Layer Perceptron for Combined Cycle Power Plant Electrical Power Output Estimation. *Energies*, 12(22), 4352. <https://doi.org/10.3390/en12224352>
- [10] Prakash, D., & Singh, O. (2019). Thermo-economic study of combined cycle power plant with carbon capture and methanation. *Journal of Cleaner Production*, 231, 529-542. <https://doi.org/10.1016/j.jclepro.2019.05.217>
- [11] Aliyu, M., AlQudaihi, A. B., Said, S. A. M., & Habib, M. A. (2020). Energy, exergy and parametric analysis of a combined cycle power plant. *Thermal Science and Engineering Progress*, 15, 100450. <https://doi.org/10.1016/j.tsep.2019.100450>
- [12] Burin, E. K., Vogel, T., Multhaupt, S., Thelen, A., Oeljeklaus, G., Gerner, K., & Bazzo, E. (2016). Thermodynamic and economic evaluation of a solar aided sugarcane bagasse cogeneration power plant. *Energy*, 117, 416-428. <https://doi.org/10.1016/j.energy.2016.06.071>
- [13] Ahmadi, G., Toghraie, D., & Akbari, O. (2019). Energy, exergy and environmental (3E) analysis of the existing CHP system in a petrochemical plant. *Renewable and Sustainable Energy Reviews*, 99, 234-242. <https://doi.org/10.1016/j.rser.2018.10.009>
- [14] Taheri, M. H., Mosaffa, A. H., & Farshi, L. G. (2017). Energy, exergy and economic assessments of a novel integrated biomass based multigeneration energy system with hydrogen production and LNG regasification cycle. *Energy*, 125, 162-177. <https://doi.org/10.1016/j.energy.2017.02.124>
- [15] Yilmaz, F., Ozturk, M., & Selbas, R. (2019). Design and thermodynamic analysis of coal-gasification assisted multigeneration system with hydrogen production and liquefaction. *Energy Conversion and Management*, 186, 229-240. <https://doi.org/10.1016/j.enconman.2019.02.053>
- [16] Mrzljak, V., Poljak, I., & Mrakovčić, T. (2017). Energy and exergy analysis of the turbo-generators and steam turbine for the main feed water pump drive on LNG carrier. *Energy conversion and management*, 140, 307-323. <https://doi.org/10.1016/j.enconman.2017.03.007>
- [17] Adibhatla, S. & Kaushik, S. C. (2014). Energy and exergy analysis of a super critical thermal power plant at various load conditions under constant and pure sliding pressure operation. *Applied thermal engineering*, 73(1), 51-65. <https://doi.org/10.1016/j.applthermaleng.2014.07.030>
- [18] Behrendt, C. & Stoyanov, R. (2018). Operational Characteristic of Selected Marine Turbounits Powered by Steam from Auxiliary Oil-Fired Boilers. *New Trends in Production Engineering*, 1(1), 495-501. <https://doi.org/10.2478/npte-2018-0061>
- [19] Ray, T. K., Datta, A., Gupta, A., & Ganguly, R. (2010). Exergy-based performance analysis for proper O&M decisions in a steam power plant. *Energy Conversion and Management*, 51(6), 1333-1344. <https://doi.org/10.1016/j.enconman.2010.01.012>
- [20] Kowalczyk, T., Ziolkowski, P., & Badur, J. (2015). Exergy losses in the Szewalski binary vapor cycle. *Entropy*, 17, 7242-7265. <https://doi.org/10.3390/e17107242>
- [21] Sutton, I. (2015). *Plant design and operations*. Elsevier.
- [22] Aljundi, I. H. (2009). Energy and exergy analysis of a steam power plant in Jordan. *Applied thermal engineering*, 29(2-3), 324-328. <https://doi.org/10.1016/j.applthermaleng.2008.02.029>
- [23] Mitrović, D., Živković, D., & Laković, M. S. (2010). Energy and exergy analysis of a 348.5 MW steam power plant. *Energy Sources, Part A*, 32, 1016-1027. <https://doi.org/10.1080/15567030903097012>
- [24] Mrzljak, V., Poljak, I., & Medica-Viola, V. (2017). Dual fuel consumption and efficiency of marine steam generators for the propulsion of LNG carrier. *Applied Thermal Engineering*, 119, 331-346. <https://doi.org/10.1016/j.applthermaleng.2017.03.078>
- [25] Hajebzadeh, H., Ansari, A. N. M., & Niazi, S. (2019). Mathematical modeling and validation of a 320 MW tangentially fired boiler: A case study. *Applied Thermal Engineering*, 146, 232-242. <https://doi.org/10.1016/j.applthermaleng.2018.09.102>
- [26] Mrzljak, V., Prpić-Oršić, J., & Senčić, T. (2018). Change in steam generators main and auxiliary energy flow streams during the load increase of LNG carrier steam propulsion system. *Pomorstvo*, 32(1), 121-131. <https://doi.org/10.31217/p.32.1.15>
- [27] Moran M., Shapiro H., Boettner, D. D., & Bailey, M. B. (2011). *Fundamentals of engineering thermodynamics*. 7th edition, John Wiley and Sons, Inc.
- [28] Hoseinzadeh, S. & Heyns, P. S. (2020). Thermo-structural fatigue and lifetime analysis of a heat exchanger as a feedwater heater in power plant. *Engineering Failure Analysis*, 113, 104548. <https://doi.org/10.1016/j.engfailanal.2020.104548>
- [29] Kakac, S., Liu, H., & Pramuanjaroenkij, A. (2012). *Heat exchangers - selection, rating, and thermal design*. 3rd edition, CRC Press, Taylor & Francis Group.
- [30] Mrzljak, V., Poljak, I., & Medica-Viola, V. (2017). Thermodynamical analysis of high-pressure feed water heater in steam propulsion system during exploitation. *Brodogradnja: Teorija i praksa brodogradnje i pomorske tehnike*, 68(2), 45-61. <https://doi.org/10.21278/brod68204>
- [31] Naserabad, S. N., Mehrpanahi, A., & Ahmadi, G. (2019). Multi-objective optimization of feed-water heater arrangement options in a steam power plant repowering. *Journal of Cleaner Production*, 220, 253-270. <https://doi.org/10.1016/j.jclepro.2019.02.125>

- [32] Laskowski, R. (2016). Relations for steam power plant condenser performance in off-design conditions in the function of inlet parameters and those relevant in reference conditions. *Applied Thermal Engineering*, 103, 528-536. <https://doi.org/10.1016/j.applthermaleng.2016.04.127>
- [33] Pattanayak, L., Padhi, B. N., & Kodamasingh, B. (2019). Thermal performance assessment of steam surface condenser. *Case Studies in Thermal Engineering*, 14, 100484. <https://doi.org/10.1016/j.csite.2019.100484>
- [34] Medica-Viola, V., Pavković, B., & Mrzljak, V. (2018). Numerical model for on-condition monitoring of condenser in coal-fired power plants. *International Journal of Heat and Mass Transfer*, 117, 912-923. <https://doi.org/10.1016/j.ijheatmasstransfer.2017.10.047>
- [35] Škopac, L., Medica-Viola, V., & Mrzljak, V. (2020). Selection Maps of Explicit Colebrook Approximations according to Calculation Time and Precision. *Heat Transfer Engineering*, 1-15. <https://doi.org/10.1080/01457632.2020.1744248>
- [36] Zhang, X., Li, Y., & Chen, H. (2019). Performance assessment of air-cooled steam condenser with guide vane cascade. *Journal of Thermal Science*, 28 (5), 993-1003. <https://doi.org/10.1007/s11630-019-1116-6>
- [37] Davies III, W. A., & Hrnjak, P. (2019). Thermo-hydraulic model for steam condensation in a large, inclined, flattened-tube air-cooled condenser. *Applied Thermal Engineering*, 149, 745-756. <https://doi.org/10.1016/j.applthermaleng.2018.12.050>
- [38] Noroozian, A., Mohammadi, A., Bidi, M., & Ahmadi, M. H. (2017). Energy, exergy and economic analyses of a novel system to recover waste heat and water in steam power plants. *Energy conversion and management*, 144, 351-360. <https://doi.org/10.1016/j.enconman.2017.04.067>
- [39] Kumar, S., Kumar, D., Memon, R. A., Wassan, M. A., & Ali, M. S. (2018). Energy and exergy analysis of a coal fired power plant. *Mehran University Research Journal of Engineering & Technology*, 37 (4), 611-624. <https://doi.org/10.22581/muet1982.1804.13>
- [40] Adibhatla, S., & Kaushik, S. C. (2017). Energy, exergy, economic and environmental (4E) analyses of a conceptual solar aided coal fired 500 MWe thermal power plant with thermal energy storage option. *Sustainable Energy Technologies and Assessments*, 21, 89-99. <https://doi.org/10.1016/j.seta.2017.05.002>
- [41] Kocijel, L., Poljak, I., Mrzljak, V., & Car, Z. (2020). Energy Loss Analysis at the Gland Seals of a Marine Turbo-Generator Steam Turbine. *Tehnički glasnik*, 14(1), 19-26. <https://doi.org/10.31803/tg-20191031094436>
- [42] Zhao, Z., Su, S., Si, N., Hu, S., Wang, Y., Xu, J., ... & Xiang, J. (2017). Exergy analysis of the turbine system in a 1000 MW double reheat ultra-supercritical power plant. *Energy*, 119, 540-548. <https://doi.org/10.1016/j.energy.2016.12.072>
- [43] Ibrahim, T. K., Basrawi, F., Awad, O. I., Abdullah, A. N., Najafi, G., Mamat, R., & Hagos, F. Y. (2017). Thermal performance of gas turbine power plant based on exergy analysis. *Applied Thermal Engineering*, 115, 977-985. <https://doi.org/10.1016/j.applthermaleng.2017.01.032>
- [44] Zhou, J., Ling, P., Su, S., Xu, J., Xu, K., Wang, Y., Hu, S., Zhu, M., & Xiang, J. (2019). Exergy analysis of a 1000 MW single reheat advanced supercritical carbon dioxide coal-fired partial flow power plant. *Fuel*, 255, 115777. <https://doi.org/10.1016/j.fuel.2019.115777>
- [45] Tontu, M., Sahin, B., & Bilgili, M. (2019). Using energy and exergy analysis to compare different coal-fired power plants. *Energy Sources, Part A: Recovery, Utilization, and Environmental Effects*, 1-16. <https://doi.org/10.1080/15567036.2019.1696429>
- [46] Mrzljak, V., & Poljak, I. (2019). Energy Analysis of Main Propulsion Steam Turbine from Conventional LNG Carrier at Three Different Loads. *NAŠE MORE: znanstveno-stručni časopis za more i pomorstvo*, 66(1), 10-18. <https://doi.org/10.17818/NM/2019/1.2>
- [47] Blažević, S., Mrzljak, V., Anđelić, N., & Car, Z. (2019). Comparison of energy flow stream and isentropic method for steam turbine energy analysis. *Acta Polytechnica*, 59(2), 109-125. <https://doi.org/10.14311/AP.2019.59.0109>
- [48] Uysal, C., Kurt, H., & Kwak, H. Y. (2017). Exergetic and thermoeconomic analyses of a coal-fired power plant. *International Journal of Thermal Sciences*, 117, 106-120. <https://doi.org/10.1016/j.ijthermalsci.2017.03.010>
- [49] Kanoğlu, M., Çengel, Y.A., & Dincer, I. (2012). *Efficiency evaluation of energy systems*. Springer Briefs in Energy, Springer.
- [50] Lorencin, I., Anđelić, N., Mrzljak, V., & Car, Z. (2019). Exergy analysis of marine steam turbine labyrinth (gland) seals. *Pomorstvo*, 33(1), 76-83. <https://doi.org/10.31217/p.33.1.8>
- [51] Bühler, F., Van Nguyen, T., Kjær Jensen, J., Müller Holm, F., & Elmegaard, B. (2018). Energy, exergy and advanced exergy analysis of a milk processing factory. *Energy*, 162, 576-592. <https://doi.org/10.1016/j.energy.2018.08.029>
- [52] Tan, H., Shan, S., Nie, Y., & Zhao, Q. (2018). A new boil-off gas re-liquefaction system for LNG carriers based on dual mixed refrigerant cycle. *Cryogenics*, 92, 84-92. <https://doi.org/10.1016/j.cryogenics.2018.04.009>
- [53] Mrzljak, V., Blecich, P., Anđelić, N., & Lorencin, I. (2019). Energy and Exergy Analyses of Forced Draft Fan for Marine Steam Propulsion System during Load Change. *Journal of Marine Science and Engineering*, 7(11), 381. <https://doi.org/10.3390/jmse7110381>
- [54] Medica-Viola, V., Mrzljak, V., Anđelić, N., & Jelić, M. (2020). Analysis of Low-Power Steam Turbine with One Extraction for Marine Applications. *NAŠE MORE: znanstveni časopis za more i pomorstvo*, 67(2), 87-95. <https://doi.org/10.17818/NM/2020/2.1>
- [55] Erdem, H. H., Akkaya, A. V., Cetin, B., Dagdas, A., Sevilgen, S. H., Sahin, B., ... & Atas, S. (2009). Comparative energetic and exergetic performance analyses for coal-fired thermal power plants in Turkey. *International Journal of Thermal Sciences*, 48(11), 2179-2186. <https://doi.org/10.1016/j.ijthermalsci.2009.03.007>
- [56] Lemmon, E. W., Huber, M. L., & McLinden, M. O. (2010). NIST Standard Reference Database 23, Reference Fluid Thermodynamic and Transport Properties (REFPROP), version 9.0, National Institute of Standards and Technology. R1234yf. fld file dated December, 22, 2010.
- [57] Lorencin, I., Anđelić, N., Mrzljak, V., & Car, Z. (2019). Multilayer Perceptron approach to Condition-Based Maintenance of Marine CODLAG Propulsion System Components. *Pomorstvo*, 33(2), 181-190. <https://doi.org/10.31217/p.33.2.8>
- [58] Baressi Šegota, S., Lorencin, I., Ohkura, K., & Car, Z. (2019). On the Traveling Salesman Problem in Nautical Environments: An Evolutionary Computing Approach to Optimization of Tourist Route Paths in Medulin, Croatia. *Pomorski zbornik*, 57(1), 71-87. <https://doi.org/10.18048/2019.57.05>
- [59] Naserbegi, A., Aghaie, M., Minuchehr, A., & Alahyarizadeh, Gh. (2018). A novel exergy optimization of Bushehr nuclear power plant by gravitational search algorithm (GSA). *Energy*, 148, 373-385. <https://doi.org/10.1016/j.energy.2018.01.119>
- [60] Baressi Šegota, S., Lorencin, I., Musulin, J., Štifanić, D., & Car, Z. (2020). Frigate Speed Estimation Using CODLAG Propulsion System Parameters and Multilayer Perceptron.

NAŠE MORE: znanstveni časopis za more i pomorstvo, 67(2), 117-125. <https://doi.org/10.17818/NM/2020/2.4>

- [61] Lorencin, I., Anđelić, N., Mrzljak, V., & Car, Z. (2019). Marine Objects Recognition Using Convolutional Neural Networks. *NAŠE MORE: znanstveno-stručni časopis za more i pomorstvo*, 66(3), 112-119. <https://doi.org/10.17818/NM/2019/3.3>

Authors' contacts:

Vedran Mrzljak, PhD, Assistant Professor
(Corresponding author)
Faculty of Engineering, University of Rijeka,
Vukovarska 58, 51000 Rijeka, Croatia
E-mail: vedran.mrzljak@riteh.hr

Sandi Baressi Šegota, mag. ing. comp.
Faculty of Engineering, University of Rijeka,
Vukovarska 58, 51000 Rijeka, Croatia
E-mail: sbaressisegota@riteh.hr

Hrvoje Meštrić, PhD
Catholic University of Croatia, University of Zagreb,
Ilica 242, 10000 Zagreb, Croatia
E-mail: hrvoje.mestric@unicath.hr

Zlatan Car, PhD, Full Professor
Faculty of Engineering, University of Rijeka,
Vukovarska 58, 51000 Rijeka, Croatia
E-mail: zlatan.car@riteh.hr

Blockchain-Based Application for Certification Management

Jovan Karamachoski*, Ninoslav Marina, Pavel Taskov

Abstract: Blockchain technology will bring a disruption in plenty of industries and businesses. Recently it proved the robustness, immutability, auditability, in many crucial practical applications. The blockchain structure offers traceability of actions, alterations, alerts, which is an important property of a system needed for development of sustainable technologies. A crucial part of the blockchain technology regarding the optimization of the processes is the smart contract. It is a self-executable computer code, open and transparent, encoding the terms of a regular contract. It is able to automate the processes, thus decreasing the human-factor mistakes or counterfeits. In this paper, we are presenting the feasibility of the blockchain technology in the certification processes, with an application developed for university diploma certification. The example is easily transferable in other areas and business models such as logistics, supply chain management, or other segments where certification is essential.

Keywords: certification; cryptographic hash; distributed ledger technology; Ethereum Blockchain; smart contract; smart record

1 INTRODUCTION

The certification procedures are part of our everyday life. A certificate is a verification of existence or possession of declared characteristics or acquired competences. In most of the cases the certificate is issued by an institution and handed in paper form to the holder. These bureaucratic procedures are time consuming, expensive and leave plenty of opportunities to issue fake documents. The advancement of technology offers a plethora of tools to the scammers to falsify the paper certificates, hence having a technology that offers protection against these malicious activities is quite beneficial.

Blockchain technology shows great potential to avert the corruption of certifications. The characteristics of the blockchain technology, like, auditability, immutability, non-repudiation, transparency, verifiability and irrevocability, make it a perfect candidate for enhancement of the traditional certification procedures. These characteristics make the blockchain technology suitable for any type of applications where certification is needed. This includes the certification of origin, possession, quality level, class, properties, measured parameters, some features, location while tracing the movement, or similar.

This paper introduces one of the pioneering works in the field of blockchain usage as certificate storage. The proposed application shows potential to overcome the long bureaucratic procedures and prevent fraudulent activities during the certification procedures. It uses the blockchain technology, also known as Distributed Ledger Technology (DLT), which is transforming the activities in a trustless environment and still keeps a single truth in the whole system.

The implementation of blockchain technology for building on-line certificate database will increase the commodity of living and ease up the administrative procedures to issue and verify the certificates.

The problem with the fake education diplomas is present in many countries. Especially it is tricky to overcome during the process of mutual recognition of foreign diplomas. In [1], Sayed points out the crucial characteristics of the blockchain

technology to overcome the fake diploma problem and mentions few projects related to the application of blockchain technology. Furthermore, the author analyzes the fraudulent activities regarding the fake diplomas and proposes structure for a concrete blockchain-based application to overcome the problems. Besides the potential to overcome the fraudulent activities over the certification and validation process, the implementation of blockchain-based application for certification will also have a financial impact. The financial impact and potential business model are analyzed in [2].

Tariq et al. in [3] are developing a blockchain-based accreditation and degree verification system by the use of Ethereum Blockchain [4]. The uniqueness of the proposal is the implementation of the private version of the Ethereum Blockchain in order to keep the system under Proof-of-Authority consensus mechanism. Similar approach of implementation private type of blockchain, is described in [5]. They are using the Hyperledger Sawtooth [6] enterprise blockchain in order to manage the credentials and privileges in a system. In contrast to these approaches, the application presented here is implemented on a public blockchain. It offers a complete decentralization of the database, while keeping the robustness of the application and managing the credentials of the users.

In addition to the use case of blockchain-based diploma certificate management, there are use-cases where the blockchain technology is used as certificate management mechanism for a birth certification [7], certificate revocation lists [8], green certification in energy sector [9], product compliance and assurance in the construction industry [10], endorsement and forestry certification [11].

2 BLOCKCHAIN-BASED CERTIFICATE STORAGE

The blockchain technology is decentralized data storage structure, capable to operate in trustless community, to track record modifications and to reduce the need of third-parties. Moreover, the blockchain database structure, also known as the distributed ledger, offers liveness, immutability, redundancy and non-repudiation of the records. The database

structure model of the blockchain technology is presented in Fig. 1.

The records in the blockchain database are organized in blocks, where the blocks are generated in predefined time intervals. All the information generated in one blockchain network is stored in every participating node, thus creating a complete copy of the common database of the system, in every participating node. This property makes the database structure redundant, reliable and very robust.

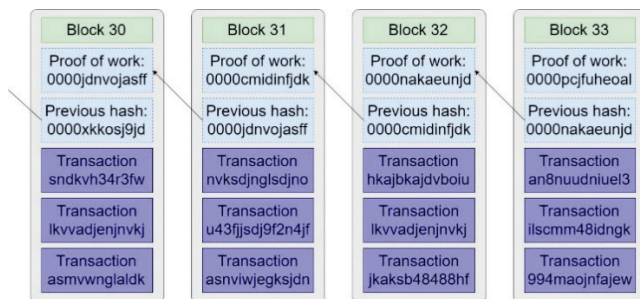


Figure 1 The structure of the blockchain

As presented in Fig. 1, the blocks are connected in a single-chain formation. The connection between two consecutive blocks is through the common data field known as block hash. The block hash is calculated by use of a cryptographic hash function, which is one-way function that creates fingerprint of the block of records, that is unique and irreversible. The block hash is calculated for the current data block and it is set in the header data of the next data block. The implementation of hashing function in the process of block creation and linking the data blocks in this way, makes the record in the database tamper-proof. Practically even the smallest change in a data record will significantly change the block hash, which will represent an attempt for modification of the database. Regarding the type of hash functions, the Bitcoin [12] network uses SHA-256 and RIPEMD-160 algorithms [13], while Ethereum uses the KECCAK-256 algorithm, which is not following exactly the FIPS 202 standard, also known as SHA-3 algorithm [14].

Besides the hash function, the blockchain technology deploys encryption functions to provide security to the user wallet and digital signature for the transactions. The main encryption algorithm is the Elliptic-curve encryption algorithm, using the elliptic curve (EC) $y^2 = x^3 + ax + b$ over a finite Galois field (GF) defined with a prime number p . Encryption algorithms over the elliptic curve work in a way that an algebra over the elliptic curve plus a neutral point at infinity is defined. Using this algebra means that any sum of two different or two same points will give again a point on the same elliptic curve. Adding the point to itself, which is multiplying by two, will again give another point on the curve. Hence we can add the same point to itself multiple times, which defines the operation of multiplication as in the classical arithmetic. Elliptic curve cryptography (ECC) algorithms start from a *base point* G and this point is multiplied by a number that represents the private key k . Using the addition rules of the ECC algebra, one can get a point that is equal to the point $K = kG = G + G + \dots + G$. This

will represent the public key K that corresponds to the private key k , using the given curve. Bitcoin and Ethereum use the Elliptic-curve Digital Signature Algorithm (ECDSA), with the elliptic curve secp256k1 [15]. This curve has the following parameters:

- $p = 2^{256} - 2^{32} - 2^9 - 2^8 - 2^7 - 2^6 - 2^4 - 1$
- $a = 0, b = 7$, making the curve $y^2 = x^3 + 7 \mod p$
- The coordinate x of the base point G is $G_x = 0279BE667E F9DCBBAC 55A06295 CE870B07 029BFCDB 2DCE28D9 59F2815B 16F81798$
- The order of the base point G is $n = \text{FFFFFFFF FFFFFFFF FFFFFFFE BAAEDCE6 AF48A03B BFD25E8C D0364141}$
- The cofactor is $h = 01$.

For protecting the data confidentiality in the digital wallet and transaction maintenance, Ethereum additionally uses the Advanced Encryption Standard (AES) [16]. The digital wallet is a file which stores user credentials, basically the private and public keys. The private key is used in the procedures to digitally sign user transactions and decrypt messages, while the public key is practically the wallet address of the user and it is used to encrypt messages sent to another user.

Another important mechanism is the consensus algorithm which helps the network to coordinate the state of the common database. Due to trust-less approach of building the network and possible malicious users in the network, the consensus mechanism offers procedures for decentralized synchronization of the databases owned by the network users. Three most common consensus algorithms are:

- Proof-of-Work (PoW) [12],
- Proof-of-Stake (PoS) [17], and
- Practical Byzantine Fault Tolerance (PBFT) [18].

Every algorithm has its own advantages and disadvantages. PoW has the most reliable properties for an anonymous usage of the network but it is the most energy inefficient algorithm due to heavy computational processes. PoS has less reliable properties but it is more energy efficient than PoW because it implements moderate computational processes. PBFT is energy efficient but it is not feasible for pure public blockchain technologies because it is designed to work in closed networks.

With the deployment of the Ethereum Blockchain technology, the feature called *smart contract* was introduced. Smart contract is a self-executable and transparent code, stored in the immutable ledger of the Ethereum Blockchain. The last property makes the smart contract code impossible to be modified. This code, or more precisely functions from this code, can be invoked by those who have credentials. Often, smart contracts have properties to follow the terms of the regular (legal) paper contracts. In that way it can often replicate and enforce the legal procedures into an automatic machine code. The implementation of smart contracts will provide unambiguous and automated procedures, transparent, reusable and publicly accessible by everyone. By the development of smart contract, that follow the regular

procedures, it is possible to store, check or revoke any information. A function in the smart contract will record the information on the blockchain, thus creating immutable evidence. Additionally, the smart contract can manage the credentials of the application users.

3 APPLICATION STRUCTURE AND FUNCTIONALITIES

3.1 Tools and Platforms

To develop our application, we use the Embark framework (v3.2) [19], which supports the whole eco-system for building a Distributed Ethereum Blockchain application. The Embark framework offers complete environment configuration for the Storage part, blockchain part, Front-end part and Back-end part of the application. Smart contracts are coded into a text editor by the use of the Ethereum custom made object-oriented programming language called Solidity (v0.4.11) [20]. The unique address of the smart contract developed for the application is publically visible in a bytecode on the Internet. The format of an Ethereum address looks like the following 40 hexadecimal character (20 bytes) sequence:

0x79Df2bf2891Be327FC859189c9d1D44eC33Df3d0.

It is obtained by hashing the public key (that corresponds to the user's private key) using Keccak-256 hash function, taking the last 40 hexadecimal characters and adding a '0x' as a prefix. In this particular case we get

0x79df2bf2891be327fc859189c9d1d44eC33df3d0.

This address has to pass the checksum process which is quite simple. First you calculate the Keccak-256 hash of the obtained hexadecimal address without the prefix 0x. If the character number i of the Keccak-256 hash is greater than or equal to 8, you convert the i -th character of the address to uppercase, otherwise you leave it lowercase. Finally, you add 0x back at the start of the resulting string. The checksum address is the same as the initial one if you ignore the case of the letters a, b, c, d, e, and f.

The application uses the Infura development suite that provides instant and scalable Application Programming Interface (API) access to the Ethereum network and the Internet Planetary File System (IPFS) [21]. By the use of Infura service, the application attaches to the Ethereum network without the use of a fully functional Ethereum node. That is a gateway service for easier deployment of distributed applications (DApps). The current version of the application is deployed on the Ropsten Ethereum test network. Moreover, Infura offers a nice gateway to the IPFS [22] storage, to access the application data. IPFS is protocol for peer-to-peer storage and sharing of files in a distributed fashion. The application content is recorded and hosted on the IPFS network, except for the IPFS record addresses, which are kept on the Ethereum Blockchain. The content on the IPFS storage cannot be erased or modified with the current version of IPFS protocol. This property

complemented with the immutability of the Ethereum Blockchain records creates a tamper-proof system. The application address on the IPFS network is as follows:

<https://ipfs.infura.io/ipfs/QmTryMjQRq8hVtVDyJTS2ixSa3AGynsKbHCGVNr6VxUqS7/>

To access and utilize the Ethereum network every user needs a wallet. The most intuitive way to use the application is in a standard web browser, such a Google Chrome or Mozilla Firefox, with an installed and enabled Metamask extension [23]. Metamask is an application for wallet management where the users have the balance information, address credentials and functionalities for interaction with application located in the Ethereum Blockchain.

3.2 Application Design

The application consists of two functional parts: one part is the certificate identification (CID) number storage procedure on the Ethereum Blockchain via Smart contract and the other segment is the front-end and the back-end of the application stored on the IPFS network. The CID number is paired to the address of the certificate record on the IPFS network.

Our application is purposely developed for university diploma certification process but can very easily be adapted to any other certification process, such as certification of origin of goods, item ownership, or feature possession, among others. The application implements four roles with different read/write credentials:

1. Visitor,
2. Administrator,
3. Staff, and
4. Rector.

The Visitor role is the default role of the application, which is given to every guest on the web site. The other roles: Administrator, Staff and Rector, have several elevated privileges. The Administrator role will have elevated privileges to manage the addresses on the page (associating the correct addresses to the Administrator, Staff or Rector role). The Staff role will have elevated privileges for insertion of newly graduated students and their credentials. The Rector role will have elevated privileges to validate and digitally sign the certificates of already inserted students. The distinct roles will be authenticated through the user wallet.

The current version of the application has five segments:

1. Student search,
2. Insert student,
3. Diploma validity,
4. Address management, and
5. Role panel.

The application organization regarding the credentials and roles is shown in Fig. 2. The Student search segment is used for searching of students by the use of the student CID number and also has verification function if the student was

previously inserted in the system, but still does not have verified the diploma by the Rector. The Insert student segment is used for insertion of students who have graduated. The Diploma verification segment is used to check the validity of the diploma for a given student. The Address management segment is used by the Administrator of the page to manage the addresses for the particular roles in the system. The Roles panel displays the addresses of the particular roles in the system. This panel gives total transparency of the certification process within the institution.

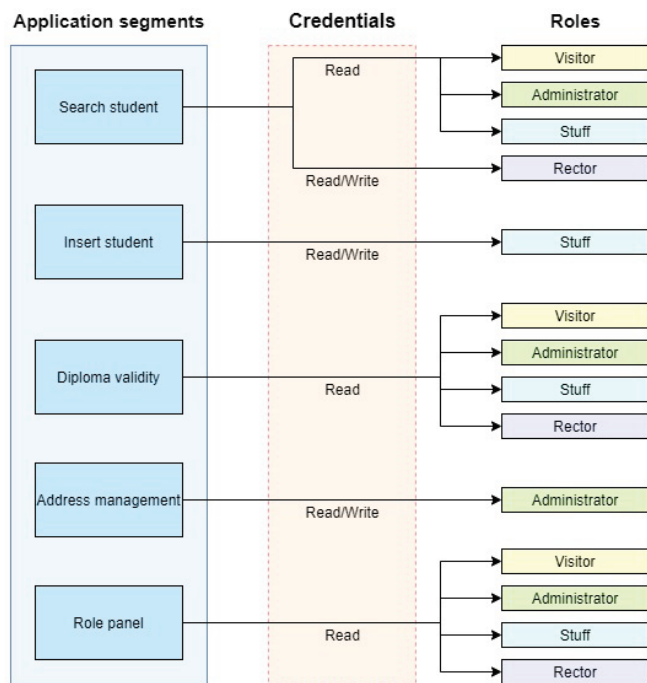


Figure 2 Credentials and roles

The smart contract of the application, beside the standard types of variables, uses variables of type *map* to store the dynamic information of the application. The map variable is a key-value type of variable where one variable can be reflected into another variable. The application implements two maps:

- one is to keep the inserted graduated students, and
- the other is to keep the verified diplomas.

```

if (search_student (CID_number) == Null)
  if (user_credentials == stuff)
    IPFS_address = insert_student (student_information)
    Graduation_record = graduated_student_map(IPFS_Address=> CID_number)
    store_data(Graduation_record)
  end
else
  show_student_information(CID_number)
  if (user_credentials == rector)
    verify_diploma(CID_number)
    Verification_record = verified_diploma_map(IPFS_Address => CID_number)
    store_data(Verification_record)
  end
end
end

```

Figure 3 Pseudo-code for diploma insertion and verification

The first action is taken over the map for inserting graduated students where the CID of the students is mapped

with the IPFS record address, and the second map is populated by reflecting the same IPFS address record from the graduated students map in the verified map. To illustrate the procedure for diploma verification, see the pseudo-code in Fig. 3.

The front-end of the application is presented in Fig. 4. The figure displays the information for a test student, previously inserted in the system. In addition, the graduation of the student is previously verified by the Rector, which is visible in the same figure.

The screenshot shows the front-end of the application. At the top is the header 'University of Information Science and Technology "St. Paul the Apostle" - Ohrid'. Below it is a navigation bar with 'Home', 'Main page', 'About', and 'Contact'. The main content area is divided into three columns. The left column has a 'Search for graduated student' section with a search bar containing '1' and a 'Search' button. Below it is the 'Information about the student' section, which displays details for a student with diploma serial number 1, including first name 'Roseanne', last name 'Knight', date of birth '26 AUGUST 1998', place of birth 'United States of America', study program 'ONE-YEAR STUDIES IN ECTS Credits', average grade '9.80', awarded title 'MASTER IN INFORMATICS', and graduation year '2019'. The right column has a 'Check the validity of the student's diploma' section with a search bar containing '1' and a 'Check' button, showing a message 'The diploma with the serial number 1 is valid'. Below this are sections for 'Set System administrator', 'Set Rector', 'Set Student affairs administrator', and 'Wallet addresses'. The bottom of the page has a footer 'UIST Blockchain Dev team'.

Figure 4 Front-end of the application

Besides the back-end segment for CID storage on the Ethereum Blockchain, the application implements back-end segment for storing the student information on the IPFS network. The current version stores the student information in plain text JSON format. The improvement of the application will implement encryption mechanism to protect the student information and enhance the privacy of the data.

4 FUTURE WORK

The current prototype of the application implements the basic functionalities, sufficient to test the feasibility of the solution and the potential of the application for mass use. Due to circulation of private data in the application, and exposure of these data in the public Internet, the application will be upgraded with encryption module to ensure privacy of the data stored in the application (either on the blockchain or on the IPFS). Also, the application will implement QR codes to make it more interactive and user friendly.

The final version of the application with extended privacy and security will be published on the Main Ethereum network and linked to the official University web site, where the graduated students will get the digital certificate.

5 CONCLUSION

It is crucial to enhance and simplify the administrative procedures. The current certification procedures are prone to falsification, and are very time consuming and expensive. The use of the blockchain technology will have immense impact on the certification processes by decreasing the bureaucratic procedures, shorten the time for certificate verification and skip the third-parties in the processes. This application is proof for the feasibility of the blockchain technology and the certification procedures, by offering transparent, reliable and robust mechanism to prevent the malicious activities.

Notice

The paper was presented at MOTSP 2020 – International Conference Management of Technology – Step to Sustainable Production, which took place from 30th September – 2nd October 2020 in Bol, island Brač (Croatia). The paper is not and will not be published anywhere else.

6 REFERENCES

- [1] Sayed, R. H. (2019). *Potential of blockchain technology to solve fake diploma problem*. University of Jyväskylä, JYX Digital Repository.
- [2] Oliver, M., Moreno, J., Prieto, G., & Benitez, D. (2018). Using blockchain as a tool for tracking and verification of official degrees: business model.
- [3] Tariq, A., Haq, H. B., & Ali, S. T. (2019). Cerberus: A blockchain-Based Accreditation and Degree Verification System. arXiv preprint arXiv:1912.06812.
- [4] Buterin, V. et al. (2014). Ethereum white paper: A next-generation smart contract and decentralized application platform. http://blockchainlab.com/pdf/Ethereum_white_paper-a_next_generation_smart_contract_and_decentralized_application_platform-vitalik-buterin.pdf, 2014.
- [5] Wegelid, F. (2019). *Storing digital certificates using blockchain*. Lund University.
- [6] Olson, K., Bowman, M., Mitchell, J., Amundson, S., Middleton, D., & Montgomery, C. (2018). *Sawtooth: An Introduction*. The Linux Foundation.
- [7] Shah, M. & Kumar, P. (2019). Tamper proof birth certificate using blockchain technology. *Int. J. Recent Technol. Eng. (IJRTE)*, 7.
- [8] Baldi, M., Chiaraluce, F., Frontoni, E., Gottardi, G., Sciarroni, D., & Spalazzi, L. (2017). Certificate Validation through Public Ledgers and blockchains. *ITASEC*, 156-165.
- [9] Andoni, M., Robu, V., Flynn, D., Abram, S., Geach, D., Jenkins, D., McCallum, P., & Peacock, A. (2019). Blockchain technology in the energy sector: A systematic review of challenges and opportunities. *Renewable and Sustainable Energy Reviews*, 100, 143-174. <https://doi.org/10.1016/j.rser.2018.10.014>
- [10] Allison, N. & Warren, M. (2019). Applying blockchain to product compliance and assurance in the construction industry. *Building Research Levy, External Research Report*.
- [11] Sylvester, G. (2019). *E-agriculture in action: blockchain for Agriculture Opportunities and Challenges*. The Food and Agriculture Organization of United Nations.
- [12] Nakamoto, S. (2008). Bitcoin: A peer-to-peer electronic cash system. Available: <https://bitcoin.org/bitcoin.pdf>
- [13] Nist, U. (2001). *Descriptions of SHA-256, SHA-384 and SHA-512*. Available: <http://www.iwar.org.uk/comsec/resources/cipher/sha256-384-512.pdf>
- [14] Bertoni, G., Daemen, J., Peeters, M., & Van Assche, G. (2011). The keccak sha-3 submission. Submission to NIST (Round 3), 6(7), p. 16.
- [15] Certicom, S. E. C. (2000). Sec 2: Recommended elliptic curve domain parameters. *Proceeding of Standards for Efficient Cryptography, Version*, vol. 1.
- [16] Standard, N.-F. (2001). Announcing the advanced encryption standard (aes). *Federal Information Processing Standards Publication*, 197(1-51), 3-3.
- [17] Thin, W. Y. M. M., Dong, N., Bai, G., & Dong, J. S. (2018). Formal analysis of a proof-of-stake blockchain. in the 23rd International Conference on Engineering of Complex Computer Systems (ICECCS), 197-200.
- [18] Buchman, E. (2016). Tendermint: Byzantine fault tolerance in the age of blockchains. Available: <https://allquantor.at/blockchainbib/pdf/buchman2016tendermint.pdf>
- [19] *Embark Framework by Status home page*. Available: <https://framework.embarklabs.io/>. (Accessed: 02-2020)
- [20] *Solidity home page*. Available: <https://solidity.readthedocs.io/en/v0.4.11/>. (Accessed: 02-2020)
- [21] *Infura home page*. Available: <https://infura.io/>. (Accessed: 02-2020)
- [22] Benet, J. (2014). *IPFS - Content Addressed, Versioned, P2P File System (DRAFT 3)*. <https://ipfs.io/ipfs/QmR7GSQM93Cx5eAg6a6yRzNde1FQv7uL6X1o4k7zrJa3LX/ipfs.draft3.pdf>.
- [23] *Metamask home page*. Available: <https://metamask.io/>. (Accessed: 02-2020)

Authors' contacts:

Jovan Karamachoski, MSc

(Corresponding author)

University of Information Science and Technology "St. Paul the Apostle",
Partizanska bb, 6000 Ohrid, North Macedonia
jovan.karamachoski@uist.edu.mk

Ninoslav Marina, PhD

University of Information Science and Technology "St. Paul the Apostle",
Partizanska bb, 6000 Ohrid, North Macedonia
ninoslav.marina@uist.edu.mk

Pavel Taskov

University of Information Science and Technology "St. Paul the Apostle",
Partizanska bb, 6000 Ohrid, North Macedonia
pavel.taskov@uist.edu.mk

Calculation of the Plastic Metal Flow in the Cold Extrusion Technology by Finite Volume Method

Hazim Bašić*, Ismet Demirdžić, Samir Muzaferija

Abstract: This paper presents an application of the finite volume method to ideal plastic metal flow in extrusion technology. Governing equations for the mass and momentum balance are used in an integral form. Solution domains in the cases considered are discretized with a Cartesian numerical mesh with computational points placed at the center of each control volume. After discretization of the governing equations, the resulting system of nonlinear algebraic equations is solved by an iterative procedure, using a segregated algorithm approach. Resulting stress fields are obtained from the Levy-Mises equations. The experimental results and numerical calculations are in good agreement.

Keywords: cold extrusion; finite volume method; ideal plasticity

1 INTRODUCTION

Extrusion processes in the metal forming by plastic deformation belong to the widespread production technology. One of the important parameters of this process is the working pressure, i.e. deformation force that determines the shape and dimensions of the extrusion tool and characteristics of the machine on which the technology will be performed. Also, a more complete knowledge of metal flow in these processes allows better design of tooling, especially in the extrusion of rods through the dies with complex cross sections.

In order to obtain a high-production rate with acceptable quality, many process parameters must be controlled. The plastic flow is conditioned by the properties of the extruded material, the geometry of the tool and the condition of the workpiece-tool contact surfaces (friction). The paper discusses the flow of ideally plastic material at plain-strain extrusion. Forward extrusion is a forming process in which a workpieces pushed through a die whose exit diameter is smaller than that of the work piece.

Two different approaches, namely the “flow approach” (flow formulation) and “solid approach”, have emerged for the simulation of metal forming processes using different numerical methods [1, 2], mainly the finite element method (FEM), [1, 3-5] and recently the finite volume method (FVM) [6-9].

Thirty years ago, Demirdžić et al. [6, 7] proposed the first application of the cell-centered finite volume method, in its modern form, to solid mechanics. This original method was applied to the simulation of thermal deformations in welded workpieces on a 2-D structured quadrilateral grid. Small strains and rotations were assumed and the material behavior was described by the so called Duhamel-Neumann form of Hooke’s law [6].

This cell-centered approach takes its name from the dependent variable, in this case velocities, residing at the cell centers (control volume centroids). Calculations performed in this paper were done with Comet software (Version 1.052) [8].

2 MATHEMATICAL MODEL

2.1 Governing Equations

The theory of plastic flow in the problems of bulk metal forming uses point velocities as dependent variables instead of displacements. The approach to problem solving according to this theory is analogous to the approach in fluid mechanics. The cold extrusion processes, which are considered in this paper, assuming a quasi-stationary (steady-state) flow, are also solved according to this theory and must satisfy the following basic conservation equations:

Mass balance equation (continuity equation) [7]:

$$\frac{\partial}{\partial t} \int_V \rho dV + \int_S \rho u_j n_j dS = 0 \quad (1)$$

Momentum balance equation [7]:

$$\frac{\partial}{\partial t} \int_V \rho u_i dV + \int_S \rho u_i u_j n_j dS = \int_S \sigma_{ij} n_j dS + \int_V \rho f_{bi} dV \quad (2)$$

Eq. (1) and (2) are valid for an arbitrary part of a continuum of volume V bounded by the surface S . Here t is the time, ρ is the density, u_j is the velocity vector, σ_{ij} is the stress tensor and f_{bi} is the resultant body force.

2.2 Constitutive Relations

According to the theory of plastic flow, the deviators of stress tensors and strain rate tensors are coaxial. The components of stress tensor are determined by the Levy-Mises equations [1]:

$$\sigma_{ij} = \sigma \delta_{ij} + \mu \left(\frac{\partial u_i}{\partial x_j} + \frac{\partial u_j}{\partial x_i} \right) \quad (3)$$

where σ is the mean stress (pressure), while the viscosity μ can be calculated as [1]:

$$\mu = \frac{1}{3} \frac{\bar{\sigma}}{\dot{\bar{\varepsilon}}} \quad (4)$$

Whence it follows that the Levy-Mises equations hold for $\bar{\varepsilon} \neq 0$ otherwise the material behaves like a rigid body.

The effective stress $\bar{\sigma}$ and effective strain-rate $\dot{\bar{\varepsilon}}$ are defined by equations [1]:

$$\bar{\sigma} = \sqrt{\frac{3}{2}} \{ \sigma'_{ij} \sigma'_{ij} \}^{\frac{1}{2}} \quad (5)$$

$$\dot{\bar{\varepsilon}} = \sqrt{\frac{2}{3}} \{ \dot{\varepsilon}_{ij} \dot{\varepsilon}_{ij} \}^{\frac{1}{2}} \quad (6)$$

where: σ'_{ij} is deviatoric stress and $\dot{\varepsilon}_{ij}$ strain-rate tensor with components [1]:

$$\dot{\varepsilon}_{ij} = \frac{1}{2} \left(\frac{\partial u_i}{\partial x_j} + \frac{\partial u_j}{\partial x_i} \right) \quad (7)$$

The viscosity μ is in the general case a function of the degree and rate of deformation and temperature, i.e. $\mu = \mu(\bar{\varepsilon}, \dot{\bar{\varepsilon}}, \theta)$. Using the assumption of ideal plasticity and the fact that cold forming is considered, viscosity becomes only a function of the strain rate gradient. The initial viscosity μ_p at which the plastic flow begins is determined by the uniaxial tensile experiment ($\sigma_z = \sigma_y = 0$, $\dot{\varepsilon}_z = \dot{\varepsilon}_y = -0.5\dot{\varepsilon}_x$).

In this case, Eq. (5) and Eq. (6) become: $\bar{\sigma} = \sigma_x$ and $\dot{\bar{\varepsilon}} = \dot{\varepsilon}_x$, so the viscosity at the beginning of plastic flow in the direction of x-axis will be [1]:

$$\mu_p = \frac{1}{3} \frac{\sigma_y}{\dot{\varepsilon}_x} \quad (8)$$

where σ_y is the yield stress, while the strain rate $\dot{\varepsilon}_x = u/h$, is equal to the ratio of the ram speed u , m/s, and workpiece high h . The value of the viscosity calculated according to Eq. (8) is also the upper limit that the viscosity can reach in the calculation. Areas in the deformed material where the viscosity is above this limiting value were considered in the calculation as rigid (stagnation) zones.

By entering the constitutive relation (3) into the momentum equation (2), a closed system of equations is obtained, which in the general 3D case consists of four equations with four unknown functions (u , v , w and σ) of spatial coordinates and, for nonstationary cases, time.

2.3 The Finite Volume Discretization

In order to solve the defined system of equations, it is necessary to discretize time, spatial domain and the equations themselves. The general case of discretization of Eq. (1) and

Eq. (2) is described in [7]. Two – dimensional discretization is considered in this paper.

With the assumption of incompressibility of the extruded material, as well as the previously introduced assumption of stationarity of the process, the first terms on the left side of Eq. (1) and Eq. (2) become zero. Also, the effect of body forces, that are present only in so-called high-speed metal forming, is neglected.

The two-dimensional spatial domain (the domain of solution) is sub-divided into a finite number (N) of contiguous control volumes (CV) or cells of volume V bounded by the surface S consisting of a number of cell faces of the area S_k . The solution domain is discretized by a rectangular numerical grid, example on Fig. 1.

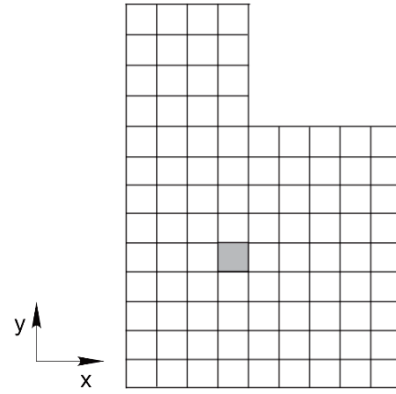


Figure 1 Example of the 2D domain discretization

The compass notation is used for definition of a boundary faces S_k of control volumes, Fig. 2.

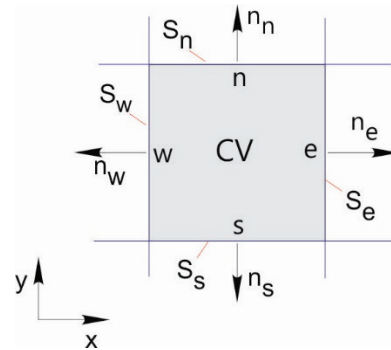


Figure 2 A control volume with compass notation

A typical and adjacent cells are shown in Fig. 3, [9]. The calculation points are located in the centers of gravity of the control volumes, while boundary nodes, needed for the specification of boundary conditions, reside at the center of boundary cell faces.

To illustrate the method of discretization of Eq. (2), the equation of balance of forces acting on one control volume, Fig. 4, will be set only for x direction.

Based on Eq. (2) for the stationary case and in the absence of volumetric forces, the equilibrium equation for one CV can be written as [9]:

$$\sum_k \int_{S_k} \rho u (u n_x + v n_y) dS = \sum_k \int_{S_k} (\sigma_{xx} n_x + \sigma_{xy} n_y) dS + \left\langle \int_V \frac{\sigma_{\theta\theta}}{x} dV \right\rangle \quad (9)$$

Where $k = e, n, w, s$ is the counter of the sides of the control volume.

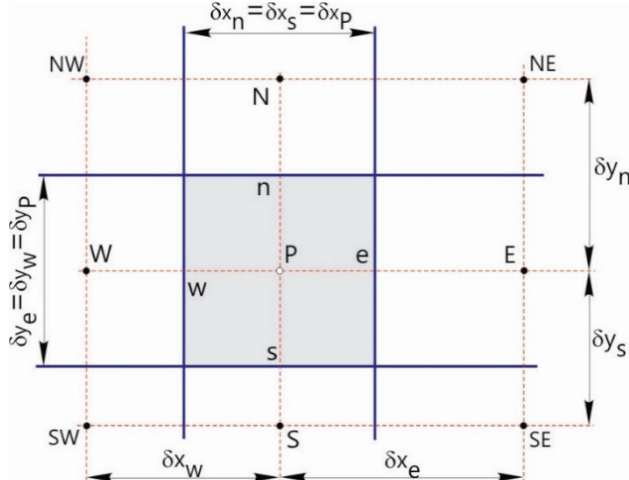


Figure 3 The numerical grid

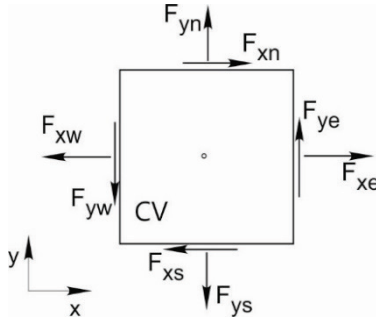


Figure 4 Control volume and acting forces

The last term in Eq. (9) appears only for axisymmetric cases of the stress state, in the equilibrium equation for the x direction. Based on Eq. (9), the forces on individual sides S_k of the observed control volume are given by the following expressions [9]:

$$\begin{aligned} F_{xe} &= \int_{S_e} \rho u u n_e dS + \int_{S_e} \sigma_{xx} n_e dS - \left\langle \int_V \frac{\sigma_{\theta\theta}}{x} dV \right\rangle \\ F_{xw} &= \int_{S_w} \rho u u n_w dS + \int_{S_w} \sigma_{xx} n_w dS \\ F_{xn} &= \int_{S_n} \rho u v n_n dS + \int_{S_n} \sigma_{xy} n_n dS \\ F_{xs} &= \int_{S_s} \rho u v n_s dS + \int_{S_s} \sigma_{xy} n_s dS \end{aligned} \quad (10)$$

After entering the expression for stress tensor (3) into Eq. (9) follows:

$$\begin{aligned} & \int_{S_e} \rho u u dS - \int_{S_w} \rho u u dS + \int_{S_n} \rho u v dS - \int_{S_s} \rho u v dS = \\ &= \int_{S_e} \left(\sigma + 2\mu \frac{\partial u}{\partial x} \right) dS - \int_{S_w} \left(\sigma + 2\mu \frac{\partial u}{\partial x} \right) dS + \\ &+ \int_{S_n} \mu \left(\frac{\partial u}{\partial y} + \frac{\partial v}{\partial x} \right) dS - \int_{S_s} \mu \left(\frac{\partial u}{\partial y} + \frac{\partial v}{\partial x} \right) dS - \\ &- \left\langle \int_{S_w} 2\mu \frac{u}{x^2} dV \right\rangle \end{aligned} \quad (11)$$

The terms on the left side of Eq. (11) represent the convective change, while the terms on the right side are the acting surface forces on the control volume.

Convective terms are discretized by applying a mixture of formulas for upstream differentiation of the first order of accuracy (implicit part) and the difference of symmetric central differentiation of the second order of accuracy and upstream differentiation (explicit part), [7].

The values of the variables between two adjacent calculation points (on the sides of the CV) are obtained by linear interpolation.

The terms on the right hand side in Eq. (11), so-called diffusion terms are discretized as follows [9]:

$$\begin{aligned} D_{xe} &\approx \mu_e \frac{S_e}{\delta x_e} (u_E - u_P) + \mu_e \frac{S_e}{\delta x_e} (u_E - u_P) + \sigma_e S_e \\ D_{xw} &\approx \mu_w \frac{S_w}{\delta x_w} (u_P - u_W) + \mu_w \frac{S_w}{\delta x_w} (u_P - u_W) + \sigma_w S_w \\ D_{xn} &\approx \mu_n \frac{S_n}{\delta y_n} (u_N - u_P) + \mu_n S_n \left(\frac{\partial v}{\partial x} \right)_n \\ D_{xs} &\approx \mu_s \frac{S_s}{\delta y_s} (u_P - u_S) + \mu_s S_s \left(\frac{\partial v}{\partial x} \right)_s \end{aligned} \quad (12)$$

The coefficients for creating a system of algebraic equations in order to solve unknown velocity components in the x direction have the form [9]:

$$\begin{aligned} a_E &= \mu_e \frac{S_e}{\delta x_e} - \min(\dot{m}_e, 0) \\ a_N &= \mu_n \frac{S_n}{\delta x_n} - \min(\dot{m}_n, 0) \\ a_W &= \mu_w \frac{S_w}{\delta x_w} - \min(\dot{m}_w, 0) \\ a_S &= \mu_s \frac{S_s}{\delta x_s} - \min(\dot{m}_s, 0) \\ a_P &= \sum_K a_K \end{aligned} \quad (13)$$

Each of four coefficients represent the sum of the implicit part of the diffusion terms and the implicit part of the

convective terms for the observed CV, where \dot{m}_k ($k = e, n, w, s$) is the mass flux through certain CV surface.

The so-called source terms (b) of the system of algebraic equations are the sum of the explicit parts of the convective and diffusion terms and the terms of the forces from the mean normal stress σ (pressure).

The final appearance of the discretized equation for one CV for calculation of the velocity component in the x direction is [9]:

$$a_p u_p - \sum_K a_K u_K = b \quad (K = E, N, W, S) \quad (14)$$

The discretized equation for the y direction is analogous to Eq. (14), where the coefficients a_K ($K = E, N, W, S$) and a_p remain the same as for the x direction. The difference is only in the source term b .

2.4 Calculation of Pressure

It is easy to notice that in the discretized equation of momentum there is an unknown mean normal stress (pressure), and that the equation of momentum (Eq. (2)) is not independent of the continuity equation. However, the pressure does not figure directly in the continuity equation, but it is used as an additional condition that must be satisfied when calculating the velocity field. Therefore, several procedures have been developed to connect the equations of momentum and continuity by which the pressure is determined. For calculation in this paper, the SIMPLE algorithm [7] was used, which results in a linear algebraic equation for pressure correction that also has the form of Eq. (14).

2.5 Boundary Condition

To start the calculation, all dependent variables (velocity components) have to be set to their initial values. The expressions for the evaluation of forces are valid for all interior cell faces which are shared by the two adjacent cells. Boundary cell faces are related to only one cell and require special treatment that depends on the type of the boundary conditions. Boundary conditions can be classified as being of Dirichlet (e.g. 'inlets', where all dependent variables are usually known), or Neumann type where values of dependent variable gradients are available. If the problem considered is symmetric in such a way that one boundary can be taken for a symmetry plane, then that is possible by looking at a near-boundary cell and its mirror image on the other side of the symmetry plane.

2.6 Solution Procedure

Writing the equations of form (14) for each velocity components and for each CV, a system of $3 \times N$ (N - number of CV-a) of nonlinear, coupled equations is obtained, which is solved by the following iterative procedure [7].

The equations are temporarily linearized and decoupled assuming that the coefficients and the source terms are known (calculated based on the values from the previous iteration) thus obtaining 3 systems of N linear algebraic equations. The coefficient matrices for each subsystem of linear equations will be sparse, symmetric, and diagonally dominant. These subsystems of the equations are solved one after the other by the conjugate gradient method. After that, the coefficients and the source terms are renewed and the procedure is repeated until the desired accuracy is achieved.

3 NUMERICAL SIMULATION OF EXTRUSION PROCESS

To verify the presented numerical procedure, two cases of the plain-strain extrusion (forward and backward) will be considered. Experiments for these cases were done by Segal [10]. In numerical simulation these processes are considered as steady-state.

The first case is forward extrusion under ideal contact conditions (contact tangential stress $\tau_k = 0$) with a cross section reduction ratio of $A_0/A_1 = 2$. The initial width of the piece is 40 mm, while the width at the output cross section is 20 mm. The discretization of the spatial domain was done with a rectangular numerical grid with 430 CVs, Fig. 5.

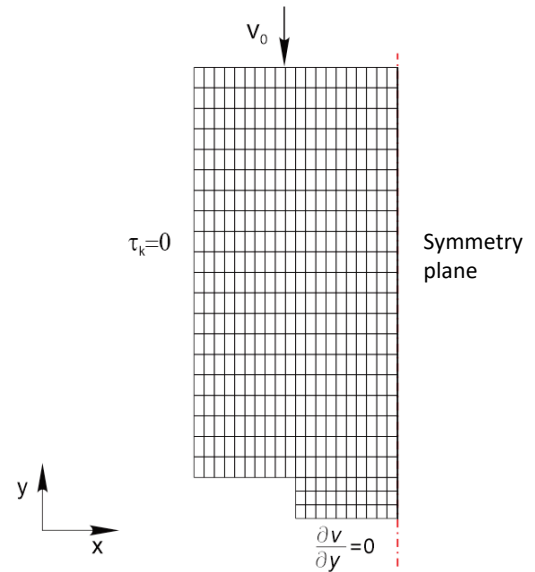


Figure 5 Numerical grid (430 CVs) and boundary conditions

In experiments the ideal contact conditions are approximately obtained by high quality contact surfaces and intensive lubrication. The extruded material is technically pure lead with a stress of the beginning of plastic flow $\sigma_Y = 14$ MPa. The extrusion speed is $v_0 = 2$ mm/s. The resulting velocity vectors obtained by the calculation after 810 iterations are given in the Fig. 6.

The effective strain-rate distribution over solution domain is given in Fig. 7. The areas which are not covered by contours represent the stagnation (dead) zones.

Fig. 8 shows the fields of the velocity components in the x -direction obtained experimentally by the Moire method

[10], and by the finite volume method. There is a very good accordance between the calculated and experimental results.

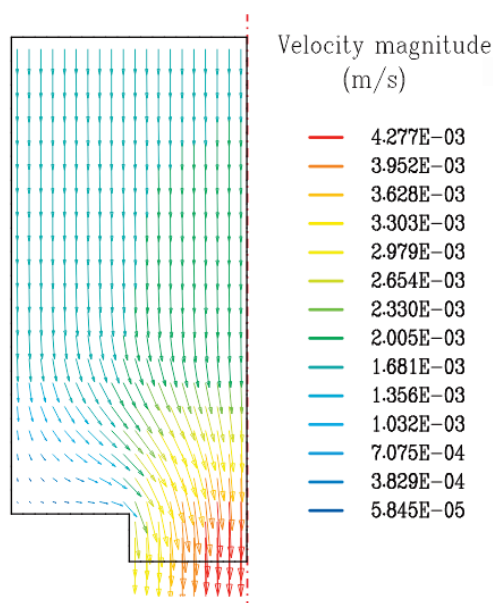


Figure 6 The velocity vectors distribution

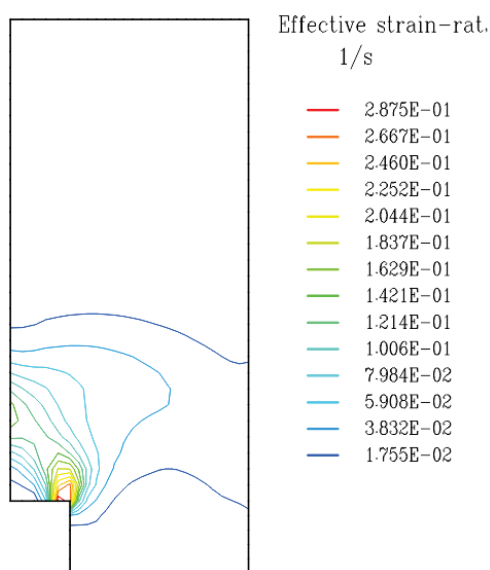
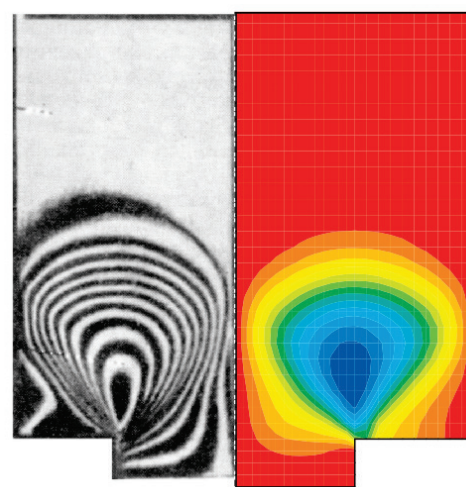


Figure 7 The effective strain-rate distribution

Another example relates to the backward extrusion of the same material and process parameters, under a plain-strain and no friction conditions, Fig. 9. The initial width of the prism is $b_0 = 80$ mm, while extrusion is done by using a $b_1 = 44$ mm wide punch. The discretization of the spatial domain was performed with 450 CVs.

Fig. 10 and Fig. 11 show the fields of the velocity components in the x and y -direction obtained experimentally, by the Moire method [10], and by the FVM. Accordance between the results is very good.



Experiment [10] FVM calculation
Figure 8 Distribution of the velocity component in x-direction

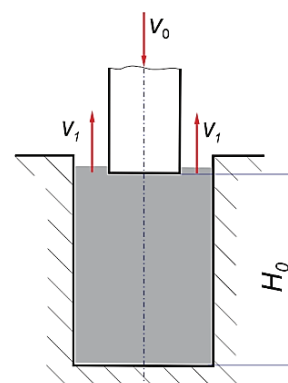


Figure 9 Backward extrusion

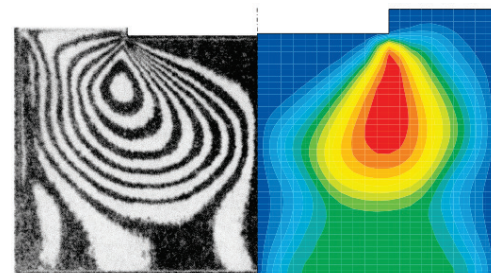


Figure 10 Distribution of the velocity vector component in x-direction (experiment on the left and FVM calculation on the right hand side)

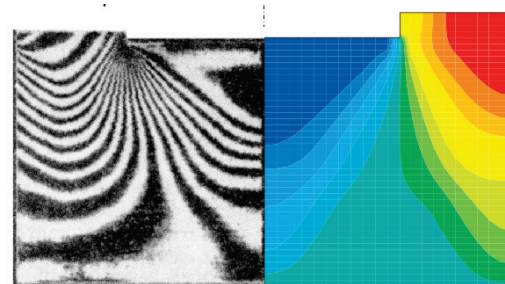


Figure 11 Distribution of the velocity component in y-direction (experiment on the left and FVM calculation on the right hand side)

The assumption of the existence of rigid (dead) zones during the deformation process is one of the common assumptions in solving the problem of the theory of plasticity by using the concept of a rigid-plastic body (for example slip-line field method, upper bound method, thin section method), [1, 2, 11, 13]. Rigid zones are most often assumed in the corners of extrusion dies (see Fig. 6, Fig. 8) or under punch (see Fig. 10, Fig. 11). The shape of these zones obtained by measuring the velocity components experimentally as well as by the FVM, indicates the accuracy of these assumptions. The height of these zones increases with increasing the contact friction between the workpiece and the die.

In the flow approach, the material is assumed to behave like a non-Newtonian viscous or visco-plastic fluid and the numerical solution is obtained by using an Eulerian reference frame (stationary mesh).

4 CONCLUSION

The finite volume method can be successfully applied in the analysis of plastic flow of metals in metal forming technologies. In this paper, the method was used for the analysis of the flow of ideally plastic material and the orthogonal geometry of tooling. Unlike approximate methods of plasticity theory, FVM gives the complete picture of the considered flow, i.e. arrangement of velocity components throughout the spatial domain, from which other relevant variables can be easily calculated: strain rates tensor components, stress tensor components, effective stress distribution, etc. Compared to other numerical methods, the advantage of FVM is in more efficient use of computer resources due to the structure of the matrices of a system of algebraic equations and solving systems of linear equations separately.

The further application of FVM in the analysis of plastic flows of metals could be: inclusion of arbitrary geometric shapes of solution domain (including 3D domains), calculation the effects of material hardening, inclusion of friction on contact boundaries and analysis of hot extrusion processes.

FVM can be applied to the above cases by generalizing the presented discretization procedure and including the energy balance equation [8]. In that case, a new subsystem of linear algebraic equations is obtained with unknown temperatures in the CVs centers. Some results of FVM application for non-orthogonal solution domains and non-zero friction boundary conditions are presented in [8].

Notice

The paper was presented at MOTSP 2020 – International Conference Management of Technology – Step to Sustainable Production, which took place from 30th September – 2nd October 2020 in Bol, island Brač (Croatia). The paper is not and will not be published anywhere else.

5 REFERENCES

- [1] Kobayashi, S., Oh, S., & Altan, T. (1989). *Metal Forming and the Finite Element Method*. Oxford University press, Oxford.
- [2] Wagoner, R. H. & Chenot, J.-L. (2004). *Metal Forming Analysis*. Cambridge University Press.
- [3] Lou, S., Zhao, G., Wang, R., & Wu, X. (2008). Modeling of aluminum alloy profile extrusion process using finite volume method. *J. of Materials Processing Technology*, 206, 481-490. <https://doi.org/10.1016/j.jmatprotec.2007.12.084>
- [4] Zhang, C., Li, L., & Zheng, Z. (2017). Numerical Simulation of Forging Process for Steam Turbine Blade. *International Journal of Mechanical & Mechatronics Engineering IJMME-IJENS*, 17(03).
- [5] Bašić, H., Duharkić, M., & Burak, S. (2019). Numerical simulation of hot forging process in production of axisymmetric automobile parts. *Periodicals of Engineering and Natural Sciences*, 7(4). <https://doi.org/10.21533/pen.v7i4.487>
- [6] Cardiff, P. & Demirdžić, I. (2018). Thirty years of the finite volume method for solid mechanics. *arXiv preprint arXiv:1810.02105*.
- [7] Demirdžić, I. & Muzaferija, S. (1995). Numerical Method for Coupled Fluid Flow, Heat Transfer and Stress Analysis Using Unstructured Moving Meshes with Cells of Arbitrary Topology. *Comput. Methods Appl. Mech. Engrg.* 125, 235-255. [https://doi.org/10.1016/0045-7825\(95\)00800-G](https://doi.org/10.1016/0045-7825(95)00800-G)
- [8] Bašić, H., Demirdžić, I., & Muzaferija, S. (2005). Finite volume method for simulation of extrusion processes. *Int. J. for Numerical Methods in Engineering*, 62, 475-494. <https://doi.org/10.1002/nme.1168>
- [9] Demirdžić, I. & Ivanković, A. (1997). *Finite Volume Stress Analysis*. Imperial College of Science, Technology and Medicine, University of London.
- [10] Segal, V. M., Makušok, E. M., & Reznikov, V. I. (1974). *Isledovanie plastičeskogo formoizmenenija metalov metodom muara*, Metalurgija, Moskva.
- [11] Alexandrov, S., Mishuris, G., Miszuris, W., & Sliwa, R. E. (2001). On the dead-zone formation and limit analysis in axially symmetric extrusion. *Int. J. of Mechanical Sciences*, 43, 367-379. [https://doi.org/10.1016/S0020-7403\(00\)00016-3](https://doi.org/10.1016/S0020-7403(00)00016-3)
- [12] Tekkaya, A. E. (1997). Current State and Future Developments in the Simulation of Forming Processes. *30th Plenary Meeting of the International Cold Forging Group ICFG*, Den Bosch.
- [13] Lange, K. (1993). *Umformtechnik band 4: Sonderverfahren, Prozesimulation, Werkzeugtechnik, Produktion*, Zweite, vollig neubearbeitete und erweiterte Auflage, Springer-Verlag.

Authors' contacts:

Hazim Bašić, prof. dr. sci.
(Corresponding author)
Mechanical Engineering Faculty,
Vilsonovo šetalište 9, 71 000 Sarajevo, Bosnia and Herzegovina
Tel: +38733729872, E-mail: basic@mef.unsa.ba

Ismet Demirdžić, prof. dr. sci.
Mechanical Engineering Faculty,
Vilsonovo šetalište 9, 71 000 Sarajevo, Bosnia and Herzegovina
E-mail: i.demirdzic@yahoo.com

Samir Muzaferija, prof. dr. sci.
Mechanical Engineering Faculty,
Siemens Industry Software GmbH,
Nordostpark 3-5, 90411 Nürnberg, Germany
E-mail: samir.muzaferija@cd-adapco.com

Case Study: Six Sigma Project for Reducing Manual Handling of Materials in Real Manufacturing Company

Atanas Kochov*, Aleksandar Argilovski

Abstract: This paper presents a case study that is focusing on the improvement of the process of materials handling in real manufacturing company. Before the implementation of this project, the company was in a concerning state of incidents and learning events towards the ergonomics, health and safety of the operators who manually handled materials as part of their daily activities. It was proposed to use the Six Sigma framework in order to improve the process or design new process for performing the task that included manual handling of materials. In this study, through selecting suitable Six Sigma framework, mapping the current process, setting key performance indicators and using various design tools and techniques, process improvement is proposed; it will solve the problem, increase ergonomics and safety, but also increase the speed of the process and reduce the cost of spilled materials that were manually handled.

Keywords: ergonomics; improvement; LEAN; manufacturing; project; Six Sigma

1 INTRODUCTION

Six Sigma is a structured problem-solving methodology widely used in the manufacturing industry. This paper will present the minimum number of tools that are needed during the execution of the Six Sigma project and will also give a short description of the results discovered during the study.

The Continuous Improvement department of the Company A is a department executing all the engineering and process improvements in the company according to the demand of the other departments. This project was initiated due to the safety issues identified during the process of dosing powder materials on an elevated platform in the production area of the Company A. The team decided to use the Six Sigma as a framework to lead this project and generate solutions through systematic and statistically supported project process.

1.1 Brief Introduction to the Six Sigma Frameworks and Their Use in this Case Study

At the core of the definition for the traditional Six Sigma, it is stated that it is a set of tools and techniques for problem solving and therefore improvement of the process and the products. The original Six Sigma framework consists of five phases: **define, measure, analyse, improve and control** [1]. This framework is also known as **DMAIC** framework and it is usually more applicable for improvement of existing processes or products. The **DMEDI** framework (**define, measure, explore, design and implement**) is also widely used framework when there is no existing process that can be improved, or the existing process should be completely replaced by new, significantly different process [3]. Fig. 1 presents the main deliverable of the mentioned Six Sigma frameworks and points out the differences between them [5]. The example in this case study is a DMEDI project. Each step of this framework is important for the project deliverable. Usually the team uses this framework in the feasibility study or in the detailed design phase of bigger projects [4]. In this

case study, the framework was used to gather all the needed information of the proposed project and decide what will be the best conceptual design that the company should use to work on further development in the future in order to solve the existing problem.

Phase	DMAIC	Phase	DMEDI
Define	Define scope, goals and resources.	Define	Define scope, goals and resources.
Measure	Map the current process, identify KPIs.	Measure	Map the current process, identify KPIs.
Analyse	Analyze the data in order to find the root cause.	Explore	Explore previous ideas, preliminary design.
Improve	Brainstorm new solutions and prioritize them.	Design	Develop detailed design of the product/process.
Control	Design a system for control of the solution.	Implement	Implement the solution and set control measures.

Figure 1 Six Sigma main frameworks and the deliverable for each different phase of the framework

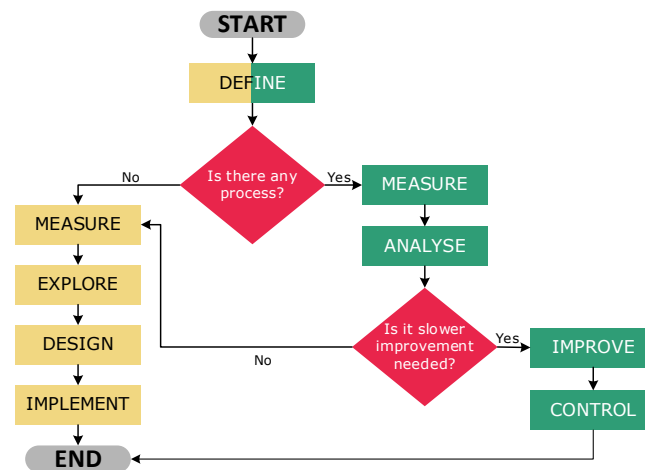


Figure 2 The process of selection of the right Six Sigma framework

The project will also establish control and monitoring plan in the last phase of the framework but will not focus on

the project on-site implementation in order to emphasize only the Six Sigma tools and not the classical project management.

Fig. 2 presents a simple process flow diagram which can be used to decide if the project should be managed through the DMAIC or the DMEDI framework [5]. If this is not obvious at the beginning of the project, it is recommended that this decision be taken after the Define phase where the team will already gather general information on the issue, goals, the process and the resources needed.

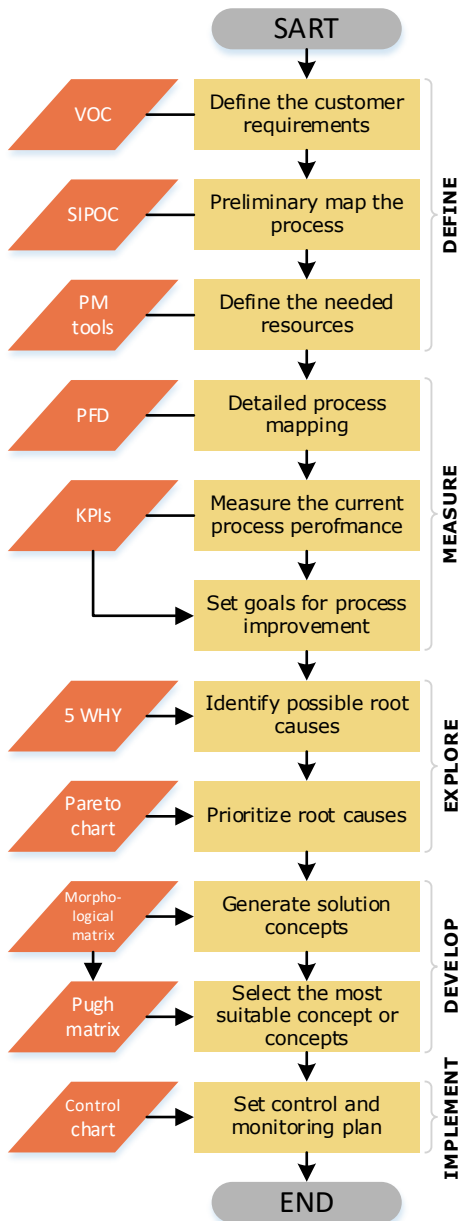


Figure 3 Six Sigma process along with tools and deliverable

1.2 Six Sigma Tools and Deliverables

This case study is focused on finding a practical solution for reducing the manual handling of materials in real manufacturing company. However, as stated above, it will not focus on the project management aspect of this project.

This Six Sigma project is meant to be fast and deliver as fast the statistically-based engineering solution of this issue. Therefore, optimal amount of tools was chosen for this study in order to minimize the needed time but still receive the desired deliverable at the end. Fig. 3 presents the entire Six Sigma process created for this case study along with the tools used in each of the process steps.

2 DEFINE

In order to successfully define the project, the least that the team should do in this phase is to collect end user requirements, preliminary map of the process, issue problem and goal statements, and define the needed resources (time, people and cost).

As stated above, at the end of this phase, the team should definitely decide if DMAIC or DMEDI framework would be followed for the project.

2.1 Voice of the Customer

Voice of the customer (VOC) is the easiest way to gather high-level customer/end user requirements without any detailed forms or surveys. Usually the end users (in this case the operators) are the ones that know the problem the best and solving this problem is in the field of their interest. To collect VOC, the team should simply talk to the operators, supervisors and department manager about their issues with the current process or product, write down the received comments, and then convert them in deliverable requirements together with the Six Sigma team. Fig. 4 is showing the VOC for this project.

END-USER COMMENT	WHY ARE THEY SAYING IT	WHAT DO THEY WANT
"The operator is not safe"	There is a risk of injury	Automated machine
"We have material (powder) spill"	Waste (spill) of raw material	New process that will reduce spills
"The process is very slow"	Waste of time	Fast process/machine
"Carrying materials trough the stairs is not ergonomic"	Risk of injury or illness	Ergonomic solution

Figure 4 Voice of the customer (VOC)

This VOC table consists of three parts. The first column states the raw comments by the end users. Then, the team is filling the rest of the table after a brainstorming analysis of the comments in order to understand what the end users are saying and finally what they want to improve their experience.

2.2 SIPOC

The SIPOC analysis is a very useful tool for smaller improvements because with this analysis the team can sum up all preliminary information on a single sheet of paper. It is also a preliminary process mapping of the project. Fig. 5 is

showing the SIPOC analysis for the example in this case study.

S	I	P	O	C
End-user department (Production) Six Sigma project facilitator (CI department)	Market analysis	Open the doors	The operator performing the job on 2,6 m height	End-user department (Production) EHS department Maintenance department
	Voice of the customer	Positioning of the load		
	Six Sigma results	Lifting the load	Safe operator	
	Procurement of new machine	Reaching highest point	The job is finished for shorter time	
	Implementation of the solution	Taking product out	The machine is used for other purposes	
		Manual dosing of the product		

Figure 5 SIPOC

This analysis is also very flexible because it can be easily updated during the project. Through this analysis, in a very tidy and a simple way, the team can identify the following important parts of the project:

- Stakeholders (S) – everyone that is interested in the outcome of this project;
- Inputs (I) – what is needed for this project to reach its goals and deliver the needed benefits;
- Process (P) – the steps of the current process;
- Outputs (O) – what the deliverables of the implementation of this project are (benefits can be also listed in this section);
- Customers (C) – or end users are all involved, parties that will be using the results of this project in any way.

2.3 Resources

This is the part of the project where project management tools set is needed to determine the needed human resources (the team), time and budget.

When it comes to resources, as a good practice it is suggested to define the Product Breakdown Structure (PBS), which will list all the final products needed at the end of this project according to the customer requirements [4]. These “products” are not only physical subjects but they can also be documents or procedures. Based on these products, the Six Sigma leader should identify the team with the needed skills to deliver these products. Cost should be defined based on relevant budgetary quotations and market analysis. When it comes to the time, many things such as internal company procedures, customer requirements, delivery terms by the vendors, availability of contractor companies etc., should be taken into consideration.

For project timeline planning, it is recommended to use the combination of Network Diagram to determinate the flow of the activities and Gantt chart to graphically show the timeline of the project and to easily have control over it.

The VOC, SIPOC and the defined resources are the inputs to the project charter, which is another Six Sigma tool that is very popular for project overview. This can be any form of a poster, which contains this information.

3 MEASURE

The purpose of this step is to thoroughly understand the current state of the process, collect reliable data on the process speed, quality and costs, and use that data to underlay the causes of the problems.

During this step, the current process map is in the focus. The team must understand and deeply analyze the process in order to generate key performance indicators, which at the end will show if there is any improvement, or not. A current process map, generated Key Performance Indicators (KPIs) and measured current KPIs of the current process should be considered as the main deliverables of this step.

3.1 Current Process Mapping

The current process for the example will be given in a simple process flow diagram (PFD) shown in Fig. 6.

The current process consists of many manual steps. First, the operator tries to find a hand pallet-truck in order to transport the materials up to the position. After that, the operator lifts materials (with the help of the pallet truck) to the highest point of a servicing platform (up to 2,6 m from the ground). While it is being lifted, the operator takes the stairs in order to reach the lifted pallet with materials. The operator reaches over the fence of the servicing platform and reaches for the raw materials placed in the bag, which is placed on the pallet. Usually the process is in a need of two operators in order to speed up the process (one operator operates with the pallet-truck and one is up on the servicing platform to manually take the material and dose it in the proper tank). When a big amount of material is not needed (less than 50 kg), it usually comes in different packages (small bags) which are manually taken by the operators through the stairs up top 2.6 m. For this case study, the Six Sigma team supervised the process several times. The process that usually occurs (with several differences from situation to situation) is presented in the process flow diagram on Fig. 6.

The process is also presented in Fig. 7 as a sketch in order to understand the process in way that is more illustrative. The sketch in Fig. 7 shows the position of the pallet and the elevated servicing platform where the bag with material is lifted.

3.1 Key performance indicators

Fig. 8 presents the Tree of Requirements for this project which will help the team to determine the measurable KPIs.

In order to generate the key performance indicators (KPIs), the team must have in mind the results of the VOC analysis before the Define phase. The end user requirements are the ones that should be converted into measurable indicators so that the team can track their improvement. If the generated requirements are not easily measurable, the Tree of Requirements can be used so that the requirements are converted into easily measurable indicators.

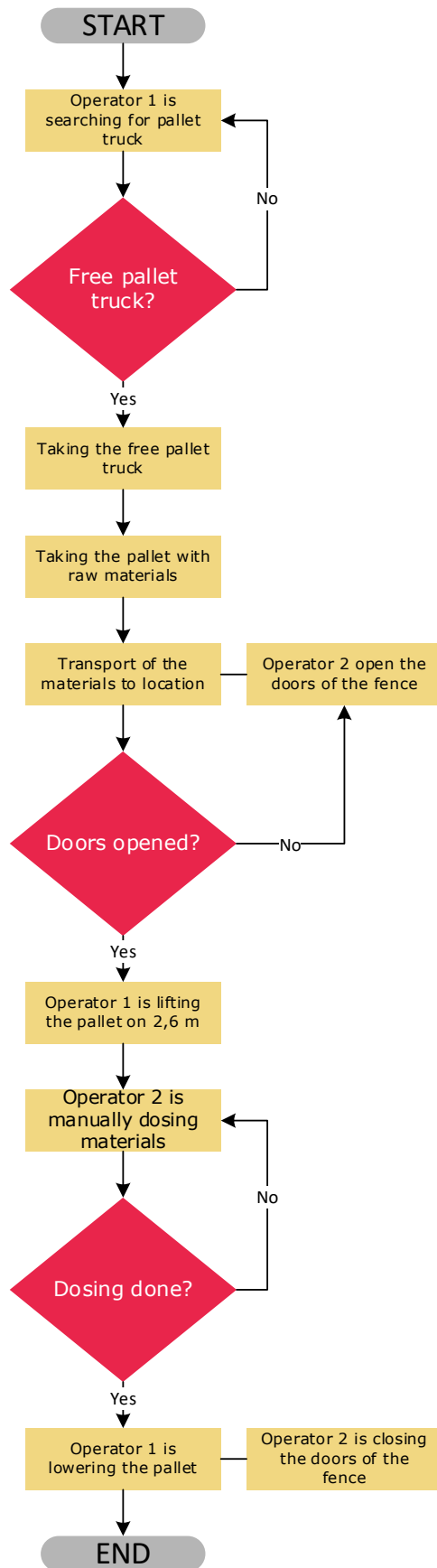


Figure 6 Process flow diagram of the current process

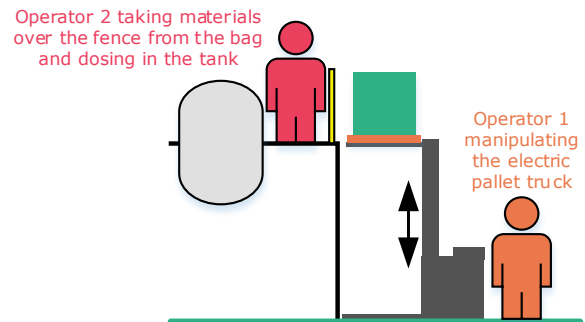
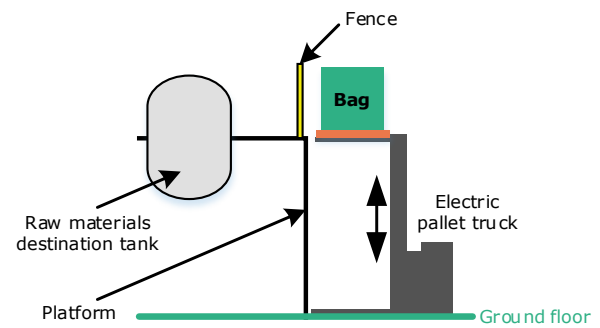


Figure 7 Sketch of the current process

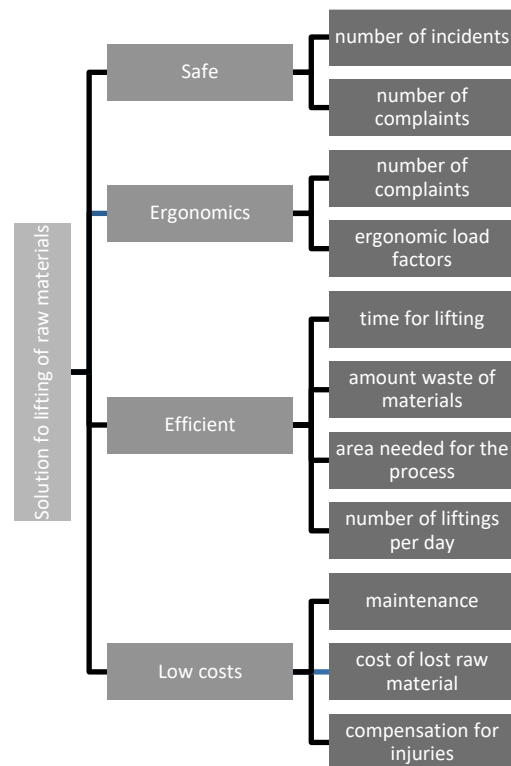


Figure 8 Tree of requirements

To explain this tool, the team highlights the requirement "waste of time/fast machine is needed". It can be already noticed that it is incredibly hard to measure this requirement and quantize it. During the Tree of requirements analysis, the team should decompose the rough end user requirement into something that can be measured with a number. For example,

waste of time can be converted to "minutes needed for lifting the load on the servicing platform". It is known that these minutes should be as few as possible, so with measuring this indicator before and after the implementation of the solution, the team can clearly see if there was an improvement and therefore if the end user requirement is fulfilled.

If the team decides that the example above can still be decomposed in an indicator that is even easier to measure, then the requirements can be decomposed as much as they can.

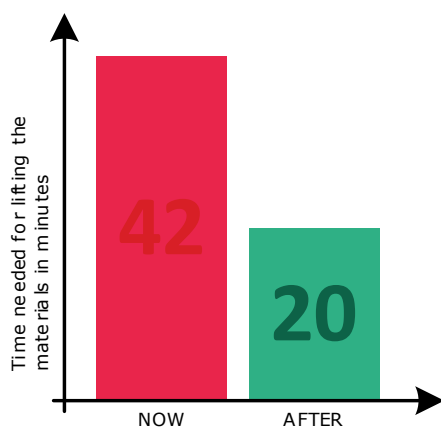


Figure 9 Time needed for lifting the materials

Figs. 9, 10 and 11 present few of the KPIs in diagrams with their current measured value. It is highly recommended that goal values be set in this phase for each indicator so that the team have initial directions "how much" to improve. The end user should set these values so that they are satisfied at the end of the project; if this is not an option, then the team should definitely set their objectives in this way.

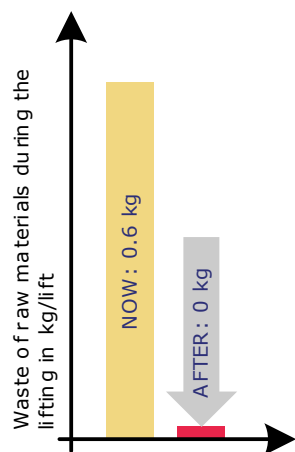


Figure 10 Waste (spill) of raw materials during the lifting

One more indicator that is not given with a diagram, but is a very important one, is that the Company A, in the last 365 days, faced 18 incidents (injuries or illnesses of operators, spills of materials and other more serious events) and 42 complaints by the operators for the ergonomics of the lifting process. After this project, the team is expecting to reduce these numbers to 0.

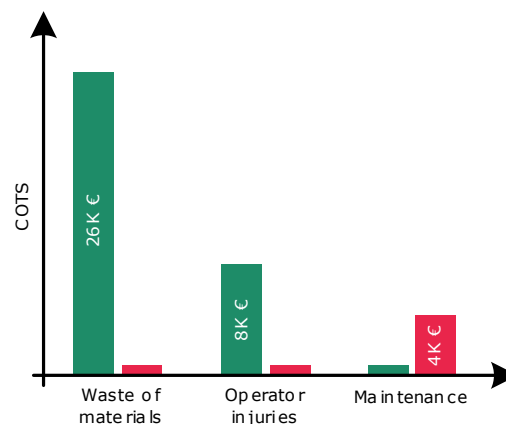


Figure 11 Costs due to spills, injuries and maintenance

4 EXPLORE

This is a step of the Six Sigma project that can usually be extremely short and straight-forward or it could be a deep analysis of the root causes of the problem. The main deliverable of this project is to define the root cause (or causes) of the issue and focus on solving it in the Design phase of the project. Sometimes the root cause is very obvious, but it is still recommended to use at least two tools to confirm this root cause. Pareto Chart, Fishbone diagram, 5 WHYS, 4CP analysis and many other tools can be used in this phase. For all of them, the entire team is always needed because the tools are usually based on brainstorming of possible issues.

4.1 5 Why

5 Why is interrogative and brainstorming based tool that helps the Six Sigma team to find the root cause of the problem by asking the team at least five questions that will lead to as many reasons for the issue as they can. The 5 Why analysis is given in Fig. 12.

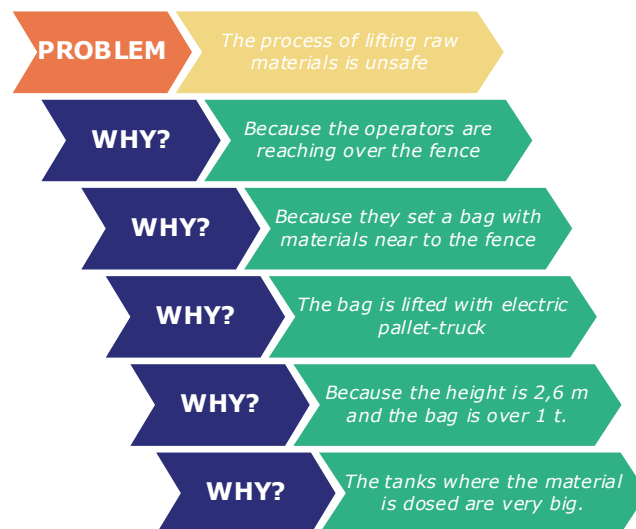


Figure 12 5 Why analysis

Since there is more than one reason for this issue, the 5 Why analysis for this case study will be shown only for one

of the main problems which is "The process of lifting raw materials is unsafe". After the problem is stated, the team is asked "Why is the process of lifting raw materials unsafe?" The team should give the answer on this question based on the gathered data during the Define and Measure phases. As an answer for this question, the team suggested "The process is unsafe because the operators are reaching over the fence (to reach for the raw materials lifted on height of 2.6 m above the ground with a help of an electric pallet-truck)". This clearly is not the root cause of the problem, so the team is continuing with the analysis and they are asking the second "Why" based on the answer of the previous question: "Why are the operators reaching over the fence?" The process continues with another answer and question until the root cause is identified according to the team.

Sometimes there can be more root causes for one problem and that is why Pareto chart is used in order to prioritize which of these root causes are causing most of the problems in the process.

4.2 Pareto Chart

The Pareto chart is a very powerful tool for showing the relative importance of the occurred problems (or the root causes for these problems). The information that is input in this diagram can be collected in various ways. For this case study, the information was taken from the previously used tools in the previous phases – VOC and KPIs. In order to construct the diagram, measuring must take place. Here all indicators must be measured in same amount of time (for example in one year) and for the Pareto chart, the team is measuring the frequency of occurring of these events (not like KPIs where the team mostly measured physical units).

Table 1 Data needed for the construction of the Pareto chart

Issues	Occurrences	Cumulative	%
Safety complaints	42	42	43
Ergonomics complaints	24	66	68
Load lifting operations	15	81	84
No free pallet truck to do the job	7	88	91
Materials spills	6	94	97
Injuries due to lifting operations	3	97	100
Total	97		

The interpretation of this diagram is very simple. The dots of the red line (cumulative frequency) that are under the 80% cut-offline are connected to the issues that should be treated with more attention than the others because theoretically they the cause of 80% of the problems. The Pareto rule also says that if the team eliminates these highlighted issues, which are 80% of all issues, a successful improvement of the process or the product was made.

The chart highlights the issues that cause 80% of the problems (Fig. 13, dark turquoise). The other issues (Fig. 13, light turquoise) are the cause of only 20% of the problems. They are also important because they are also identified issues but the team cannot focus on so many issues and find one solution for them all. That is why it is always important to prioritize the issues. After this Pareto analysis, the team will focus on finding a solution that will be reducing the safety and ergonomics complaints during the lifting process.

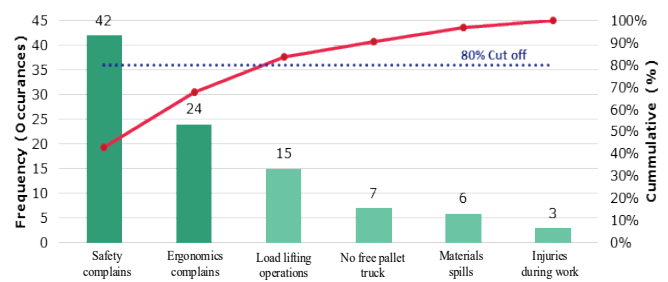


Figure 13 Pareto chart

5 DESIGN

As mentioned before, this Six Sigma project will not define the detailed design of the solution, nor will it generate any technical drawings for manufacturing of it but will definitely confirm the design specifications of the solution so that the solution meets the end user's requirements, improve the measured KPIs of the current process, and remove the previously identified issues with the root cause analysis.

5.1 Morphological Matrix

For this case study, Morphological Matrix will be used as a tool for generating new concepts. This matrix is constructed of two columns. The first column is for the needed functions of the new product/process. Next to them, in the second column, for each function the team brainstorms solutions how these functions can be executed. With combination of the different solutions (one for each function), many different concepts can be generated and after proper evaluation of the concepts according to the end users' needs, the best concept (or concepts) can be selected for further development.

5.2 Selection of the Best Concepts

For evaluation of the selected concepts as well as selection of the best concept, Pugh matrix will be used in this case study. The selected concepts for evaluation (according to the Morphological matrix on Fig. 14) are:

- Concept 1 (C1): 1.3, 2.1, 3.2, 4.2
- Concept 2 (C2): 1.2, 2.4, 3.2, 4.4
- Concept 3 (C3): 1.5, 2.2, 3.1, 4.1

Table 2 Pugh matrix

Criteria	C1	C2	C3
Positioning to be easy and flexible	5	3	5
The current habits of the operators to be considered	5	1	3
Easy for maintenance	4	2	2
Can be manipulated from both close and far	5	5	0
Total	19	11	10

In the Pugh matrix, the randomly selected concepts were scored from 1 to 5 according to how much they fulfil the needed criteria (based on the end user requirements). According to the matrix, Concept 1 is the most suitable concept for the end user. This matrix can also include weighting factor. This factor will prioritize one criterion

above the other and give them higher importance in the matrix. In this example, all the criteria have the same importance.

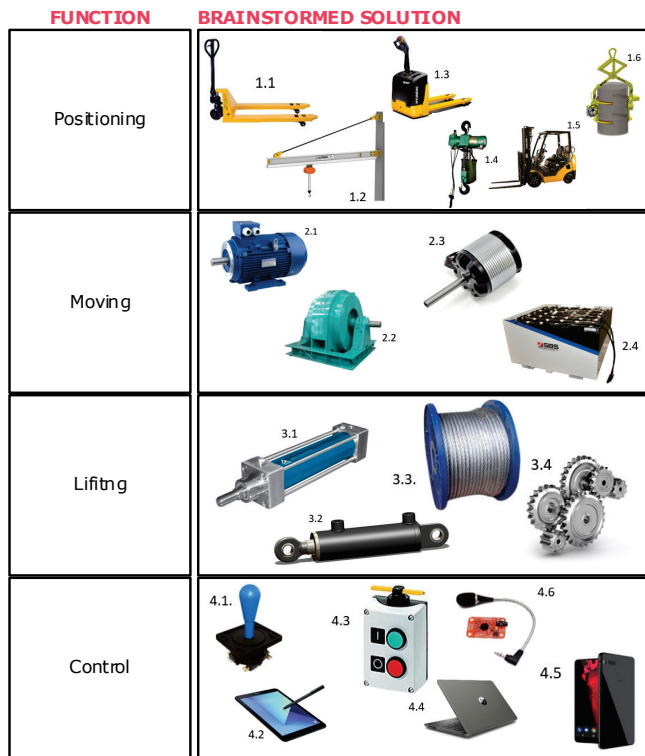


Figure 14 Morphological matrix

In order to confirm that the selection of this concept is the right one, Six Sigma offers one more tool called Force Field analysis shown in Fig. 15 [3].

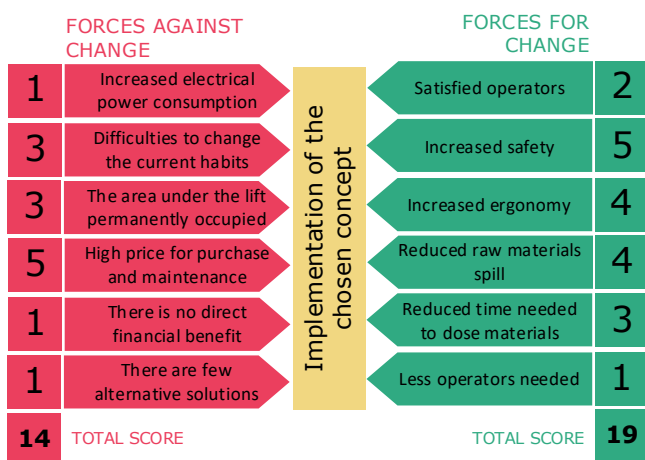


Figure 15 Force-Field analysis

6 IMPLEMENT

Since this project involves implementation of entirely new machine in the production area, this should undergo a heavy project management process and that is why this will not be covered in this study. The contracts with external vendors, method statements for the activities on site and other

project management tools such as risk assessments for the installation, commissioning of the equipment etc., will not be a subject of this study but it is very important to say that if the project charter of the Six Sigma project in the Define phase is such that the customer is expecting these activities to occur at the end of the project, then the Six Sigma team should definitely execute the entire installation of the equipment and fulfill the agreed scope of work.

In the light of Six Sigma and the tools that it offers for this phase, few deliverables are expected for this project in the last phase: define how this solution will be sustained and set up control chart. Failure mode matrix (or FMEA) can also be executed in order to prevent any of the identified risks to become issues over the time [2].

6.1 Sustainability and Solution Control

For solution control and sustainability over the time, the Six Sigma suggests several options such as:

- Training for the employees – all operators that will be directly involved in the process, including their supervisors and maintenance technicians, should get detailed training about the new process and eventually the new machine that will be installed. The training should focus on ergonomics, safety and optimization of their time;
- Occasional measuring of the KPIs - plan for measuring of the established KPIs in the Measure phase must be created in order to see if the solution lost the benefits of the improvement (Control chart is a recommended tool);
- 5S – setting visible labels and keeping the area tidy will help the operators to optimize the process;
- Standardized Work Instruction (or Operational procedure) – standardized procedure for work for each operator will enhance the quality of the process.

6.2 Control Chart

The control chart is a statistical tool that can assure the quality of the newly introduced process or product [3]. The control chart is constructed of one reference line that represents the ideal process and two margins (upper and lower margin). The fourth line is the actual process and this line is constructed of the measured values through the time for the assigned KPI. This control chart should be made for all critical KPIs identified previously in the Measure phase to assure that the solution is still an improvement compared to the old process. All the results of the measurements should be between the lower and the upper margins (of course, as close as possible to the ideal line). If any of the samples is out of the margins, that is an initial indicator that there is a malfunction in the newly introduced process. If seven samples in a row are out of the margins, it means that there is already an issue and the improvement is degraded (improvement no longer exists).

For the case study, the team selected one of the indicators in order to create the control chart. The selected indicator is "Number of registered complaints for ergonomics in one month". This indicator at the beginning of the project (in the

Measure phase) was 48 complaints per year, which means 4 complaints per month. In order to construct this diagram with this indicator, it must be measured every month. The upper margin for the control chart is set at three complaints per month (which is one less than the situation before the implementation of the lifting solution). The lower margin is 0. Fig. 16 presents what the diagram looks like if the process of measuring is applied in six months after the implementation.

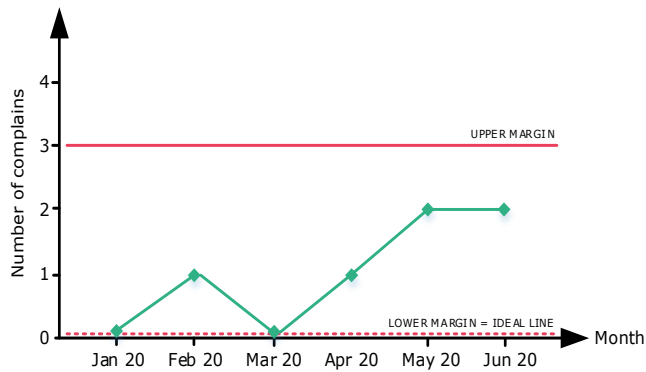


Figure 16 Control chart example

7 CONCLUSION

The DMEDI framework of Six Sigma is a very detailed and creative approach to finding solutions for the issues. Through this Six Sigma framework, the team managed to gather valuable information and set up initial control measures for the selected conceptual design in order to solve the identified problem that makes the work quite hard and unsafe for the operators of the Company A.

The number of Six Sigma tools was kept to the minimum of tools that are sufficient to deliver the main and most important deliverable of this project and in the meantime satisfy the end user of this project. Such were Voice of the Customer (VOC), SIPOC, Process Flow Diagram (PFD), Tree of Requirements, Key Performance Indicators (KPI), 5 Whys, Pareto Chart, Morphological Matrix, Pugh Matrix, Force Field analysis and Control chart.

The combination of these tools made sure that Company A would receive a solution that would solve their ergonomics, safety, spills and time issues of the process of manual dosing of raw powder materials. This promotes a contemporary LEAN culture in the company. The reduction of the costs, reduction of the time needed to produce the final product and the enhancement of the quality also enhance the competitiveness of the company on the market. This shows that even smaller improvements can lead to significant changes in the companies. Besides this, the Six Sigma approach also helps in building entirely new culture in the companies, which promotes systematic approach to the problems and leads to very fast process of problem solving and end user satisfaction.

Notice

The paper was presented at MOTSP 2020 – International Conference Management of Technology – Step to Sustainable Production, which took place from 30th September – 2nd October 2020 in Bol, island Brač (Croatia). The paper is not and will not be published anywhere else.

8 REFERENCES

- [1] KIT. (2015). Industrial Engineering and Management - University of the State of Baden-Wuerttemberg and Research Center of the Helmholtz Association. Available from: https://www.wiwi.kit.edu/downloads/2015ss_mhb_wiing_BS_c_lang_en.pdf
- [2] Toutenburg, H. & Knöfel, P. (2009). Six Sigma - Methoden und Statistik für die Praxis. Springer, Berlin, p. 349.
- [3] Meran, R., John, A., Roenpage, O., Staudter, C., & Schmitz, A. (2013). Six Sigma+Lean Toolset: mindset for successful implementation of improvement projects. Second edition. Lunau, S., editor. Vol. Management for professionals. Berlin: Springer. Available from: [http://ezproxy.derby.ac.uk/login?url=https://www.vlebooks.com/vleweb/product/openreader?id=DerbyUni&isbn=9783642358821&uid=^uPMBOK® Guide – Sixth Edition. \(2017\). A guide to Project Management Body of Knowledge, Project Management Institute.](http://ezproxy.derby.ac.uk/login?url=https://www.vlebooks.com/vleweb/product/openreader?id=DerbyUni&isbn=9783642358821&uid=^uPMBOK® Guide – Sixth Edition. (2017). A guide to Project Management Body of Knowledge, Project Management Institute.)
- [4] www.isixsigma.com – To use DMAIC or to use DMEDI? That is the question! – blog by Steven H. Jon
- [5] Singh, S. K., Sharma, K., Kumar, D., & Gupta, T. (2014). Role & Importance of Lean Manufacturing in Manufacturing Industry. *The International Journal of Engineering and Science (IJES)*, 1-14.

Authors' contacts:

Atanas Kochov, PhD
(Corresponding author)
Faculty of Mechanical Engineering - Skopje
Karposh II bb, 1000 Skopje, Republic of North Macedonia
+389(0)71-299-299,
atanas.kochov@mf.edu.mk

Aleksandar Argilovski, BSc
Faculty of Mechanical Engineering - Skopje
Karposh II bb, 1000 Skopje, Republic of North Macedonia
+389(0)71-254-429,
argilovski@hotmail.com

UAV, Digital Processing and Vectorization Techniques Applied to Building Condition Assessment and Follow-up

Carles Serrat*, Sebastian Banaszek, Anna Cellmer, Vicenç Gibert, Anna Banaszek

Abstract: The aim of the paper is to explain the basic principles of carrying out an inventory and follow-up of buildings and their condition assessment, by using the Full Interactive Visualization Method for Building Condition Assessment platform. It is a platform enabling the implementation of construction inventory based on the remote cooperation of many specialists in the field of, among others: building construction, architecture, civil engineering, photogrammetry, CAD, UAV. This type of cooperation is of particular importance especially in the context of the current epidemiological situation related to COVID-19. The idea of the presented platform fits into the broadly understood Building Information Modeling. After introducing the methodology, stages of the inventory and follow-up process carried out within the platform are illustrated and discussed on the basis of a case study. Based on the obtained results it can be concluded that the proposed methodology creates a convenient, efficient and inexpensive tool for massive inspection of building resources in large areas. The inventory is based primarily on high-quality photo and video material obtained from the deck of an unmanned aerial vehicle and the expert knowledge of the inspector conducting the inspection. By combining digital images data (photos, 3D model, orthophotos) with substantive data (facade element classification tables, wear / defect classification tables), we get a platform that allows intuitive access to viewing, classification, editing and analysis of selected data.

Keywords: BIM; building condition assessment; GIS; monitoring; UAV

1 INTRODUCTION

Innovative technology applied to building condition assessment should be flexible, achievable, reliable, accessible, updating data and ensuring stakeholder participation. An example of this direction is the use of digital technologies, especially in the field of the use of unmanned aerial vehicles (UAVs) in order to improve inventory activities and improve the work of an inspector, in particular when assessing the technical condition of buildings. The idea presented in the article concerns the Full Interactive Visualization Method for Building Condition Assessment platform and is part of the broadly understood Building Information Modeling. As a real-time capturing of data technology, UAV is used in the construction industry. In the recent years, the UAVs have been successfully used for different construction and operation applications of various types of construction projects [1].

The use of unmanned aerial vehicle technologies to efficiently collect information for effective updating of Building Information Modeling, building management and documentation is a topic that is being studied and considered in terms of systematic use by various authors [2-4].

The main aim of this paper is to introduce the further research about the tool previously introduced by Banaszek et al. (2019) [5] for the accurate assessment of the technical condition of buildings, as an efficient strategy for the massive inspection of building stocks, in big residential areas. The development of the Full Interactive Visualization Method for Building Condition Assessment platform (IVP4BCA) [5] requires the selection of technical measures of data collection and computational methods of data processing (including software) as well as the requirements for cooperation of many specialists:

- Inspector - a specialist in the field of construction - thanks to the use of modern technologies integrated through the described platform in the inventory process, the Inspector does not have to carry out a personal

inspection in the field, thanks to this solution the labor intensity of a single process decreases and the Inspector's efficiency increases. Responsible for indicating the building and making its inventory.

- The operator of an unmanned aerial vehicle (UAV) - a specialist in piloting unmanned aerial vehicles and photogrammetry - in the proposed solution, he is the only person whose presence is required at the inventory site. In the future, when Beyond Visual Line of Sight (BVLOS) flights become commonplace, it will be possible to reduce the need for field visits also for the UAV operator. Responsible for the planning and execution of the raid and the quality of the obtained material.
- Photogrammetrist - specialists in the field of data processing and analysis, responsible for data processing, generating products and assessing their accuracy.
- Computer Aided Design (CAD) operator - a specialist in the field of CAD software, responsible for generating a square grid and classifying building elements subject to inventory.

The paper is organized as follows. In chapter 2 it will be shown the main methodology illustrated by the 3D model as well picture of the all building its facades and roof in flat form. Chapter 3 contains description of the case study. The final product is influenced by the requirements regarding the detail of image geoinformation necessary for analysis and the area of inspection as a factor in the time of execution of planned works. Further results and discussion will compose chapter 4. The paper ends with a summary of the main conclusions.

2 METHODOLOGY

As an important means of obtaining spatial data, the unmanned aerial vehicle (UAV) remote sensing has such advantages as real-time, flexible high-resolution and cost-

effectiveness [6]. The type and quality of the data obtained using UAVs depends largely on installed on them sensor, camera resolution, the technical capabilities and planning of photogrammetric flights [7]. The flight mission of the UAVs must be technically protocolized in order to get the proper high-quality information about the real condition of the building [8].

Based on that, the following methodology for the implementation of the inventory based on the platform is proposed, which is used for building condition assessment:

- Indication of the object for inventory - building inspector.
- Analysis of the legal situation in the area designated for the inventory - UAV operator.
- Analysis of the field situation in the area intended for inventory - UAV operator.
- Development of a raid plan - UAV operator.
- Implementation of the raid - UAV operator.
- Analysis of the quality of the obtained material - photogrammeter.
- Digital processing, generation of orthophotos and a 3D model - photogrammeter.
- Analysis of the accuracy of the generated orthophoto planes - photogrammetry.
- Generating a square grid - CAD operator.
- Classification of object elements - CAD operator.
- Visual inventory - Building inspector.

Fig. 1 illustrates in detail the IVP4BCA steps. The methodology is empowered by the results of processing data obtained from the board of the unmanned aerial vehicle. The data is acquired using an RGB sensor, and then, using the Pix4D class software, processed into orthophotos, point clouds and a 3D model. The processing is an iterative process, usually requires 2 to 4 iterations. The first iteration is performed in an unattended process. Materials that are created as a result become the basis of which the obtained data and its completeness are assessed. In the second iteration, the supervised process removes excess data and visible artifacts. After reprocessing, the geometry is analyzed, and the generated materials are visually assessed. If the results of the test are satisfactory, the materials are imported into IVP4BCA, otherwise an iterative process takes place in order to eliminate the observed errors in the geometry and the visual side of the materials.

More specifically, all digital images obtained from the unmanned aerial vehicle deck are geotagged. In order to be able to indicate the location of images on orthophotoplan in open-source GIS software [9], you must first extract the coordinates from the EXIF data of each of the digital images. This can be done with any software that enables batch reading and saving of EXIF data to a .txt file or use the option to import coordinates of processed images in the application used for data processing and generating orthophotoplans.

After importing the materials (orthophotos, cloud point, 3D model, photos etc.), selection of the size of the square grid that will be used for further analysis is needed. In order to properly select its size, it is necessary to carry out a visual analysis of the facade and its parts classification. In the next

stage, the damage is visually assessed with selection of analytical algorithms.

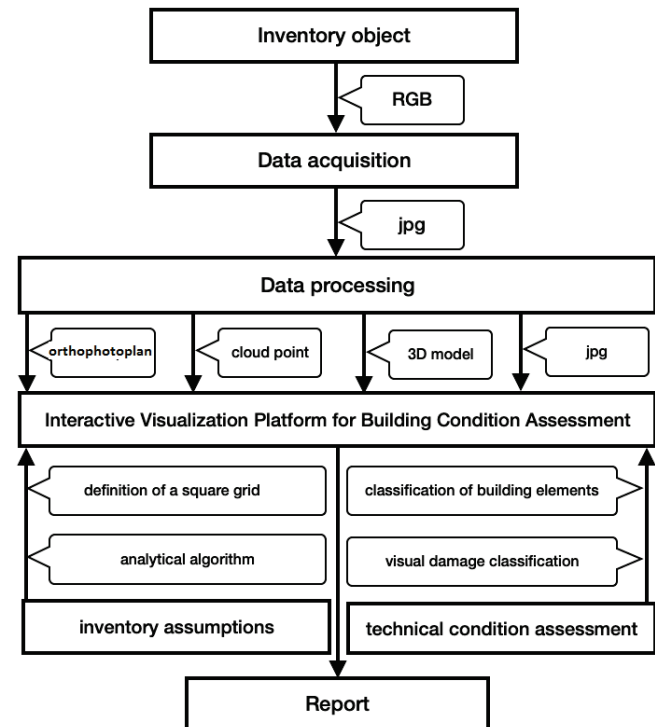


Figure 1 IVP4BCA Methodology

At the end, a report is generated, which, as a document signed by the Building Inspector, may be an element of the documentation from the course of the inspection.

Research results [7] showed that the UAVs orthophotos satisfactorily passed the spatial quality tests. Assessment of the influence of UAV image quality on the orthophoto production presented in such articles as [8, 10]. The tested area covered urban, flat, agricultural and woodland terrains.

In recent years, researches have proposed building damage detection algorithms using remote sensing technology. 3D building damage detection and urban structural damage methods using UAV images described in the research of [11-13]. The results show that geometric parameters derived from the 3D point cloud can reveal damage indicators that are difficult to detect in the original imagery.

3 CASE STUDY

A residential building located in Olsztyn et al. Grunwaldzka. (Poland) was indicted to carry out the inventory. The building is owned by the Commune and is managed by the Board of Municipal Buildings in Olsztyn. The building is situated on a small plot additionally developed with outbuildings. The building is three-story, L-shaped and covered with a two-pitched roof. It was built in the 1960s. Despite proper renovation management, the building shows signs of technical wear, especially in terms of façade wear.

For the purposes of the UAV raid, the operator conducted an analysis of the aviation legal situation in the area designated for the inventory.

The analysis of the field situation in the area intended for the UAV raid showed that the inventoried object is located in a compact urban development, on both sides directly adjacent to the road lane. An additional obstacle is the narrow sidewalk adjacent to the building, about 1.5 m wide, and a two-way road, about 9 m wide, on which there is traffic, including public transport buses. In the off-peak hours, pedestrian traffic can be considered as low-intensity and vehicle traffic moderate.

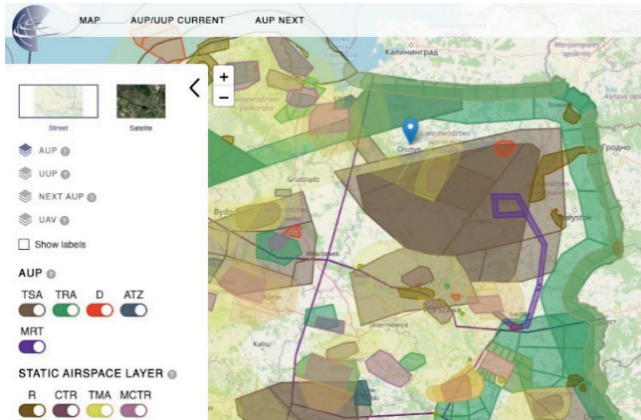


Figure 2 Visualization of the airspace in the area of planned flights

When developing the flight plan, the position of the sun in relation to the inventoried object was taken into account. The order of the façade inventory was planned in such a way that it was properly illuminated during the raid.

The take-off and landing sites are designated separately for each elevation. When planning the flight, attention was also paid to the difficult accessibility of one of the elevations. The flights were carried out using the DJI Inspire One drone. It is a drone with a weight not exceeding 3.5 kg MTOM, classified in the MR (multirotor) category in the so-called the X4 system. The camera installed on board the drone is X3 ZENMUSE with a 12 Mpix matrix with a size of 4000×3000 Pix. 7 flights (6 facades + roof) have been planned. Flights for the façade inventory were carried out in manual mode using the native DJI GO drone control application. The roof inventory was carried out in automatic mode, using the DJI GS application for photogrammetric flights. All flights are to be carried out as Visual Line of Sight (VLOS) flights, in accordance with the diagram shown in Fig. 3. Design coverage of min. 80/80%, distance from the facade approx. 2 m, height above the roof level approx. 10 m. Shutter release manually or with an interval - 2 seconds. GSD is planned at the level of <0.5 cm.

The flight was carried out at high humidity and transient slight rainfall, the temperature was about +5 degrees, wind at about 5 m/s (in gusts up to 10 m/s). At the stage of the raid implementation, changes were made to its implementation consisting in a change in the number of take-off points - finally, the inventory of the building was made from 3 positions. Due to the distance from the neighboring building

not exceeding 2 m, the material for the north-west façade was obtained only from diagonal raids carried out at large angles to the wall plane. Interval release shutter.

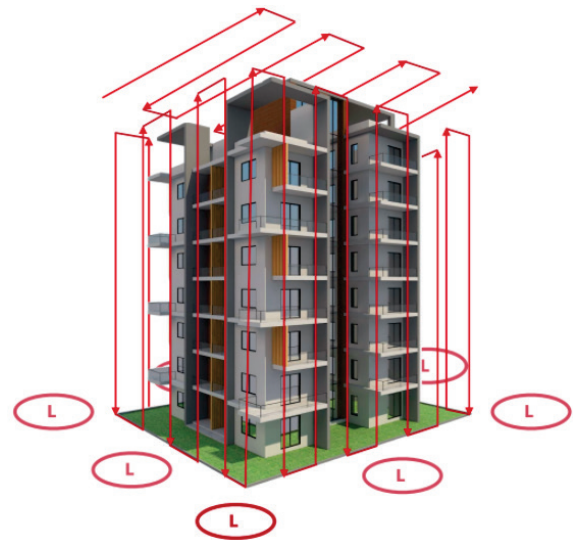


Figure 3 Design of a manual cubature raid for the building inventory (landing strip)

3.1 Digital Processing, Orthophotoplans Generation and 3 D Model

As part of the inventory, a total of 818 good quality .jpg photos were obtained. The photos were properly exposed, lacking high contrast in shadows and highlights and sharp. Despite the fact that the flight was carried out manually, all the photos were calibrated, and the assumed for coverage and resolution were achieved (GSD = 0.36 cm).

The Pix4D mapper software was used to generate orthophotos of the elevation and the 3D model, the pre-processing on a PC (i7-2600 CPU @ 3.40GHz; RAM: 16GB; GPU: NVIDIA GeForce GTX 750) took almost 7 hours. The data was processed in the UTM zone 34N (egm96) coordinate system. As a result of this process, a point cloud was created, represented by 12 005 271 2D key points (3 676 555 3D points) with a mean reprojection error of 0.278 pixels. Such a result allowed to obtain a median number of points per 1 photo at the level of: 24 724 for 2D points and 13 924 3D points.

Due to the GPS signal disturbances occurring during the raid, the data was processed in two blocks:

- Block I included the following elevations: south-west, west, north-west, north-east and a roof.
- Block II included the south-eastern elevation.

To align the blocks, it was necessary to enter the 11 manual tie point and reprocess the data. After these activities, the cloud was generated in one block, the inventoried object was characterized by the correct geometry, shape and proportions. Finally, the relative camera position and orientation of the uncertainties X , Y , Z was obtained at <0.025 for mean and <0.015 for sigma.

In order to generate a 3D model devoid of artifacts, it was necessary to carry out manual cleaning and classification of

the point cloud (Fig. 4 and Fig. 5). The process took almost 6 hours and resulted in the generation of a model practically free from contamination. The model allows it to be used for the visualization of selected, inventoried phenomena in 3D space in a natural way for the user. The carried-out process of cleaning the point cloud additionally influenced the quality of the generated orthophotoplans of the facade and roof. As part of this stage, an orthophotoplan separation was generated for each of the elevations (Fig. 6).



Figure 4 Visualization of the generated model in 3D space



Figure 5 3D model of an inventoried building in a flat projection



Figure 6 Orthophotoplan of North-East elevation

3.2 Accuracy Analysis of Generated Orthophotoplans

Work on orthoplanes takes place in a local system, the accuracy of the GPS module used for geotagging photos (accuracy of determining the position ± 2.5 m), which is standard UAV equipment, does not affect the usability of the generated material. In the local system, the distortion recorded inside the system is important, and not the external error of the point position in the selected coordinate system (UTM zone 34N). Due to the above, the quality of the generated orthophotoplans is described by the GSD coefficient, which is 0.36 cm, and the length measurement error, which is 0.50 cm. The length measurement error was determined by performing control measurements on an inventoried object using the Leica Disto D810 laser rangefinder. For the control purposes, about 50 measurements were made in different planes.

3.3 Generation of a Square Grid and Classification of Building Elements

In order to additionally view the selected image directly from the GIS application by indicating its center, the above-mentioned data should be enriched with the path to the directory in which the images will be ultimately stored. The easiest way to do this is to use batch directory inventory software that saves data most often in a .txt file in the form of an absolute path "c: / project / image.jpg" or the relative "... project / image.jpg". Thanks to the possibilities offered by today's spreadsheets, you can easily combine the contents of both files and generate a .txt or .csv file with the structure: "Filename.jpg [Tab] X coordinate [Tab] Y coordinate [Tab] Z coordinate [Tab] c: / design / name.jpg ". A file prepared in this way, imported into the GIS software, after indicating columns containing the selected coordinates, enables visualization of image centers and preview of images directly from the application without the need to know their physical location.



Figure 7 Orthophotoplan with a squared grid

In the case of visualization of images in the orthophotomap area, we use the X , Y coordinates, in the case of orthophotos of elevations (orthophotos the façade) vertical Z , Y . The experiment generated a file consisting of 926 records, containing 5,556 attribute values.

The next step to assign specific values of selected attributes for a previously defined part of the façade is to create a matrix of squares of the selected size and size.

Based on the conducted analyses, a matrix made of squares with a side of 0.4 m was considered optimal (Fig. 7).

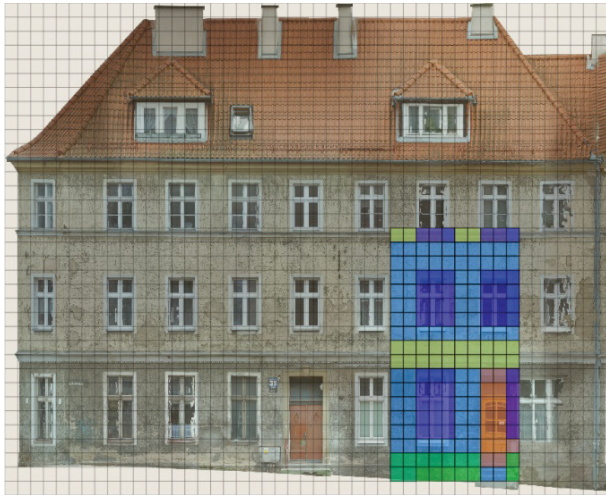


Figure 8 Orthophotoplan with completed qualification of inventoried elements



Figure 9 A fragment of the orthophoto plan with the performed qualification of the inventoried elements

The basic elements of the façade classified in the manual process include, first of all, the geometry of the façade and the roof, window and door joinery and architectural details (Fig. 8 and Fig. 9). Depending on the assumed accuracy of the final inventory of the above-mentioned elements can be

subjected to classic polygon vectorization (for the most accurate inventories) or indicated by assigning individual mesh squares a value corresponding to the inventoried elements (for the inventory requiring less accuracy). In our case, method 2 was used, for the needs of which 5 classes of elements they were created: 1 - wall, 2 - molding, 3 - window, 4 - plinth, 5 - door (Fig. 10).

Etykieta	Regula
<input checked="" type="checkbox"/> Fasade	"_Fasade" = 1
<input checked="" type="checkbox"/> Wall	"_Wall" = 1
<input checked="" type="checkbox"/> Door	"_Door" = 5
<input checked="" type="checkbox"/> Window	"_Window" = 3
<input checked="" type="checkbox"/> Plinth	"_Plinth" = 4
<input checked="" type="checkbox"/> Molding	"_Molding" = 2

Figure 10 List of classes of identified facade elements

The matrix was created in 2 stages. The first stage consisted of creating a square grid using the QGIS tool: vector / research tools / create a grid, resulting in a linear vector layer. In the second stage, linear objects were transformed into polygonal objects using the tool: vector / geometry tools / lines into polygons. As a result, an attribute table was created with the number of records equal to the number of polygons. A total of 1,645 polygons were generated based on the created 47×35 matrix. At this stage, the table contained only 5 attributes: polygon ID and top, down, left, right - coordinates of the polygon corners.

3.4 Visual Inventory

The last step is to carry out a visual assessment of the technical condition of the façade by the inspector, determining the degree and type of wear on the basis of orthophotoplanes based on a square grid and classification (Fig. 11). Its implementation enables the automatic visualization of wear in accordance with the indicated criteria and the determination of the area and position of each type of defects found (Fig. 12 and Fig. 13).

Location	1068	1069	1070	1071	1072	1073	1074	1075	1076	1077	1078	1079	1080	1081	1082	1083	1084
Facade	X	X	X	X	X	X	X	X	X	X	X	X	X	X	X	X	X
Body	X	X	X	X	X	X	X	X	X	X	X	X	X	X	X	X	X
Outdoor enclosure	X	X	X	X	X	X	X	X	X	X	X	X	X	X	X	X	X
Wall	X	X	X	X	X	X	X	X	X	X	X	X	X	X	X	X	X
Masonry																	
Brick																	
Seen	X	X	X	X	X	X	X	X	X	X	X	X	X	X	X	X	X
Coating and painting	X	X	X	X	X	X	X	X	X	X	X	X	X	X	X	X	X
Ledge																	
Eave																	
Cornice																	
Molding																	
Brick																	
Seen																	
Coating and painting																	
Plinth																	
Coating and painting																	

Figure 11 A fragment of an orthophoto plan with the performed qualification of inventoried elements

In order to enter data obtained during manual examination of generated orthophotoplanes, the attribute table was expanded with another 138 attributes, for which the values found were then introduced. As a result, it became possible to conduct surface analyzes of the façade's technical condition both on the basis of entered, directly observed

attribute values and using any combination of their values using the so-called GIS application available in the GIS application called field calculator.



Figure 12 Visualization of a specific degree of wear, depending on the type found

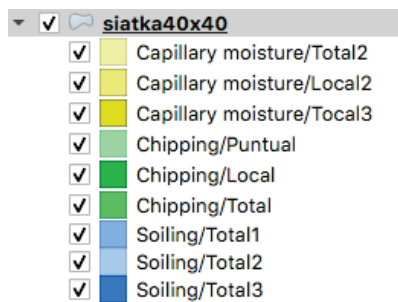


Figure 13 A fragment of the list of inventoried types of use

4 CONCLUSION

The proposed Full Interactive Visualization Method for Building Condition Assessment is based primarily on high-quality digital information obtained from the deck of an unmanned aerial vehicle and the expert knowledge of the inspector conducting the inspection. By combining digital images and geoinformation data (photos, 3D model, orthophotos) with substantive data (facade element classification tables, wear / defect classification tables), we get a platform that allows intuitive access to viewing, classification, editing and analysis of selected data:

- 3D module - enables the visualization of selected, inventoried phenomena in 3D space in a natural way for the user and is most often used to carry out inspections and move around the model;
- 2D module - allows you to visualize selected, inventoried phenomena in 2D space in a way that enables their identification, location and accurate measurement.

Factors that have a negative impact on the efficiency of the proposed methodology for Building Condition Assessment should be mentioned.

The first group of factors is related to UAV technology:

- The possibility of flying depends on the weather - in some cases it is impossible to carry out tasks in accordance with the previously agreed schedule. It becomes especially visible in the autumn and winter period;
- Obtaining the required permits for flights from the property owner or manager - not everyone understands

the nuisance associated with the implementation of flights within their property.

The second group is related to digital processing:

- Large volume of acquired material - gigabytes of acquired data require storage, processing, analysis and archiving, for which an efficient, stable and high-capacity Network Attached Storage (NAS) system is needed;
- High hardware requirements for the proper operation of data processing software (obtained from UAV) - currently used processing algorithms cause that data processing processes are often processes lasting many hours, and the prices of the appropriate class of computer equipment make it difficult to implement the so-called parallel processing.
- Imperfection of automatic data processing algorithms - orthophotos, point clouds and 3D models generated in an unattended process contain many artifacts. Therefore, removing them in a supervised process requires a large amount of time by a specialist.

After considering the above-mentioned limitations based on the conducted research, it can be concluded that the proposed methodology creates a convenient and efficient tool for massive inspection of building resources in large areas. The use of the described platform in the inventory process enables the optimization of the work of human resources involved in the implementation of the process, especially in relation to the construction inspector, who can carry out his activities without the need to visit inventoried facilities each time, thanks to which the costs of logistics and time lost on commuting are eliminated.

Creation of a platform based on the proposed methodology will allow to provide users with the use of a modern tool enabling full integration of the construction inventory process with BIM.

By optimizing the work of the task force, it is possible to lead to a situation in which the inspector's work will be carried out completely online from the office.

Notice

The paper was presented at PBE2020 – International Scientific Conference "People, Buildings and Environment 2020". The 14th conference was held in the Rožnov pod Radhoštěm city, the Czech Republic, from 7 to 9 October 2020. The paper will not be published anywhere else.

5 REFERENCES

- [1] Asnafi, M. & Dastgheibifard, S. (2018). A Review on Potential Applications of Unmanned Aerial Vehicle for Construction Industry. *Sustainable Structures and Materials, An International Journal*, 1(2), 44-53.
- [2] Grosso, R., Mecca, U., Moglia, G., Prizzon, F., & Rebaudengo, M. (2020). Collecting Built Environment Information Using UAVs: Time and Applicability in Building Inspection Activities. *Sustainability, MDPI, Open Access Journal*, 12(11), 1-15. <https://doi.org/10.3390/su12114731>

- [3] Chen, Y., Zhang, J., & Min, B. (2019). Applications of BIM and UAV to construction safety. *CSCE Annual Conference*, 1-7.
- [4] Vacanas, Y., Themistocleous, K., Agapiou, A., & Hadjimitsis, D. (2015). Building Information Modelling (BIM) and Unmanned Aerial Vehicle (UAV) technologies in infrastructure construction project management and delay and disruption analysis. *Proc. SPIE 9535, Third International Conference on Remote Sensing and Geoinformation of the Environment (RSCy2015)*, 95350C.
<https://doi.org/10.1117/12.2192723>
- [5] Banaszek, A., Banaszek, S., Cellmer, A., Gibert, V., & Serrat, C. (2019). A Fully Interactive Visualization Method for Building Condition Assessment. *IOP Conf. Ser.: Mater. Sci. Eng.* 603 022011, 1-10.
<https://doi.org/10.1088/1757-899X/603/2/022011>
- [6] Li, C., Shen, L., Wang, H. B., & Lei, T. (2010). The research on unmanned aerial vehicle remote sensing and its applications. *2nd International Conference on Advanced Computer Control, Shenyang*, 644-647.
- [7] Mesas-Carrascosa, F. J., Rumbao, I. C., Berrocal, J. A. B., & Porras, A. G.-F. (2014). Positional Quality Assessment of Orthophotos Obtained from Sensors Onboard Multi-Rotor UAV Platforms. *Sensors*, 14, 22394-22407.
<https://doi.org/10.3390/s141222394>
- [8] Lin, Z. J. (2008). UAV for mapping — low altitude photogrammetric survey. *The International Archives of the Photogrammetry, Remote Sensing and Spatial Information Sciences*, Vol. XXXVII. Part B1, 1183-1186.
- [9] Niethammer, U., Rothmund, S., Schwaderer, U., Zeman, J., & Joswig, M. (2011). Open source image-processing tools for low-cost UAV-based landslide investigations. *International Archives of the Photogrammetry, Remote Sensing and Spatial Information Sciences*, Volume XXXVIII-1/C22, 161-166.
<https://doi.org/10.5194/isprsarchives-XXXVIII-1-C22-161-2011>
- [10] Wierzbicka, D., Kedzierska, M., & Fryskowska, A. (2015). Assessment of the influence of UAV image quality on the orthophoto production. *The International Archives of the Photogrammetry, Remote Sensing and Spatial Information Sciences*, Volume XL-1/W4, 1-8.
<https://doi.org/10.5194/isprsarchives-XL-1-W4-1-2015>
- [11] Fernandez Galarreta, J., Kerle, N., & Gerke, M. (2015). UAV-based urban structural damage assessment using object-based image analysis and semantic reasoning. *Nat. Hazards Earth Syst. Sci.*, 15, 1087-1101. <https://doi.org/10.5194/nhess-15-1087-2015>
- [12] Torok, M. M., Golparvar-Fard, M., & Kochersberger, K. B. (2014). Image-based automated 3D crack detection for post-disaster building assessment. *Journal of Computing in Civil Engineering*, 28(5).
[https://doi.org/10.1061/\(ASCE\)CP.1943-5487.0000334](https://doi.org/10.1061/(ASCE)CP.1943-5487.0000334)
- [13] Malihi, S., Valadan Zoej, M. J., Hahn, M., Mokhtarzade, M., & Arefi, H. (2016). 3D Building Reconstruction Using Dense Photogrammetric Point Cloud. *The International Archives of the Photogrammetry, Remote Sensing and Spatial Information Sciences*, Volume XLI-B3, 71-74.
<https://doi.org/10.5194/isprsarchives-XLI-B3-71-2016>

Authors' contacts:

Carles Serrat, PhD

(Corresponding author)
IEMAE-EPSEB and Dept. of Mathematics,
Universitat Politècnica de Catalunya-BarcelonaTECH,
Dr Marañón, 44-50, 08028-Barcelona, Spain
E-mail: carles.serrat@upc.edu

Sebastian Banaszek, PhD

Training and Research Center "DroneTechCamp"
Ul. Jarocka 64/2, 10-699, Olsztyn, Poland
E-mail: sebastian.banaszek@banaszekgroup.pl

Anna Cellmer, PhD

Dept. of Geoinformatics,
The Faculty of Civil Engineering, Environmental Engineering and Geodesy,
Koszalin University of Technology,
Ul. Śniadeckich 2,75-453 budynek E pokój 212-2 E, Koszalin, Poland
E-mail: anna.cellmer@tu.koszalin.pl

Vicenç Gibert, PhD

LABEDI-EPSEB and Dept. of Architectural Technology,
Universitat Politècnica de Catalunya-BarcelonaTECH,
Dr Marañón, 44-50, 08028-Barcelona, Spain
E-mail: vicenc.gibert@upc.edu

Anna Banaszek, PhD

banaszek group,
Ul. Jarocka 64/2, 10-699, Olsztyn, Poland
E-mail: anna.banaszek@banaszekgroup.pl

THD Analysis of a Seven, Nine, and Eleven Level Cascaded H-Bridge Multilevel Inverter for Different Loads

Manoj Kumar Sahu*, Madhusmita Biswal, Jagan Mohana Rao Malla

Abstract: A multilevel inverter is implemented for generating the required staircase AC voltage of output from various steps of voltages of DC sources. The multilevel inverter gives a better harmonic spectrum and a compatible quality of output. This article delves into an analytical analysis of the total harmonic distortion (THD) of different multilevel inverters which employ a multicarrier PWM technique. This technique is implemented for operating the switches at their respective angle of conduction. This paper deals with various cascaded H-Bridge multilevel inverters (CMI) with various loads that are modelled by implementing the MATLAB/Simulink platform. The output gives a better result of the proposed model in terms that it is helpful towards reducing the THD and the losses of switching.

Keywords: APD; CMI; IPD; phase shifted modulation technique; POD; THD

1 INTRODUCTION

The multilevel inverter can be categorized as a power semiconductor device along various sources of dc voltage. Those sources may be a solar cell, fuel cell or a battery. Higher voltage and lower switching losses can be achieved by properly, i.e. with proper sequence, turning on and off the devices. There are various advantages of the multilevel inverter in comparison with the two-level inverter. It can operate over a wider range of switching frequencies. It draws the output current of a lower THD and generates the output voltage of a lower harmonic content. Additionally, it has a much lower common mode voltage. The PWM technique can be successfully applicable. It also has certain demerits that by increasing various switching devices, also increase the requirements of gate drive circuits. Such system configurations become complex and by default, there is an increase in the cost of devices.

The common recognized topologies of the multilevel inverter are known as the cascaded H-bridge and neutral point clamped inverters, among which the cascaded H-bridge inverter is popularly used for single-phase systems [1]. The PWM-based technique can give a better dynamic response in addition to the lower THD of current, and the staircase modulation (SCM) based operation can also be directed (when required) over PWM due to having a lower burden of commutation, which can result in reduced switching losses [2-5]. The method of selected harmonic elimination (SHE), based upon the concept of the elimination of harmonics, proposed by Patel for inverters of a high-power range, offers enhanced operations at the lower range of the switching frequency by decreasing the size and price of the bulky types of passive filters [6-8]. These have been effectively implemented in various topologies of the cascaded H-bridge multilevel types converters, whose N-level output of ac voltage improves the performance of the reduced THD [8-17].

The commonly implemented switching methods for a 3-phase voltage source inverter (VSI) are the space vector pulse width modulation (SVPWM) techniques and the carrier pulse

width modulation (CPWM) [18-20] and the five-phase VSI [18, 20-25]. The survey verifies that CPWM reigns over SVPWM at an increased number of phases because of its speed and the structure of the modular computing type [18, 26]. However, SVPWM has greater dominance compared to the CPWM and sinusoidal PWM (SPWM) [18] due to its operational evidence such as fault-tolerant capabilities, common-mode voltage (CMV) and switching losses [27-29]. The different modulation topologies are normally computed by taking into account its computational capability, with THD being most commonly used for a specified inverter application [30]. Another general basis would be the particular harmonic amplitude limitation set up by exhortation and excellence such as RMS CMV [31, 32], IEEE Std. 519 [33], the harmonic distortion factor (HDF) [34], and peak common-mode voltage (CMV) [35].

The NPC inverter initially implemented the PWM techniques such as a simple uniform PWM [36, 37] and the selective harmonic elimination PWM (SHEPWM) [38]. Eventually, significant research was worked out based upon the SHEPWM topology [37, 39, 40]. Voltage signal pulses have a consistent amplitude over a cycle of lines for a uniform nature of PWM [37]. In the sinusoidal PWM, the width of the pulses of voltage are sinusoidally modulated based on the trend of the fundamental pattern for achieving proper spectral properties [41-46].

The development of non-conventional energy resources at higher power and voltage levels demands a sustained upgrade in power electronics converters [47-50]. The multilevel inverter has been successfully implemented at higher power and voltage levels for a single/three-phase system utility in the last decade [51, 52]. The multilevel inverter topology generates more levels of voltage in a way that it decreases the voltage stress and THD while increasing the semiconductor devices [53]. During operation at the higher ranges of switching frequencies, these additional switching devices can raise the losses of power [54-56]. The switching frequency of SHEPWM can be regulated by a proper selection of the pulses of signals in preset voltage waveforms [57-60].

In the analysis, a different study is conferred with having a 15-level inverter by implementing an asynchronous machine drive having single-phase system such that it is in the construction stage of the inverter, 16 numbers of power switches (e.g. IGBTs) are implemented [61]. Hence, in this case, a linear pulse width modulation (LPWM) may be preferred for these types of 15-level inverters [61]. The 35-level inverter can also be implemented for achieving the power line's ac voltage from the solar power plant's dc voltage [62].

There are three principal classifications of multi-level inverters [63]. These are known as the cascaded H-bridge [64] multilevel inverter, diode clamped and capacitor clamped [65] type. A comparison analysis of various multilevel inverters of the cascaded H-bridge such as the 3-level, 5-level, 7-level, 9-level and 11-level inverter is carried out in this paper. The multicarrier pulse width modulation (PWM) technique is [65] implemented in this H-bridge. Through this type of the phase shifted-PWM analogy, among two carrier waves, the Φ_1 phase displacement is achieved. It is represented as

$$\Phi_1 = \frac{360^\circ}{m-1} \quad (1)$$

Where, m = the inverter level. In the case of the level shifted-PWM, there will be a vertical displacement of the carrier signals of triangular waves. Here, carrier waves have identical frequency. These types of PWM are principally categorized into three types. These can be represented as: a phase disposition pulse width modulation technique (IPD-PWM), a phase opposition disposition pulse width modulation technique (POD-PWM) and an alternate phase opposition disposition pulse width modulation technique (APOD-PWM).

2 TOPOLOGY OF THE MULTILEVEL INVERTER

2.1 Operational Principle

The (CMI) [66] generally consists of a certain number of inverters of full bridge types whose AC terminals are set in a series manner for synthesizing the desired output signal.

Fig. 1 represents the general diagram of the CMI, where each bridge is supplied by an individual dc voltage source. As per from Fig. 1, for an inverter of the m -level, the inverter of a full bridge has $[(m-1)/2]$ number which is joined in pattern of series, and also, the same value of the separate sources of the DC voltage is used. In this topology, $2(m-1)$ switching devices are used. CMI consists of less switching devices as compared to other multilevel inverter topologies.

2.1 Modulation Methodology of CMI

In this paper, the PWM method is used to produce the desired gate pulse for the switching devices. This method requires a fewer number of components and helps reduce the harmonics of a lower order. The harmonics of a higher order will be minimized by implementing filter circuits. Basically,

in the sinusoidal PWM technique, there are two signals, and one is the reference signal (sinusoidal signal) which is compared with a frequency of the higher range of the carrier signal (triangular signal), which generates the ON and OFF state. The magnitude of the voltage of output can be regulated by adjusting the modulation index (M). In the case of the inverter of the m -level, the triangular waves of $(m-1)$ numbers are compared with a sinusoidal wave.

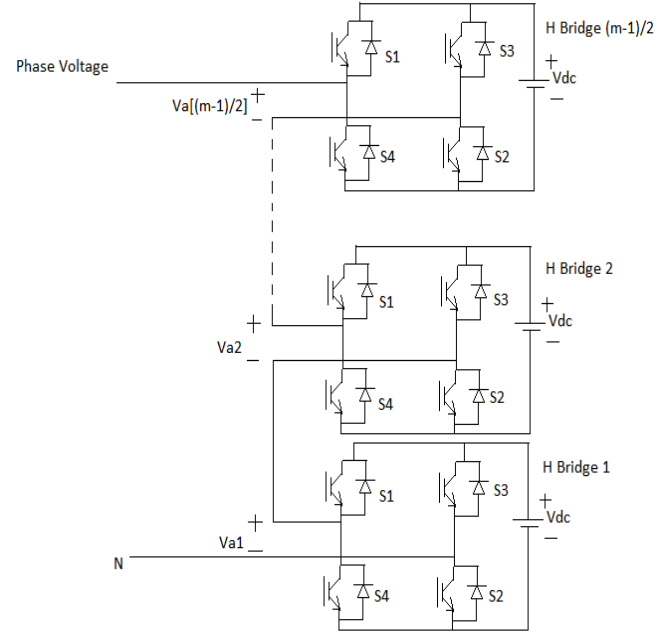


Figure 1 Basic structure of a CMI

3 METHODOLOGY

The operation of different multilevel inverters with different loads is done in the MATLAB Simulink. Among different multilevel inverters, the nine level inverter topology and its switching states are explained in Fig. 2 and Tab. 1 respectively. Fig. 2 represents 9-level multilevel inverters which have four individual bridges and are connected in a series, and four dc voltage sources are given to the individual bridge so that each bridge can be operated by single dc voltage. In this case, each dc voltage value is the same, i.e. 100 V.

In a similar manner, other multilevel inverter topologies and switching states can be verified.

In the case of the multilevel inverter, each level indicates a particular voltage level in a cycle. The multilevel inverter of a cascaded H-bridge type produces almost sinusoidal waveforms by increasing the level of voltages, and it can be implemented in HVDC systems, high power drives, SVC, renewable energy systems, traction drive systems, etc. It can be also used in variable speed drive induction motors that have a medium voltage range of an induction motor.

In the 9-level multilevel inverter, there is series connection of four numbers of full bridges that have a single phase [67]. The 9-level inverter has a voltage of output of nine values. These are: zero, V_{dc} , $2V_{dc}$, $3V_{dc}$, $4V_{dc}$, $-V_{dc}$, $-2V_{dc}$, $-3V_{dc}$, $-4V_{dc}$ [68], which is why it is called a 9-level

inverter. To get the output DC voltage V_{dc} , the semiconductor switches a, d, g, h, k, l, o, p should be turned ON. In this switching pattern, for getting a desired step voltage, there

should be eight semiconductor switches turned ON. Similarly, other voltage of output can also be computed by using the pattern of switching shown in Tab. 1.

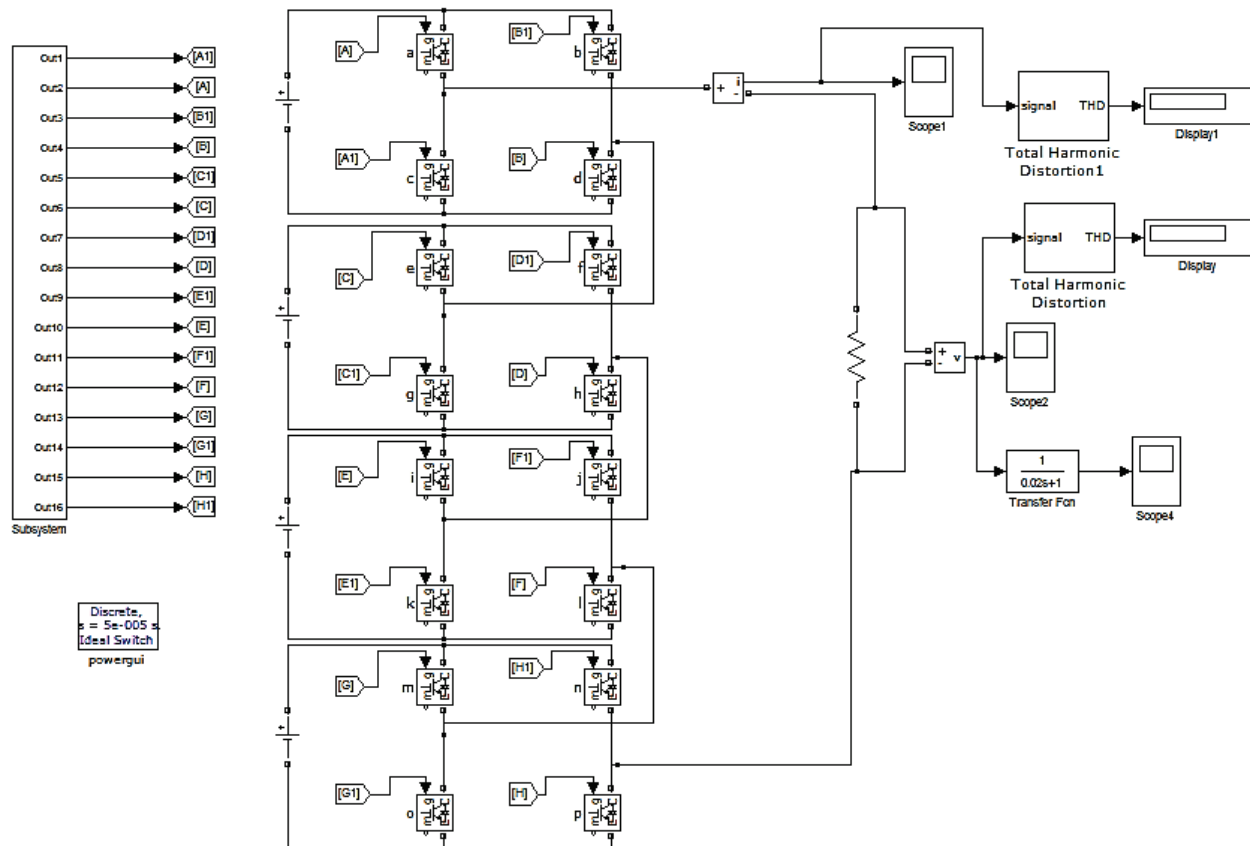


Figure 2 MATLAB model of a 9-level inverter

Table 1 The 9-level inverter switching states [72]

DC Voltage	a	b	c	d	e	f	g	h	i	j	k	l	m	n	o	p
0	0	0	0	0	0	0	0	0	0	0	0	0	0	0	0	0
V_{dc}	1	0	0	1	0	0	1	1	0	0	1	1	0	0	1	1
$2V_{dc}$	1	0	0	1	1	0	0	1	0	0	1	1	0	0	1	1
$3V_{dc}$	1	0	0	1	1	0	0	1	1	0	0	1	0	0	1	1
$4V_{dc}$	1	0	0	1	1	0	0	1	1	0	0	1	1	0	0	1
$3V_{dc}$	1	0	0	1	1	0	0	1	1	0	0	1	0	0	1	1
$2V_{dc}$	1	0	0	1	1	0	0	1	0	0	1	1	0	0	1	1
V_{dc}	1	0	0	1	0	0	1	1	0	0	1	1	0	0	1	1
0	0	0	0	0	0	0	0	0	0	0	0	0	0	0	0	0
$-V_{dc}$	0	1	1	0	1	1	0	0	1	1	0	0	1	1	0	0
$-2V_{dc}$	0	1	1	0	0	1	1	0	1	1	0	0	1	1	0	0
$-3V_{dc}$	0	1	1	0	0	1	1	0	0	1	1	0	1	1	0	0
$-4V_{dc}$	0	1	1	0	0	1	1	0	0	1	1	0	0	1	1	0
$-3V_{dc}$	0	1	1	0	0	1	1	0	0	1	1	0	1	1	0	0
$-2V_{dc}$	0	1	1	0	0	1	1	0	1	1	0	0	1	1	0	0
$-V_{dc}$	0	1	1	0	1	1	0	0	1	1	0	0	1	1	0	0
0	0	0	0	0	0	0	0	0	0	0	0	0	0	0	0	0

4 SIMULATION RESULTS

The simulations of different multilevel inverters, as discussed above, are computed through the MATLAB Simulation and the desired performances are verified. The THD is analysed for different multilevel inverters with different loads.

4.1 Phase – Shifted PWM Technique

In this method, the triangular waves will be phase displaced by a certain phase angle Φ_1 between the adjacent triangular waves. The phase angle Φ_1 can be calculated as per Eq. (1).

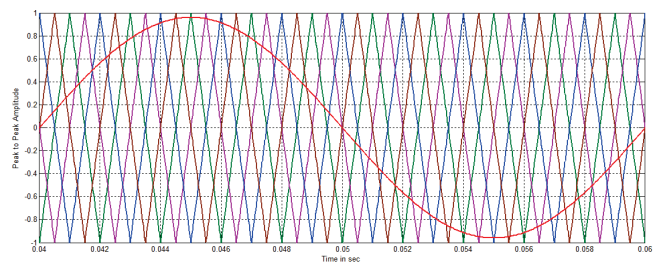


Figure 3 Simulation of a PWM topology

Fig. 3 represents the PWM method of a 5-level inverter, where the signal of a sinusoidal wave is compared with four high frequency triangular signals. It gives an idea of pulse generation for a 5-level inverter. It is produced by juxtaposing the sinusoidal signal with four high frequency carrier triangular signals. In a similar way, the gate pulse can be generated by juxtaposing a number of triangular waves with a sinusoidal reference wave for other multilevel

inverters. The harmonic spectrum present at the output voltage can be analysed through the FFT analysis. Fig. 4 represents the 3-level inverter's output voltage, and by carrying out the FFT analysis, the THD value is 56.13%. Fig. 5 shows a 5-level CMI whose THD value is 30.31%. Figure 6 shows a 7-level phase shift multilevel inverter whose THD value is 20.22%. Similarly, Figs. 7 shows a 9-level phase shift multilevel inverter, and by doing the FFT analysis, its THD value is 15.3%. As previously stated in the preceding figures, Fig. 8 shows an 11-level inverter that uses the phase shift modulation technique and generates the THD value of 13.21%.

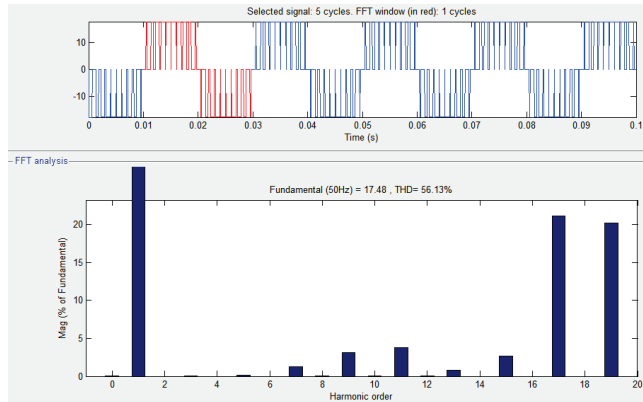


Figure 4 Output voltage's FFT analysis of a 3-level inverter [70, 71]

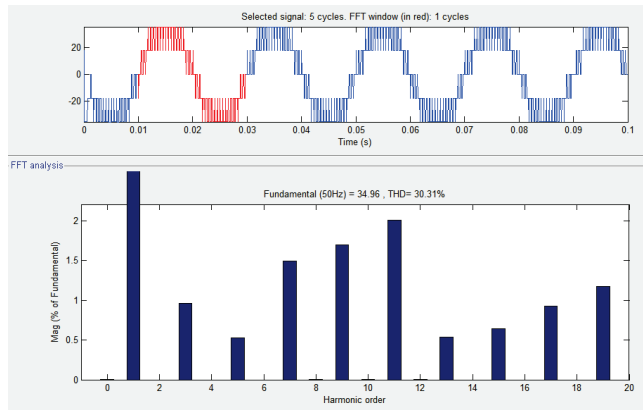


Figure 5 Output voltage's FFT analysis of a 5-level inverter [70, 71]

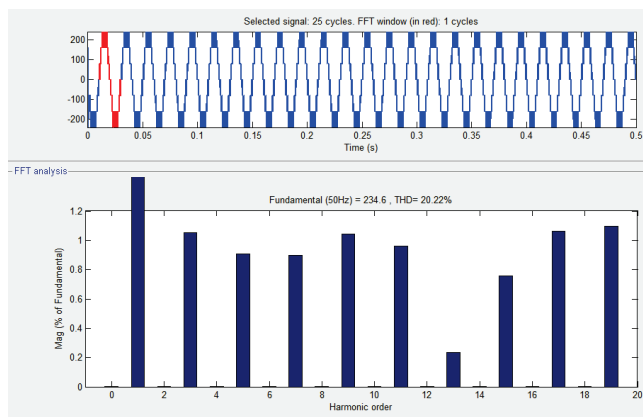


Figure 6 Output voltage's FFT analysis of a 7-level inverter [70, 71]

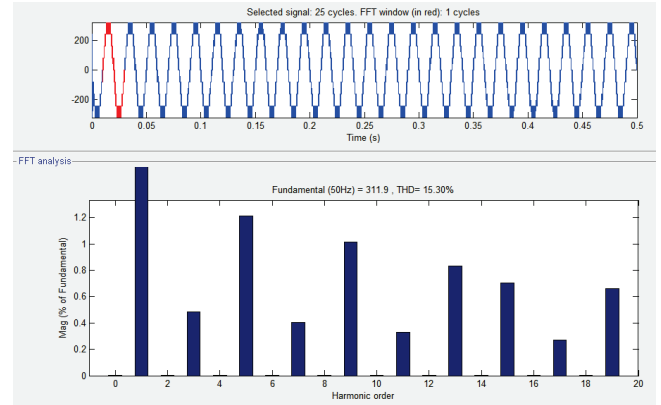


Figure 7 Output voltage's FFT analysis of a 9-level inverter [70, 71]

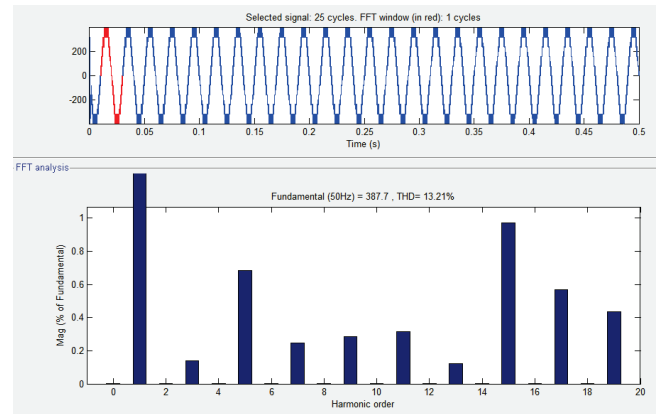


Figure 8 Output voltage's FFT analysis of an 11-level inverter [71]

4.2 Level-Shifted PWM Technique

In this case, there is a vertical shift of the triangular waves, and their peak to peak amplitude – including the frequency – is the same. There are mainly three types of strategies and they can be represented as: 1) in phase disposition (IPD) [72], 2) phase opposition disposition (POD) [72] and 3) alternate phase opposition disposition (APOD) [72] PWM technique.

4.2.1 IPD-PWM Technique

Carrier waves are here in [73] the same phase.

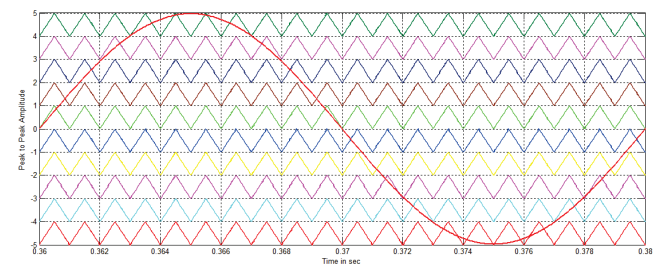


Figure 9 Gate pulse generation of an 11-level inverter [77]

Fig. 9 represents the gate pulse generated by comparing ten triangular waves with one sinusoidal wave, where each triangular wave has some magnitude for an in phase

disposition (IPD) PWM techniques of an 11-level multi-level inverter.

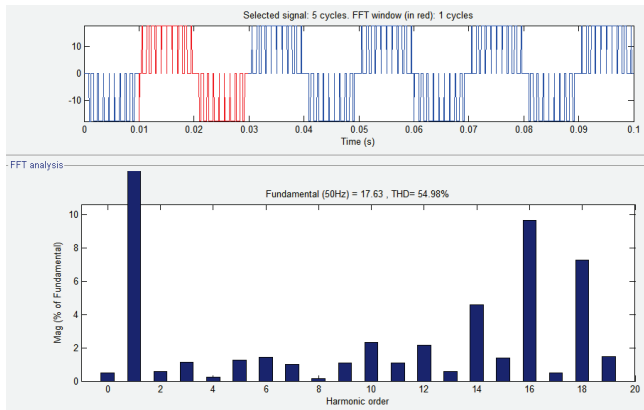


Figure 10 Output voltage's FFT analysis of a 3-level inverter [70, 71]

In a similar manner, the firing pulse can be generated for other multilevel inverter topologies. The harmonic quantity present in the output voltage can be evaluated through the FFT analysis. Fig. 10 represents the THD value of a 3-level inverter by doing the FFT analysis. The THD value is 54.98%. Fig. 11 represents the THD value of a 5-level inverter by using the IPD-PWM technique. The THD value is 28.75% by doing the FFT analysis.

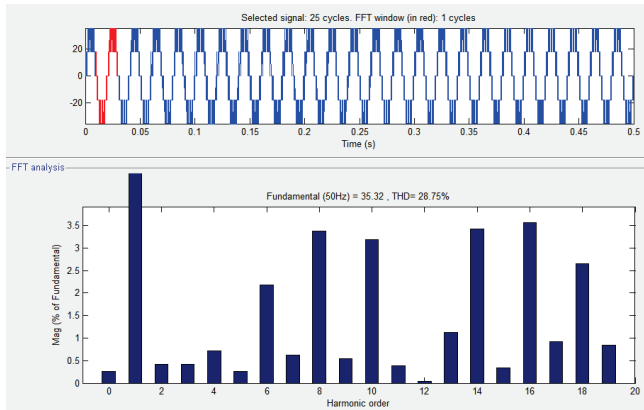


Figure 11 Output voltage's FFT analysis of a 5-level inverter [70, 71]

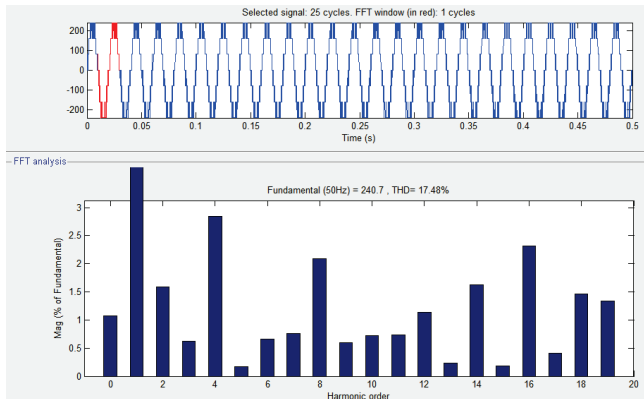


Figure 12 Output voltage's FFT analysis of a 7-level inverter [70, 71]

Fig. 12 represents the THD value of a 7-level inverter, which is 17.48% by doing the FFT analysis. Fig. 13

represents the THD value of a 9-level inverter, which is 14.4% by using the IPD technique. Fig. 14 represents the THD value of an 11-level inverter by implementing the IPD-PWM technique. Therefore, by doing the FFT analysis, the THD value is 11.11%.

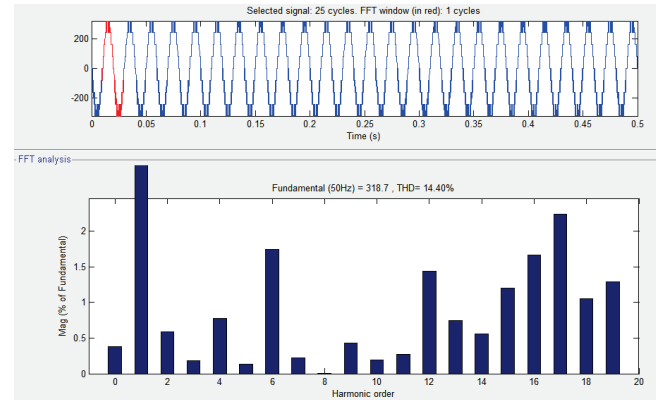


Figure 13 Output voltage's FFT analysis of a 9-level inverter [70, 71]

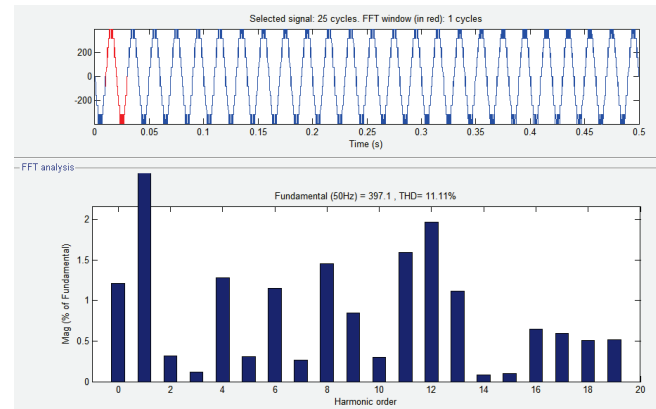


Figure 14 Output voltage's FFT analysis of an 11-level inverter [70, 71]

4.2.2 POD-PWM Technique

Here, all carrier [74] waves are in the same phase on the top and bottom sides of the zero reference and of the 180° phase displacement.

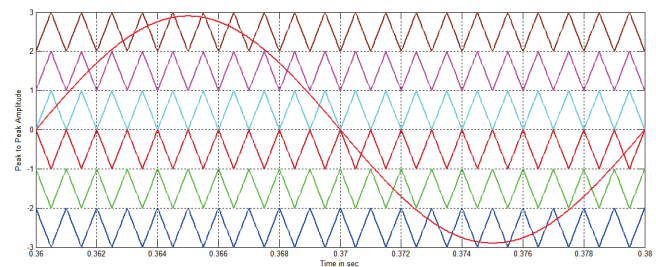


Figure 15 Gate pulse generation of a 7-level inverter [77]

Fig. 15 represents the gate pulse generation of a 7-level inverter by using the POD technique, where the firing angle is generated by comparing six high frequency triangular signals with a fundamental sinusoidal signal. In a similar way, the gate pulse can be generated for other inverters. The presences of harmonics in the output voltage are calculated

through the FFT analysis. Fig. 16 represents the THD of the output voltage of a 3-level inverter as 56.03% by doing the FFT analysis.

Similarly, Fig. 17 represents the THD value of a 5-level inverter, which is 30.63%. Fig. 18 represents the distortion value of the output voltage of a 7-level inverter, which is calculated as 18.12% through the FFT analysis. Fig. 19 represents the THD value of a 9-level inverter, which is 17.62%. Fig. 20 represents the output voltage's THD value of an 11-level inverter by using the POD-PWM technique and the THD value obtained by the FFT analysis is 11.40%.

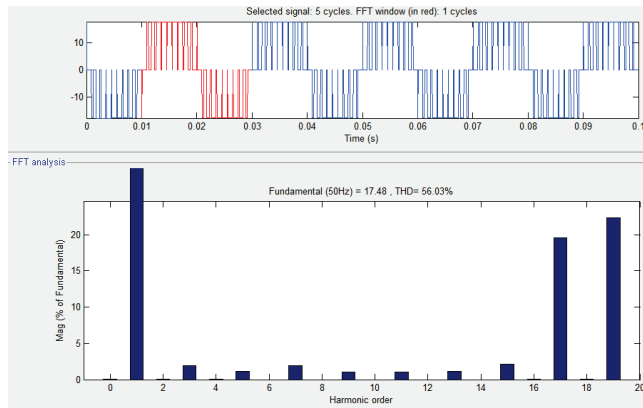


Figure 16 Output voltage's FFT analysis of a 3-level inverter [70, 71]

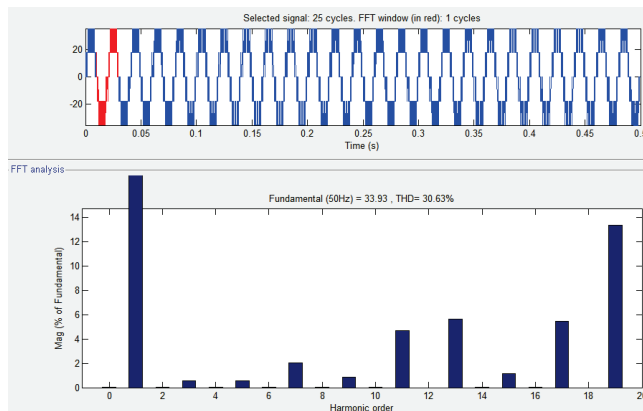


Figure 17 Output voltage's FFT analysis of a 5-level inverter [70, 71]

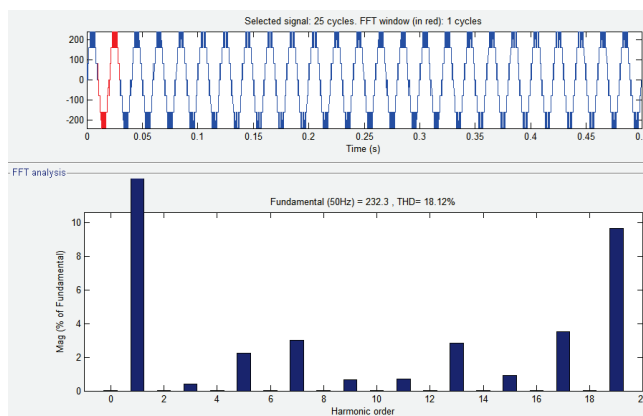


Figure 18 Output voltage's FFT analysis of a 7-level inverter [70, 71]

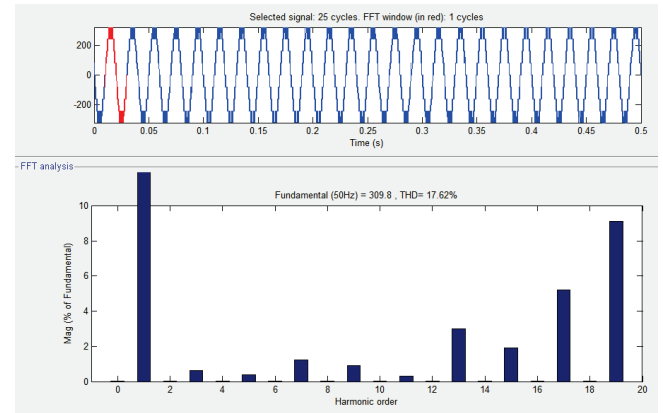


Figure 19 Output voltage's FFT analysis of a 9-level inverter [70, 71]

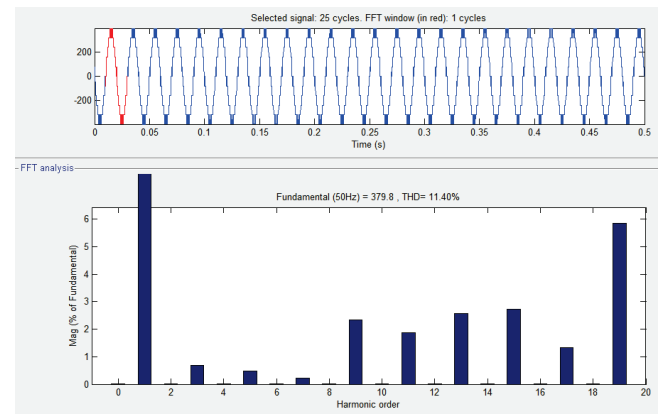


Figure 20 Output voltage's FFT analysis of an 11-level inverter [71]

4.2.3 APOD-PWM technique

Here, carrier waves are phase displaced by 180° alternately.

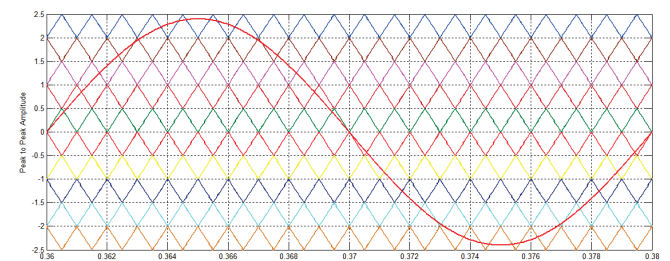


Figure 21 Gate pulse generation of an 11-level inverter [77]

Fig. 21 shows the firing angle generated by using the APOD technique of an 11-level inverter, where ten numbers of signals of high frequency are juxtaposed with a reference signal of the sinusoidal wave to get the desired gate pulse. Fig. 22 shows the THD value of a 3-level inverter, where the THD value is 58.33% by doing the FFT analysis. Fig. 23 represents the THD value of the output voltage of a 5-level inverter, which is 31.42% by using the APOD-PWM technique. Fig. 24 represents the distortion value of a 7-level inverter's output voltage, which is 19.77% by doing FFT analysis. Fig. 25 represents the percentage of the THD value of the output voltage of a 9-level inverter, which is 16.43%. Fig. 26 shows the THD value of the output voltage of an 11-

level inverter by using the APD-PWM technique, which is calculated as 12.29% through the FFT analysis.

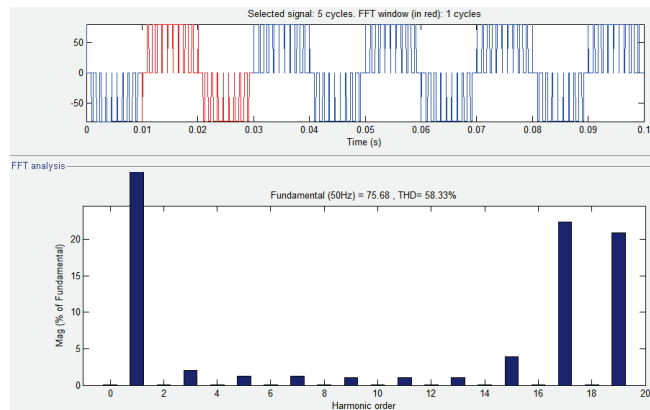


Figure 22 Output voltage's FFT analysis of a 3-level inverter [70, 71]

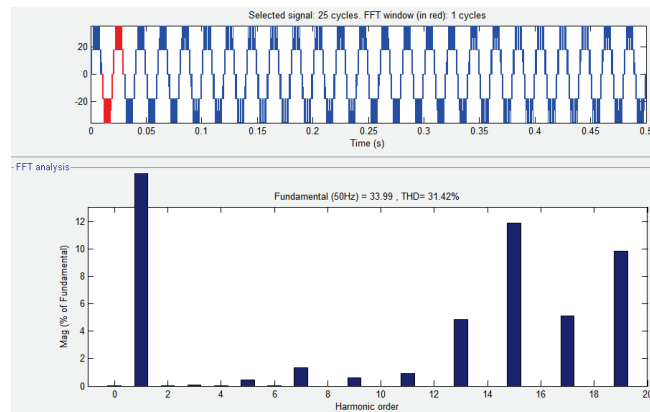


Figure 23 Output voltage's FFT analysis of a 5-level inverter [70, 71]

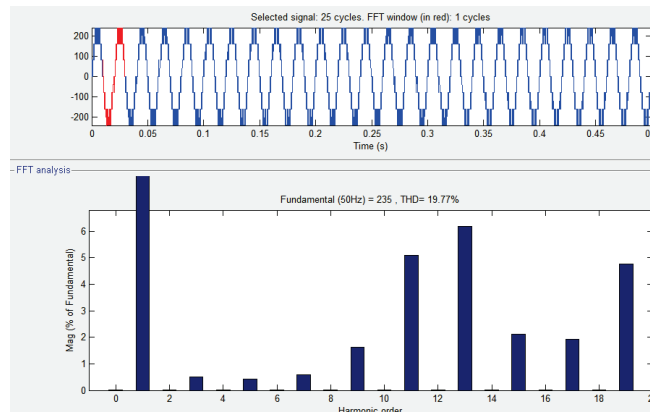


Figure 24 Output voltage's FFT analysis of a 7-level inverter [70, 71]

In the case of both the R-load and the R-L load, the harmonic quantity is the same at the output phase voltage. However, the THD value for current is different for both the R-load and the R-L load. In the case of the R-load, voltage and current are in same phase [76], which is why the THD value is same for both the phase voltage and output current.

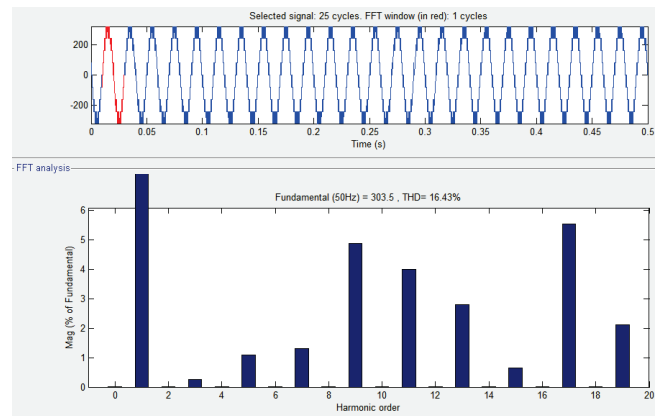


Figure 25 Output voltage's FFT analysis of a 9-level inverter [70, 71]

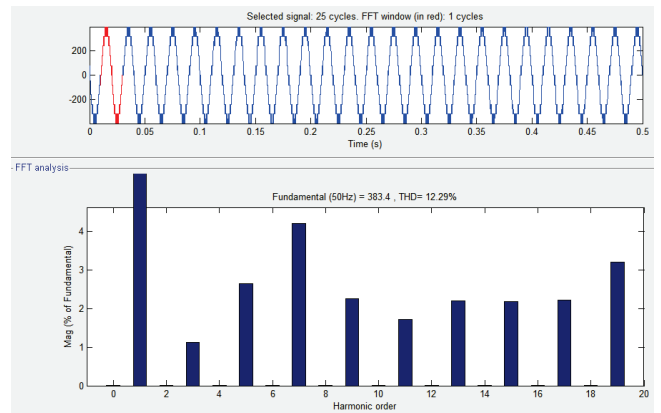


Figure 26 Output voltage's FFT analysis of an 11-level inverter [75]

Table 2 THD analysis of different multilevel inverters with an [75] R-load and without a filter [77]

Phase Voltage	IPD	POD	APD	Phase shifted (PS)
3 Level	54.98%	56.03%	58.34%	56.13%
5 Level	28.75%	30.63%	31.42%	30.31%
7 Level	17.48%	18.12%	19.77%	20.22%
9 Level	14.4%	17.62%	16.43%	15.3%
11 Level	11.11%	11.41%	12.3%	13.21%

Table 3 THD analysis of different multilevel inverters with an R-load and with a filter circuit [77]

Phase Voltage	IPD	POD	APD	Phase Shifted (PS)
3 Level	2.28%	2.36%	2.51%	2.34%
5 Level	1.35%	1.36%	1.38%	0.78%
7 Level	1.32%	1%	0.97%	0.53%
9 Level	0.76%	0.83%	0.95%	0.37%
11 Level	0.67%	0.65%	1%	0.23%

Table 4 THD analysis of different multilevel inverters with an R-L load and without a filter [77]

Output Current	IPD	POD	APD	Phase Shifted (PS)
3 Level	2.68%	2.83%	3%	2.73%
5 Level	1.64%	1.63%	1.67%	1%
7 Level	1.59%	1.23%	1.21%	0.76%
9 Level	1%	1.06%	1.19%	0.62%
11 Level	0.9%	0.87%	1.27%	0.52%

5 CONCLUSION

This paper focuses on seven, nine, and eleven-level multilevel inverters, in addition to three and five-level multilevel inverters with different loads. By analysing the THD value for different multilevel inverters, it has been concluded that by increasing the level number, the %THD value decreases. Harmonics can further be decreased by using the appropriate filter circuit. It is observed that among all simulated multilevel inverters discussed in this paper, the cascaded 11-level multilevel inverter with the IPD modulation technique gives a better THD result at the output phase voltage. The computation of the generation of a signal in the IPD modulation is simpler than other discussed modulations. The harmonics present in the output current in the case of the R-L load can also be minimized by increasing the number of levels. It can also be further decreased by implementing a compatible filter circuit. The multilevel inverter reduces the THD value to large extents, hence why the filter size is also reduced. The multilevel inverter can be implemented where the quality of the output is the primary need.

6 REFERENCES

- [1] Barbie, E., Rabinovici, R., & Kuperman, A. (2019). Closed-Form Analytic Expression of Total Harmonic Distortion in Single-Phase Multilevel Inverters with Staircase Modulation. *IEEE Transactions on Industrial Electronics*, 67(6), 5213-5216. <https://doi.org/10.1109/TIE.2019.2922934>
- [2] Rodriguez, J., Lai, J. S., & Peng, F. Z. (2002). Multilevel inverters: a survey of topologies, controls, and applications. *IEEE Trans. Ind. Electron.*, 49(4), 724-738. <https://doi.org/10.1109/TIE.2002.801052>
- [3] Rodriguez, J., Franquelo, L. G., Kouro, S., Leon, J. I., Portillo, R. C., & Martin, M. A. (2009). Multilevel converters: An enabling technology for high power applications. *Proc. IEEE*, 97(11), 1786-1817. <https://doi.org/10.1109/JPROC.2009.2030235>
- [4] Rodriguez, J., Bernet, S., Wu, B., Pontt, J. O., & Kouro, S. (2007). Multilevel voltage-source-converter topologies for industrial medium-voltage drives. *IEEE Trans. Ind. Electron.*, 54(6), 2930-2945. <https://doi.org/10.1109/TIE.2007.907044>
- [5] Holmes, D. G., & Lipo, T. A. (2003). Pulse width modulation for power converters: Principles and practice. *IEEE Press*. <https://doi.org/10.1109/9780470546284>
- [6] Patel, H. S., & Hoft, R. G. (1973). Generalized harmonic elimination and voltage control in thyristor converters: Part I—Harmonic elimination. *IEEE Trans. Ind. Appl.*, IA-9(3), 310-317. <https://doi.org/10.1109/TIA.1973.349908>
- [7] Patel, H. S., & Hoft, R. G. (1974). Generalized harmonic elimination and voltage control in thyristor converters: Part II—Voltage control technique. *IEEE Trans. Ind. Appl.*, IA-10(5), 666-673. <https://doi.org/10.1109/TIA.1974.349239>
- [8] Buccella, C., Cecati, C., Cimatorini, M. G., & Razi, K. (2014). Analytical Method for Pattern Generation in Five-Level Cascaded H-Bridge Inverter Using Selective Harmonic Elimination. *IEEE Transactions on Industrial Electronics*, 61(11), 5811-5819. <https://doi.org/10.1109/TIE.2014.2308163>
- [9] Napoles, J., Watson, A., Padilla, J., Leon, J., Franquelo, L., Patrick, W., & Aguirre, M. (2013). Selective harmonic mitigation technique for cascaded H-bridge converters with non-equal DC link voltages. *IEEE Trans. Ind. Electron.*, 60(5), 1963-1971. <https://doi.org/10.1109/TIE.2012.2192896>
- [10] Napoles, J., Leon, J. I., Portillo, R., Franquelo, L. G., & Aguirre, M. A. (2010). Selective harmonic mitigation technique for high-power converters. *IEEE Trans. Ind. Electron.*, 57(7), 2315-2323. <https://doi.org/10.1109/TIE.2009.2026759>
- [11] Franquelo, L. G., Napoles, J., Portillo, R., Leon, J. I., & Aguirre, M. A. (2007). A flexible selective harmonic mitigation technique to meet grid codes in three-level PWM converters. *IEEE Trans. Ind. Electron.*, 54(6), 3022-3029. <https://doi.org/10.1109/TIE.2007.907045>
- [12] Gopakumar, K., Azeez, N. A., Mathew, J., Dey, A., & Kazmierkowski, M. (2014). A medium voltage inverter fed IM drive using multilevel 12-sided polygonal vectors, with nearly constant switching frequency current hysteresis controller. *IEEE Trans. Ind. Electron.*, 61(4), 1700-1709. <https://doi.org/10.1109/TIE.2013.2266083>
- [13] Sanzhong, B., & Lukic, S. M. (2013). New method to achieve AC harmonic elimination and energy storage integration for 12-pulse diode rectifiers. *IEEE Trans. Ind. Electron.*, 60(7), 2547-2554. <https://doi.org/10.1109/TIE.2012.2196903>
- [14] Filho, F., Maia, H. Z., Mateus, T. H. A., Ozpineci, B., Tolbert, L. M., & Pinto, J. O. P. (2013). Adaptive selective harmonic minimization based on ANNs for cascade multilevel inverters with varying DC sources. *IEEE Trans. Ind. Electron.*, 60(5), 1955-1962. <https://doi.org/10.1109/TIE.2012.2224072>
- [15] Pulikanti, S. R., Konstantinou, G., & Agelidis, V. G. (2013). Hybrid seven-level cascaded active neutral-point-clamped-based multilevel converter under SHE-PWM. *IEEE Trans. Ind. Electron.*, 60(11), 4794-4804. <https://doi.org/10.1109/TIE.2012.2218551>
- [16] Guzman, J. I., Melin, P. E., Espinoza, J. R., Moran, L. A., Baier, C. R., Munoz, J. A., & Guinez, G. A. (2013). Digital implementation of selective harmonic elimination techniques in modular current source rectifiers. *IEEE Trans. Ind. Informat.*, 9(2), 1167-1177. <https://doi.org/10.1109/TII.2012.2210232>
- [17] Lai, J. S., & Peng, F. Z. (1996). Multilevel converters—A new breed of power converters. *IEEE Trans. Ind. Appl.*, 32(3), 509-517. <https://doi.org/10.1109/28.502161>
- [18] Chikondra, B., Muduli, U. R., Behera, R. K. (2020). Performance comparison of Five-phase three-level NPC to Five-phase Two-level VSI. *IEEE Transactions on Industry Applications*, 56(4), 3767-3775. <https://doi.org/10.1109/TIA.2020.2988014>
- [19] Bose, B. K., & Sutherland, H. A. (1983). A high-performance pulse width modulator for an inverter-fed drive system using a micro computer. *IEEE Trans. Ind. Appl.*, IA-19(2), 235-243. <https://doi.org/10.1109/TIA.1983.4504187>
- [20] Das, S., Narayanan, G., & Pandey, M. (2014). Space-vector-based hybrid pulse width modulation techniques for a three-level inverter. *IEEE Trans. Power Electron.*, 29(9), 4580-4591. <https://doi.org/10.1109/TPEL.2013.2287095>
- [21] Iqbal, A. & Levi, E. (2005). Space vector modulation schemes for a five phase voltage source inverter. In *2005 European Conference on Power Electronics and Applications*, 1-12. <https://doi.org/10.1109/EPE.2005.219194>
- [22] Lopez, O., Alvarez, J., Gandoy, J. D., & Freijedo, F. D. (2009). Multilevel multiphase space vector PWM algorithm with switching state redundancy. *IEEE Trans. Ind. Electron.*, 56(3), 792-804. <https://doi.org/10.1109/TIE.2008.2004390>
- [23] Dujic, D., Jones, M., & Levi, E. (2009). Analysis of output current ripple RMS in multiphase drives using space vector approach. *IEEE Trans. Power Electron.*, 24(8), 1926-1938. <https://doi.org/10.1109/TPEL.2009.2017746>
- [24] Gao, L., & Fletcher, J. E. (2010). A space vector switching strategy for three level five-phase inverter drives. *IEEE Trans. Ind. Electron.*, 57(7), 2332-2343.

- <https://doi.org/10.1109/TIE.2009.2033087>
- [25] Bharatiraja, C., Jeevananthan, S., & Munda, J. L. (2018). A timing correction algorithm-based extended SVM for three-level neutral-point-clamped MLI in over modulation zone. *IEEE J. Emerg. Sel. Top. Power Electron.*, 6(1), 233-245. <https://doi.org/10.1109/JESTPE.2017.2723518>
- [26] Liu, Z., Zheng, Z., Sudhoff, S. D., Gu, C., & Li, Y. (2016). Reduction of common-mode voltage in multiphase two-level inverters using SPWM with phase-shifted carriers. *IEEE Trans. Power Electron.*, 31(9), 6631-6645. <https://doi.org/10.1109/TPEL.2015.2499380>
- [27] Dordevic, O., Jones, M., & Levi, E. (2013). A comparison of carrier-based and space vector PWM techniques for three-level five-phase voltage source inverters. *IEEE Trans. Ind. Informat.*, 9(2), 609-619. <https://doi.org/10.1109/TII.2012.2220553>
- [28] K. K. N. & Sivakumar, K. (2015). A quad two-level inverter configuration for four-pole induction-motor drive with single DC link. *IEEE Trans. Ind. Electron.*, 62(1), 105-112. <https://doi.org/10.1109/TIE.2014.2327577>
- [29] Tan, C., Xiao, D., Fletcher, J. E., & Rahman, M. F. (2016). Analytical and experimental comparison of carrier-based PWM methods for the five-phase coupled-inductor inverter. *IEEE Trans. Ind. Electron.*, 63(12), 7328-7338. <https://doi.org/10.1109/TIE.2016.2592860>
- [30] Farokhnia, N., Vadizadeh, H., Fathi, S., & Anvariasl, F. (2011). Calculating the formula of line-voltage thd in multilevel inverter with unequal dc sources. *IEEE Transactions on Industrial Electronics*, 58(8), 3359-3372. <https://doi.org/10.1109/TIE.2010.2089938>
- [31] Dagan, K. J., & Rabinovici, R. (2015). Criteria- Based Modulation for Multilevel Inverters. *IEEE Transactions on Power Electronics*, 30(9), 5009-5018. <https://doi.org/10.1109/TPEL.2014.2362171>
- [32] Lai, Y. S., Chen, P. S., Lee, H. K., & Chou, J. (2004). Optimal common-mode voltage reduction PWM technique for inverter control with consideration of the dead-time effects-part ii: applications to IM drives with diode front end. *IEEE Transactions on Industry Applications*, 40(6), 1613-1620. <https://doi.org/10.1109/TIA.2004.836151>
- [33] IEEE Recommended Practices and Requirements for Harmonic Control in Electrical Power Systems, *IEEE Std 519-1992*.
- [34] Dahidah, M., Konstantinou, G., Flourentzou, N., & Agelidis, V. (2010). On comparing the symmetrical and non-symmetrical selective harmonic elimination pulse-width modulation technique for two-level three-phase voltage source converters. *IET Power Electronics*, 3(6), 829-842. <https://doi.org/10.1049/iet-pel.2009.0306>
- [35] Hava, A. M. & Üm, E. (2011). A high-performance PWM algorithm for common-mode voltage reduction in three-phase voltage source inverters. *IEEE Transactions on Power Electronics*, 26(7), 1998-2008. <https://doi.org/10.1109/TPEL.2010.2100100>
- [36] Das, S., & Narayana, G. (2012). Novel switching sequences for a space-vector modulated three-level inverter. *IEEE Transactions on Industrial Electronics*, 59(3), 1477-1487. <https://doi.org/10.1109/TIE.2011.2163373>
- [37] Bhagwat, P. M. & Stefanovic, V.R. (1983). Generalized structure of a multilevel PWM inverter. *IEEE Trans. Ind. Appl.*, IA-19(6), 1057-1069. <https://doi.org/10.1109/TIA.1983.4504335>
- [38] Nabae, A., Takahashi, I., & Akagi, H. (1981). A new neutral-point-clamped PWM inverter. *IEEE Trans. Ind. Appl.*, IA-17(5), 518-523. <https://doi.org/10.1109/TIA.1981.4503992>
- [39] Fei, W., Du, X., & Wu, B. (2010). A generalized half-wave symmetry SHE-PWM formulation for multilevel voltage inverter. *IEEE Trans. Ind. Electron.*, 57(9), 3030-3038. <https://doi.org/10.1109/TIE.2009.2037647>
- [40] Zhang, Y., Zhao, Z., & Zhu, J. (2011). A hybrid PWM applied to high power three-level inverter-fed induction motor drives. *IEEE Trans. Ind. Electron.*, 58(8), 3409-3420. <https://doi.org/10.1109/TIE.2010.2090836>
- [41] Carrara, G., Gardella, S., Marchesoni, M., Salutati, R., & Sciutto, G. (1992). A new multilevel PWM method: A theoretical analysis. *IEEE Trans. Power Electron.*, 7(3), 497-505. <https://doi.org/10.1109/63.145137>
- [42] McGrath, B. P. & Holmes, D. G. (2002). Multicarrier PWM strategies for multilevel inverters. *IEEE Trans. Ind. Electron.*, 49(4), 858-867. <https://doi.org/10.1109/TIE.2002.801073>
- [43] Banerjee, D., Ghosh, R., Narayanan, G., & Ranganathan, V. T. (2005). Comparison of various sine-triangle PWM techniques for three level voltage source inverters in space vector domain. *In Proc. NPEC, IIT Kharagpur, West Bengal, India, Dec. 2005*.
- [44] Wang, F. (2002). Sine-triangle vs. space vector modulation for three-level PWM voltage source inverters, *IEEE Trans. Ind. Appl.*, 38(2), 500-506. <https://doi.org/10.1109/28.993172>
- [45] Yao, W. X., Hu, H. B., & Lu, Z. Y. (2008). Comparisons of space-vector modulation and carrier-based modulation of multilevel inverter. *IEEE Trans. Power Electron.*, 23(1), 45-51. <https://doi.org/10.1109/TPEL.2007.911865>
- [46] Pereira, I. & Martins, A. (2009). Multicarrier and space vector modulation for three-phase NPC converters: A comparative analysis. *In Proc. 13th EPE, Barcelona, Spain, Sep. 2009*, 9, 2435-2444.
- [47] Franquelo, L. G., Rodriguez, J., Leon, J. I., Kouro, S., Portillo, R., & Prats, M. A. (2008). The age of multilevel converters arrives. *IEEE industrial electronics magazine*, 2. <https://doi.org/10.1109/MIE.2008.923519>
- [48] Wu, F., Li, X., Feng, F., & Gooi, H. B. (2017). Multi-topology-Mode Grid Connected Inverter to Improve Comprehensive Performance of Renewable Energy Source Generation System. *IEEE Transactions on Power Electronics*, 32, 3623-3633. <https://doi.org/10.1109/TPEL.2016.2589974>
- [49] Xiao, B., Hang, L., Mei, J., Riley, C., Tolbert, L. M. & Ozpineci, B. (2015). Modular cascaded H-bridge multilevel PV inverter with distributed MPPT for grid-connected applications. *IEEE Transactions on Industry Applications*, 51, 1722-1731. <https://doi.org/10.1109/TIA.2014.2354396>
- [50] Vahedi, H., Sharifzadeh, M., & Al-Haddad, K. (2018). Modified Seven Level Pack U-Cell Inverter for Photovoltaic Applications. *IEEE Journal of Emerging and Selected Topics in Power Electronic*, 6(3), 1508-1516. <https://doi.org/10.1109/JESTPE.2018.2821663>
- [51] Vahedi, H., P.-A. Labbé, P. A., & Al-Haddad, K. (2016). Sensor-Less Five-Level Packed U-Cell (PUC5) Inverter Operating in Stand-Alone and Grid Connected Modes. *IEEE Transactions on Industrial Informatics*, 12, 361-370. <https://doi.org/10.1109/TII.2016.2578183>
- [52] Elias, M. F. M., Rahim, N. A., Ping, H. W., & Uddin, M. N. (2014). Asymmetrical cascaded multilevel inverter based on transistor clamped H-bridge power cell. *IEEE Transactions on Industry Applications*, 50, 4281-4288. <https://doi.org/10.1109/TIA.2014.2346711>
- [53] Sharifzadeh, M., Vahedi, H., Al-Haddad, K. (2018). New Constraint in SHE-PWM for Single Phase Inverter Applications. *IEEE Transactions on Industry Applications*, 54(5), 4554-4562. <https://doi.org/10.1109/TIA.2018.2831177>
- [54] Vahedi, H. & Al-Haddad, K. (2016). Real-time implementation of a seven level packed u-cell inverter with a low-switching-frequency voltage regulator. *IEEE Transactions on Power Electronics*, 31, 5967-5973. <https://doi.org/10.1109/TPEL.2015.2490221>
- [55] Edpuganti, A. & Rathore, A. K. (2015). Fundamental switching frequency optimal pulswidth modulation of medium-voltage

- cascaded sevenlevel inverter. *IEEE Transactions on Industry Applications*, 51, 3485-3492.
<https://doi.org/10.1109/TIA.2015.2394485>
- [56] Vahedi, H., Sharifzadeh, M., & Al-Haddad, K. (2017). Topology and control analysis of single-DC-source five-level packed U-cell inverter (PUC5). in *Industrial Electronics Society, IECON 2017-43rd Annual Conference of the IEEE*, 8691-8696. <https://doi.org/10.1109/IECON.2017.8217527>
- [57] Yang, K., Chen, L., Zhang, J., Hao, J., & Yu, W. (2016). Parallel resultant elimination algorithm to solve the selective harmonic elimination problem. *IET Power Electronics*, 9, 71-80. <https://doi.org/10.1049/iet-pel.2015.0070>
- [58] Dahidah, M. S., Konstantinou, G., & Agelidis, V. G. (2015). A review of multilevel selective harmonic elimination PWM: formulations, solving algorithms, implementation and applications. *IEEE Transactions on Power Electronics*, 30, 4091-4106. <https://doi.org/10.1109/TPEL.2014.2355226>
- [59] Wang, J. & Ahmadi, D. (2010). A precise and practical harmonic elimination method for multilevel inverters. *IEEE transactions on industry applications*, 46, 857-865.
<https://doi.org/10.1109/TIA.2010.2041620>
- [60] Yang, K., Zhang, Q., Zhang, J., Yuan, R., Guan, Q., & Yu, W. (2017). Unified selective harmonic elimination for multilevel converter. *IEEE Transactions on Power Electronics*, 32, 1579-1590. <https://doi.org/10.1109/TPEL.2016.2548080>
- [61] Can, E. (2018). Analysis and performance with vertical divided multilevel voltage on phase of induction engine. *Tehnički vjesnik*, 25(3), 687-693.
<https://doi.org/10.17559/TV-20170425110919>
- [62] Can, E. (2018). The modeling and analysis of a power transmission line supplied by a solar power plant. *Tehnički glasnik*, 12(3), 124-130.
<https://doi.org/10.31803/tg-20180521111744>
- [63] Khamooshi, R., & Namadmalan, A. (2016). Converter Utilization Ratio Assessment for THD Optimization in Cascaded H-Bridge Multi-level Inverters. *IET Power Electronics*, 9(10). <https://doi.org/10.1049/iet-pel.2015.0787>
- [64] Solanki, V. K., Hoang, M. K., Lu, Z., & Pattnaik, P. K. (Eds.). (2020). Intelligent Computing in Engineering. *Springer Science and Business Media LLC*.
<https://doi.org/10.1007/978-981-15-2780-7>
- [65] Das, K. N., Bansal, J. C., Deep, K., Nagar, A. K., Pathipooranam, P., & Naidu, R. C. (Eds.). (2020). Soft Computing for Problem Solving. *Springer Science and Business Media LLC*.
<https://doi.org/10.1007/978-981-15-0184-5>
- [66] Gholinezhad, J. & Noroozian, R. (2012). Application of cascaded H-bridge multilevel inverter in DTC-SVM based induction motor drive. *3rd Power Electronics and Drive Systems Technology (PEDSTC)*, 2012.
<https://doi.org/10.1109/PEDSTC.2012.6183311>
- [67] Angulo, M., Lezana, P., Kouro, S., Rodriguez, J., & Wu, B. (2007). Level-shifted PWM for Cascaded Multilevel Inverters with Even Power Distribution. *IEEE Power Electronics Specialists Conference*, 2007.
<https://doi.org/10.1109/PESC.2007.4342382>
- [68] Biju, K. & Ramchand, R. (2018). Control strategy for single phase cascaded nine-level inverter with sinusoidal pulse width modulation using LPC 1769 ARM cortex-M3 Microcontroller. *International Journal of Power Electronics, Inder Science Publishers*, 9(4), 349-365.
<https://doi.org/10.1504/IJPELEC.2018.095081>
- [69] Payami, S., Behera, R. K., Iqbal, A., & Al-Ammari, R. (2015). Common-Mode Voltage and Vibration Mitigation of a Five-Phase Three-Level NPC Inverter-Fed Induction Motor Drive System. *IEEE Journal of Emerging and Selected Topics in Power Electronics*, 3(2), 349-361.
<https://doi.org/10.1109/JESTPE.2014.2313153>
- [70] Bhanutej, J. N. & Naidu, R. C. (2020). A 7-level Inverter with Multi-Carrier Pulse Width Modulation Technique for PV Systems. *International Journal of Innovative Technology and Exploring Engineering (IJITEE)*, 9(4), 2818-2822.
<https://doi.org/10.35940/ijitee.C8543.029420>
- [71] Kumar, K. S., Edward, J. B., Chimonyo, K., & Rushambwa, M. C. (2018). Implementation of Single Phase Cascaded H-Bridge Nine Level Inverter and Simulation Study with PI Controller. *International Conference on Smart Grid and Clean Energy Technologies (ICSGCE)*, 2018.
- [72] Sundar, R., Gnanavel, C., & Muthukumar, P. (2019). A Unique Single Source Nine Level Inverter with Reduced Switching Devices for Single Phase AC Applications. *International Journal of Engineering and Advanced Technology (IJEAT)*, 9(2), 4098-4101. <https://doi.org/10.35940/ijeat.B4953.129219>
- [73] Manjesh, Ananda, A. S., Bhoi, A. K., & Sherpa, K. S. (2018). Evaluation of harmonics and THD in Five-phase inverter constructed with high-pass filter by MATLAB Simulation. *Advances in Systems, Control and Automation", Springer Science and Business Media LLC*.
https://doi.org/10.1007/978-981-10-4762-6_1
- [74] Teja, R. R., Sateesh, C., & Chowdari, M. A. (2016). Single Phase 9- Level Symmetrical Cascaded H-Bridge Inverter for different PWM techniques. *International Conference on Electrical Power and Energy Systems (ICEPES), IEEE Conference, 2016*. <https://doi.org/10.1109/ICEPES.2016.7915972>
- [75] Puse, P. B. & Bhasme, N. R. (2020). Performance Analysis of Three Phase Multilevel Inverter with SPWM Techniques used in Railway System. *International Journal of Engineering and Advanced Technology (IJEAT)*, 9(3), 2964-2971.
<https://doi.org/10.35940/ijeat.A1449.029320>
- [76] Chakraborty, S., Reza, S. M. S., Hasan, W., & Abdur Razzak, M. (2015). Design of a transformer-less single switch-mode photovoltaic grid-connected boost inverter with immittance conversion topology. *IEEE Innovative Smart Grid Technologies - Asia (ISGT ASIA)*, 2015.
<https://doi.org/10.1109/ISGT-Asia.2015.7387189>
- [77] Sahu, M. K., Biswal, M., Jena, R. K., & Malla, J. M. R. (2020). Simulation of different levels of multilevel inverter using Cascaded H-Bridge for various loads. *TEST Engineering & Management*, 83(May-June 2020), 7527-7535.
- [78] Malarvizhi, M. & Gnanambal, I. (2014). Harmonics elimination in multilevel inverter with unequal DC sources by fuzzy-ABC algorithm. *Journal of Experimental & Theoretical Artificial Intelligence*, 27(3), 1-20.
<https://doi.org/10.1080/0952813X.2014.930596>

Authors' contacts:

Manoj Kumar Sahu, Associate Professor, PhD
 (Corresponding Author)
 Department of Electrical Engineering,
 Centre for Advanced Post Graduate Studies,
 BPUT, Chhend Campus, Rourkela, Odisha-769015, India
 +91-9437225468,
 E-mail: capgs.mksahu@bput.ac.in

Madhusmita Biswal, Mrs., Assistant Training Officer
 Government ITI Berhampur,
 Berhampur, Odisha-769015, India

Jagan Mohana Rao Malla, Mr., Assistant Professor
 Department of Electronics and Communication Engineering,
 Rishi Institute of Engineering and Technology for Woman,
 Kukatpally, Hyderabad-500090, India
 E-mail: nitya5311@gmail.com

The Importance of SD Goals Indicators 7, 8, 9 and 12 in the Industry Development by Using Multi Criteria and Decision Making Method

Fisnik Osmani, Atanas Kochov*, Betim Shabani, Mirjeta Ilazi

Abstract: Sustainable Development and Decision Making are just two of the many processes that affect the industry sector. SDG7, SDG8, SDG9 and SDG 12 as four goals of sustainable development show the indicators we have to deal with, given that the energy, industry, economy and production are closely connected. This research focuses on promoting sustainable development in the industry, by testing very important indicators using the MCDM method. Our analysis was carried out with the help of a multi-criteria decision-making method - the Hierarchical Analytical Process. Through this method, we have identified specific areas that need improvement, the importance of the indicators separately, ranking so by their importance and impact in the industry, economy and production.

Keywords: decision-making; energy; industry; MCDM; sustainable development

1 INTRODUCTION

Energy is a vital need for a functioning society. Add here the economic development, the need for foreign investment, consumption, and production – all members of the system that have a significant impact on sustainable development in the industry.

Developing countries are trying to improve their standard of living through industrialization. In this regard, it is important to analyze the indicators that have an impact on improving the overall situation, and this can be done based on the Sustainable Development Goals (SDG 17). This, in fact, is the focus of this paper – to figure the relevance of each factor based on scientific methods of decision-making and on expert opinion (based on interviews with twenty experts). Most countries in the Western Balkans region face similar issues and thus a thorough analysis can bring a solution that can serve and be applied to all [1].

Since the fact that the process of monitoring regional industrial sustainability could be rather difficult, due to the many stakeholders and objectives, empirical literature has proposed a variety of indicators for the assessment of the industrial sustainability, including social, economic, and environmental determinants [2].

One of the most important indicators, especially when talking about sustainable development, is the investment indicator, which is of great importance in our analysis. To deal with decision making for different kinds of problems and try to solve them is difficult even more if there is a need to obtain information from a group of decision-makers [3]. Therefore, especially in the recent years, the need to improve sustainability in industrial activities has increased the interest of policy-makers and industrial decision-makers (IDMs). Even if firms started to include sustainability at a strategic level, current modes of production cannot be considered sustainable, and significant changes are needed at a technological, managerial, organizational, and behavioral level [4].

One of the most important goals is the economic development in the industrial sector, particularly in developing countries [5] where it should be maintained and needs to be taken into consideration, as required by the nature of sustainable development.

Given the factual situation, we have analyzed the possibility of applying the indicators according to SDG7-SDG8-SDG9 and SDG12 in theoretical terms, thus achieving results/solutions to guarantee the participation of clean energy factors, innovation and infrastructure, as more important elements for sustainable development.

2 CONSIDERABLE INDICATORS IN THE DECISION-MAKING ANALYSIS

SDG's, especially in the industry, are closely related to Clean and Sustainable Energy, Investment, Work and Economy Growth, Consumption and Production (Fig. 1). Based only on the broader meaning of these two purposes by the UN, we conclude that sustainable development in the industry has to do with the idea that all requirements that we have towards the environment can be met without harming the opportunities of others but by improving the situation for future generations.

We have come to a situation where we need to understand the importance of incorporating indicators from SDG7- SDG8-SDG9 and SDG12 where vital/key issues for sustainable development in the industry are touched upon. Therefore, in order to define key indicators for sustainable development in the industry (Fig. 2), we have considered indicators as in Tab. 1.

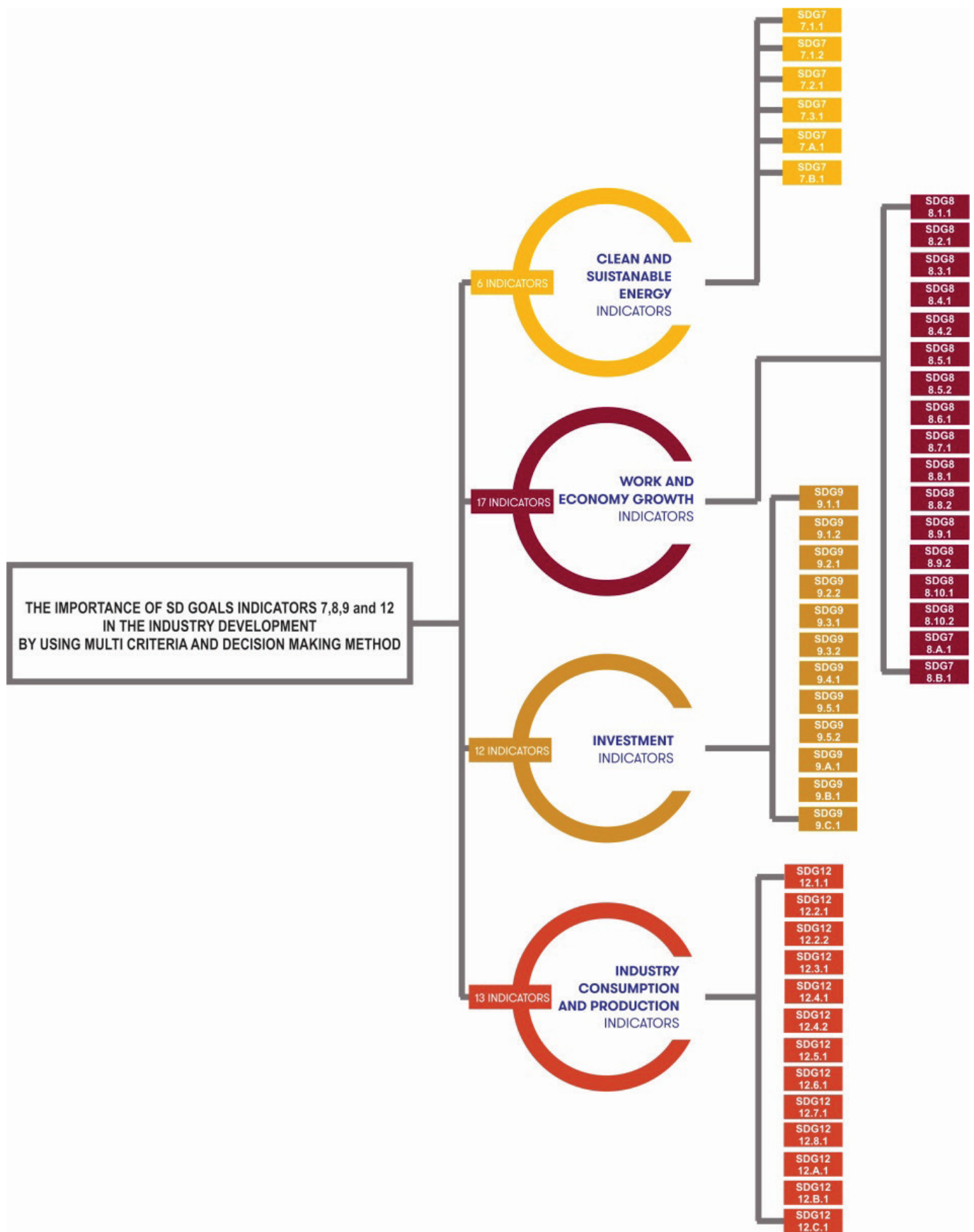


Figure 1 Sustainable Development Goals SDG7 / SDG8 / SDG9 / SDG12 [6]



Figure 2 Sustainable Development Goals SDG7 / SDG8 / SDG9 / SDG12 [6]

Table 1 Analyzed indicators of all levels of the hierarchy of the problem

Table 1 Analyzed indicators of all levels of the hierarchy of the problem										
<div> <div>7 AFFORDABLE AND CLEAN ENERGY</div> <div>6 INDICATORS 7.1.1 - 7.B.1.</div> </div>										
<div> <div>8 DECENT WORK AND ECONOMIC GROWTH</div> <div>17 INDICATORS 8.1.1 - 8.B.1.</div> </div>										
<div> <div>9 INDUSTRY, INNOVATION AND INFRASTRUCTURE</div> <div>12 INDICATORS 9.1.1 - 9.C.1.</div> </div>										
<div> <div>12 RESPONSIBLE CONSUMPTION AND PRODUCTION</div> <div>13 INDICATORS 12.1.1 - 12.C.1.</div> </div>										
N	1	2	3	4	5	6	7	8	9	10
RI	0.00	0.00	0.58	0.90	1.12	1.24	1.32	1.41	1.45	1.49

3 DECISION-MAKING PROCESS APPLICATION OF AHP METHOD

The AHP method developed by Thomas L. Saaty [7] stands as one of the most commonly used methods of multi-criteria analysis. This method sees the decision-making process to be a hierarchical process with multiple levels.

In decision making, especially when we talk about sustainable development in the industry, it is very important which method we decide to use to achieve optimal solutions. So why have we decided to use the Analytic Hierarchy process in particular?

The AHP works as a hierarchy, breaking down the decision top to bottom. The goal is at the top level, the criteria and sub-criteria are in middle levels, and the alternatives are at the bottom layer of the hierarchy.

Input of experts and decision-makers is considered as pair-wise comparison and the best alternative can be selected according to the highest rank between alternatives. It is noticed that AHP is the most used methodology of all the MCDM methods. This can be credited to its simple structure and the ability of an analyst to negotiate results until consistency is achieved, offering near consensus on judgment. [8]

Table 2 Theoretical basis of MCDM - AHP Method [11, 12, 1]

The characteristics of matrix A . $a_{ij} = 1/a_{ji}$ for $i, j = 1, \dots, n$; $\det A \neq 0$											1																					
Determining the weights can be solved same as solving a matrix equation with matrix columns w solution for eigenvalues λ different from 0 i.e.											2																					
$A \cdot w = \lambda \cdot w, \text{ or } \begin{bmatrix} a_{11} & a_{12} & \dots & a_{1n} \\ a_{21} & a_{22} & \dots & a_{2n} \\ \dots & \dots & \dots & \dots \\ a_{n1} & a_{n2} & \dots & a_{nn} \end{bmatrix} \cdot \begin{bmatrix} w_1 \\ w_2 \\ \dots \\ w_n \end{bmatrix} = \begin{bmatrix} \lambda_1 w_1 \\ \lambda_2 w_2 \\ \dots \\ \lambda_n w_n \end{bmatrix} \quad (3) [10]$																																
Priority vectors (w) from the pair-wise comparison matrix A by solving an eigenvalue problem with the relation. $A \cdot w = \lambda_{\max} \cdot w$ Where λ_{\max} is the maximum eigenvalue of A											3																					
Assessment, or to calculate index of consistency. $CI = (\lambda_{\max} - n)/(n - 1)$											4																					
Based on this index we determine the index of inconsistency $CR = CI/RI$ Where: RI (Random Index)											5																					
The value of $CR \leq 0.10$ shows that the estimates for a and j are consistent. In case they are not, the evaluation should be repeated.											6																					
<table><tr><td>N</td><td>1</td><td>2</td><td>3</td><td>4</td><td>5</td><td>6</td><td>7</td><td>8</td><td>9</td><td>10</td></tr><tr><td>RI</td><td>0.00</td><td>0.00</td><td>0.58</td><td>0.90</td><td>1.12</td><td>1.24</td><td>1.32</td><td>1.41</td><td>1.45</td><td>1.49</td></tr></table>												N	1	2	3	4	5	6	7	8	9	10	RI	0.00	0.00	0.58	0.90	1.12	1.24	1.32	1.41	1.45
N	1	2	3	4	5	6	7	8	9	10																						
RI	0.00	0.00	0.58	0.90	1.12	1.24	1.32	1.41	1.45	1.49																						
Saaty's 9-point scale of pair-wise comparison.											7																					
Scale		Compare factor of i and j																														
1		Equally important																														
3		Weakly important																														
5		Strongly important																														
7		Very strongly important																														
9		Extremely important																														
2, 4, 6, 8		Intermediate value between adjacent scales																														

Analytic Hierarchy Process (AHP) has many advantages including its adaptive application; it is scalable; it has a hierarchy structure that can easily adjust to fit many sized problems; it is not data intensive, etc. [9] Inside MCDM,

AHP is one of the most efficient methods for dealing with different problems. [10]

The procedure follows numerous steps, including: assigning a relative assessment in pairs with attributes of a hierarchical level, for given attributes of the first and higher hierarchical level, and then repeating the process for all levels of the hierarchy. [1] Naturally, the application of the theoretical basis is required, which is given in Tab. 2.

4 HIERARCHY OF THE PROBLEM AND ALTERNATIVES BASED ON AHP METHOD

The analysis of indicators is examined in three main areas/main indicators. There are 48 indicators from the second level of the hierarchy that will be compared with the four alternatives (Investment in Education, Investment in the Energy Sector, Investment by Foreign Investment, Investment in the Infrastructure and Innovation). The whole analysis is done based on the diagram below (Figure 3). After analyzing the data and processing with Expert Choice

Software, we have obtained the results. The results structure a hierarchy that will be a good basis for decision-making and policy-making for the impact of sustainable development in the industry. Diagrams with the results obtained after processing all the data will be presented in the following chapters.

The results (Tab. 3) show that Alternative 1 - Investment in Education has an advantage over the other three alternatives. From this point of view, sustainable development suggests the scale towards Alternative 1 with a slight advantage over other alternatives. However, Alternatives 2 and 3, based on our analysis, are very close and should not be neglected completely as they represent the corresponding alternatives derived from the model. Based on these results, we note that Sustainable Development Goals are closely related to Investment in Education, Investment by Foreign Investors, Investment in Energy, and Investment in Infrastructure and Innovation.

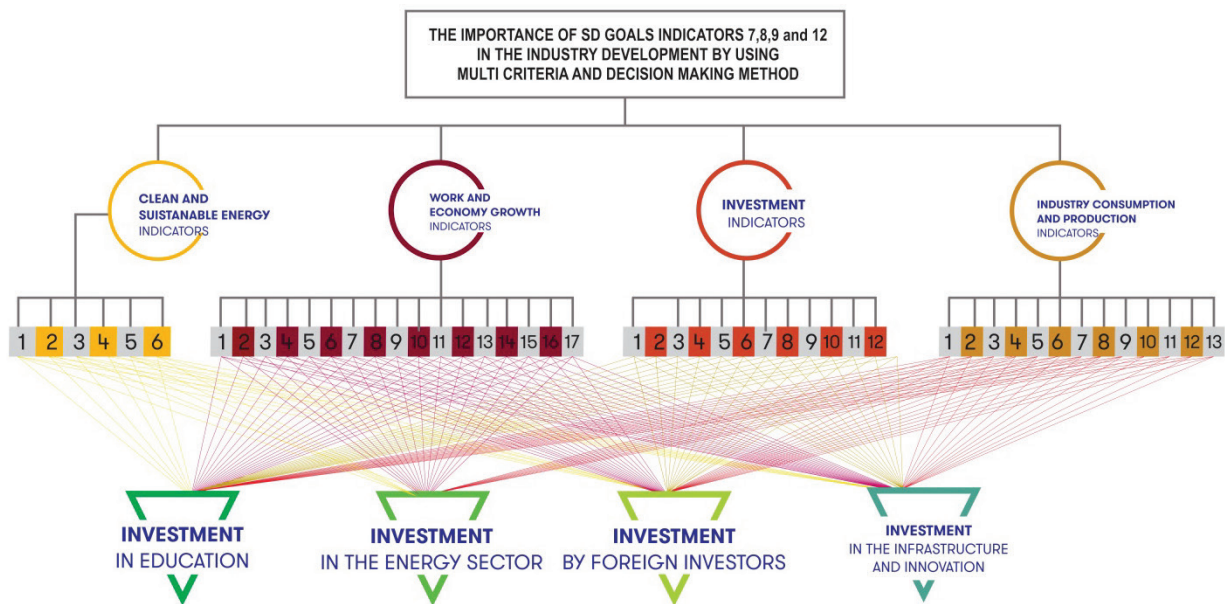


Figure 3 The comparative link between the second hierarchical level and alternatives

Table 3 Ranking of Alternatives

Alternative 1	Investment in Education	0.382	1
Alternative 2	Investment in the Energy Sector	0.208	3
Alternative 3	Investment by Foreign Investors	0.266	2
Alternative 4	Investment in the Infrastructure and Innovation	0.143	4

The successful implementation of the AHP method requires that experts maintain the dominant role in ranking the indicators and alternatives. They contributed through the interviews they provided based on Saaty's rules. The university professors' opinions are crucial for our analysis, as universities are the main actors in teaching, research, and support for the implementation of clean production activities [1]. Since we are dealing with theoretical analysis, we have focused mainly on getting the opinion of university professors. However, the participants in our analysis were not

just members of the academic community, but also decision-makers in relevant institutions such as mayors, department directors, board directors, etc.

The complete calculations of the analysis for all indicators – part of the model for three levels of the hierarchy – were made by applying Expert Choice Software. Through it, it is possible to achieve results in all the steps followed by the AHP methodology through Expert Choice. Here are the steps: Pairwise Comparisons, Judgment Scales, Priorities Derivation, Consistency, Aggregation - which are displayed at the end through sensitivity analysis (performance sensitivity, dynamic sensitivity, gradient sensitivity, head to head sensitivity) as a final step (Fig. 4).

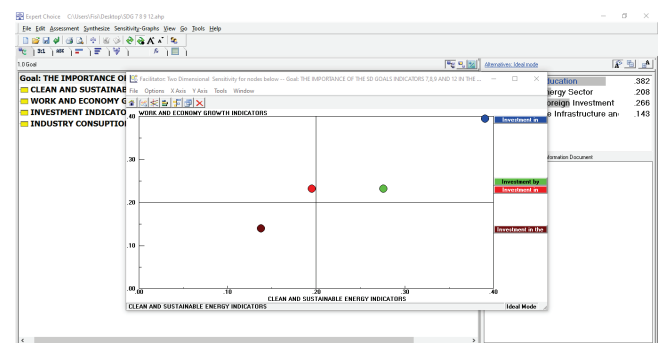
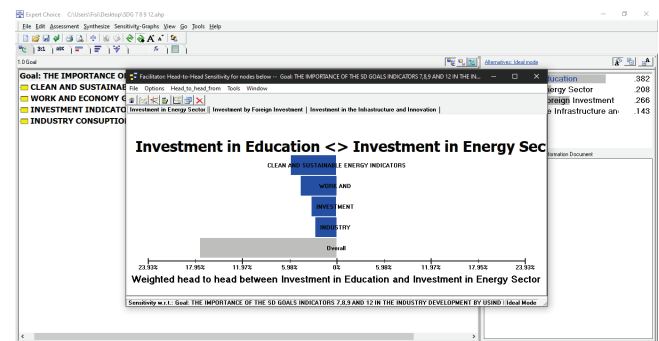
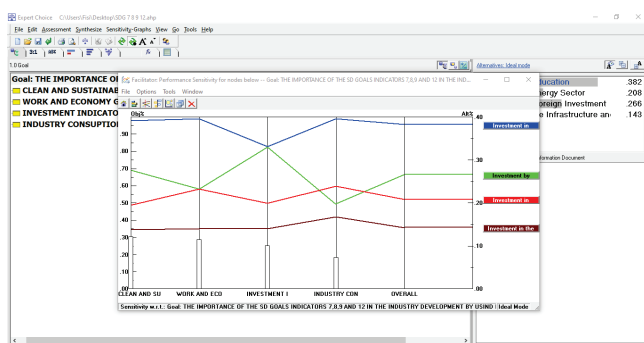
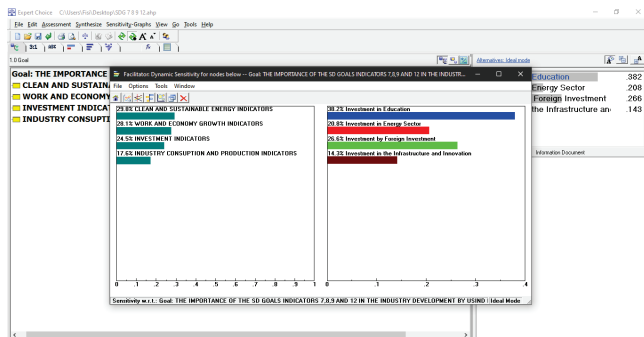
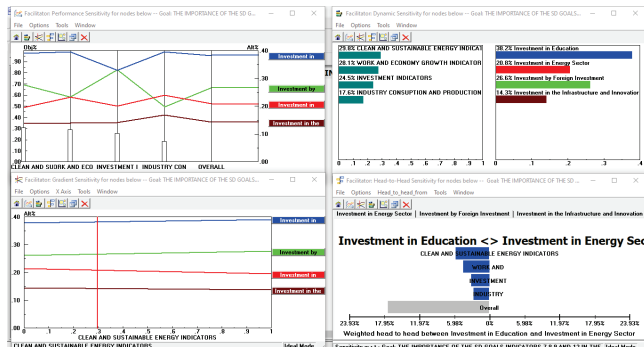
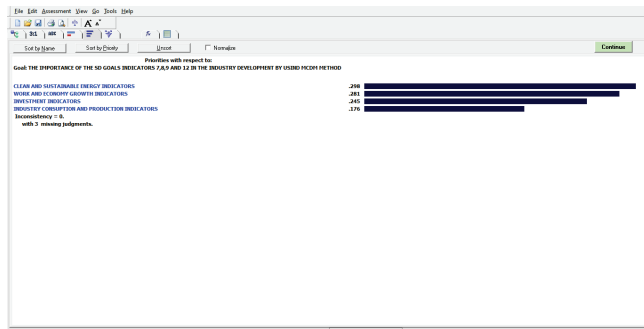
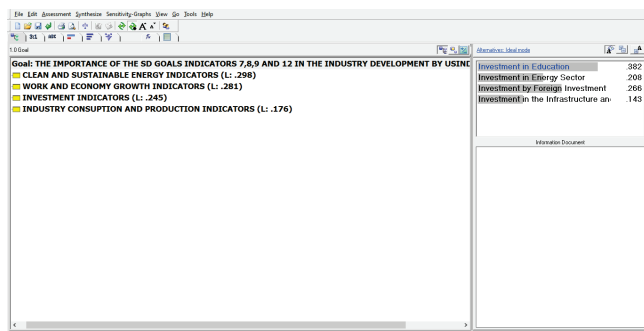


Figure 4 The program interface through which the calculations for the Technical-energetic Indicators, Environmental and Social Indicators, Economic-Investment Indicators have been made

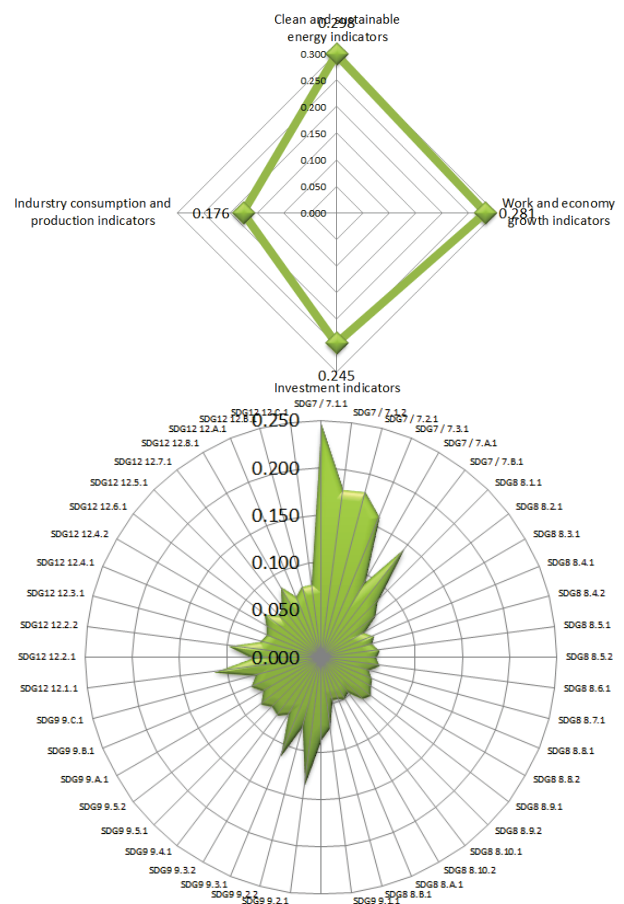


Figure 5 Graphic presentation of the final results for the Clean and Sustainable Energy Indicators, Work and Economy Growth Indicators, Investment Indicators, Industry Consumption and Production Indicators distributed in the three hierarchical levels of the model.

The summary of the results we obtained through the application of Expert Choice, are presented in summary form in Fig. 5. Here the final values of the alternatives tested in the analysis are presented with the values of all indicators analyzed in the whole model.

5 CONCLUSIONS AND RECOMMENDATIONS

Using the AHP Method, we have set the indicators, identified their weight, defined the hierarchy of the problem, and offered alternatives. This does not imply that we are talking about a method through which we can solve real problems that mankind faces nowadays. Nevertheless, we have managed to define our future goal, use, and application of other methods in the field of decision-making and multi-criteria policy for Developing Countries (Western Balkans region) in projects that enable sustainable development.

The results acquired can give a fair picture of the appropriate steps to be taken to intervene and change the situation, based on the indicators that we have taken into account. According to the Clean and Sustainable Energy Indicators (0.298) resulted in Indicator 7.1.1 Proportion of population with access to electricity worth (0.246).

In the second part of the Work and Economy Growth Indicators we have reached the highest value in the annual growth rate of real GDP per capita (0.083).

Investment Indicators (0.245) achieved its highest value through the Proportion of rural population indicator who live within 2 km of an all-season road (0.135).

The last indicators, Industry Consumption and Production Indicators (0.176), reach the maximum value in the indicator Number of countries with sustainable consumption and production (SCP) or SCP mainstreamed as a priority or target in national policies with value (0.114).

The results of the analysis will be used as a base for developing countries (Western Balkans) in the logic of identifying, analyzing, and taking appropriate steps in the right direction. The research has raised many new questions and paves the way for potential new research in this field of study. The Republic of Kosovo in particular and the region in general, need to address these issues in the future in order to define more indicators that have an impact on the sustainable development of their respective territories. The span of the applicability of this particular model can easily expand to include other countries in the region. With some alterations, the model can reach a broader acceptance in the region. As for the term "wider", it is comprised of institutional inclusion of the proven scientific methods and techniques in decision making, as well as applying existing models and studies from one country into another country in the region of Western Balkans.

Moreover, the model (besides contributing towards the identification of problems) will offer these solutions:

- To identify, define, and plan the most crucial criteria in the hierarchy of the sustainable industry based on the SDG's;
- To alter/modify models which will be established carefully for each different case specifically;

- To establish the model to solve similar problems, in accordance with the recommendations for further work, by the use of the analytic hierarchy process;
- Our analysis can also be utilized for similar cases in the field of decision making concerning sustainable industry.

Notice

The paper was presented at MOTSP 2020 – International Conference Management of Technology – Step to Sustainable Production, which took place from 30th September – 2nd October 2020 in Bol, island Brač (Croatia). The paper is not and will not be published anywhere else.

6 REFERENCES

- [1] Osmani, F. & Kochov, A. (2018). Definition of indicators for decision-making to contribute to sustainable development through Cleaner Production and Resource Efficiency by using the AHP method. *Lietuvos mokslų akademija, Energetika*, 64(3), 149-160. <https://doi.org/10.6001/energetika.v64i3.3808>
- [2] Condon, E., Goldenb, B., & Wasil, E. (2003). Visualizing group decisions in the analytic hierarchy process. *Computers & Operations Research*, 30, 1435-1445. [https://doi.org/10.1016/S0305-0548\(02\)00185-5](https://doi.org/10.1016/S0305-0548(02)00185-5)
- [3] Neri, A., Cagno, E., Di Sebastiano, G., & Trianni, A. (2018). Industrial sustainability: Modelling drivers and mechanisms with Barriers. *Journal of Cleaner Production*, 194, 452-472. <https://doi.org/10.1016/j.jclepro.2018.05.140>
- [4] Wang, C., Wang, L., & Dai, S. (2018). An indicator approach to industrial sustainability assessment: The case of China's Capital Economic Circle. *Journal of Cleaner Production*, 194, 473-482. <https://doi.org/10.1016/j.jclepro.2018.05.125>
- [5] Kates, R. W., Parris, T. M., & Leiserowitz, A. A. (2005). Environment: Science and Policy for Sustainable Development what is Sustainable Development? *Goals, Indicators, Values, and Practice*, 47(3), 8-12. <https://doi.org/10.1080/00139157.2005.10524444>
- [6] Saaty, T. L. (1980). *Multicriteria Decision Making: The Analytic Hierarchy Process*. McGraw-Hill, New York. <https://doi.org/10.21236/ADA214804>
- [7] Saaty T. L. & Gholamnezhad A. H. (1982). High-Level Nuclear Waste Management: Analysis of Options. *Environmental Planning*, 9, 181-196. <https://doi.org/10.1068/b090181>
- [8] Rimal, T. A. & Tugrul, D. (2013). Multi-Criteria Applications in Renewable Energy Analysis, a Literature Review. *Research and Technology Management in the Electricity Industry*. Springer, VIII. p. 359.
- [9] Velasquez, M. & Hester, P. T. (2013). An Analysis of Multi-Criteria Decision Making Methods. *International Journal of Operations Research*, 10(2), 56-66.
- [10] Triantaphyllou, E., Shu, B., Nieto Sanchez, S., & Ray, T. (1998). Multi-Criteria Decision Making: An Operations Research Approach. *Encyclopaedia of Electrical and Electronics Engineering*, (Webster, J. G. Ed.), John Wiley & Sons, New York, NY, Vol. 15, 175-186.
- [11] Miller, G. (1956). The magical number seven, plus or minus two: some limits on our capacity for processing information. *The Psychological Review*, 63(2), 81-97. <https://doi.org/10.1037/h0043158>

- [12] Saaty, T. L. (1994). How to make a decision – The Analytic Hierarchy Process. *Interfaces*, 19-43.
<https://doi.org/10.1287/inte.24.6.19>

Authors' contacts:

Prof. ass. dr. **Fisnik Osmani**
University of Mitrovica, Faculty of Mechanical Engineering and Computer,
Fabrika e Akumulatorëve, 40000 Mitrovica, Kosovo
fisnik.osmani@umib.net

Prof. dr. sc. **Atanas Kochov**
(Corresponding author)
University "St. Cyril and Methodius" Skopje,
Faculty of Mechanical Engineering,
Karpos II b.b. P. O. Box 464,
1000 Skopje, Republic of North Macedonia
atanas.kochov@mf.edu.mk

MSc. **Betim Shabani**, PhD Candidate
University "St. Cyril and Methodius" Skopje,
Faculty of Mechanical Engineering,
Karpos II b.b., 1000 Skopje, Republic of North Macedonia

MSc. **Mirjeta Ilazi**, PhD Candidate
University "St. Cyril and Methodius" Skopje,
Faculty of Mechanical Engineering,
Karpos II b.b., 1000 Skopje, Republic of North Macedonia

Selection of an Optimal Supplier

Predrag Ćosić*, Zdenka Keran, Vedran Kokot

Abstract: The paper describes the selection of an optimal supplier from China based on three obtained bids to produce 120 000 forged pieces, which is the primary process for shaft production. The choice was made using the AHP method based on the Expert Choice software program and Multiple-Criteria Decision-Making (MCDM). The key information when choosing the optimal supplier of large number of forgings is to define the objective of the task, decision tree with weighted criteria and sub-criteria, consistency checking and possible reconsideration using brain storming when defining the strength of criteria/sub-criteria. To some extent, this may reduce initial subjectivity in the decision-making process in the Decision Support System.

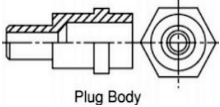
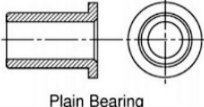
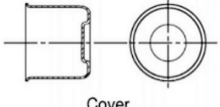

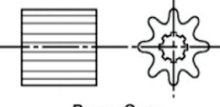
Keywords: Analytical Hierarchy Process (AHP); Multiple-Criteria Decision-Making (MCDM); optimization of selection optimal supplier

1 INTRODUCTION

Choosing the primary forging process as the best between the potential processes – forging, extrusion or casting – was the initial step towards the idea of choosing the optimal shaft supplier between three forges in PR China. A Chinese forge made three offers to produce 120 000 forgings. The comparison and final selection of the optimal offer was

made depending on the criteria and sub-criteria. Defining and weighting of criteria and sub-criteria was the key to defining decision tree and AHP models. The selection of the optimum primary process as well as the selection of the optimum supplier was done by using the Expert Choice 11 software program based on the AHP method.

Table 1 Materials, number per year, manufacturing process and relative cost [5]

Component	Material	Number Per Year	Manufacturing Process	Relative Economic and Technical Merits	Relative Cost
 Plug Body	Low Carbon Steel	1 000 000	Machining	High waste Low to medium production rates Poor strength	3.9
			Cold Forming	Little waste Very high production rates High strength	1.0
 Plain Bearing	Bronze	50 000	Machining	High waste Low to medium production rates Non-porous product properties	2.2
			Powder Metal Sintering	No waste High production rates Porous product	1
 Cover	Aluminum Alloy	5000	Spinning	High labor costs Low production rates Limited detail and accuracy	1.8
			Deep Drawing	Low labor costs High production rates High detail and accuracy	1
 Connecting Rod (after (1.6))	Medium Carbon Steel	100 000	Closed Die Forging	Long lead times High tooling costs High equipment costs	1.3
			Sand Casting	Short lead times Low tooling costs Low equipment costs	1
 Pump Gear	Low Carbon Steel	5000	Machining	High waste Low to medium production rates Poor strength	2.6
			Cold Extrusion	Little waste Very high production rates High strength	1

2 IMPORTANCE OF SELECTION PRIMARY PROCESS IN PROCESS PLANNING

Process planning [1-3] is essential in production preparation process because it defines processing parameters,

machine tools, cutting tools, production times, and production costs. These data are useful for technological improvement and management of production costs. Process planning provides basic data for the production designer because these data define the distribution of jobs for the

realization of orders and delivery times. The primary process has a significant influence on after-treatment processing time, the machine occupancy, the production cost, and the delivery period.

Tab. 1 provides examples of how different shapes, materials, number of pieces, relative production time, and the manufacturing process affect the production costs. The key fact is that the observed product is a shaft that must be resistant to twisting and bending stresses. Data sources according to Halevi [1], ASM Handbook [4] and Swift-Booker [5] were used to help select the primary process [3-5].

3 DECISION SUPPORT THROUGH MULTI-CRITERIA OPTIMIZATION

Decision support systems are based on artificial intelligence and strive for an optimal solution (so-called multi-criteria optimization). In a single-objective optimization, with objective function and constraints, a solution is relatively easy to find.

But a real situation, in most cases, requires multi-criterial optimization. This results in the necessary compromises if the criteria are conflicted (for example, one criterion increases the observed variable, the other reduces it). This necessarily indicates the expected subjectivity of the decision-making support, since the assessment of the "criterion strength" is the result of the experience, knowledge and intuition of the experts in the considered field. The expected subjectivity is being somewhat reduced by team building and brainstorming of more experts.

3.1 Analytic Hierarchical Process (AHP method)

AHP first enables interactive structuring (hierarchy formatting) of problems to prepare decision-making scenarios. A hierarchically structured decision-making model consists of a goal, criteria, several possible levels of sub-criteria and alternatives. The goal is always at the top and it cannot be compared with any other element. The AHP method is not the only method, there are also the Electre and the Promethee methods.

Analytical hierarchical process (AHP) is solved in four phases [6-9]:

- 1) Structuring the problem
- 2) Determining the most important criterion
- 3) Determining the most significant alternative
- 4) Determining the final solutions (goal).

4 EXPERT CHOICE SOFTWARE

The Expert Choice software is used to solve semi-structured and unstructured decision-making problems. It is based on the AHP [7] method, and Tomas Saaty [6, 8], an author of the AHP method, participated in its development. The idea is that the assessment of the importance of criteria and sub-criteria, as well as the assessment of the importance

of alternatives in relation to the criteria, is carried out by the decision-maker. This allows the method to better cover all subjective views and objectives used by the decision-maker.

4.1 Consistency

The consistency of the whole process is checked through a consistency index, which must be less than 10% in order to make a decision that can be accepted as valid and consistent. Consistency means *the consistency of decision makers in their decisions and assessments* [6].

5 CASE STUDY OF PRIMARY PROCESS SELECTION

At first, the primary process is selected according to Halevi, then by the ASM Handbook and finally by Swift-Booker [1, 4, 5]. The eccentric effect of the considered shaft influences the process of selecting the primary process and subsequent processing.

5.1 Process Selection in Process Planning

The defined forging has a symmetry axis; the shape is a shaft (Fig. 1) with different cross-sections. The length of the forging is greater than its width. Influential factors are the *asymmetric part, the outer and inner threads at the ends, the slots to be milled and the relatively large L/D ratio*.

Product features:

- Material: St 44-2 - unalloyed steel or E275 (1.0225)
- Weight: 19.24 kg
- Minimum wall thickness: 15 mm
- Cam length: 124 mm
- Hole length: 205 mm
- Maximum diameter: $\varnothing 123$ mm
- Most demanding surface quality: Ra 0.4 (other Ra 1.6 and Ra 6.3)

Thought guides for 120 000 pieces are:

- 1) Less influence of the executors,
- 2) More uniform quality,
- 3) The production should be as short as possible,
- 4) More precise processing,
- 5) No measurements before processing for each workpiece.

The hierarchical structure (Fig. 2) is designed to determine the optimal primary process through multi-criteria decision making. When using the AHP method, the basic and functional properties of the workpiece were considered. Closed die forging has no alternatives; the only variant is precise forging that is not considered. In the observed shaft, the eccentric part of geometry causes a problem when choosing the primary process, and later when the machining process takes place.

Fig. 2 shows the hierarchical structure of the problem introduced with the final goal and defined criteria and sub-criteria.

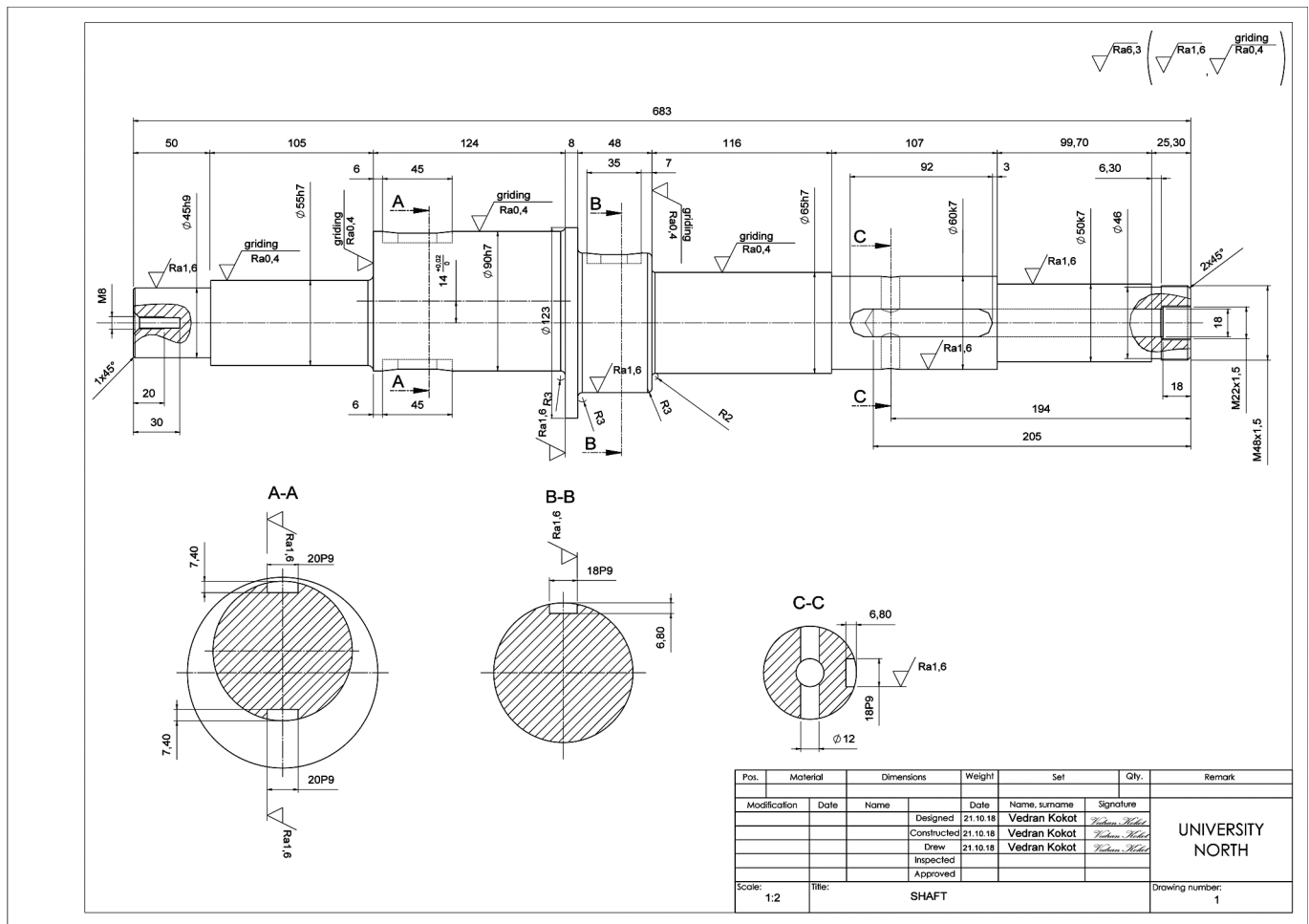


Figure 1 Technical drawing of a final part

5.1.1 Halevi's Primary Process Selection

The first step of primary process determination, according to Halevi [1], is to define the workpiece complexity. Therefore, the most similar shape is selected in Fig. 3. As with any general solution, it must be noticed that there are too few forms offered, making the choice more difficult and therefore less precise. The second step is, based on the selected shape and quantity, to weight primary process technology that is suggested, from best to worst (Fig. 3). The interval boundaries are tightly set. For non-existent intervals the designer can search for the solution from the nearest interval.

The boundaries between intervals are not set and this is the biggest problem when selecting the primary process according to Halevi. In addition, the problematic fact is that the influence of the material type is not initially taken as a

factor according Halevi. By comparing the basic offered forms with the product form that we have, it is concluded that it is an open form with a variable cross-section along the axis. After selecting the shape type, it is necessary to select one of the production processes that can be seen in Fig. 3.

The primary processes are as follows (Fig. 3):

- A – Casting process
- B – Metal forming process
- C – Cutting (machining) process
- D – Joining process
- E – Mounting process
- F – Magnifying process.

Fig. 3 displays the product shape type. For the quantity of 120 000 pieces, it is suggested to choose the *processing type B – metal forming*.

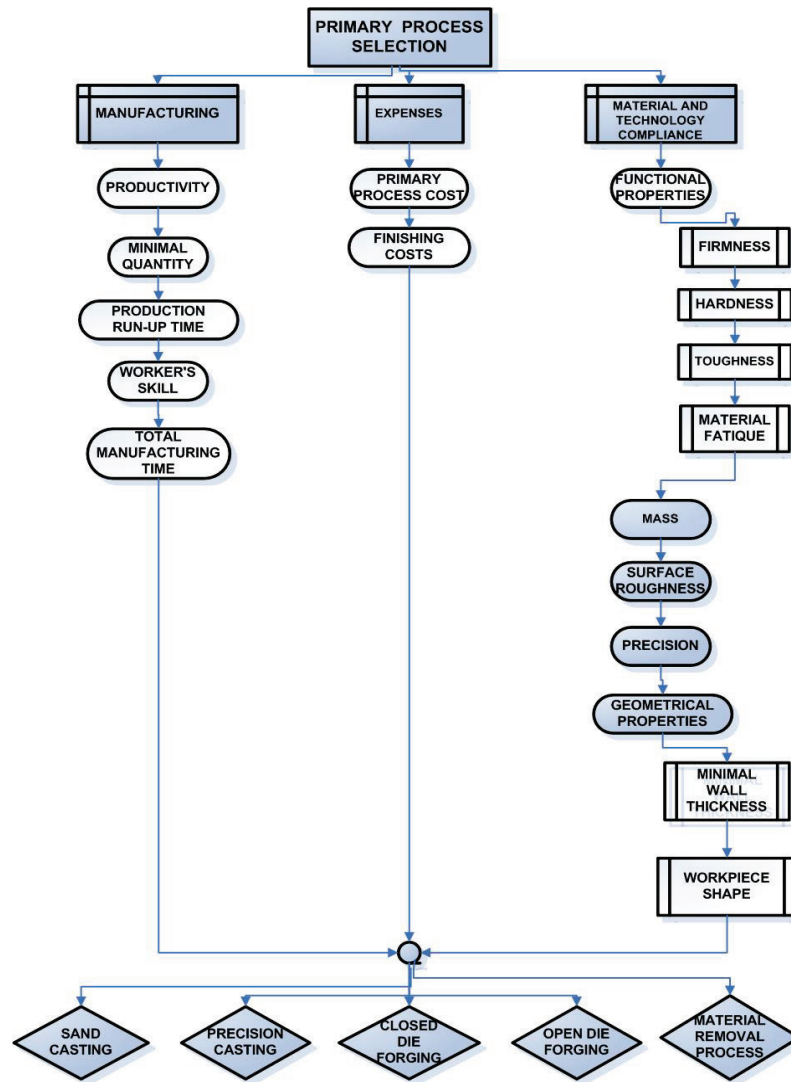


Figure 2 Hierarchical structure selection of the primary process

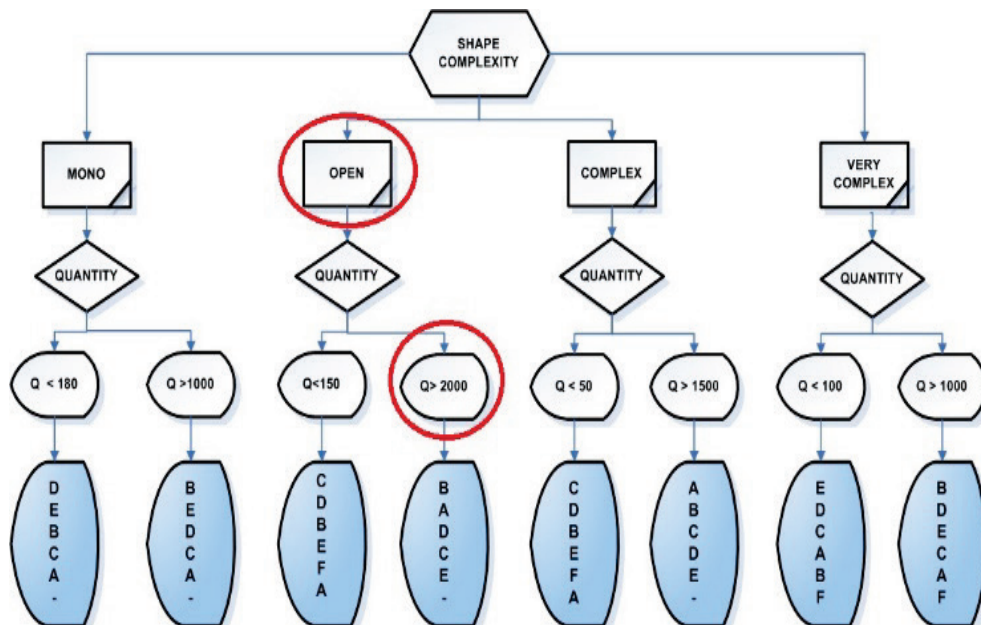


Figure 3 Halevi's selection of the primary process [4]

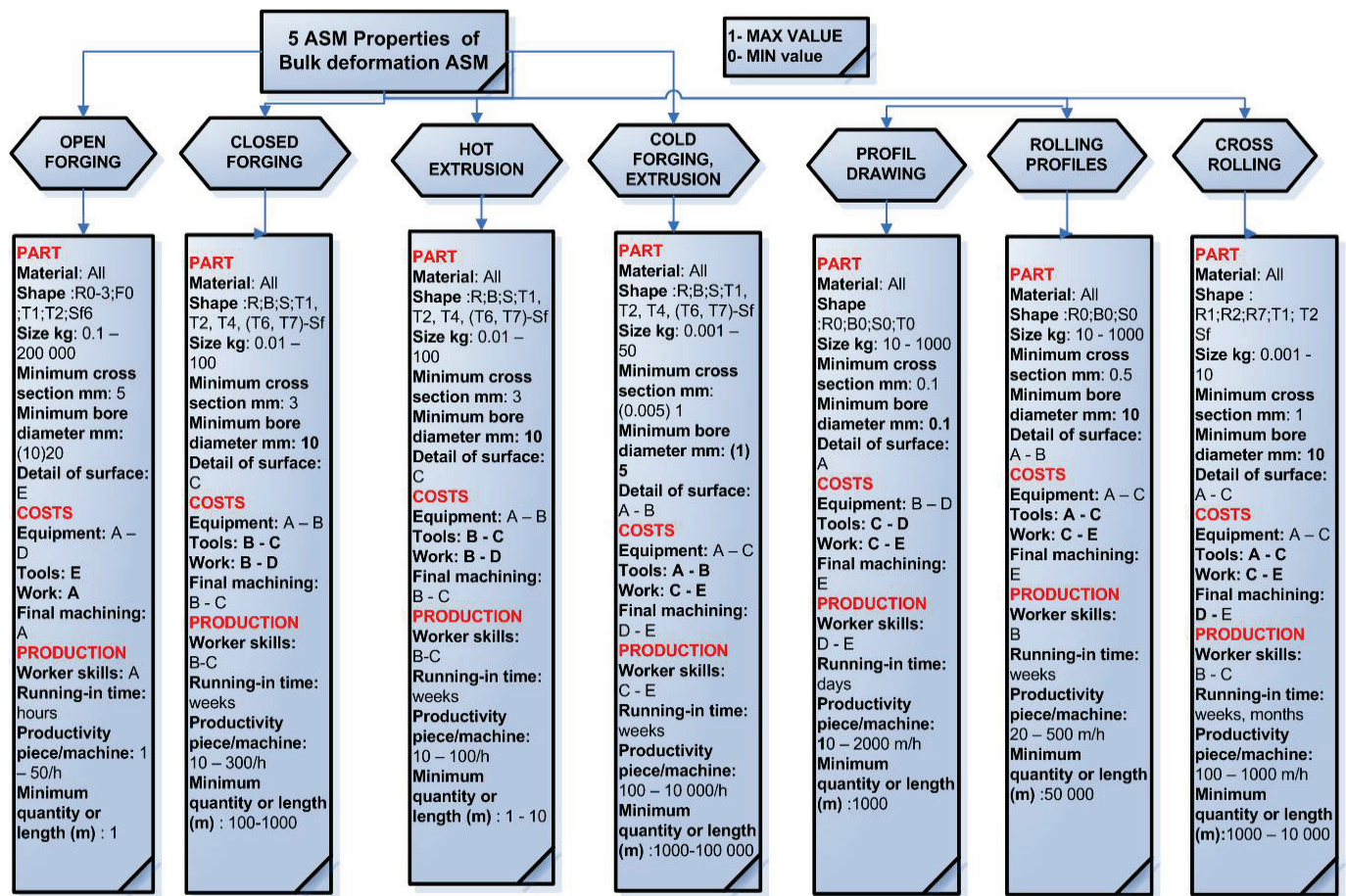


Figure 4 ASM's selection of the primary process [4]

5.1.2 ASM's Primary Process Selection

The first step of the primary process determination, by ASM [4], is to select possible primary process technologies (Fig. 4) only based on the type of material. The second step is to determine the type of the shape complexity of the desired product. The conclusion is that it is a complex form with a round cross-section. In this step, there is a "type of gap" because there is no logical step sequence how to narrow down the choice of offered technologies, after selecting possible technologies and choosing shapes. According to the ASM handbook, there is a "gap" to be "filled" by the intuition and knowledge of the technologist because the process of narrowing down potential primary process procedures is not defined. When defining metal forming process by ASM, attributable features of the finished piece are applied (Fig. 4); they are highly subjective and can have major influence on the final selection. Thus, someone's experience here comes to the fore by introducing the criterion of functionality.

5.1.3 Swift-Booker's Primary Process Selection

The starting point is a table in Fig. 5. It provides information that the primary process, closed die forging, is economically viable for a combination of material and production quantity. Tab. 2 defines the dimensions of the forging diameter calculated according to reference [10]. The

applied contour angles (5° - 7°) serve the purpose of easy ejection from the die (in hammer forging process), without special ejector pin.

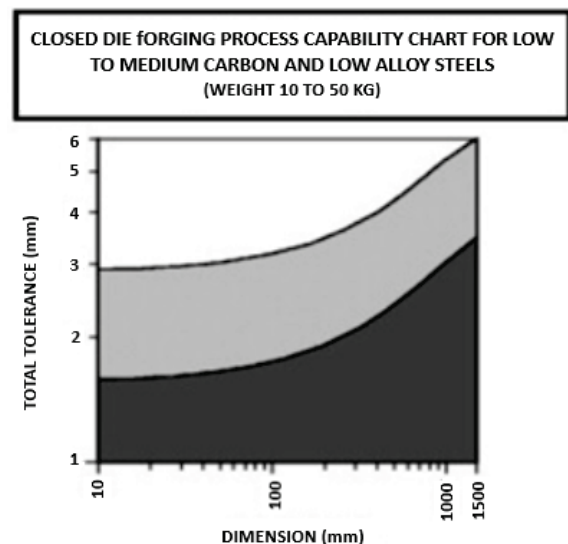


Figure 5 Features of closed die forging process capability [3]

By comparing calculated tolerances (Tab. 2) and process capability diagrams (Fig. 5), we see that closed die forging

represents a normal working ability, in the diagram presented in a light grey area.

The dimension adding in forging can be reduced from 7 mm (according to [10]) to 4 mm because of technology modernization. This option would significantly shorten the

cutting process on the CNC machine. What is imposed as an obstacle in reducing the dimension adding is that this can lead to the strain appearance in workpiece due to the activity of horizontal forces (excenter), so the quality of the product itself will be questionable.

Table 2 Spreadsheet of processing features (diameters) and tolerances

Determination of dimension D	Ø45	Ø55	Ø90	Ø123	Ø90	Ø65	Ø60	Ø50	Ø48
Quality of processing	Δ2	Δ2	Δ2	Δ2	Δ2	Δ2	Δ2	Δ2	Δ2
Processing allowance $\delta/2$	3.5	3.25	3.25	3.5	3.5	3.25	3.5	3.5	3.5
$D_k = D + \delta$	52	61.5	96.5	130	97	71.5	67	57	55
D_k (rounded)	Ø52	Ø62	Ø97	Ø130	Ø97	Ø72	Ø67	Ø57	Ø55
Tolerances	Δc	0.1	0.24	0.24	0.36	0.24	0.24	0.24	0.1
	x	2.37	2.27	2.51	2.63	2.51	2.51	2.51	2.37
	y	1.16	1.3	1.3	1.42	1.3	1.3	1.3	1.16

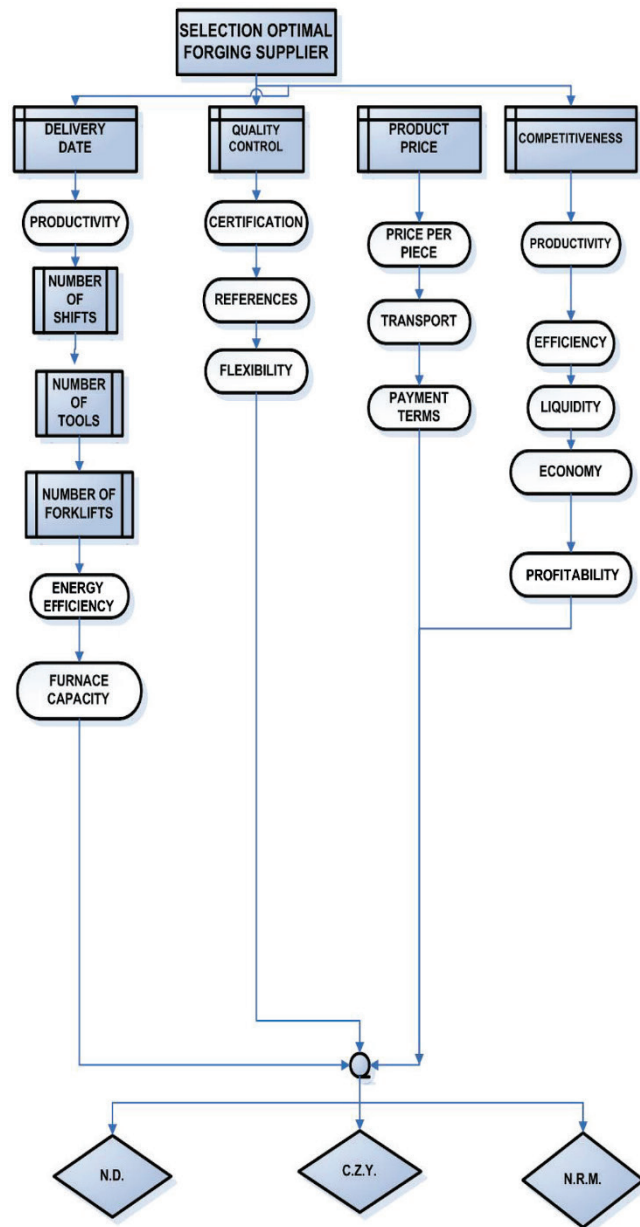


Figure 6 Hierarchical structure selection of suppliers

5.2 Selection of Optimal Supplier

For the default workpiece, the optimal forging offer should be selected according to defined criteria. The offer request has been sent and three offers have been received from China that differ in delivery time, price and quality. The production and delivery of 120 000 pieces of the final product were considered. Several data should have been assumed because they represent a technological and trade secret, for example, hourly labor costs, hourly machine costs, productivity, efficiency, liquidity and profitability. It is therefore important to highlight the subjectivity when assessing the weights of sub-criteria and criteria. Fig. 6 shows the hierarchical structure of the criteria and sub-criteria with the goal of selecting the forging offer.

The competitiveness criteria with sub-criteria – productivity, efficiency, liquidity, economy and profitability – are set as a reason why. It was not possible, for the purposes of the previous project, to obtain such exact data concerning the business of the considered forging companies.

5.2.1 Delivery Date

Because of a large series, it is primarily necessary to concentrate on the short delivery period in order to make the entire production cycle as short as possible. This means that the default production forging process must be done in a short period, so the first container shipment could arrive as soon as possible. The forging time and the transport from China, first by boat and later by truck, are related to the production time, which means that if it is possible to shorten the time of forging and transport, the price will be reduced. As the number is 120 000 pieces, time saving can be expected. The delivery time will be improved so that the cutting (CNC machining) starts immediately after the pick-up of the first container shipped from China. This means that the operator of the CNC machine will begin the preparation of the numerically operated machine one month after the first shipment from China is sent. In this way, the production cycle, i.e. delivery deadlines, and thus the occupancy of a high-speed and high-productive CNC processing center, are shortened. In addition, further production planning is

possible, thus achieving greater competitiveness in the market.

5.2.2 Productivity

Productivity is affected by the following:

- number of working shifts,
- number of machines and number of forging tools,
- number of forklifts and number of employees.

The level of automation and the number of robots in the production reduce the time needed to introduce the new model and reduce the time and material loss. Of course, the questions that do not have answers in [3, 4] still remain: What type of heating to choose (flame furnace, induction heating); What type of machines to choose (bat, press); What kind of forging die design to choose – how many engravings in one die; How many forgings (according to the size and mass) can be forged at the same time? According to [4], which uses the practical research and experience, the mass adding for die filling insurance increases both the mass of the workpiece, the price of the material, and the cost of heating for the material which is later removed as a waste.

5.2.3 Quality Control

The elimination of the strain in the forging workpiece due to the appearance of horizontal forces could be avoided by forging two forgings in one forging die, which would halve the forging time, and the quality would be higher. But these factories do not have such large forging machines or dies for the expected dimensions of the default shaft. It should be emphasized that the simultaneous forging of two workpieces depends on the mass of drop-down parts of forging hammers. The offer states that additional product control that improves quality and productivity reduces risk and ensures fast shipping. A SGS control provides solutions involving control, certification, auditing and verification. SGS is a Geneva-based multinational company that also ensures that products, systems or services meet the requirements set by SGS customers. An internal audit of the company submits a daily production report to the client.

5.2.4 Certification

The market competition is serious, and the buyer has the choice. The tenders require additional quality assurance to reduce the cost of input control and reduce the risk of substandard purchases. Additional warranty includes ISO certificates 9001, 20001 and 14001. The forging factories N.R.M. and N.D. claim that they have the three mentioned certificates, while the forge of C.Z.Y. is certified by IATF 16949. It is not possible to know whether these forges implement quality systems because deeper analysis is not done.

5.2.5 References

Looking at the process of forging and acquiring from China, from an organizational point of view, all parts of the business are well considered and planned, as evidenced by the fact of long-term cooperation on the global level with many world-famous companies. The most significant external clients of the forge factory N.D. are "McLaren" and "Subitomo Rubber". The clients of the forge factory C.Z.Y. are "Bosch", "Volvo" and "Scania", while the most famous references of the forge factory N.R.M. are "CCL UK" and "HMI USA". Of course, it is not possible to compare which company is "more present" in the market because there is no information available on which products they produced for them, so there is a certain subjectivity when giving importance to references. *Important criteria* for such a business are the *success of the arrangement, compliance of the delivery time and quality of production, flexibility and adaptability to changes* in the arrangement. Further organizational improvements concern production directly and further processing of ordered forgings.

5.2.6 Product Price

Since the big series is concerned, a small price difference of a few dollars (USD dollar) per piece (forging) means a big difference of several hundred thousand dollars of the total forging price. A big role in the price is played by the exchange rate which varies and which of the currencies of USD/HRK, EUR/HRK, USD/EUR are calculated. In the offers, the exchange rate was calculated in USD compared to the Chinese RMB (YUAN) from the PBOC ("People's Bank of China") and the exchange rate was 6.8 with the date of December 28, 2018. The shipping price of the container from China is not the same for every month of the year. At the beginning of the year (i.e. January 2019), the fares are at a much higher level than for the rest of the year; this especially applies to containers with dimensions of 40' (inches), which were about \$200-500 cheaper during the last year.

5.2.7 Payment Terms

The payment method is 30% in advance, and the other 70% in cash on delivery as required by the forge factories C.Z.Y. and N.R.M., while the forge factory N.D. requires paying 50% in advance and the other 50% on delivery. However, they are open to negotiations and explain that if a long-term relationship is established, the terms of payment can be discussed.

6 ANALYSIS OF RESULTS

Based on the set of criteria and the alternatives, the decision is to be made. By using the AHP method, it is necessary to decide about the selection of the forging offer. As explained earlier in Chapter 5, when weighting individual criteria, the *most important criterion* is the *delivery time* when choosing the optimal primary process. The deadline

should be shortened in order to shorten the entire production cycle.

The forge factory comparison (Tab. 3) was used to simplify the entry and display of data in Expert Choice.

The results show that the best choice is the forge factory N.R.M., where the priority vector has the highest value, although the remaining two forge factories do not fall far behind. The second choice is the N.D. and the third is C.Z.Y., which is also shown in Fig. 7.

Table 3 Comparison of three forges

Forges	N. D.	C. Z. Y.	N. R. M.
Delivery time	3 months	10 months	12 months
Productivity per day	1333 forgings	600 forgings	455 forgings
Productivity per worker per day	8 forgings	17 forgings	4 forgings
Price per piece	40.5\$	52.11\$	35.17\$
Mold for price	6,618\$	22,332\$	5,880\$
Total price (120 000 pcs.)	4,860,000\$	6,253,200\$	4,220,400\$
Payment terms	50% in advance, the balance is paid on delivery	30% in advance, the balance is paid on delivery	30% in advance, the balance is paid on delivery
Certification	ISO 9001, 20000	IATF 16949	ISO 9001, 14001
References	McLaren, Subitomo	Bosch, Volvo	CCL UK, HMI USA
Number of shifts	Two nine-hour shifts	One twelve-hour shift	One ten-hour shift
Number of employees	150	35	120
Number of forklifts	6	1	6
Number of forging machines	12	3	1
Type of heating in furnaces	Electric heating	Electric heating	Induction heating

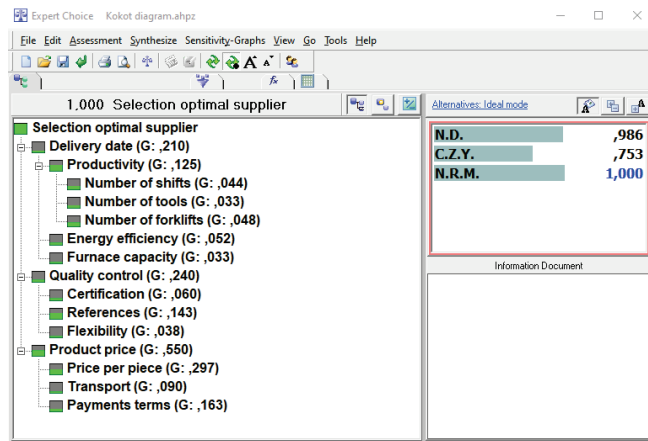


Figure 7 Model view of the results obtained by Expert Choice

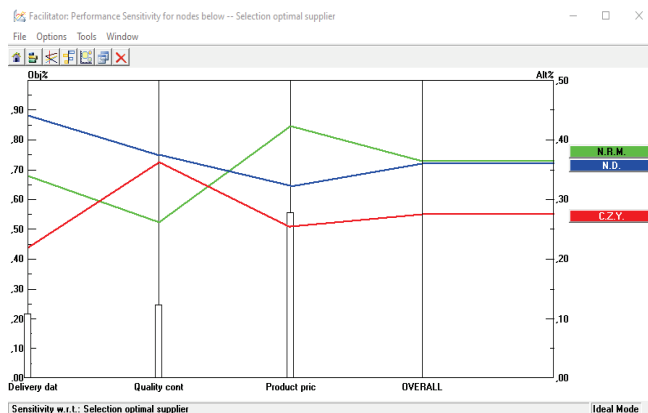


Figure 8 Diagram of the results obtained by Expert Choice

Graphic analysis (Fig. 8) clearly shows that forge N.D. is the best alternative. The result was expected as the delivery time is the most important criterion.

If the relation between the criteria were changed, i.e. if the price of the product was the most important criterion, different results would be generated as shown by Fig. 9.

The graphic analysis of the changed relations (Fig. 10) clearly shows that the forge factory N.D. is the best alternative. It was obtained when the price of the product was set as the most important criterion.

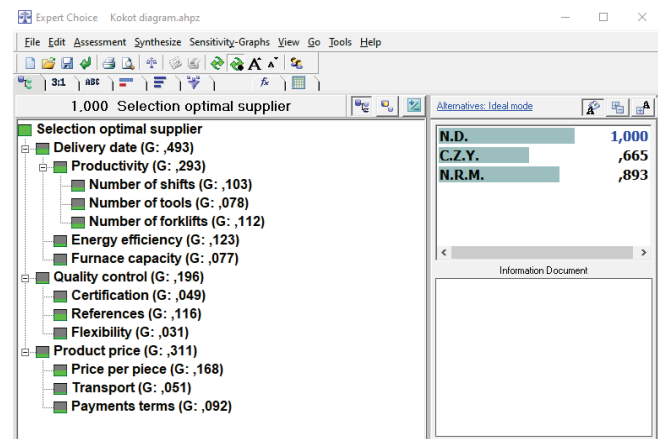


Figure 9 Model view of the results obtained by changed criteria

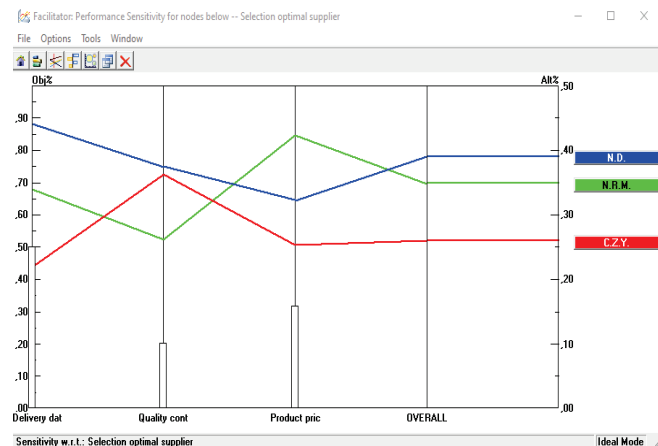


Figure 10 Diagram of the results obtained by changed criteria

7 CONCLUSION

The implementation of the AHP method was performed for a concrete shaft workpiece, using Expert Choice 11. Based on the analysis of the results, the relation between each one of the weighted criteria affects the goal of selecting the optimal forging supplier. Three criteria that have an intense impact on selection have been analyzed, especially the delivery time and product price. The results show that the optimal forge factory is N.D. The specified forge is the best according to the following criteria: delivery time and quality management. This choice is logical since the delivery criterion is the most important. It is explained that the competitiveness criterion also affects the selection of the optimal provider, but due to the unavailability of the data, it

was not considered in the analysis of the results. The subjectivity of the decision-maker has a great impact on the result. The preparation of the business environment itself and the insight into the business process of the three forge factories, between which the selection was carried out, is very important. Thus, if the cooperation with Chinese forge factories had been longer and deeper, more exact data would have been obtained, such as rejects percentage, product return, productivity, efficiency, economy, liquidity, profitability, etc. If these data had been known, the criteria would have been differently evaluated, and they would certainly influence the final decision. It would be interesting to compare, according to presented criteria, the difference between precise forging and closed die forging.

Notice

The paper was presented at MOTSP 2020 – International Conference Management of Technology – Step to Sustainable Production, which took place from 30th September – 2nd October 2020 in Bol, island Brač (Croatia). The paper is not and will not be published anywhere else.

8 REFERENCES

- [1] Adithan, M. (2007). *Process Planning and Cost Estimation*, New Age International (p) Limited, Publishers, New Delhi.
- [2] Slack, N., Chambers, S., Johnston, R., & Betts, A. (2009). *Operations and Process Management*, 2nd edition, FT Prentice Hall, Harlow.
- [3] Swift, K. G. & Booker, J. (2003). *Process Selection: From Design to Manufacture*. Second Edition. Process Selection: From Design to Manufacture: Second Edition. 1-316. <https://doi.org/10.1016/B978-075065437-1/50000-7>
- [4] Halevi, G. (2003). *Process and Operation Planning: Revised Edition of the Principles of Process Planning: A Logical Approach*, Kluwer Academic Publishers.
- [5] Davis, J. R., Semiatin, S. L. et al. (1989). *ASM Metals, Handbook, Vol. 14: Forming and Forging*, 9th edition (#06360G).
- [6] Saaty, T. L. (2008). Decision making with the analytic hierarchy process. *Int. J. Services Sciences*, 1(1), 83-98. <https://doi.org/10.1504/IJSSCI.2008.017590>
- [7] Coyle, G. (2004). *Practical Strategy*. Open Access Material. AHP The Analytic Hierarchy Process (AHP).
- [8] Saaty, T. L. & Vargas, L. G. (2012). *Models, Methods, Concepts & Applications of the Analytic Hierarchy Process*, Springer, New York. <https://doi.org/10.1007/978-1-4614-3597-6>
- [9] Clemen, R. T. (1996). *Making Hard Decisions, An Introduction to Decision Analysis*, 2nd Edition, Fuqua School of Business, Duxbury Press.
- [10] Musafija, B. (1988). *Obrada metala plastičnom deformacijom*. Svjetlost, Sarajevo. (in Bosnian)

Authors' contacts:

Predrag Ćosić, PhD, Full Professor
(Corresponding author)
University of Zagreb,
Faculty of Mechanical Engineering and Naval Architecture,
Ivana Lučića 5, 10000 Zagreb, Croatia
385 91 413 1450, e-mail: pcosic3@gmail.com

Zdenka Keran, PhD, Assistant Professor
University of Zagreb,
Faculty of Mechanical Engineering and Naval Architecture,
Ivana Lučića 5, Zagreb, Croatia
e-mail: zdenka.keran@motsp.eu

Vedran Kokot, BSc, student of Master Study
University North,
Jurja Križanića 31b, 42000 Varaždin, Croatia
e-mail: vekokot@unin.hr

The Simulation Model of a Student Restaurant

Zvonimir Mihaljevic, Goran Dukic*

Abstract: This paper features a simulation model of the FSB canteen. The data required for the simulation was collected through direct observation of the canteen during the busiest time of the day, that is, lunchtime. The simulation model was verified and validated based on the collected data. The model and the results of the simulation were presented. In order to reduce the waiting time, two modifications of the existing model were proposed and simulation models for both cases were also developed. After simulating the modified models, in order to determine the effects of the proposed modifications, the obtained results were analyzed and compared with the results of the existing system.

Keywords: model; modification; simulation; validation; verification

1 INTRODUCTION

When a demand for a service exceeds the ability of a provider to respond to orders, a waiting line occurs. The set of statistical laws and theorems that deal with various problems related to the clients waiting for a service is called Queuing theory. Queuing theory is a mathematical study of the congestion and delays of waiting in line. "Queuing theory (or "queueing theory") examines every component of waiting in line to be served, including the arrival process, service process, number of servers, number of system places, and the number of customers which might be people, data packets, cars, etc." [1]. Waiting in line at the canteen is a part of every student's daily routine. Generally, students have limited periods of free time which they use to go to the canteen. The length of the queue often determines whether they decide to wait or decide it is not worth waiting for. Waiting in line is perceived negatively by students and is associated with poor service quality. Interestingly, the queues often occur when the system is not actually overloaded, that is when its capacity is not fully utilized. The main problem is in the patterns of arrivals and the process of serving; they are very variable and can cause a temporary overload on the system. The aim of this paper is to analyze the operation of the canteen as a multichannel system. The paper is derived from the master diploma work. Chapter 2 is followed by a brief theoretical background about simulations and simulation modelling. The third chapter presents the steps of a simulation project through the FSB canteen (FSB - Fakultet Strojarsstva i Brodogradnje = FMENA - Faculty of Mechanical Engineering and Naval Architecture, University of Zagreb, Croatia). In order to get the most accurate simulation, before even creating a simulation, it is necessary to analyze the system in detail and measure all of its essential elements. Later on, with the help of all of those elements, we will improve the system and ultimately reduce the time spent waiting in line.

2 SIMULATION AND SIMULATION MODELLING

According to Meng [2], simulation is the imitation of the operation of a real-world process or system over time. The steps of a simulation process include:

- Generating an artificial history of a system.

- Observing the behavior of that artificial history.
- Drawing inferences concerning the operating characteristics of the real system.

Main advantages of simulation include:

- Studying the behavior of a system without building it.
- Results are accurate in general and compared to the analytical model.
- It helps to find an unexpected phenomenon in behavior of the system.
- It is easy to perform "What-If" analysis.

Main disadvantages of simulation include:

- It is expensive to build a simulation model.
- It is expensive to conduct a certain simulation.
- Sometimes it is difficult to interpret the simulation results.

2.1 Systems and System Environment

According to [2], a system is a group of objects which are joined together in some form of a regular interaction or interdependence towards the accomplishment of a certain purpose. A system is often affected by changes occurring outside of it. Such changes are said to occur in the system environment. In modelling a system, it is necessary to decide on the boundary between the system and its environment. System can be both discrete and continuous. A discrete system is one in which the state variable(s) change only at a discrete set of points in a certain time period. A continuous system is one in which the state variable(s) change continuously over time. The system consists of the following components:

- An *entity* is an object of interest in the system.
- An *attribute* is a property of an entity.
- An *activity* represents a time period of a specified length.
- The *state* of a system is defined as a collection of variables necessary to describe the system at any time, and relative to the objectives of the study.
- An *event* is defined as an instantaneous occurrence that may change the system's state.

As it evolves over time, the behavior of a system is being studied through developing a simulation model.

2.2 Modelling

According to Basch and Žagar [3], modeling is the process of describing a model in a simulation language. In doing so, the actual system is displayed in a way enabled by the simulation language. There are different languages for different types of systems. A model is a means by which we represent a realistic system. The model only shows the most important aspects of the system, that is, the model describes the system only with a certain level of accuracy. In this paper, to create a simulation model of a student restaurant, Enterprise Dynamics 10.3. is used. Enterprise Dynamics represents a state of the art modular object oriented simulation platform created to help solve any complex people, processes, technology, and infrastructure related challenges. Moreover, Enterprise Dynamics offers data-driven answers for the majority of commercial, governmental, education and industrial applications [4]. The steps of making a simulation model of the FSB canteen are presented in next chapter.

3 THE STEPS OF MAKING A SIMULATION MODEL OF THE FSB CANTEEN

3.1 Operation Flow

In order to describe the real system and give us a rough picture of what the simulation model should look like, a conceptual model was created prior to the simulation model. The conceptual model of the canteen is shown in Fig. 1.

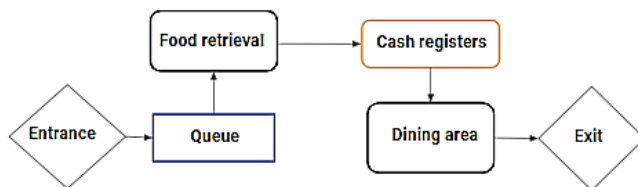


Figure 1 Operational flow

3.2 Data Collection

The input data for the canteen simulation was obtained on the basis of measurements performed during the canteen operation. Using a stopwatch to record the operation of the system, the data was collected through direct observation of the system. The description of the system required measurements of:

- arrival time of each student,
- time necessary to receive food,
- a possible number of students in a queue,
- a number of cash registers,
- invoicing time,
- a possible number of students in a queue for each cash register,
- dining time,
- canteen capacity,
- tray disposal time,

- a number of students entering the canteen at the opening.

Measurement of inter-arrival time consisted of noting the time whenever a new student joined the queue. This measurement also obtained the total number of students who came to the canteen during that particular day. A sample of 50 students was chosen to measure certain elements such as the amount of time for students to pick up food, for the cashier to issue an invoice, and the amount of time for student to pay for the meal. When measuring dining time, a sample of 100 students was taken. The amount of time students spend eating was measured. While measuring this amount of time, it was noticed that students who came to the canteen on their own, left it much faster, unlike the groups of students of three or more who tend to stay in the canteen longer despite finishing their lunch. In the end, for the measurement of tray disposal time, a sample of 50 students was taken. The amount of time for the canteen staff to pick up and clean the trays with plates and cutlery was measured. During this process of staff cleaning up the trays, especially during the busiest time in the canteen, a queue of students waiting tends to create. Furthermore, in theory, such a queue can cause a standstill, but it does not happen in practice. As a result, the type of measurement concerning the amount of time for the staff to clean the trays was chosen.

3.3 Simulation Model of FSB Canteen

Based on the conceptual model and a detailed observation of the canteen operation, a simulation model of the FSB canteen was developed in the Dynamics Enterprise simulation program. Fig. 2 shows the overall model used to analyze the FSB canteen operation.

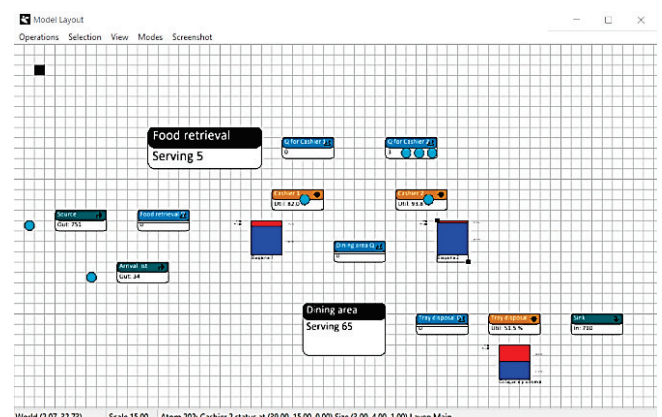


Figure 2 Simulation model of FSB canteen

The basic atoms used in this model are Source, Queue, Server, Multiserver and Sink atoms. The simulation was conducted through a time period of three hours, that is, during lunchtime from 11:00 to 14:00, a time period when the system is at its busiest. The measurement results described in the previous chapter were used as input data to simulate the operation of the canteen. In order to capture the variability of the data, AutoFit option was used. The option was also used to find the probability distributions that best fit the observed data. The Source atom, which on average takes 14.25 seconds

to perform its activity, generates students. Alongside the Source atom, Poisson distribution was assumed. Arrival list generated 34 students who initially loaded the system. When entering the canteen, students may have to wait in a queue before being served in Food retrieval atom. The average time required for students to pick up their food is 73.39 seconds for which the Logistic distribution fitted the data best. According to a random open channel rule, Multiservice Food retrieval chooses a random channel from all the open output channels and sends student to it. Then, students approach one of the cash register queues from which they go to the corresponding cash register. An average time for the first cashier to issue an invoice is 22.75 seconds for which the normal distribution fitted the data best. An average time for the second cashier is 26.25 seconds and pearsont5 distribution fitted the data best. After students pay for their food, they go to Dining area. An average dining time is 922.34 seconds for which an AutoFit suggests a Gamma distribution. When students finish their lunch, they are required to return the trays with plates and cutlery. An average time for an employee to clean a tray is 7.77 seconds for which the lognormal distribution fitted the data best.

3.4 Verification and Validation of the Simulation Model

According to [5], verification is a process which ensures that the model is constructed correctly, that is, it raises the question whether the mathematical model is correctly implemented in the simulation software or not. Verification also takes care of the correctness of the input parameters and logical structure of the model. Validation is a process of evaluating the accuracy of a model relative to the actual system it describes.

3.4.1 Verification

The simulation model is verified by investigating whether the model is built correctly. The model in Fig. 2 is built according to specifications by implementing the observed data. After running the model for three hours no errors occurred and all the students who had arrived at the canteen were served and eventually left the canteen. During this period of time, all atoms behaved as they were programmed.

3.4.2 Validation

This model was validated based on the data of the total number of students who arrived at the canteen the day the measurement was carried out. According to the canteen staff, 811 invoices were issued during lunchtime, while simulation generated 796 students during a three-hour period. The number of 796 students was obtained through the sum of students which was generated both by the atom Source (762 students) and students from the Arrival list (34 students). The comparison of the data obtained from the canteen staff (811 students in the canteen that day) and the simulation (796 students generated), validates the simulation model.

3.5 Simulation Results of the Current System

This section presents the results obtained by running the simulation model for a three-hour period for which certain measurements were performed. In the Run Control menu, the simulation is set to stop after three hours. Recording was turned on so simulation results could be read from the summary report. Fig. 3 shows the output of the summary report for the simulation model of the current system.

name	content	current average		throughput		staytime average
		current	average	input	output	
Source	0	0.000		762	762	0.000
Food retrieval	0	1.322		796	796	17.938
Food retrieval	5	5.817		796	791	79.178
Q for Cashier 2	1	2.160		390	389	59.844
Q for Cashier 1	1	1.357		401	400	36.628
Cashier 1	1	0.847		400	399	22.903
Cashier 2	1	0.941		389	388	26.174
Dining area Q	0	0.000		787	787	0.000
Dining area	64	63.898		787	723	910.141
Tray disposal Q	0	0.302		723	723	4.505
Tray disposal	0	0.518		723	723	7.742
Sink	0	0.000		723	0	0.000
Cashier 1 statu	0	0.000		0	0	0.000
Cashier 2 statu	0	0.000		0	0	0.000
Product	0	0.000		0	0	0.000
StatusMonitorSt	0	0.000		0	0	0.000
Product	0	0.000		0	0	0.000
Arrival list	0	0.000		34	34	0.000
Model start time	nedjelja, lipanj 21 2020 12:27:33					
Model end time	nedjelja, lipanj 21 2020 15:27:33					
Runlength (seconds)	10800.00					

Figure 3 Summary report for the simulation model of the current system

The calculated utilization of the current system is 89.45 %. This was calculated using the arithmetic mean of the utilization of Cashier 1 (84.7%) and Cashier 2 (94.2%). The average time spent in the system (W) obtained by the simulation is 169.89 seconds. The calculated time spent in the system (W) includes all elements of the system placed in front of the Dining atom in the model and as such is taken into account in further analysis. Although this particular system does not include all elements of a regular system, it is still called a system because it includes the elements such as the time spent in queues, the time spent in the multiserver Food retrieval, and the time spent on servers (cash registers). The period of time a student spends eating is not affected by any part of the system, but is defined by the students themselves. As a result, the element of dining time is not included in the analysis. The time spent in the tray disposal queue is negligible compared to the total amount of time spent in the system. Since that amount of time can be compensated for the dining time reduction, it is also not used in further analysis.

4 SYSTEM MODIFICATIONS

After the system's operational characteristics were obtained by simulating the canteen operation, certain modifications of the system were made in order to obtain more favorable values of such characteristics. Those modifications of the system include adding the third cash register and also adding another waiting line. Both system

modifications are feasible in reality and they have both yielded some improvements in the system's operational characteristics. After that, a "What-if" analysis of the system was performed. In such an analysis the behavior of all three models in relation to the increased system load was analyzed.

4.1 3-Cash Register System

Fig. 4 shows a model of the canteen with three cash registers.

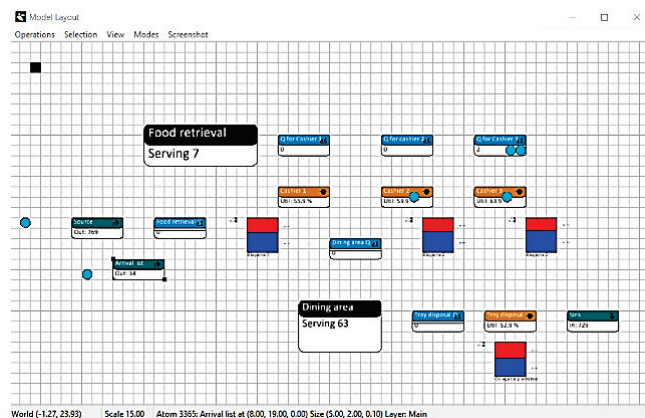


Figure 4 Simulation model of FSB canteen with 3 cash registers

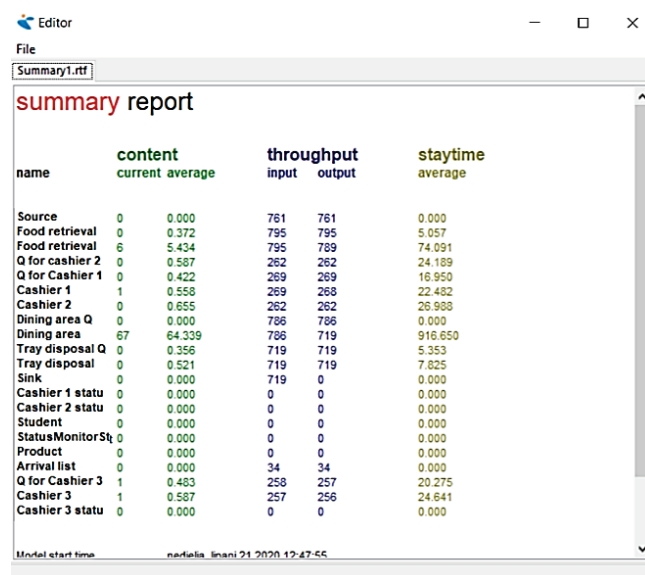


Figure 5 Summary report for the three-cash register canteen system

Unlike the initial model, this one has two additional atoms: Server (Cashier 3) and Queue (Queue for third cashier). Multiserver Food retrieval now has 3 output channels that are connected to the queues of each cash register. Random channel rule randomly selects the channel and outputs the Product (student) to it. After waiting in one of the queues, the student goes to the next cashier and further into the system that has remained the same. The simulation was also conducted throughout a period of three hours, for which the results are shown in Fig. 5.

By simulating a three-cash register canteen system, the system utilization of 60 % was obtained. The total efficiency

of 60 % was obtained by the arithmetic mean of the usability of Cashier 1, Cashier 2, and Cashier 3. The average amount of time spent in the system (W) obtained by the simulation is 124.323 seconds.

4.2 2-Row Waiting Line System

Fig. 6 shows a two-row waiting line system.

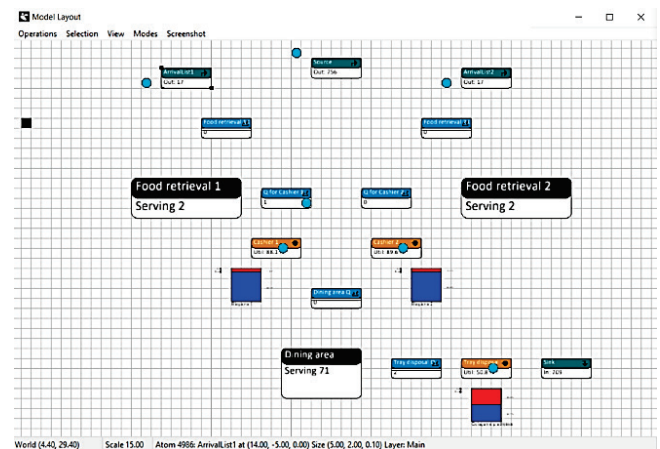


Figure 6 Simulation model of the two-row waiting line system

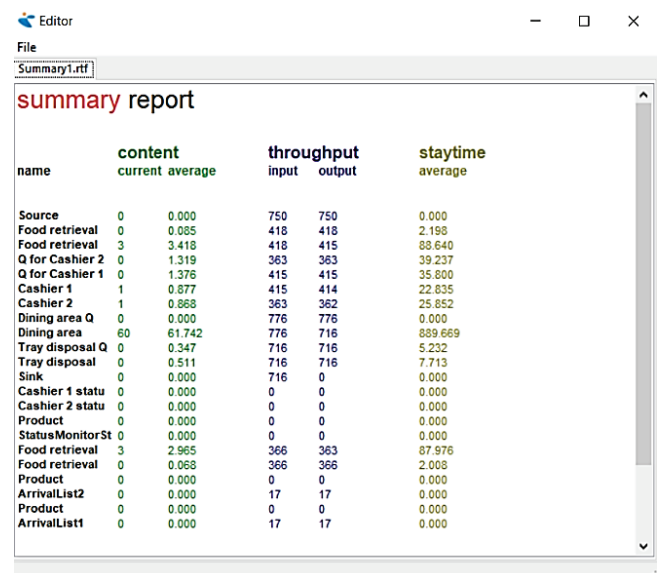


Figure 7 Summary report for the two-row waiting line system

Unlike the initial model, this model has two Food retrieval Multiservers, where each one has its own queue. Atom Source now has two output channels and randomly selects the queue to which the Product (student) is sent. It was assumed that out of 34 students who loaded the system at the beginning, half of them would fit in one row and the other half would fit in another one. This is done by adding another Arrival list to the system. The simulation was performed throughout the period of three hours for which the results are shown in Fig. 7.

System utilization of the current system was calculated at the percentage of 87.25. This was calculated using the arithmetic mean of the utilization of Cashier 1 (87.7%) and

Cashier 2 (86.8%). The average amount of time spent in the system (W) obtained by the simulation is 152.273 seconds.

4.3 Model Comparison

Tab. 1 shows a comparison of the system utilization and the average time spent in the system for all three developed models.

Table 1 Comparison of simulation model results

	System utilization, %	Average time spent in the system, s
Current system	89.45	169.89
three-cash register system	60	124.323
two-row waiting line system	87.25	152.273

The average waiting time in the three-cash register system is 124.323 seconds, which is almost 27% less than in the existing system. The system utilization was also reduced by 29 percentage points. The average waiting time in the two-row waiting line system is 152.273 seconds, which is 10% less than in the existing system. Compared to the current system, the system utilization reduced by two percentage points. Looking at the comparison, the high utilization of the system can be directly related to the higher average of waiting time. As a result, it can be inferred that the cash registers are the bottleneck of the system. Analyzing the simulation of the current system, a slight increase in the number of students coming into the system is visible. After the system suffers an initial shock where 34 students instantly load the system, Multiserver Food retrieval rarely reaches maximum capacity since queues are regularly filled before reaching the cash registers. As the number of students coming into the system increases, the usability of the cash registers reaches 99% very quickly with a result of endless queues starting to form. Based on this observation, it can be concluded that cash registers are the bottleneck of the system.

4.4 "What-If" system analysis

In order to reveal the bottleneck of the system mentioned in the previous subchapter, an analysis of the model which observes what happens if the number of students coming to the canteen increases was made. "What-if" analysis is an analysis that looks at what would happen to the system if any of its parameters changed. The following table shows what happens to all the three systems if the number of students coming to the canteen increases by 10%, that is, how this increase affects the usability of the system and the average time students spend waiting in the system.

Increase in the number of students coming to the canteen by 10% results in significant changes of characteristics inside the two systems. The current system and the two-row waiting line system, which have been heavily burdened so far, show that they are able to withstand such an increase in the number of students. As a result, this kind of increase also causes a sharp increase in the average waiting time in the system. In the current system, there was an increase of 41% in the waiting time, while in the system with two rows, the increase was 33%. The three-cash register system withstood this

increase very well. Its utilization increased only by 4.23 percentage points and the average time spent in the system increased only by 2.35%. The results show that adding another cash register to the system has a greater potential than adding another waiting line. The three-cash register system withstood an increase without any problems and with a minimal increase in the average time spent in the system. Further testing showed that this system is able to handle up to 40% more students than the current system, without compromising its operational characteristics.

Table 2 Results comparison of the "What-If" analysis

	System utilization, %	Average time spent in the system, s
Current system	98.50	287.18
three-cash register system	64.23	127.32
two-row waiting line system	95.45	227.69

5 CONCLUSIONS

In order to analyze the work of the FSB student canteen and to find out how much time students spend waiting in line at the canteen, canteen simulation model was created with the help of the Enterprise Dynamics simulation platform. The data used in the simulation was obtained through direct observation of the system during lunchtime when the number of students visiting the canteen is the greatest. The high accuracy of the simulation results enabled further modifications of the model with the aim of optimizing the whole process, and ultimately reducing the average time spent in the system. It can be concluded from the obtained results that both modifications offer an improvement in terms of the average waiting time in the system. However, the addition of a third cash register in the system has a greater potential. Carrying out a "What-if" analysis leads to the conclusion that the three-cash register system is able to handle up to 40% more students than the existing one, without compromising operational characteristics. As a result, serious consideration should be given to reconstructing the existing system.

Notice

The paper was presented at MOTSP 2020 – International Conference Management of Technology – Step to Sustainable Production, which took place from 30th September – 2nd October 2020 in Bol, island Brač (Croatia). The paper is not and will not be published anywhere else.

6 REFERENCES

- [1] <https://www.investopedia.com/terms/q/queuing-theory.asp>
- [2] Meng, X. (1998). *Simulation CSCI 6337*. University of Texas - Pan American, <https://www.eg.bucknell.edu/~xmeng/Course/CS6337/Note/master/master.html>
- [3] Basch, D. & Žagar, M. (2011). *ATLAS - simulacije arhitekture mikroročunala*, 1. internetsko izdanje. Sveučilište u Zagrebu, Fakultet elektrotehnike i računarstva, Zagreb. <http://docbook.rasip.fer.hr/ddb/public/index.php/publication/html/rasipbook/id/3?chapter=TOC&rce=0&tts=0&css=original&edit=0> (in Croatian)

- [4] <https://www.incontrolsim.com/software/enterprise-dynamics/>
- [5] Banks, J., Carson II, J. S., Nelson, B. L., & Nicol, D. M. (2005). *Discrete-Event System Simulation*, 4th edition. Prentice Hall.

Authors' contacts:

Zvonimir Mihaljevic, mag. ing. mech.
University of Zagreb,
Faculty of Mechanical Engineering and Naval Architecture,
Ivana Lučića 1, 10000 Zagreb, Croatia
E-mail: zvone.miha@gmail.com

Goran Dukic, PhD, Full Professor
University of Zagreb,
Faculty of Mechanical Engineering and Naval Architecture,
Department of Industrial Engineering, Chair of Production Design,
Ivana Lučića 1, 10000 Zagreb, Croatia
Tel. +385 1/61 68 381
E-mail: goran.dukic@fsb.hr

ERES 2021

WIT
CONFERENCES
Call for Papers

**13th International Conference on Earthquake
Resistant Engineering Structures**

26 – 28 May 2021 | Rome, Italy

Organised by

Wessex Institute, UK

Link Campus University, Italy

Sponsored by

WIT Transactions on the Built Environment



www.witconferences.com/eres2021

Article Title Only in English (Style: Arial Narrow, Bold, 14pt)

Ivan Horvat, Thomas Johnson, Marko Marić (Style: Arial Narrow, Normal, 10pt)

Abstract: Article abstract contains maximum of 150 words and is written in the language of the article. The abstract should reflect the content of the article as precisely as possible. TECHNICAL JOURNAL is a trade journal that publishes scientific and professional papers from the domain(s) of mechanical engineering, electrical engineering, civil engineering, multimedia, logistics, etc., and their boundary areas. This document must be used as the template for writing articles so that all the articles have the same layout. (Style: Arial Narrow, 8pt)

Keywords: keywords in alphabetical order (5-6 key words). Keywords are generally taken from the article title and/or from the abstract. (Style: Arial Narrow, 8pt)

1 ARTICLE DESIGN

(Style: Arial Narrow, Bold, 10pt)

(Tab 6 mm) The article is written in Latin script and Greek symbols can be used for labelling. The length of the article is limited to eight pages of international paper size of Letter (in accordance with the template with all the tables and figures included). When formatting the text the syllabification option is not to be used.

1.1 General Guidelines

(Style: Arial Narrow, 10pt, Bold, Align Left)

The document format is Letter with margins in accordance with the template. A two column layout is used with the column spacing of 10 mm. The running text is written in Times New Roman with single line spacing, font size 10 pt, alignment justified.

Article title must clearly reflect the issues covered by the article (it should not contain more than 15 words).

Body of the text is divided into chapters and the chapters are divided into subchapters, if needed. Chapters are numbered with Arabic numerals (followed by a period). Subchapters, as a part of a chapter, are marked with two Arabic numerals i.e. 1.1, 1.2, 1.3, etc. Subchapters can be divided into even smaller units that are marked with three Arabic numerals i.e. 1.1.1, 1.1.2, etc. Further divisions are not to be made.

Titles of chapters are written in capital letters (uppercase) and are aligned in the centre. The titles of subchapters (and smaller units) are written in small letters (lowercase) and are aligned left. If the text in the title of the subchapter is longer than one line, no hanging indents.

Typographical symbols (bullets), which are being used for marking an item in a list or for enumeration, are placed at a beginning of a line. There is a spacing of 10pt following the last item:

- Item 1
- Item 2
- Item 3

The same rule is valid when items are numbered in a list:

1. Item 1
2. Item 2
3. Item 3

1.2 Formatting of Pictures, Tables and Equations

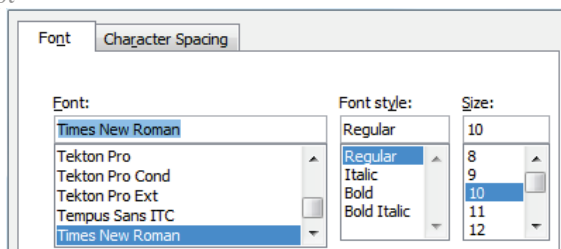
(Style: Arial Narrow, 10pt, Bold, Align Left)

Figures (drawings, diagrams, photographs) that are part of the content are embedded into the article and aligned in the centre. In order for the figure to always be in the same position in relation to the text, the following settings should be defined when importing it: text wrapping / in line with text.

Pictures must be formatted for graphic reproduction with minimal resolution of 300 dpi. Pictures downloaded from the internet in ratio 1:1 are not suitable for print reproduction because of unsatisfying quality.

Figure 1 Text under the figure [1]

(Style: Arial Narrow, 8pt, Align Centre)



The journal is printed in black ink and the figures have to be prepared accordingly so that bright tones are printed in a satisfactory manner and are readable. Figures are to be in colour for the purpose of digital format publishing. Figures in the article are numbered with Arabic numerals (followed by a period).

Text and other data in tables are formatted - Times New Roman, 8pt, Normal, Align Center.

When describing figures and tables, physical units and their factors are written in italics with Latin or Greek letters,

while the measuring values and numbers are written upright.

10pt

Table 1 Table title aligned centre
(Style: Arial Narrow, 8pt, Align Centre)

	1	2	3	4	5	6
ABC	ab	ab	ab	ab	ab	ab
DEF	cd	cd	cd	cd	cd	cd
GHI	ef	ef	ef	ef	ef	ef

10 pt

Equations in the text are numbered with Arabic numerals inside the round brackets on the right side of the text. Inside the text they are referred to with equation number inside the round brackets i.e. "... from Eq. (5) follows" (Create equations with MathType Equation Editor - some examples are given below).

10pt

$$F_{\text{avg}}(t, t_0) = \frac{1}{t} \int_{t_0}^{t_0+t} F[q(\tau), p(\tau)] d\tau, \quad (1)$$

$$\cos \alpha + \cos \beta = 2 \cos \frac{\alpha + \beta}{2} \cdot \cos \frac{\alpha - \beta}{2}, \quad (2)$$

$$(AB)^T = B^T A^T. \quad (3)$$

10pt

Variables that are used in equations and also in the text or tables of the article are formatted as *italics* in the same font size as the text.

10pt

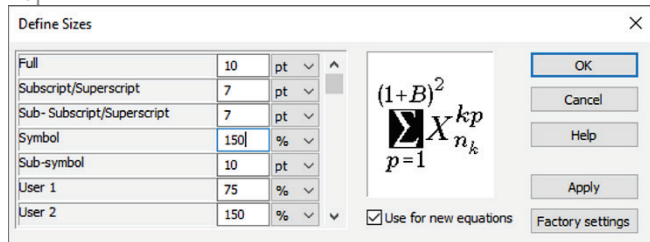


Figure 2 The texts under figures
(Style: Arial Narrow, 8pt, Align Centre)

10pt

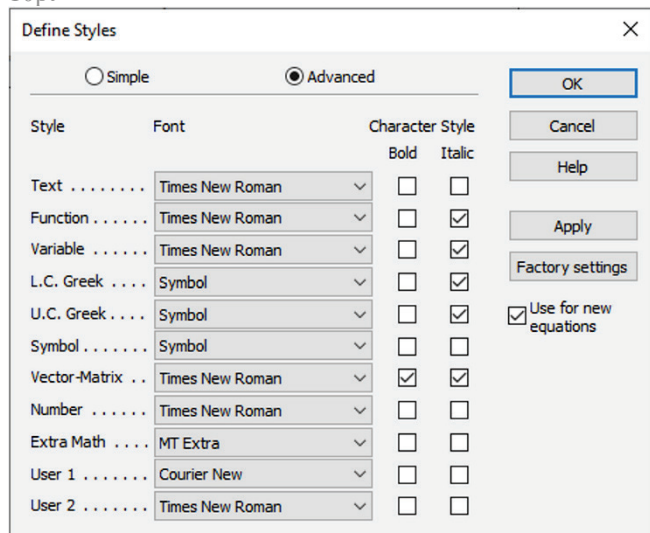


Figure 3 The texts under figures
(Style: Arial Narrow, 8pt, Align Centre)

Figures and tables that are a part of the article have to be mentioned inside the text and thus connected to the content i.e. „... as shown in Fig. 1...” or „data from Tab. 1...” and similar.

10pt

2 PRELIMINARY ANNOTATION

10pt

Article that is offered for publication cannot be published beforehand, be it in the same or similar form, and it cannot be offered at the same time to a different journal. Author or authors are solely responsible for the content of the article and the authenticity of information and statements written in the article.

Articles that are accepted for publishing are classified into four categories: original scientific papers, preliminary communications, subject reviews and professional papers.

Original scientific papers are articles that according to the reviewer and the editorial board contain original theoretical or practical results of research. These articles need to be written in such a way that based on the information given, the experiment can be repeated and the results described can be achieved together with the author's observations, theoretical statements or measurements.

Preliminary communication contains one or more pieces of new scientific information, but without details that allow recollection as in original scientific papers. Preliminary communication can give results of an experimental research, results of a shorter research or research in progress that is deemed useful for publishing.

Subject review contains a complete depiction of conditions and tendencies of a specific domain of theory, technology or application. Articles in this category have an overview character with a critical review and evaluation. Cited literature must be complete enough to allow a good insight and comprehension of the depicted domain.

Professional paper can contain a description of an original solution to a device, assembly or instrument, depiction of important practical solutions, and similar. The article need not be related to the original research, but it should contain a contribution to an application of known scientific results and their adaptation to practical needs, so it presents a contribution to spreading knowledge, etc.

Outside the mentioned categorization, the Editorial board of the journal will publish articles of interesting content in a special column. These articles provide descriptions of practical implementation and solutions from the area of production, experiences from device application, and similar.

10pt

3 WRITING AN ARTICLE

10pt

Article is written in the English language and the terminology and the measurement system should be adjusted to legal regulations, standards (ISO 80 000 series) and the SI international system of units. The article should be written in third person.

Introduction contains the depiction of the problem and an account of important results that come from the articles that are listed in the cited literature.

Main section of the article can be divided into several parts or chapters. Mathematical statements that obstruct the reading of the article should be avoided. Mathematical statements that cannot be avoided can be written as one or more addendums, when needed. It is recommended to use an example when an experiment procedure, the use of the work in a concrete situation or an algorithm of the suggested method must be illustrated. In general, an analysis should be experimentally confirmed.

Conclusion is a part of the article where the results are being given and efficiency of the procedure used is emphasized. Possible procedure and domain constraints where the obtained results can be applied should be emphasized.

10pt

4 RECAPITULATION ANNOTATION

10pt

In order for the articles to be formatted in the same manner as in this template, this document is recommended for use when writing the article. Finished articles written in MS Word for Windows and formatted according to this template must be submitted using our The Paper Submission Tool (PST) (<https://tehnickiglasnik.unin.hr/authors.php>) or eventually sent to the Editorial board of the Technical Journal to the following e-mail address: tehnickiglasnik@unin.hr

The editorial board reserves the right to minor redaction corrections of the article within the framework of prepress procedures. Articles that in any way do not follow these authors' instructions will be returned to the author by the editorial board. Should any questions arise, the editorial board contacts only the first author and accepts only the reflections given by the first author.

10pt

5 REFERENCES (According to APA)

10pt

The literature is cited in the order it is used in the article. Individual references from the listed literature inside the text are addressed with the corresponding number inside square brackets i.e. "... in [7] is shown ...". If the literature references are web links, the hyperlink is to be removed as shown with the reference number 8. Also, the hyperlinks from the e-mail addresses of the authors are to be removed. In the literature list, each unit is marked with a number and listed according to the following examples (omit the subtitles over the references – they are here only to show possible types of references):

9pt

- [1] See <http://www.bibme.org/citation-guide/apa/>
- [2] See http://sites.umuc.edu/library/libhow/apa_examples.cfm
- [3] (Style: Times New Roman, 9pt, according to APA)
- [4] Amidzic, O., Riehle, H. J., & Elbert, T. (2006). Toward a psychophysiology of expertise: Focal magnetic gamma bursts as a signature of memory chunks and the aptitude of chess players. *Journal of Psychophysiology*, 20(4), 253-258. <https://doi.org/10.1027/0269-8803.20.4.253>
- [5] Reitzes, D. C. & Mutran, E. J. (2004). The transition to retirement: Stages and factors that influence retirement adjustment. *International Journal of Aging and Human Development*, 59(1), 63-84. Retrieved from

<http://www.baywood.com/journals/PreviewJournals.asp?Id=0091-4150>

- [6] Jans, N. (1993). *The last light breaking: Life among Alaska's Inupiat Eskimos*. Anchorage, AK: Alaska Northwest Books.
- [7] Miller, J. & Smith, T. (Eds.). (1996). *Cape Cod stories: Tales from Cape Cod, Nantucket, and Martha's Vineyard*. San Francisco, CA: Chronicle Books.
- [8] Chaffe-Stengel, P. & Stengel, D. (2012). *Working with sample data: Exploration and inference*. <https://doi.org/10.4128/9781606492147>
- [9] Freitas, N. (2015, January 6). People around the world are voluntarily submitting to China's Great Firewall. Why? Retrieved from http://www.slate.com/blogs/future_tense/2015/01/06/tencent_s_wechat_worldwide_internet_users_are_voluntarily_submitting_to.html

(Style: Times New Roman, 9pt, according to APA)

10pt

10pt

Authors' contacts:

8pt

Full Name, title
Institution, company
Address
Tel./Fax, e-mail

8pt

Full Name, title
Institution, company
Address
Tel./Fax, e-mail

Note: Gray text should be removed in the final version of the article because it is for guidance only.

BEM/MRM 44

WIT
CONFERENCES
Call for Papers

**44th International Conference on Boundary Elements
and other Mesh Reduction Methods**

15 – 17 June 2021 | Valencia, Spain

Organised by

Wessex Institute, UK

University of Mississippi, USA

Sponsored by

WIT Transactions on Engineering Sciences

International Journal of Computational Methods
and Experimental Measurements



www.witconferences.com/bem44



CALL FOR ABSTRACTS

ICPADM2021

13th International Conference on the Properties
and Applications of Dielectric Materials

11–15 JULY 2021 | JOHOR BAHRU, MALAYSIA

Emerging Dielectrics for Energy Sustainability

KEY AREAS

- ☐ Aging of HV insulation
- ☐ Bio-dielectrics
- ☐ Conduction and breakdown in dielectrics
- ☐ Dielectrics phenomena and applications
- ☐ Eco-friendly dielectrics
- ☐ Emerging dielectric materials
- ☐ Gaseous breakdown and discharges
- ☐ HV insulation design via computational analysis
- ☐ HVDC insulation systems
- ☐ Monitoring and diagnostics of electrical insulation
- ☐ Nano-technology and nano-dielectrics
- ☐ New diagnostic applications for dielectrics
- ☐ New functional dielectrics for electrical systems
- ☐ Partial discharges
- ☐ Space charge and its effects
- ☐ Surface and interfacial phenomena

KEY DATES

Receipt of Abstract

SEPTEMBER 15, 2020

Notification of Abstract Acceptance

NOVEMBER 15, 2020

Receipt of Full Paper

JANUARY 15, 2021

Notification of Paper Acceptance

MARCH 15, 2021

For more details, please visit :

<https://attend.ieee.org/icpadm-2021/>

Hosted by:



Sponsored by:



TEHNIČKI GLASNIK / TECHNICAL JOURNAL – GODIŠTE / VOLUME 14 – BROJ / NUMBER 4

PROSINAC 2020 / DECEMBER 2020 – STRANICA / PAGES 403-545



Sveučilište
Sjever

SVEUČILIŠTE SJEVER / UNIVERSITY NORTH – CROATIA – EUROPE

ISSN 1846-6168 (PRINT) / ISSN 1848-5588 (ONLINE)

TEHNICKIGLASNIK@UNIN.HR – [HTTP://TEHNICKIGLASNIK.UNIN.HR](http://tehnickiglasnik.unin.hr)